ULTRA WIDEBAND RADAR ANTENNA DESIGN FOR SNOW MEASUREMENT APPLICATIONS

by

John Samy Mosy

A thesis submitted in partial fulfillment
of the requirements for the degree

of

Master of Science

in

Electrical Engineering

MONTANA STATE UNIVERSITY
Bozeman, Montana

November 2009

APPROVAL

of a thesis submitted by

John Samy Mosy

This thesis has been read by each member of the thesis committee and has been found to be satisfactory regarding content, English usage, format, citation, bibliographic style, and consistency, and is ready for submission to the Division of Graduate Education.

Richard S. Wolff

Approved for the Department of Electrical and Computer Engineering

Robert C. Maher

Approved for the Division of Graduate Education

Dr. Carl A. Fox

STATEMENT OF PERMISSION TO USE

In presenting this thesis in partial fulfillment of the requirements for a master's degree at Montana State University, I agree that the Library shall make it available to borrowers under rules of the Library.

If I have indicated my intention to copyright this thesis by including a copyright notice page, copying is allowable only for scholarly purposes, consistent with "fair use" as prescribed in the U.S. Copyright Law. Requests for permission for extended quotation from or reproduction of this thesis in whole or in parts may be granted only by the copyright holder.

John Samy Mosy

November 2009

ACKNOWLEDGEMENTS

First and foremost, I would like to thank my advisor, Richard Wolff, for the opportunity to work on this project, and also for his encouragement and confidence in my work; I am greatly thankful to him for giving me the chance to experience the beauty of research, and for giving me the support I needed when research results did not. I am also thankful to Andy Olson, without whom I would surely have been lost. I would also like to express my gratitude to those who made this entire project possible including Doug Roberts and the Flat Earth team, Jared Campbell and the Campbell Scientific team, and Brock LaMeres and his DSP team. Thanks to Dwayne Folden and everyone that helped in building and providing the tools and programs for testing the antennas in MSU-Bozeman. Many thanks to Brent Olson for making every tool I needed available, and for providing me with afterhours access to machines.

I would like to thank my parents who taught me to love learning and to always acquire the highest level of academic excellence. I would also like to thank my sisters, Germaine and Maryam, and my many great friends in Egypt, Montana, and Tunisia for their support.

TABLE OF CONTENTS

TABLE OF CONTENTS- CONTINUED

TABLE OF CONTENTS- CONTINUED

LIST OF TABLES

Table Page

LIST OF FIGURES

Figure Page

LIST OF FIGURES – CONTINUED

Figure Page

LIST OF FIGURES – CONTINUED

Figure Page

LIST OF FIGURES – CONTINUED

Figure Page

LIST OF FIGURES – CONTINUED

Figure Page

LIST OF FIGURES – CONTINUED

Figure Page

LIST OF FIGURES – CONTINUED

Figure Page

LIST OF FIGURES – CONTINUED

Figure Page

ABSTRACT

Creating a high-precision, compact and low cost snow structure and depth sensor has always been the dream of many industries, and yet hard to achieve all together. Snow depth sensors are used in avalanche search and rescue and widely in recreational snow industry, as well as in environmental monitoring systems for snow water equivalence measurements. The use of radar for snow depth measurement is not new and many techniques -such as Frequency Modulated Continuous Wave (FMCW) - have been used but they prove to be costly, bulky, and have relatively low precision. Today with the availability of chip-scale Ultra Wide-Band (UWB) technology, it is possible to create Snow Depth Sensor (SDS) and Snow Water Equivalent (SWE) measuring systems in low cost, small size and possibly mobile devices, with very high precision. One problem that remains at the RF (Radio Frequency) end of the UWB technique in measuring snow parameters is the antenna used in transmitting and receiving UWB pulses. UWB pulses are characterized by an instantaneous fractional energy bandwidth greater than about 0.20-0.25. The FCC has allocated spectrum for UWB use in the 3.1-10.6 GHz band and available chipsets generate pulses in the lower 3-6 GHz band. For creating applications that use UWB in measuring snow parameters such as SWE and snow depth, a UWB antenna is required. A successful UWB radar antenna needs to have high gain, linear phase, low dispersion and low Voltage Standing Wave Ratio (VSWR), and high directivity throughout the entire band. The antennas are to have physically compact design with high gain, linear phase, low VSWR and high directivity for UWB radar applications in the snow measurements industry. This thesis presents several antenna designs for the 3.1-10.6 GHz UWB band and the 3-6 GHz UWB lower band that have the potential to meet these requirements, and show, through laboratory measurements, modeling and simulations, that the required attributes can be achieved.

CHAPTER 1

INTRODUCTION

Ultra Wideband (UWB) has a number of advantages that make it attractive for a variety of applications including radar measurements in the time domain; UWB systems have potentially low complexity and low cost, a noise-like signal (no significant interference to existing radio systems), and more importantly, they have a very good time domain resolution [1]. The Federal Communications Commission (FCC) defines a UWB system as any device where the fractional bandwidth is greater than 0.20, or occupies 500 MHz or more of spectrum [2]. UWB systems can be characterized either by a large relative bandwidth, or a large absolute bandwidth. For large relative bandwidth characterization, systems with relative bandwidth of larger than 20 % are considered as UWB, while large absolute bandwidth refers to systems with more than 500 MHz of bandwidth. With such spreading in frequency the power spectral density (PSD) is brought to such low levels that it does not disturb other systems operating at the same frequency range under most operating conditions. The frequency range and power levels of UWB systems are regulated by the FCC in accordance to its 'report and order' issued in 2002 [2][3]. This ruling allowed the emission of intentional UWB radiations, subject to restrictions on emitted power spectral density. The ruling restricts the admissible peak power to 0 dBm/ 50 MHz [4] and the PSD is limited to a -10 dB bandwidth lying between 3.1 and 10.6 GHz. It also sets stringent limits on out-of-band emission, as shown

in figure 1, with a maximum PSD of -41.3 dBm/MHz permitted in the frequency band 3.1- 10.6 GHz [3].

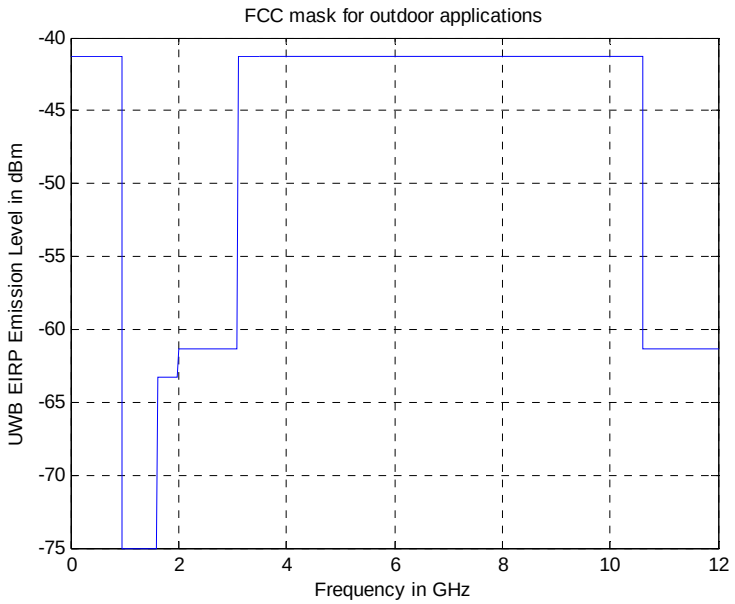

Figure 1. FCC mask for outdoor UWB applications.

The main focus of this project is to design an antenna for a UWB radar system to be used in snow measurements. In measuring snow parameters the Time Domain PulsON technology was selected for initial trials. This system uses the UWB lower band between 3 and 6 GHz. The Time Domain's PulsON technology uses very short pulses to generate ultra-wide bandwidths of spectrum at a very low transmit power as shown in figure 2. The system generates pulses with a width of 316 picoseconds at a repetition rate of 9.6 million pulses per second, as shown in figure 3. Another similar system that was used later in this project is the Novelda R2A. Detailed characterization for these two systems is presented in chapter three of this thesis.

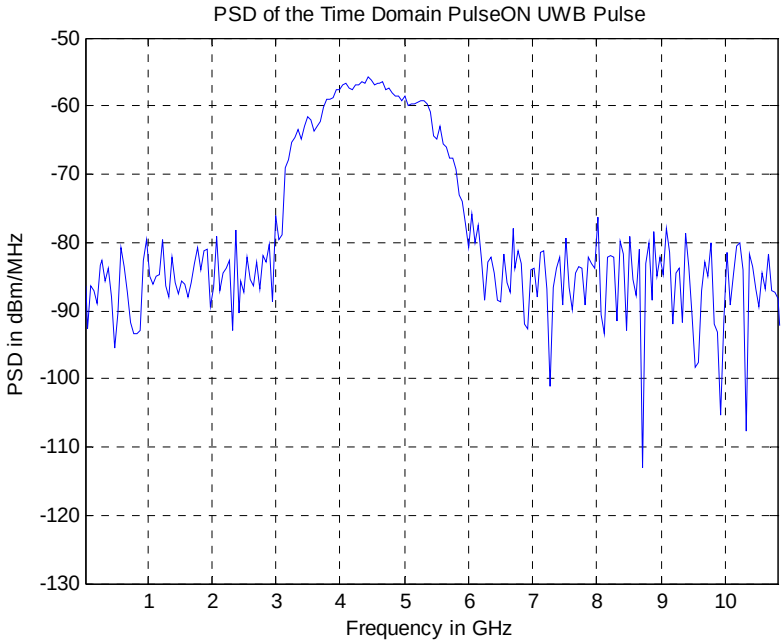

Figure 2. The PSD of Time Domain's Pulse ON UWB Pulse, calculated from the signal measurement provided by Time Domain for the Pulse ON 220 Module.

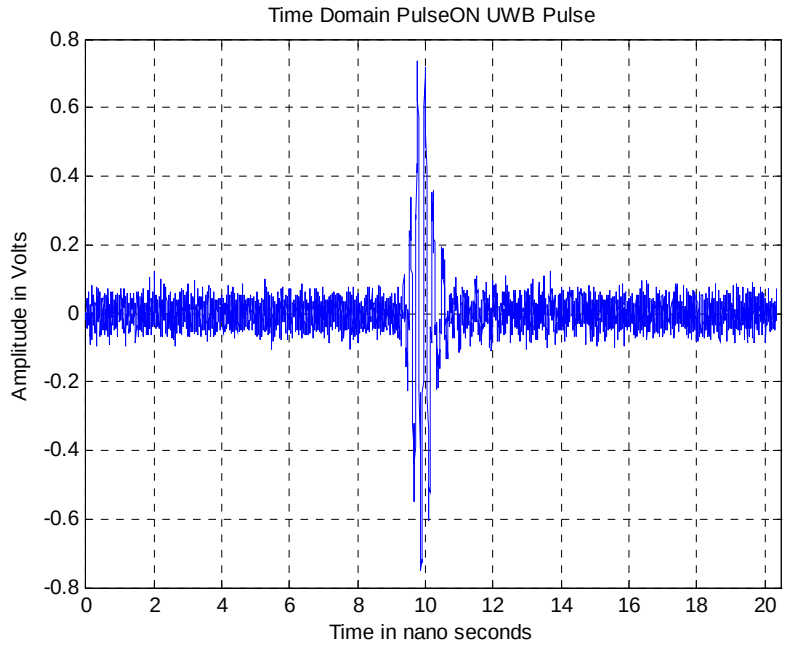

Figure 3. Time Domain's Pulse ON UWB Pulse, provided by Time Domain for the Pulse ON 220 Module.

Several UWB antennas will be presented which were designed, modeled, simulated and tested at Montana State University in Bozeman (MSU-Bozeman). The designs include: a quasi-horn antenna, a log periodic dipole array (LPDA) antenna, a Vivaldi antenna, and a bowtie antenna. Various tradeoffs are considered between these antennas based on specifications such as physical profile, radiation efficiency, impedance matching, and directivity.

CHAPTER 2

BACKGROUND

The IEEE standard definition of terms for antennas (IEEE std 145-1983) defines the antenna as “a means for radiating or receiving radio waves.” [5] Such a medium is a crucial part of any radar system. The basic role of the radar antenna is to provide a transducer between the free-space propagation and the guided-wave propagation of electromagnetic waves [6]. The antenna concentrates the radiated energy into a shaped directive beam that illuminates the target in a desired direction. The energy contained in the reflected target echo signals is then collected by the antenna and delivered to the receiver. In this radar system two antennas are required for transmitting and receiving of the signal. Due to the reciprocal behavior of antennas, however, only one design is needed for both ports. Several parameters are used to characterize any antenna such as, gain, directivity, efficiency, and return loss. To help better understand these parameters, and therefore, the requirements and challenges in designing UWB radar antennas, a background on antenna parameters is given here.

Antenna Parameters

Understanding basic antenna principles helps in selecting the best antenna for the UWB snow measurements system. These principles are reviewed in this section. The three basic parameters for any antenna are gain, radiation pattern, and VSWR. Other parameters will be discussed in this chapter as well.

Gain

The ability of an antenna to concentrate energy in a narrow angular region (a directive beam) is described in terms of antenna gain [6]. The antenna gain measurement is related to the directivity through the antenna radiation efficiency –defined later in this chapter. It is defined as "the ratio of the intensity, in a given direction, to the radiation intensity that would be obtained if the power accepted by an antenna were radiated isotropically [5]." Where the intensity of isotropically radiated power equals to the input power to the antenna divided by 4π (equation 1); and the direction of the gain measurement is the maximum gain direction unless otherwise indicated. Antenna gain can be expressed as

$$\text{Gain} = 4\pi \frac{radiation\ intensity}{total\ input\ power} = 4\pi \frac{U(\theta,\varphi)}{P_{in}} \text{ (dimensionless)} \qquad \text{Equation 1}$$

Another formula for the gain is shown in equation 2 which takes into account the radiation efficiency (e_{cd}).

$$G(\theta,\varphi) = e_{cd}\left[4\pi\frac{U(\theta,\varphi)}{P_{rad}}\right] \qquad \text{Equation 2}$$

It is important to note that for directive antennas, the high gain is a desired attribute. This comes from the fact that the gain is linearly proportional to directivity, provided that the antenna has good radiation efficiency.

Radiation Pattern

Antenna radiation pattern is defined as "a mathematical function or graphical representation of the radiation properties of the antenna as a function of space coordinates [7]." In the usual case the radiation pattern is determined in the far field region and is represented as a function of directional coordinates. The common set of such coordinates is shown in figure 4. Radiation properties include power flux density, radiation intensity, field strength, directivity, phase or polarization [5]. The radiation property of most concern, however, is the spatial distribution of radiated energy as a function of the observer's position along a path or surface of constant radius. Three dimensional pattern plots show the radiation power in the far field sphere surrounding the antenna, but extensive data are required to a plot radiation pattern in such a format. More frequently, however, two dimensional plots are sufficient and more convenient to measure and plot. If planes are chosen correctly for the two dimensional representation of radiation patterns, three dimensional patterns can easily be inferred. The two most important measurements for creating the full picture of the radiation pattern are the E-plane and H-plane patterns. The E-plane is a principal plane containing the direction of the electric filed (E-field) vector of the radiation from the antenna. The H-plane is orthogonal to it,

therefore containing the magnetic (H-field) vector radiation. It should also be noted that a two dimensional pattern view does not always represent a planar (vertical) cut. In a planar cut, the angle φ stays at a constant value –usually 0°- and θ is swept from 0 to 360°. Another representation is the conical cut; for a conical cut, the angle θ is kept constant while φ is swept through the 360 degrees, as shown in figure 5.

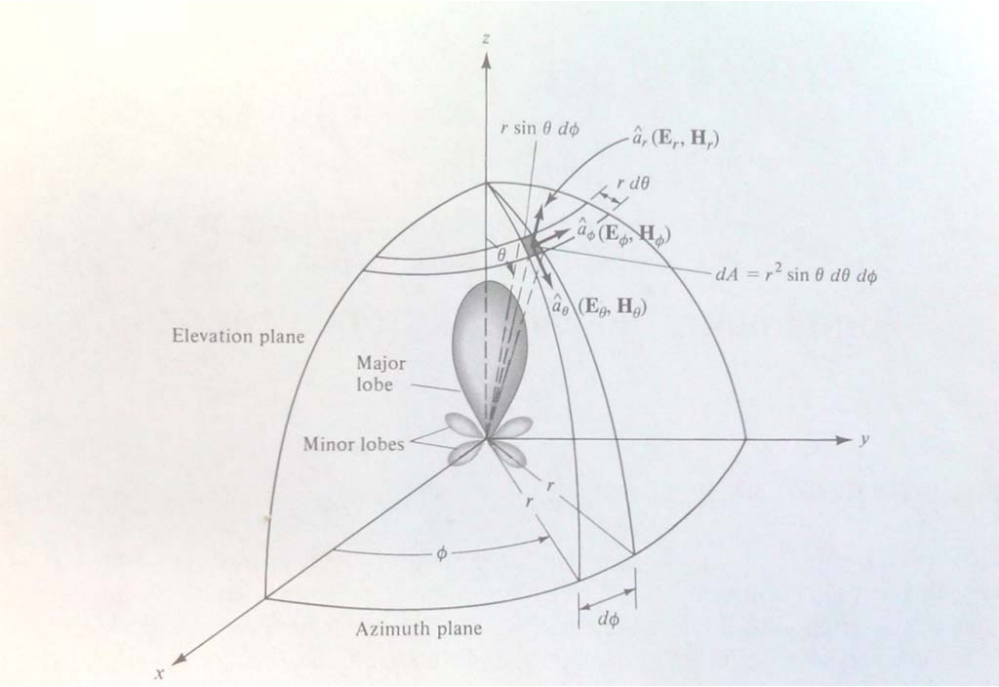

Figure 4. Coordinate system for antenna analysis. [5]

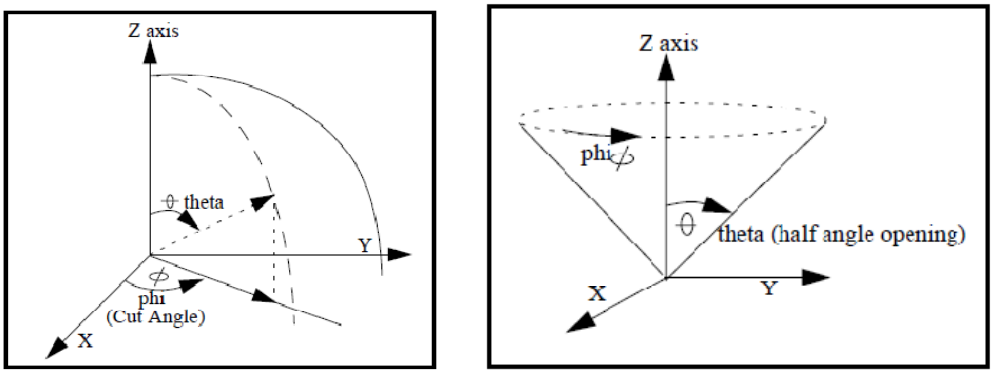

Figure 5. Planar (left) and conical (right) cuts in antenna analysis. [8]

Radiation patterns are designed based on the application for which an antenna will be used. For example most mobile communications like cell systems use omnidirectional antennas, i.e. the radiation power is uniformly distributed around the antenna. For radar applications, however, directional antennas are used so that the radiated energy is directed to a specific target. A high radiated power is desired to illuminate a target, yielding a stronger return signal and greater range. Figure 6 shows examples of omnidirectional and directional antennas radiation patterns.

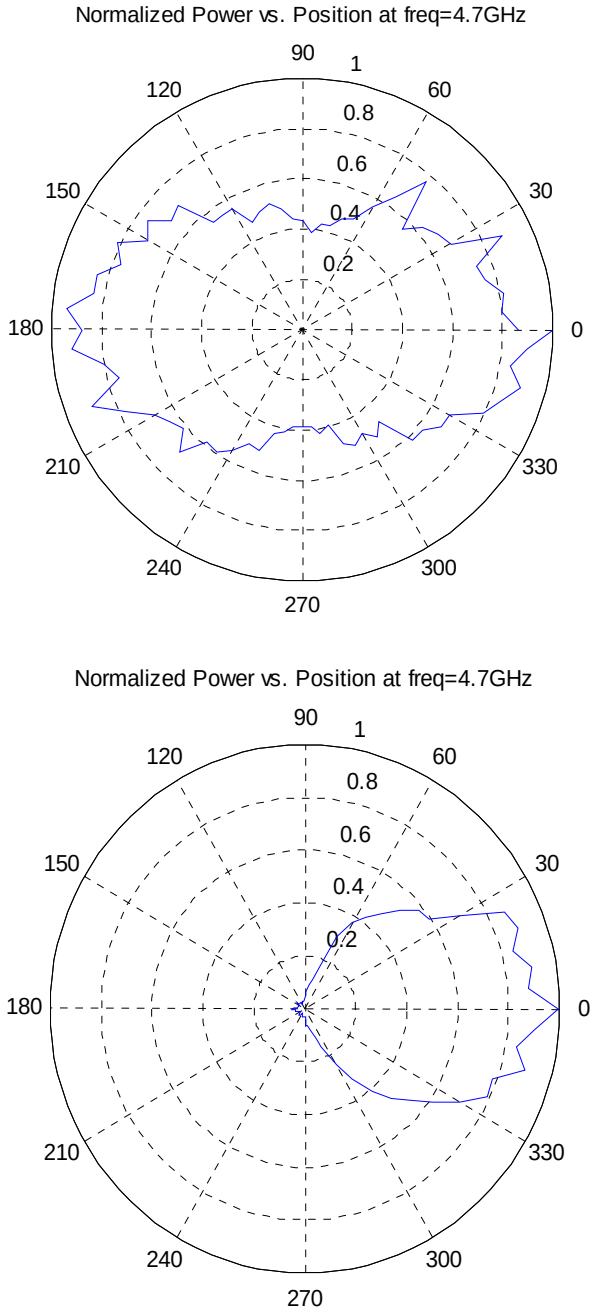

Figure 6. A near-omnidirectional pattern of the Pulse ON 220 antenna measured at 4.7 GHz (top), and directional radiation pattern of the Vivaldi antenna measured at 4.7GHz (bottom). Measurements were made in the MSU antenna test chamber (see 6.3.2).

There are several ways to represent radiation patterns. For example, the most common method is to normalize the field and power patterns with respect to their maximum value. This method results in normalized patterns that give a more readable view of the antenna's directivity rather than its absolute gain in different directions. For absolute values of power as a function of angular space, the logarithmic (dB) scale is preferred as it accommodates for both major and minor lobes of the pattern, which typically have widely different gains. The logarithmic scale representation can also be normalized. Figure 7 demonstrates the different methods of representing radiation patterns.

Half Power Beam Width (HPBW)

While radiation patterns help in understanding the nature of antenna radiation, some metric is required to distinguish antennas of different directivity. This measurement is known as half power beam width (HPBW). The HPBW is defined by the IEEE as: "In a plane containing the direction of the maximum of a beam, the angle between the two directions in which the radiation intensity is one-half value of the beam" [7]. The HPBW can also be translated into the logarithmic frame of reference as the angle between the two points at which the radiation intensity is reduced by 3dB relative to its maximum value in that plane, as shown in figure 7. Because HPBW is an indicator of the antenna's directivity, it is also usually a measure of the resolution of an antenna. Two identical targets at the same range are said to be resolved in angle if separated by at least the half-power beamwidth. The HPBW is a function of both the aperture of the antenna and the wavelength as given by equation 3.

$$HPBW = k\lambda/D \qquad \text{Equation 3}$$

In equation 3, D is the aperture dimension, λ is the free-space wavelength, and k is a proportionality constant known as the beamwidth factor [6]. From this equation it is noted that the HPBW decreases with increasing antenna operating frequency.

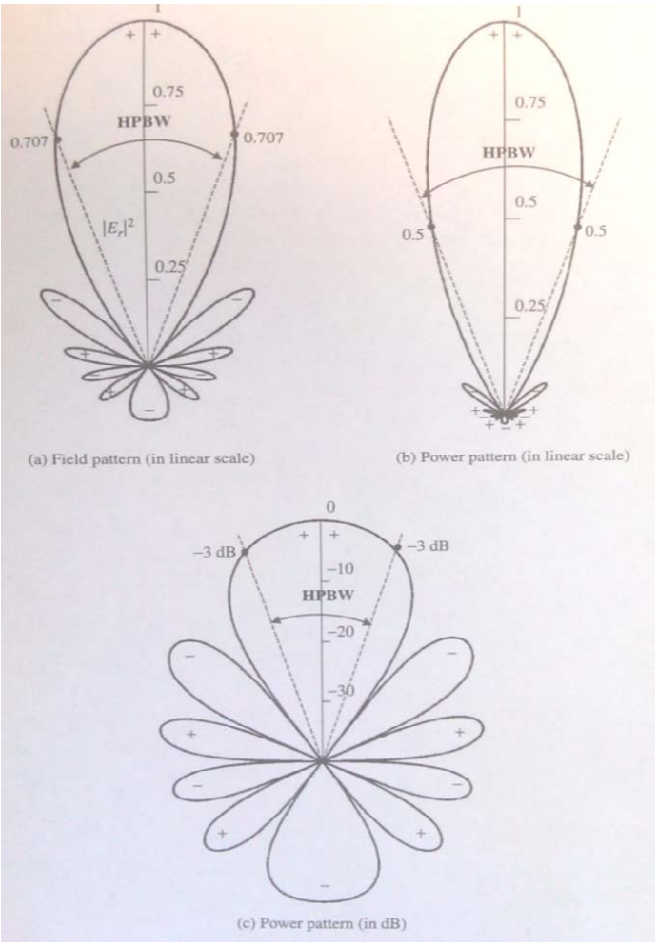

Figure 7. The different methods of representing radiation patterns with HPBW shown on each plot. [5]

Directivity

To complete the discussion we look at directivity**,** which in [9] is defined as "the ratio of the radiation intensity in a given direction from the antenna to the radiation intensity averaged over all directions. The average radiation intensity is equal to the total power radiated by the antenna divided by 4π. If the direction is not specified, the direction of maximum radiation intensity is implied." Or simply for a nonisotropic source, directivity is the ratio of its radiation intensity in a given direction over that of an isotropic source, as given in equation 4.

$$D = \frac{U}{U_0} = \frac{4\pi}{P_{rad}} \quad \text{(Dimensionless)} \qquad \text{Equation 4}$$

The radiation intensity is the power radiated from an antenna per unit solid angle [7] or mathematically,

$$U = r^2 S_{rad} \qquad \text{Equation 5}$$

and the total power radiated is given by

$$P_{rad} = \oiint_{\Omega} U_0 d\Omega = U_0 \oiint_{\Omega} d\Omega = 4\pi U_0 \qquad \text{Equation 6}$$

Antenna gain and directivity are referenced to the radiation intensity of an isotropic source, but that is highly theoretical. For this reason gain and directivity are usually measured in reference to the most commonly used half-wavelength dipole antenna and scaled to the isotropic antenna as a reference using equation 7.

0dBd = 2.15dBi Equation 7

In equation 7, dBd is dB(dipole), dBi is dB(isotropic)

Finally, it should be noted that the definition of directivity does not involve any dissipative losses in the antenna but only the concentration of radiated power. Other parameters are used to account for losses such as voltage standing wave ratio (VSWR) and efficiency – which is directly related to VSWR as shown below.

Voltage Standing Wave Ratio (VSWR)

Great attention will be given to the voltage standing wave ratio (VSWR) throughout this project as the VSWR relates directly to the antenna's performance and is used to characterize its efficiency. VSWR is the ratio between the amplitudes of the maximum standing wave to the minimum standing wave and is given by:

$$\text{VSWR}=\frac{V_{max}}{V_{min}}=\frac{1+|\Gamma|}{1-|\Gamma|} \quad \text{Equation 8}$$

Here Γ is voltage reflection coefficient at the input terminals of the antenna and calculated using equation 9.

$$\Gamma=\frac{Z_{in}-Z_0}{Z_{in}+Z_0} \quad \text{Equation 9}$$

The antenna input impedance is Z_{in}, and Z_0 is the characteristic impedance of the transmission line, as shown in figure 8.

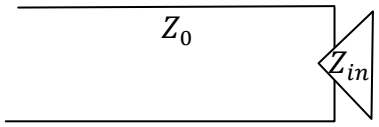

Figure 8. Antenna and transmission line model.

VSWR is important in the characterizing antenna's bandwidth. Bandwidth is defined as "the range of frequencies within which the performance of the antenna, with respect to some characteristics, conforms to a specific standard." [5] Such characteristics are tied directly to impedance matching that lead to higher or lower return loss in the range of frequency.

Return Loss

Return loss is proportional to the reflection coefficient squared, as shown in equation 10, where the reflection coefficient is the ratio of the transmitted to the reflected voltage [10]. For an antenna that is well matched to its input transmission line, 10% or less of the incident signal is lost due to reflections. This value can be translated as a -10dB or less return loss, where the return loss is calculated using the following equation:

Return Loss= $-10\log|S_{11}|^2$ or equivalently, $-10\log|\Gamma|^2 = -20\log|\Gamma|$ Equation 10

Although return loss is heavily used in the RF and microwave research field, VSWR is preferred instead in the commercial world and used in antenna datasheets. VSWR and return loss are related to each other as both values are concluded from Γ as

shown in equations 8 and 10. A commercially acceptable antenna has a VSWR of 2:1 or less.

Efficiency

Less commonly used but highly related to VSWR is antenna efficiency. Total antenna efficiency $e_0$takes into account losses at the input terminal and within the structure of the antenna such that:

$$e_0 = e_r e_c e_d \qquad \text{Equation 11}$$

Factors e_r, e_c, e_d are the reflection, conduction, and the dielectric efficiencies respectively, with the last two being very difficult to compute but can be determined theoretically and e_r calculated using the following equation:

$$e_r = (1 - |\Gamma|^2) \qquad \text{Equation 12}$$

Radiation Efficiency

Finally, radiation efficiency ,which takes into account both the conduction and dielectric efficiency, is defined as the ratio of the total power radiated by the antenna to the total power accepted by the antenna at its input terminal during radiation. [5]

CHAPTER 3

CHARACTERIZATION OF UWB PULSES

It is important to study and characterize the signals generated by available UWB chipsets in order to design practical radar antennas that can be used in applications such as the proposed SDS and SWE systems. Two UWB radio systems are considered in this project: the Time Domain Pulse ON 220, and the Novelda R2A development kit. These were selected after an examination of UWB chipsets that are becoming available, as they offer pulsed waveforms ideal for this application as explained in the next sections.

Time Domain Pulse ON 220

The Time Domain Pulse ON 220 UWB radio generates a high order derivative of a Gaussian pulse. The pulse has a width of 316 picoseconds as shown in figure 3 and is transmitted at a rate of 9.6 Mpulses/sec [2]. As discussed in chapter one, the frequency range and power level of UWB systems are regulated by the FCC in accordance to its "report and order" issued in 2002. The FCC restricts the admissible peak power to 0 dBm/50 MHz and the PSD is limited to a -10 dB bandwidth lying between 3.1 and 10.6 GHz. It also sets stringent limits on out-of-band emission, as shown in figure 1, with a maximum average PSD of -41.3 dBm/ MHz permitted in the frequency band 3.1- 10.6 GHz [8]. Measuring the transmit power for the Pulse ON 220 permits inspecting the system's compliance with the FCC UWB constraints. Characterizing the UWB pulses generated by the Pulse ON 220 also helps in better understanding how the UWB pulse

shape impacts the antenna design. The process of measuring the transmit signal and its characterization is discussed in the following sections.

Power Measurement Procedure

The Time Domain Pulse ON 220 transceiver has two standard SMA connectors for a transmitter and a receiver antenna. Figure 10 shows the block diagram of the setup for the power measurement. The receiver side was terminated and the transmitter was connected directly to an Advantest R3273 spectrum analyzer through a low loss cable. An auto calibration was performed on the spectrum analyzer before the measurement process. The losses in the cable were measured for calibration using an HP 8720D network analyzer. Due to the default 10 dB attenuation at the spectrum analyzer input port and the low power of the Pulse ON 220, no further attenuation was needed at the input port of the spectrum analyzer. The signal was above the noise floor of the spectrum analyzer and no amplifier was used in the measurement process. The spectrum analyzer provided limited capabilities for storing the data from the measurement performed but displayed directly on its screen. The total power was recorded in the graph captured from the spectrum analyzer screen and was -14.26 dBm as shown in figure 9. A LabVIEW virtual instrument (VI) was created to copy the power spectrum from the spectrum analyzer using the GPIB commands in the National Instrument drivers for the spectrum analyzer. The recorded PSD was further processed in Matlab to subtract cable insertion losses at different frequencies, smooth the PSD, and calculate the total power.

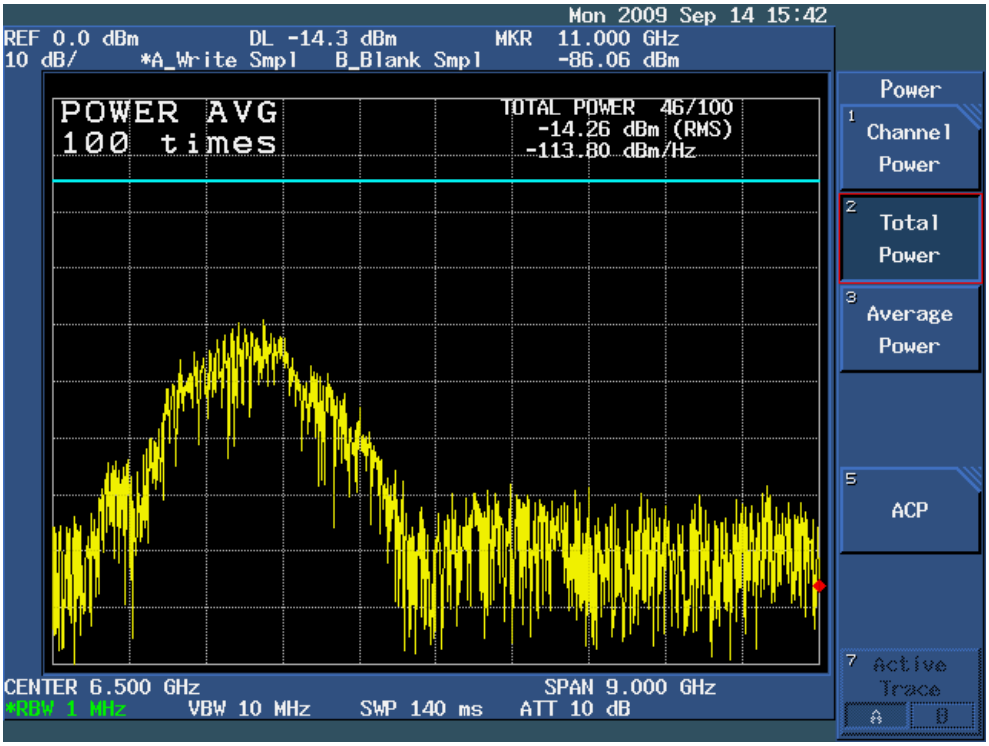

Figure 9. The power spectral density of the transmitted signal of Pulse ON 220 as seen on the spectrum analyzer.

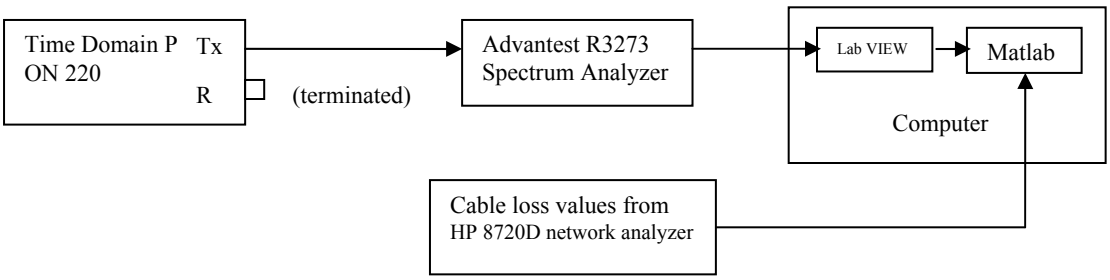

Figure 10. Time Domain Pulse ON 220 transmit power measurement block diagram.

Power Spectral Density

The power spectral density of the Time Domain Pulse ON 220 transmit signal was measured using a resolution bandwidth (RBW) of 1MHz. The measured PSD was copied from the spectrum analyzer into a comma separated (.csv) file using the Lab VIEW VI application created for this purpose. The file was then loaded into Matlab along with the loss values for the cables measured using the network analyzer. The measurement was calibrated using the cable losses and the resulting PSD is shown in figure 11. Due to the noisy nature of the measured PSD, smoothing was performed on the data using a third order Savitzky-Golay smoothing filter in Matlab. The resulting PSD of the smoothing process is shown in figure 12. The PSD has a maximum of -48.86 dBm/MHz at 4.4 GHz, that stays under the FCC limit of -41.3 dBm/MHz. The PSD has a 10 dB bandwidth that lies between 3.494 and 5.196 GHz as shown in figure 13.

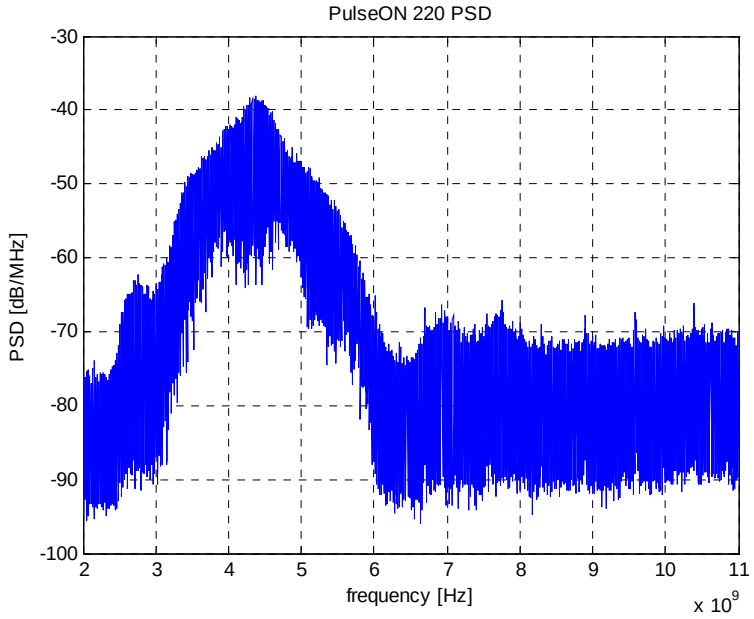

Figure 11. Measured power spectral density of the transmitted signal from Pulse ON 220.

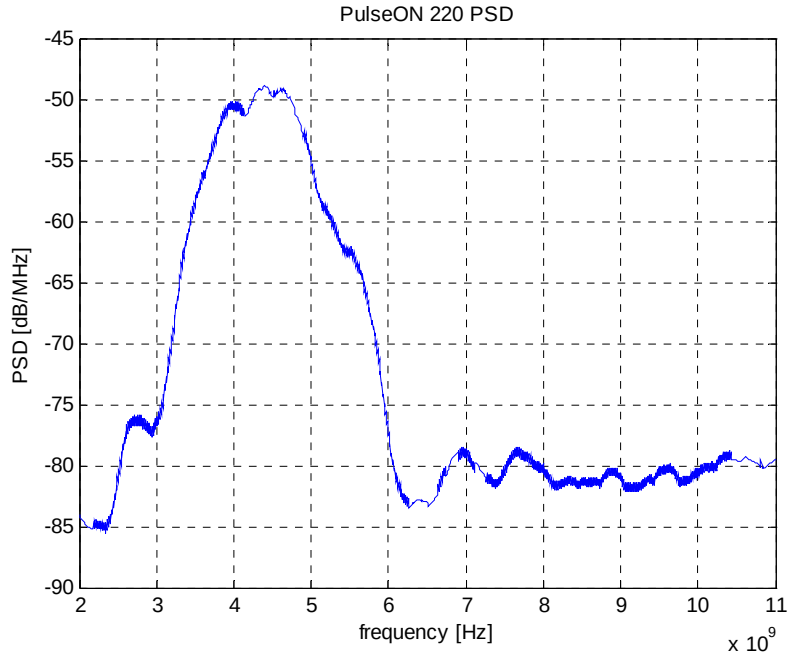

Figure 12. Measured power spectral density of the transmitted signal from Pulse ON 220 smoothed using a third order Savitzky-Golay filter.

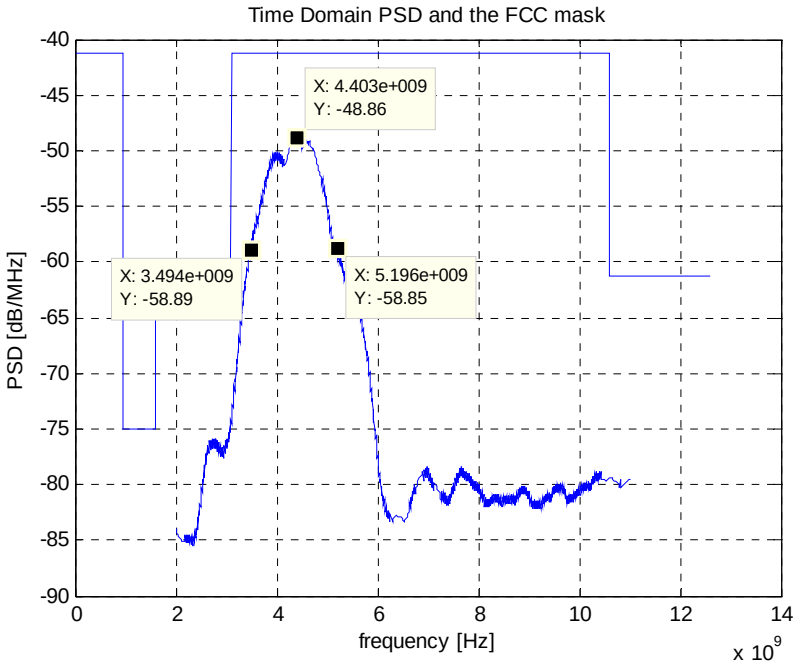

Figure 13. Measured power spectral density of the transmitted signal from Pulse ON 220 under the FCC UWB outdoor mask;
shown on the plot are the peak power and the -10 dB points.

Full Bandwidth Peak Power

Fontana explains in detail in an article entitled "*Observations on Low Data Rate, Short Pulse UWB Systems"* how the FCC regulations on the full bandwidth (FBW) peak power of UWB systems should be measured and interpreted [11]. For a UWB system that has a pulse repetition frequency (PRF) much greater than the spectrum analyzer resolution bandwidth (RBW), the Full Bandwidth (FBW) peak power is limited by the FCC to the value calculated using equation 13. In our case, the Pulse ON 220 has a PRF of 96 MHz and the spectrum analyzer RBW is 1 MHz.

$$P_{peak} \leq 7.5x10^{-8}\left(\frac{B_p}{R}\right)^2 \text{Watts} \qquad \text{for } R \gg B_R \qquad \text{Equation 13}$$

In equation 13, R= PRF, B_p is the -10 dB bandwidth of the signal, and B_R= RBW (1MHz for FCC measurements).

For the Pulse ON 220 system, R= 96 MHz, $B_{p(-10dB)}$= 1.7 GHz, as shown in Figure 13. The maximum allowed peak power is then calculated as follows:

$$P_{peak} \leq 7.5x10^{-8}\left(\frac{1.7x10^9}{96x10^6}\right)^2 \text{ or } P_{peak} \leq 3.71dBm$$

The actual peak power of the measured signal is calculated using equation 14

$$P_{peak} = \frac{P_{peak}^m}{\tau^2 R^2} \qquad \text{Equation 14}$$

In equation 14, P_{peak}^{m} is the measured peak power, $\tau = \frac{1}{B_p}$, and R= PRF

$\therefore P_{peak} = \frac{P_{peak}^{m}}{\tau^2 R^2} = \frac{P_{peak}^{m}}{(\frac{1}{1.7x10^{-9}})^2 x (9.6x10^6)^2} = P_{peak}^{m} + 44.96\text{dB}$

P_{peak}^{m} = -48.86 dBm

Therefore, the Pulse ON 220 transmit signal has a peak power $P_{peak} = -48.86 + 44.96 = -3.9\ dBm$. The peak power of the transmit signal is less than the maximum peak power of 3.71 dBm set by the FCC.

Novelda R2A

Novelda R2A is a development kit for the NAV3000 UWB chip which is capable of generating brief UWB pulses for radar applications. The NAV3000 chip includes a transmitter and a receiver. The transmitter part of the chip creates and transmits third order Gaussian pulses of various pulse widths. In the R2A development kit, the generated UWB pulse has a duration of 0.4 nanoseconds. The NAV3000 pulse has relatively small overall power values for a radar signal. The transmit signal from NAV3000 is amplified using the Hittite HMC 462LP5 low noise amplifier (LNA), which is included on the R2A evaluation board. The measurements were performed on the output of the LNA that is the amplified UWB transmit signal generated by NAV3000.

Power Measurement Procedure

The same procedure for measuring the Pulse ON 220 transmit signal is followed here for measuring the Novelda R2A transmit signal. The receiver side was terminated

and the transmitter was connected directly to an Advantest R3273 spectrum analyzer through a low loss cable. The losses in the cable were measured for calibration using an HP 8720D network analyzer. The total power was recorded in the graph captured from the spectrum analyzer screen and was -4.05 dBm as shown in figure 14. The Lab VIEW VI application used in the Pulse ON 220 measurements was used to copy the PSD from the spectrum analyzer. The recorded PSD was further processed in Matlab to subtract cable insertion losses at different frequencies, smooth the PSD, and calculate the total power.

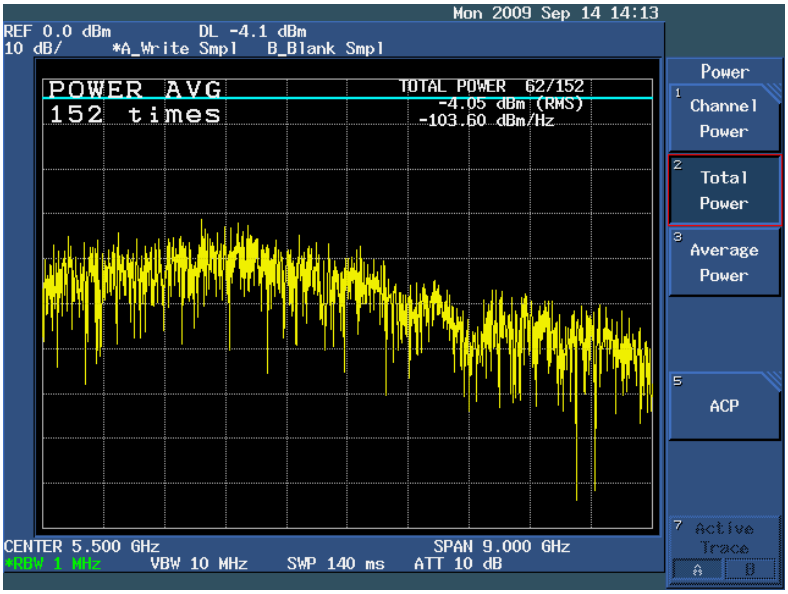

Figure 14. The power spectral density of the transmitted signal of Novelda R2A as seen on the spectrum analyzer.

Power Spectral Density

The power spectral density of the Novelda R2A transmit signal was measured using a spectrum analyzer resolution bandwidth (RBW) of 1MHz. The measured PSD

was calibrated using the cable losses and the resulting PSD is shown in figure 15. Due to the noisy nature of the measured PSD, smoothing was performed on the data using a third order Savitzky-Golay smoothing filter in Matlab. The resulting PSD of the smoothing process is shown in figure 16. The PSD has a maximum of -42.93 dBm/MHz at 3.97 GHz –that stays under the FCC limit of 41.3 dBm/MHz. The PSD has a 10 dB bandwidth that occupies from 1.08 to 6.06 GHz as shown in figure 17.

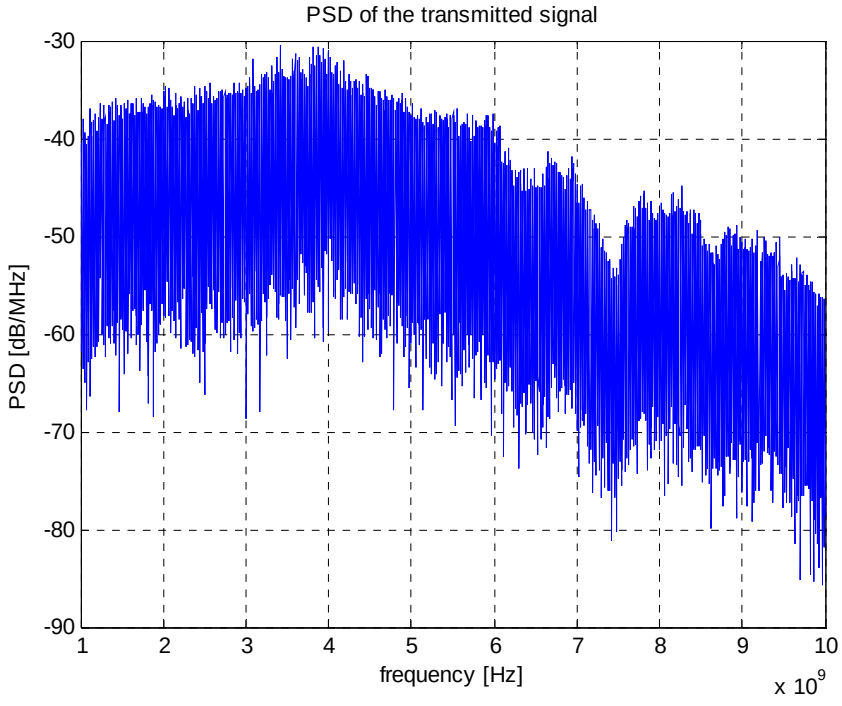

Figure 15. Measured power spectral density of the transmitted signal from Novelda R2A.

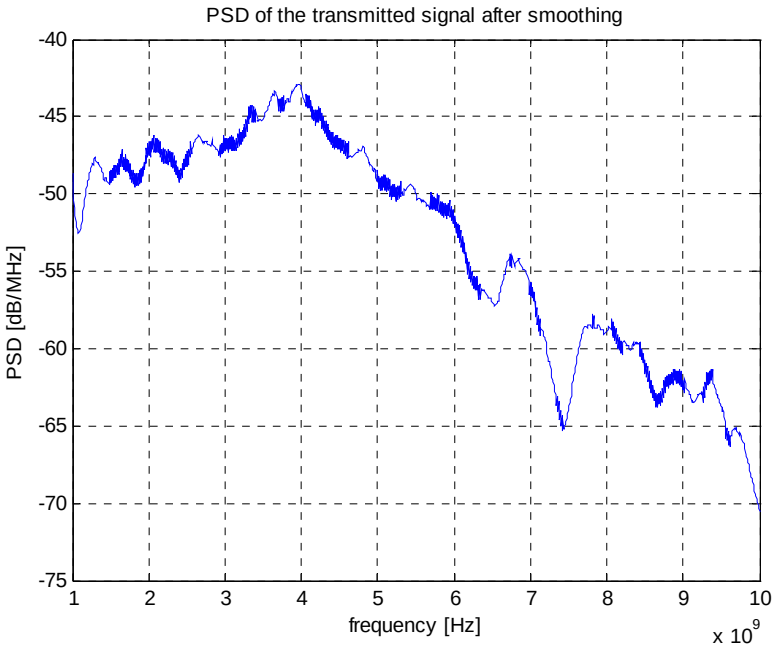

Figure 16. Measured power spectral density of the transmitted signal from Novelda R2A smoothed using a third order Savitzky-Golay filter.

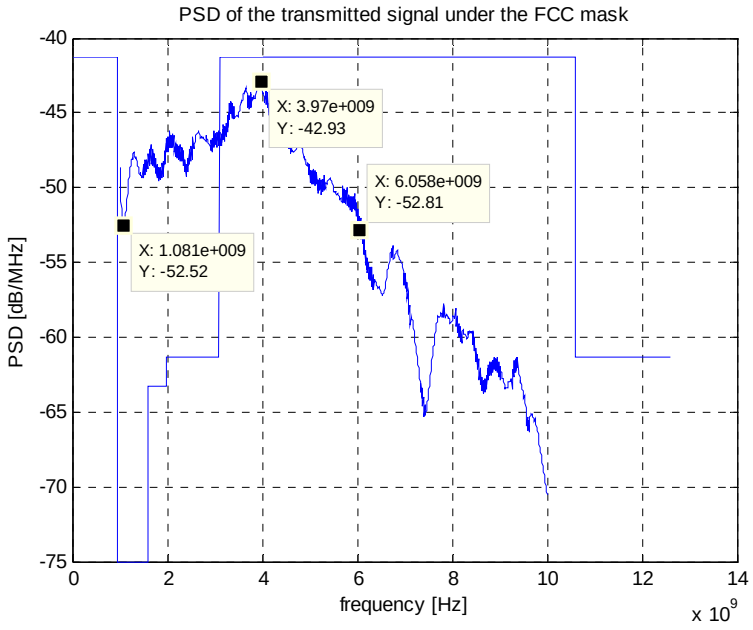

Figure 17. Measured power spectral density of the transmitted signal from Novelda R2A under the FCC UWB outdoor mask;
shown on the plot are the peak power and the -10 dB points.

Full Bandwidth Peak Power

The full bandwidth peak power is limited by the FCC to the value calculated using equation 13. The PRF for Novelda R2A was set to its maximum at 100 MHz and the spectrum analyzer RBW was 1 MHz. The maximum allowed peak power is then calculated as $-7.27dBm$. From the collected PSD, the measured peak power, P_{peak}^{m} = -42.93 dBm. The actual peak power of the measured signal was calculated using equation 14, and found to be

$P_{peak} = -42.93 + 33.98 = -8.95\ dBm.$

Therefore, the peak power of the transmit signal is less than the maximum peak power of -7.27 dBm set by the FCC.

CHAPTER 4

UWB RADAR ANTENNA REQUIREMENTS

Due to the very low transmit power spectral density of the UWB signals, high radiation efficiency of the antenna is a must. As a consequence, all forms of losses, including dielectric and return losses, must be kept low. In addition to the return loss, the other parameters presented in the previous chapter are considered in the process of designing the antenna. Due to the wideband nature of the signal, it is important to have the antenna parameters as independent of frequency as possible. To avoid deformation of the pulse shape the antenna efficiency, VSWR, and gain pattern are desired to be frequency-independent in the UWB range.

The primary goal of this project is to achieve a radar UWB antenna designs for the specific snow measurements applications. The antennas are to operate in the 3-6 GHz UWB bandwidth occupied by the Time Domain Pulse ON 220 signal and in the 1-6 GHz UWB bandwidth occupied by the Novelda R2A signal. The applications include stationary and mobile measurement devices; therefore a physically compact design is preferred. Several geometries will be evaluated and presented, considering tradeoffs between each design. Physical profile, ease of manufacturing, efficiency and directivity are to be considered in the designs comparison process. The antenna requirements for the Time Domain Pulse ON 220 are summarized in table 1; while the antenna requirements for the Novelda R2A are summarized in table 2.

Table 1. Summary of the UWB Radar Antenna design requirements for the Pulse ON 220 signal.

Operation Bandwidth	3-6 GHz
Radiation Efficiency	High, VSWR< 2:1
Radiation Pattern	Directional
Directivity and Gain	High (>8 dBi)
HPBW	Narrow (< 60°), in the azimuth or elevation plane
Physical profile	-Small, and compact (to enable usage in mobile applications), -Easy to manufacture (e.g. two-dimensional, single layered PCB)

Table 2. Summary of the UWB Radar Antenna design requirements for the Novelda R2A signal.

Operation Bandwidth	1-6 GHz
Radiation Efficiency	High, VSWR< 2:1
Radiation Pattern	Directional
Directivity and Gain	High (>8 dBi)
HPBW	Narrow (< 60°), in the azimuth or elevation plane
Physical profile	-Small, and compact (to enable usage in mobile applications), -Easy to manufacture (e.g. two-dimensional, single layered PCB)

CHAPTER 5

ANTENNA TYPES

Schantz in [10] categorizes UWB antennas into the following four different classes according to their form and function:

Frequency-Independent Antennas

In this category the antenna elements vary in geometry to contribute for the different frequencies in the UWB band. Due to the fact that $\lambda = \frac{c}{f}$, small-scale portions of the antenna account for the high frequencies, while larger-scale portions account for lower frequencies. Examples of antennas that fall into this category include spiral, log periodic, and conical spiral antennas. A log periodic dipole array (LPDA) antenna design is considered in this project and presented in chapter seven.

Small-Element Antennas

These antennas tend to be small and usually omnidirectional in pattern. Some designs, however, have directional radiation patterns like the Vivaldi and the bow tie antennas presented later in chapter seven. Examples of omnidirectional small-element antennas include Lodge's biconical antenna, Master's diamond dipole, and Thomas's circle dipole.

Horn Antennas

A horn antenna is nothing more than a hollow pipe of different cross sections that has been flared to a larger opening. As simple as it sounds, a horn antenna design offers very high gain and relatively narrow beams, but usually at a much higher cost and larger size than most simple antennas. Some variations of the horn antenna are suited for cheaper, mobile designs like the quasi-horn antenna discussed in chapter seven.

Reflector Antennas

Like horn antennas, reflector antennas concentrate energy in a particular direction resulting in a high gain and directive beams. The most popular shapes of reflector antennas are the plane, corner, and parabolic reflectors. The use of corner reflectors for concentrating energy of a planar antenna is discussed in chapter seven.

Discussion

LPDA antennas are desired for their frequency independence and the possibility of manufacturing them in small sizes given the frequency bands used in this project. Vivaldi and bowtie antennas have the advantage of being small in size, but they are hard to match in UWB. The issue of matching these antennas is investigated and solved using microstrip feed methods as explained in chapter seven. Quasi-horn antennas overcome the need for balun or matching circuit but have the disadvantage of being three-dimensional antennas. Each design is presented and investigated independently in chapter seven and the final designs are compared in chapter eight.

CHAPTER 6

DESIGN PROCEDURE AND TOOLS

The design process consists of several steps as follows:

-Problem definition and antenna characterization.

-Design and simulation.

-Building and testing.

-Optimization and prototyping.

-Design evaluation.

Problem Definition and Antenna Characterization

The first step in any design is defining the problem and characterizing the requirements; this was discussed in detail in chapter four. A summary of these requirements is represented in tables 1, 2.

Design and Simulation

Several antenna designs are discussed in the next chapter. The design of an LPDA antenna and a quasi-horn antenna are a slight modification of the previous work of Dwayne Folden, a former MSU graduate student [13]. No simulation was performed for these two designs but rather direct in-lab testing was conducted. In that earlier project, the design constraints described above and summarized in table 1 were explicitly taken into account. For the other new designs, however, a computer simulation was performed for

each antenna before building and testing the models. The simulated designs include a dual elliptically tapered antipodal slot antenna (Vivaldi) and a slotline-fed bowtie horn antenna. After reviewing references and scientific papers on the candidate antenna designs, initial designs were modeled and simulated for impedance matching, return loss, and VSWR. The Simulation process was important because the largest part of the design optimization was done in this phase. Before building the antennas, modifications were applied to their designs based on the simulation results. Several Electronic Design Automation (EDA) tools and Finite Element Method (FEM) solvers were tried in the process of simulating the antenna design performance. Following, is a list of these programs and how the simulation software was selected for this project:

Computer Simulation Technology (CST) (version 2009.02) was first used to simulate the Vivaldi antenna performance. The *transient* solver component of the program provided the *S* parameters of the antenna, but at the high cost of lengthy simulation runs. Moreover, the *integral equation solver* component was not available due to a license limitation in the version available at MSU-Bozeman. For these reasons, CST was eliminated as a simulation environment for the designs. Zeland (version 3.71) and Antenna Measurement Studio (version 5.5) software did not provide flexibility in importing external drawings needed for the advanced optimization of the designs.

HFSS from Ansoft (Ansoft Designer Student Version 2.2.0) allowed the importing and building of the design in the simulation environment but did not support the simulation of such large structures in the academic version of the software.

Advanced Design System (ADS) (Version 350.500) -an EDA software system produced by Agilent- provided the capability of importing complicated structures and simulating its electromagnetic behavior as an antenna. Details on the simulation of each design are presented in the next chapter.

Building and Testing

Building

The different antenna designs in this thesis are planar designs with addition of copper flares in some of the designs. In the initial design phase before final prototyping, the antennas were built at MSU-Bozeman using the tools available in the stock room in the ECE department. The LPKF's ProtoMat machine was suitable for building the single-layered Printed Circuit Boards (PCB) of the antennas, shown in figure 18. For simplicity and ease of manufacturing, the designs were optimized to have the strip line widths, transmission line widths, and vias diameters in the order of 0.25 mm or larger. The ProtoMat LPKF machine had the capability of cutting and drilling the PCBs in this resolution range with acceptable tolerance.

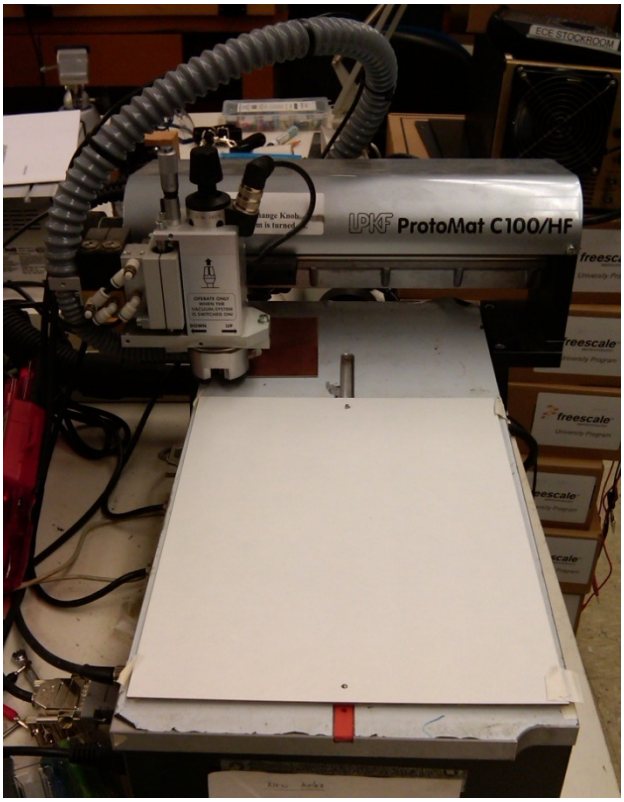

Figure 18. LPKF ProtoMat PCB prototyping machine.

Some of the designs included copper parts that needed to be cut and shaped before being attached to the PCBs of the antennas. Several tools were used in building the copper parts including, a stomp shear, a corner notch, and a finger break shown in figure 19.

Figure 19. Stomp shear (top left), corner notch (top right), finger break (bottom) machines at the stock room in the ECE department.

Testing

After building each antenna, several tests were performed. The testing includes measuring the return loss, VSWR, absolute gain, and HPBW. Based on the results of these tests, the design was optimized – when needed- for better performance. Return loss and VSWR were measured using the HP 8720D network analyzer shown in figure 20. This network analyzer has a frequency range of 50 MHz to 20 GHz which covers the entire UWB bandwidth. With the variety of formats available directly on the network

analyzer, the task of switching between magnitude and phase measure of losses and VSWR is easy. Results of each measurement were stored on a floppy disk for further processing. An important step before using the network analyzer for measuring the return loss was calibration. The HP 8720D network analyzer is easily calibrated using the calibration kit and the calibration function available in the device's main menu. An S11 calibration was performed in the range from 3 to 11 GHz and the antenna was then connected to Port1 of the network analyzer for measuring S11.The number of points measured with the HP 8720D was limited to 201 points corresponding to a resolution of 40 MHz when measuring from 3 to 11 GHz. The collected data was further processed in Matlab for VSWR values. Figure 21 shows the block diagram of the process.

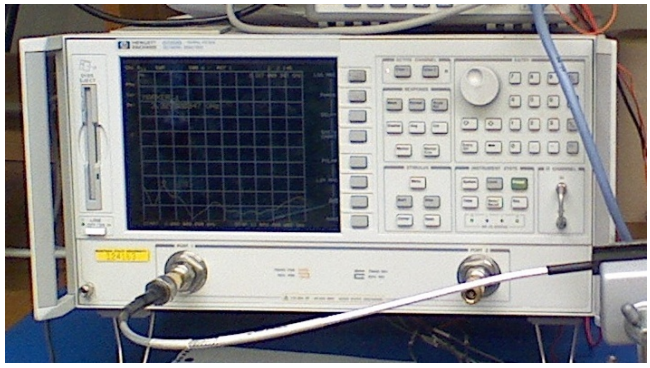

Figure 20. HP 8720D network analyzer.

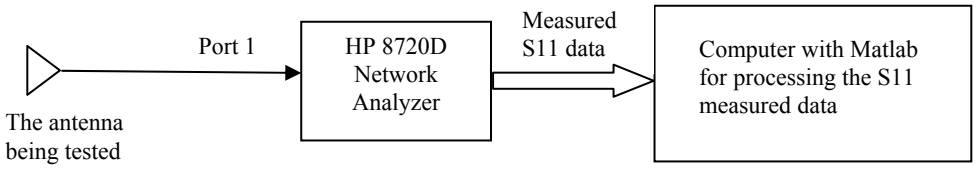

Figure 21. Antenna return loss measurement block diagram.

Absolute gain and HPBW were measured using the automated antenna test facility in the communications lab in the ECE department at MSU-Bozeman. The facility is designed for the general testing of antenna parameters. With the components that cover a wide range of frequencies, the testing of UWB antennas was possible. The facility consists mainly of:

- An Anritsu 68369A/ NV signal generator. That generator produces a nearly linear power level over the range from 10 MHz to 60GHz, shown in figure 22.
- An HRN-0118 TDK horn antenna attached to the signal generator serving as a reference transmitter. The horn antenna generates a high gain over the range of frequencies from 1 GHz to 18 GHz. The calibrated values of the gain from the horn antenna were used to calculate the gain of the receiver antenna under test.
- An Advantest R3273 spectrum analyzer covering from 100 MHz to 26.5 GHz, shown in figure 22. The spectrum analyzer was used to measure the power received by the antenna being tested. The received power values were then processed for absolute gain and HPBW.
- The tested antenna, along with the reference horn antenna, were placed in an anechoic chamber to eliminate any secondary reflections, as show in figure 23. The anechoic chamber is lined with absorbent foam designed and cut in a pyramidal shape to encounter for a wide range of frequencies including those in the UWB bandwidth. Furthermore, a stepper motor underneath the chamber provided a controlled rotational movement to the antenna being tested.

- The signal generator, network analyzer and the stepper motor were connected to a computer and controlled through a LabVIEW program. Programs built in LabVIEW were in the form of Virtual Instruments (VI's). The VI for this test environment was built by former graduate students at MSU-Bozeman, and modified for better data storage and handling for further processing. LabVIEW was used for the ability of creating a Graphical User Interface (GUI) that are easy to edit without the need of rewriting large number of lines of codes. In addition LabVIEW communicates easily with the equipments attached to the computer without a lot of effort. LabVIEW uses Matlab for its mathematical computations, which makes further processing of the data in Matlab an easy task. The two important GUI components of this VI are shown in figure 24, for more details on the facility refer to [12]. The frequency span and scan step were adjustable in the windows shown in figure 24. A proper value for the frequency span was set at 100 MHz and the scan step is 5 degrees resulting in 72 locations in the 360 degrees full range. A block diagram of the entire automated test facility is shown in figure 25.

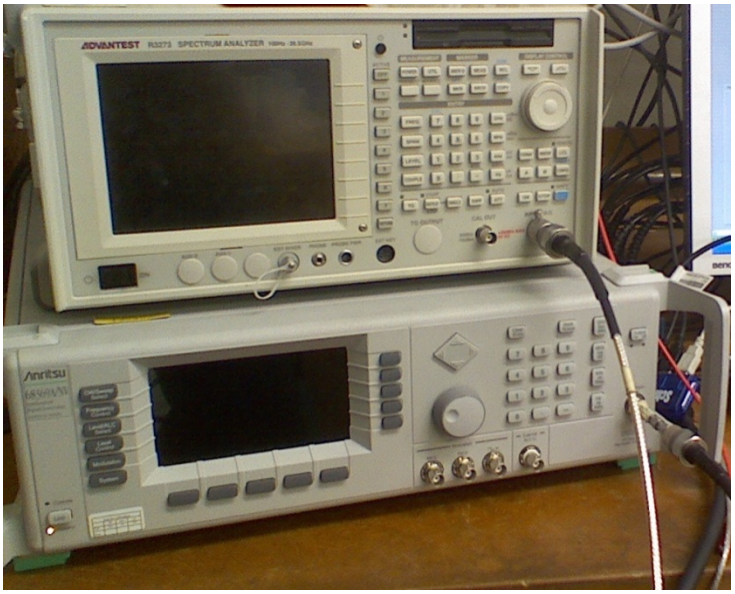

Figure 22. Advantest R3273 spectrum analyzer (top) connecting to the antenna being tested, Anritsu 68369A/NV Signal generator (bottom) connecting to the reference horn antenna.

Figure 23. The anechoic chamber (left) used for testing antennas eliminating secondary reflections, and the interior of the anechoic chamber (right) containing the horn antenna on the left and the tested antenna on the right

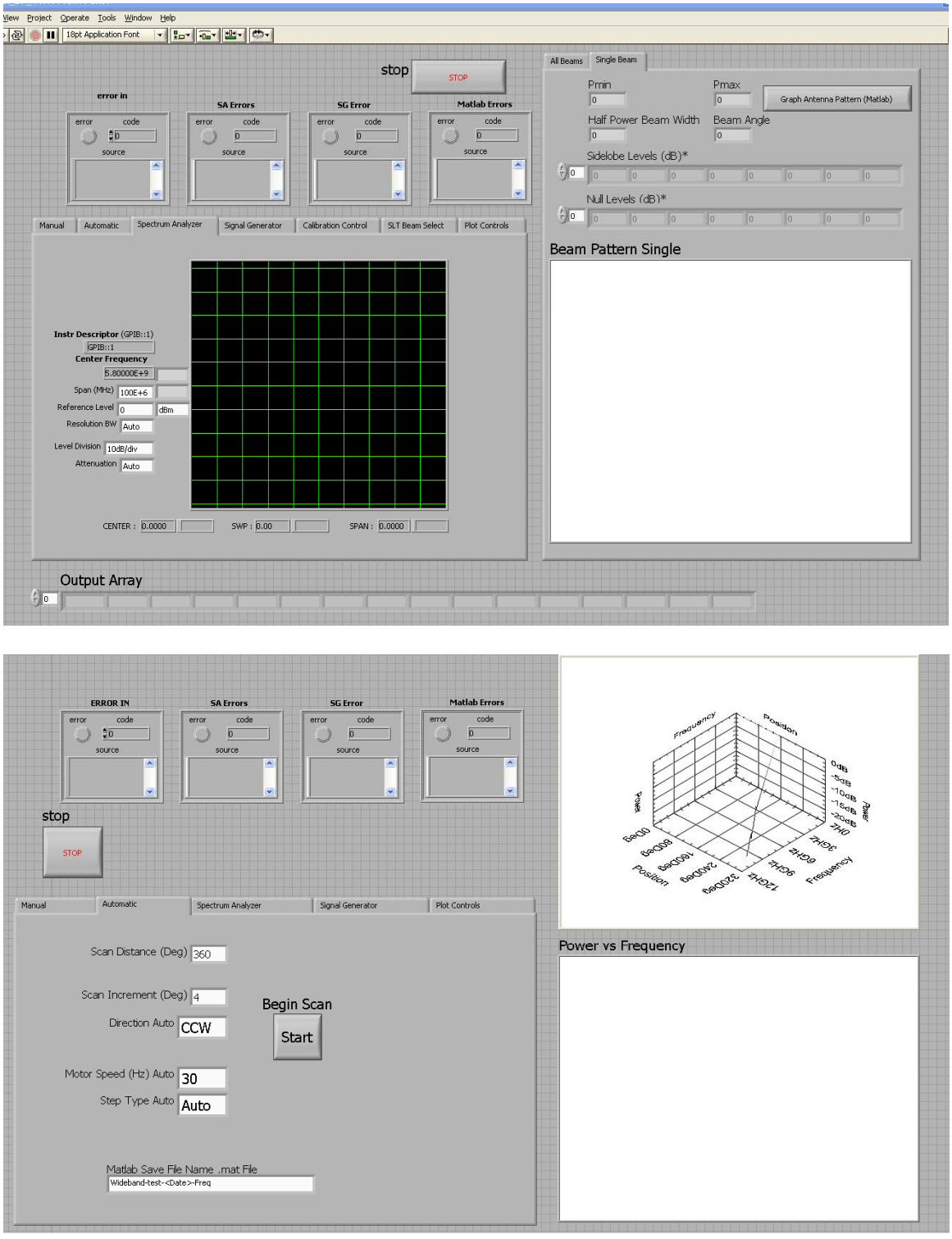

Figure 24. The automated antenna test LabVIEW's VI components:
the GUI control for the signal generator (top), and the stepper motor (bottom).

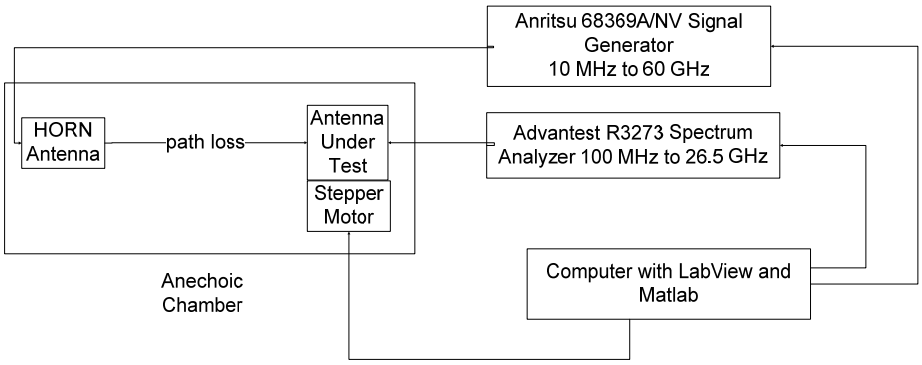

Figure 25. Automated antenna test facility block diagram.

Optimization and Prototyping

The optimization process leading to the prototype of each antenna design was an iterative process. Each modification in the design was based on the results of the simulation first and then the in-lab testing when needed. The simulation gave a very clear picture of the return loss and VSWR values. The design was then optimized for the lowest losses before the process of building and testing. The antenna was then tested using the network analyzer for return loss and VSWR and modified noticing the changes immediately on the network analyzer's screen. Finally, the antenna was tested in the anechoic chamber using the automated antenna testing system described in the previous section. Recorded data from the test were then processed using a Matlab-based program for absolute gain and HPBW. The resulting values were then compared to the expected results from the simulation process, and optimization for final prototypes was performed when needed.

Design Evaluation

After a prototype was manufactured and tested, it was evaluated in a software environment, in an in-lab controlled environment, and in a field test. Chapter 9 discusses the evaluation of the final antenna designs in detail.

CHAPTER 7

ANTENNA DESIGN, SIMULATIONS AND RESULTS

In this chapter several antenna designs are presented including a log periodic dipole array (LPDA) antenna, a quasi-horn antenna, a Vivaldi antenna, and a bowtie antenna. The LPDA and quasi-horn antennas were designed by Dwayne Folden, a previous graduate student at MSU-Bozeman [13]. For the LPDA antenna, measurements and test results are presented here. For the quasi-horn antenna, optimization, measurements, and test results are also discussed here. Finally, the design process and results are presented and discussed in details for the Vivaldi and bowtie antennas. The process for each of these two antennas include: design, simulation, building, testing, and optimization. Tradeoffs regarding the UWB required parameters are analyzed for each antenna.

Log Periodic Dipole Array Antenna

As mentioned in chapter four, due to the wideband nature of the UWB signal, it is important to have the antenna parameters as independent of frequency as possible. A type of antenna that closely parallels the frequency independent concept is the log periodic dipole array (LPDA) antenna [14]. LPDA antennas consist of a sequence of side-by-side parallel linear dipoles forming a coplanar array [5]. A famous example of directive LPDA is the Yagi-Uda array. The directivity of an LPDA antenna is related to the parameters σ and τ that are defined by equations 15 and 16 [15]. For this design, σ was set to 0.15 and

τ was set to 0.9. Furthermore the width of the traces was set to four times the radius. The width of the smallest element was arbitrarily set to 1mm, which defines all the widths of the subsequent elements. [13]

$$\tau = \frac{R_{n+1}}{R_n} = \frac{D_{n+1}}{D_n} = \frac{L_{n+1}}{L_n} \quad \text{, see figure 26} \qquad \text{Equation 15}$$

$$\sigma = \frac{1-\tau}{4\tan\alpha} = \frac{D_n}{2L_n} \quad \text{, see figure 26} \qquad \text{Equation 16}$$

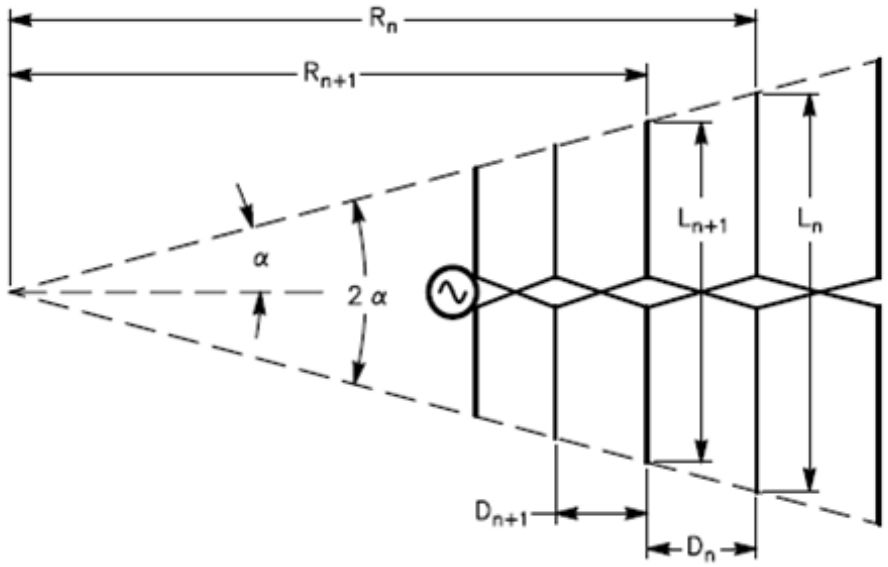

Figure 26. LPDA antenna and its element dimensions.

LPDA antennas are built as wire type antennas or as planar antennas. Our design used a planar structure utilizing stripline technology to create a feed structure that was

matched to 50 Ω. The design also took into account the effects of the dielectric substrate on the antenna design [13]. A pictorial representation of the design is shown in figure 27.

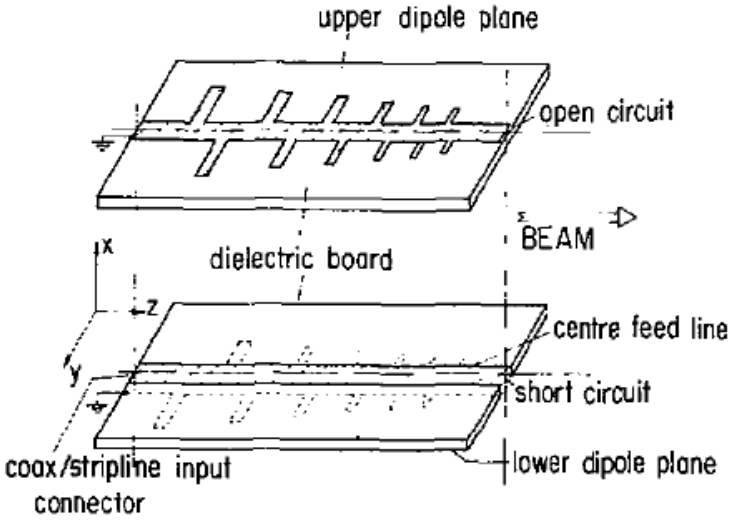

Figure 27. Pictorial representation of the log periodic dipole planar structure [16].

The design was created in PADS as a two-layer board, with one board having only a single layer (the top antenna structure) and one board having two layers (the feed line and the bottom antenna structure). Figure 28 shows the PCB routes of the board layers from the layout program. The top board was designed with two cutout portions. The cutout on the right hand side was used to short the feedline to the top conducting elements as required by the design. The left cutout was used to attach the stripline launch SMA. The alignment holes were used to ensure that there is very little misalignment of the conducting structures. The design was tested following the procedure described in the "Building and Testing" section in Chapter 6. Measurements included VSWR, and absolute gain and HPBW.

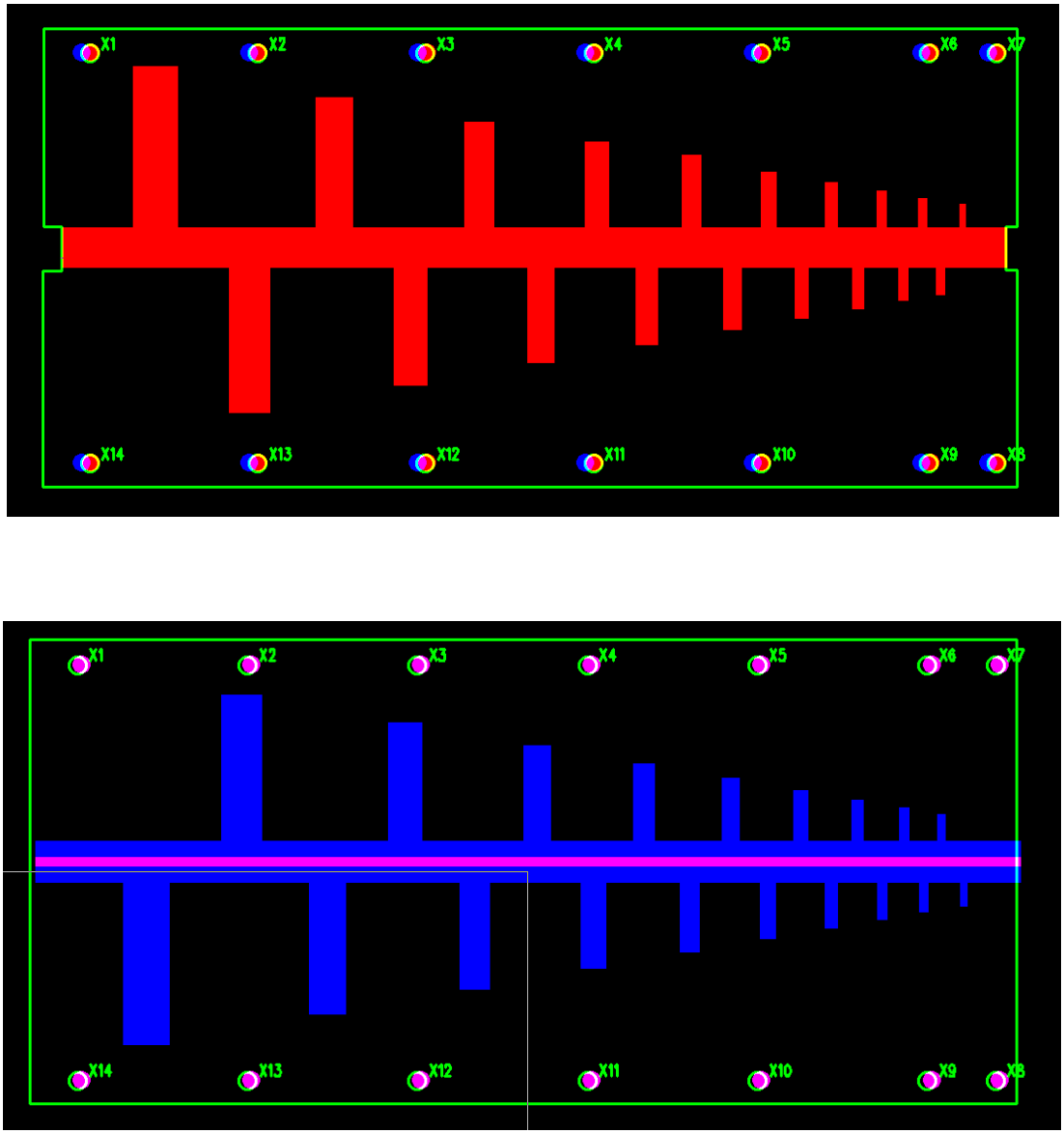

Figure 28. Top conducting elements of LPDA (top),
Bottom conducting structure of LPDA (bottom) [13].

VSWR

The LPDA antenna showed a high return loss for most of the UWB frequency range. The VSWR measurement results for this design is shown in figure 29 and has an average of 2.5:1. A good antenna design should have a VSWR of 2:1 or less.

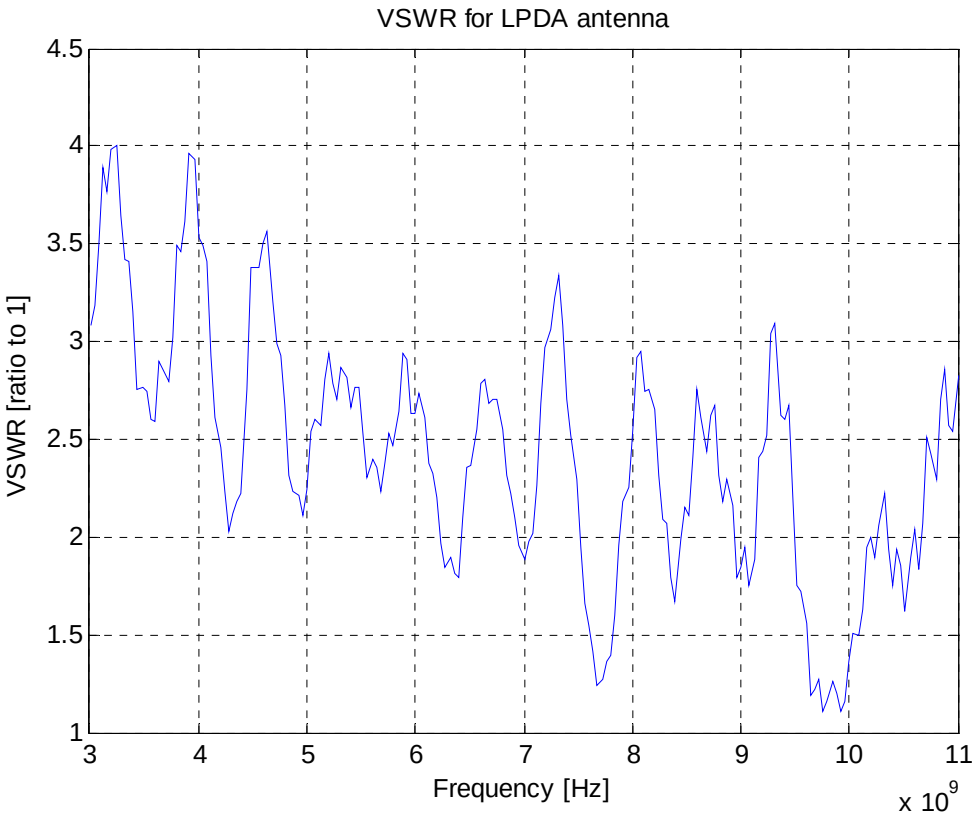

Figure 29. VSWR for the LPDA antenna.

Gain and HPBW

The LPDA antenna showed a linearly dropping boresight gain with the increase of frequency as shown in figure 30. The boresight gain has a maximum value of 10.4 dBi at 4 GHz and drops down to 0 dB at 6 GHz. HPBW, however, has an average of 75 degrees for most of the UWB frequency range as shown in figure 31. While the LPDA has a low gain, it is directive in the frequency band of operation for the Pulse ON 220 radar system. Figure 32 shows the normalized power pattern- in linear scale- for the LPDA antenna at 4.5 GHz- that is the peak frequency for Pulse ON 220. A full set of graphs showing the

normalized power pattern at different frequencies for the LPDA antenna is provided in appendix A.

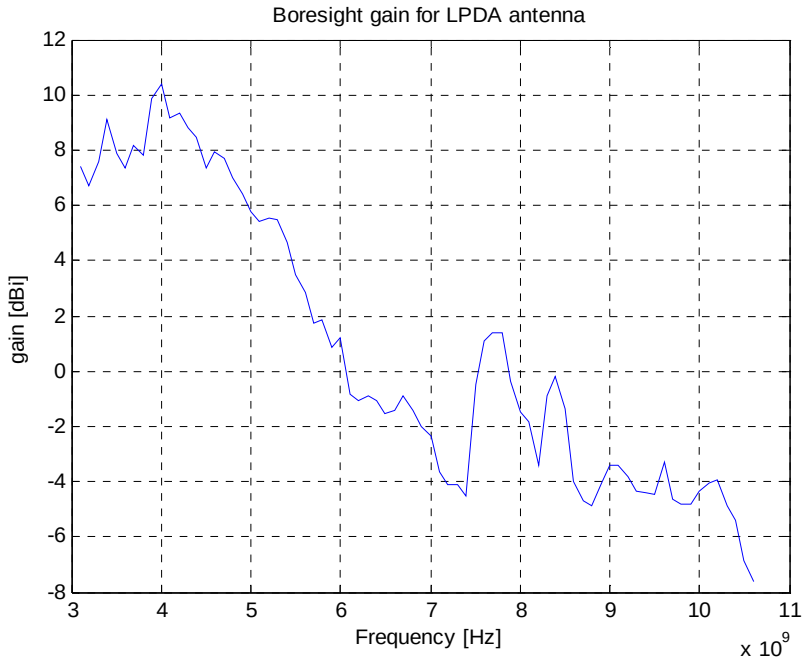

Figure 30. Boresight gain for LPDA antenna.

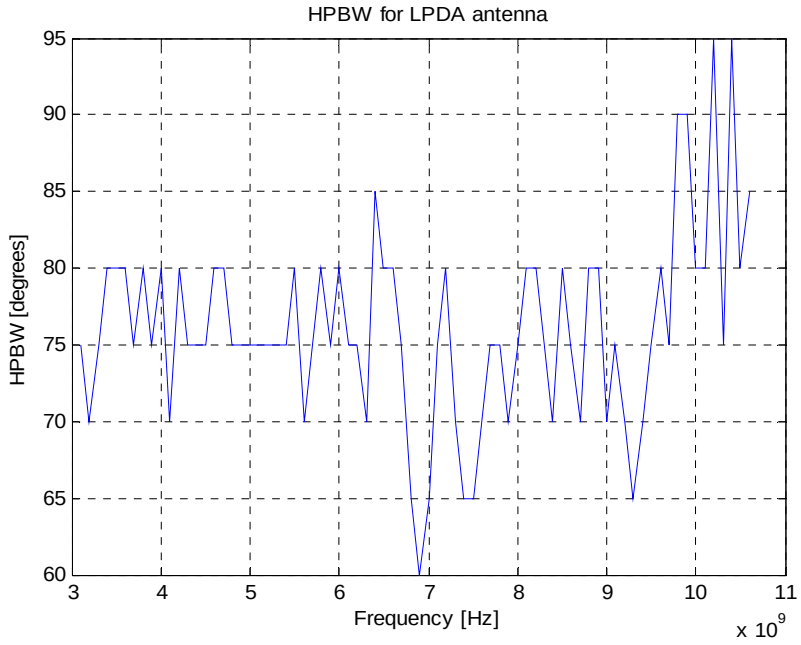

Figure 31. HPBW for LPDA antenna.

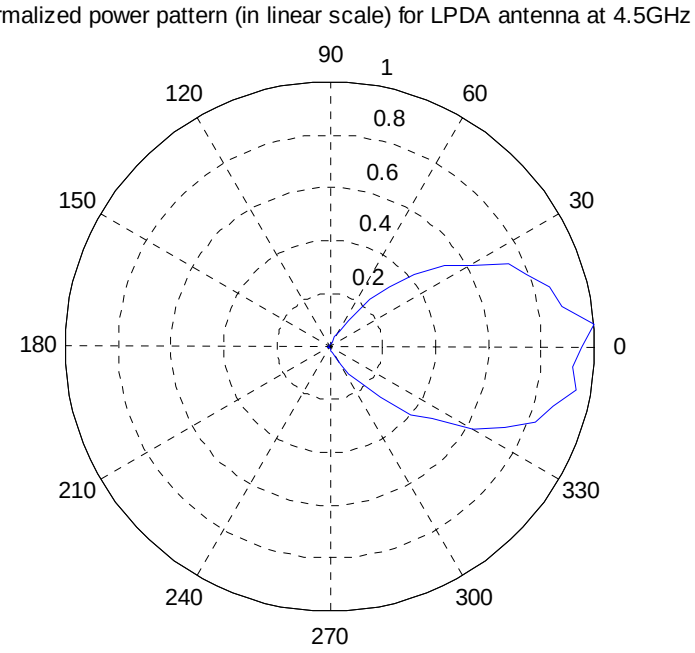

Figure 32. The normalized power pattern (in linear scale)
for the LPDA antenna at 4.5 GHz.

Quasi-Horn Antenna

The quasi-horn antenna is an example of a small, low cost, directive, wideband microstrip antenna. Because of these characteristics, microstrip antennas are very appealing from a system perspective making them an important subject in antenna technology. The basic principle of the UWB microstrip quasi-horn antenna is based on the theory of wave propagation along a transmission line [17]. A balun or transition is not needed at the antenna input. The initial design of the quasi-horn antenna was done by Dwayne Folden [13]. The design of the antenna is shown in figure 33.

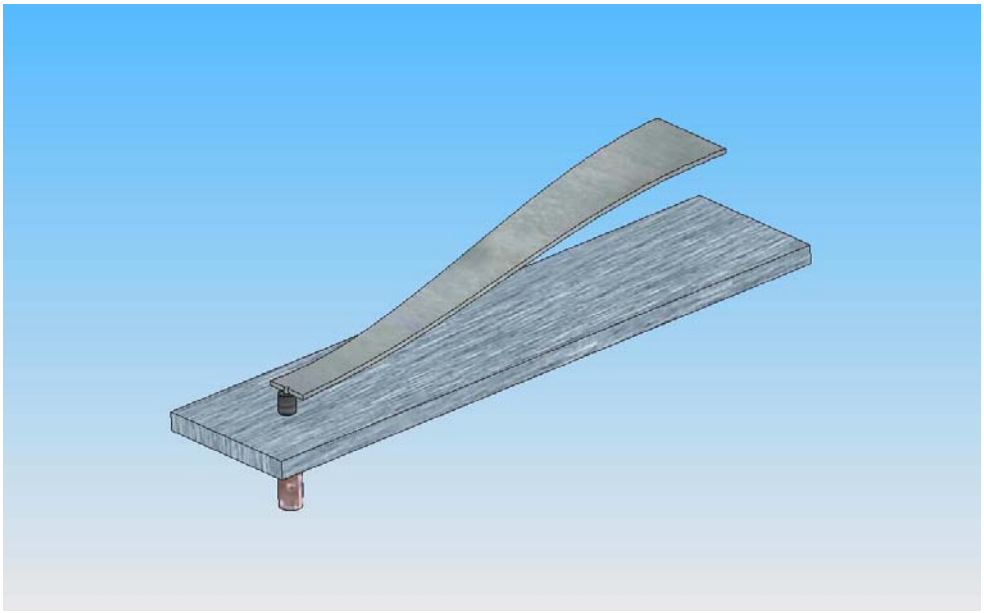

Figure 33. Quasi-horn structure showing ground plane and 50 Ω SMA connection, image captured from SolidWork. [13]

The basic theory behind radiation in quasi-horn antennas is explained by Li and Zhou as follows:

> In the uniform section of the microstrip line, where the separation between the top radiating patch and the ground plane is very small compared to a wavelength, wave propagation is mostly confined within the dielectric between the top radiating patch and the ground plane, the wave is guided between the radiating patch and ground plane. However, as the spacing between the radiating patch and the ground plane gradually increases and approaches approximately one half-wavelength or more, the energy begins to radiate in the end-fire mode, consequently the wave is no longer guided between the radiating patch and the ground plane. The entire structure effectively behaves as an antenna [18].

In the design for UWB systems, the highest frequency is 10.6 GHz resulting in a half-wavelength of less than 14 mm. This value was considered when modifying the quasi-horn antenna design for better performance.

Three modifications were applied to the design. First, the top conductor was adjusted experimentally to reach a low return loss taking into account the limitations on the separation from the bottom ground plane based on the wavelengths in the bandwidth of operation. The second modification was on the feed structure. The original design was fed vertically as shown in figure 33. Feeding the antenna horizontally [19] resulted in better performance when tested for VSWR. Finally, a radar absorber material was used to cover the top conductor yielding improvement in the performance of the input matching and antenna gain [20]. The modified quasi-horn antenna is shown in figure 34. The antenna was tested for VSWR, and absolute gain and HPBW following the procedure described in the "Building and Testing" section in Chapter 6.

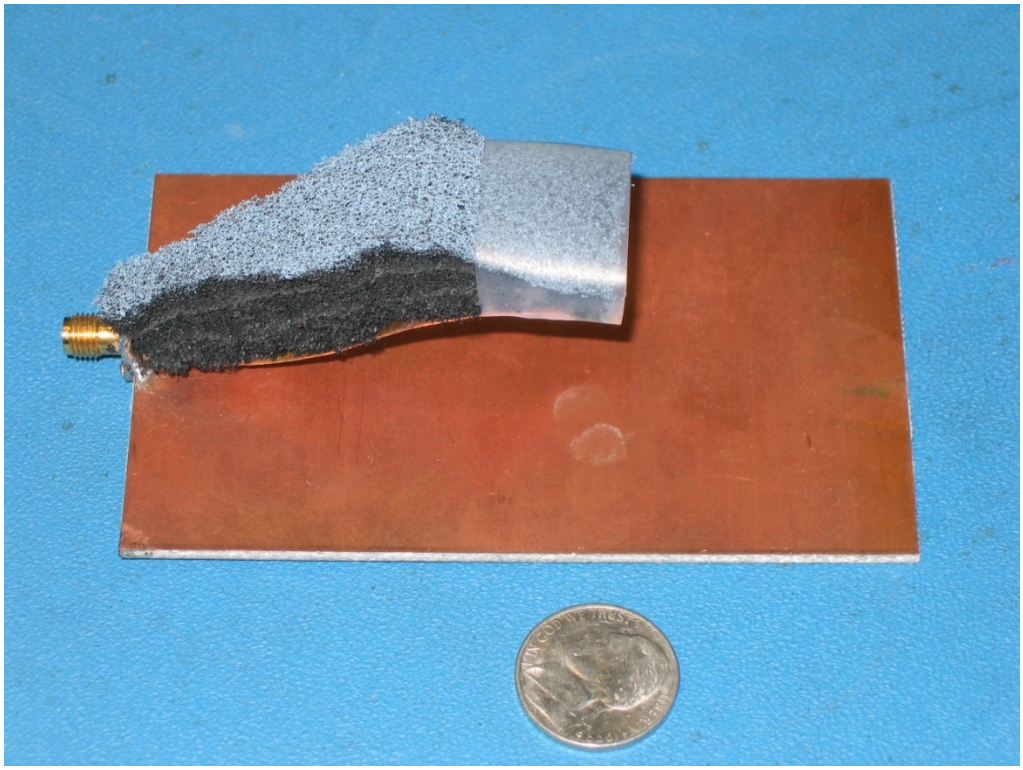

Figure 34. The modified quasi-horn antenna, horizontally fed, and the top conductor is covered with radar absorber material.

VSWR

The quasi-horn antenna –after the modifications described above- showed a low VSWR for most of the UWB range as shown in figure 35. The VSWR is less than 1.6:1 in the 3 to 6 GHz area which makes using the antenna possible with systems like the Pulse ON 220- described in chapter three.

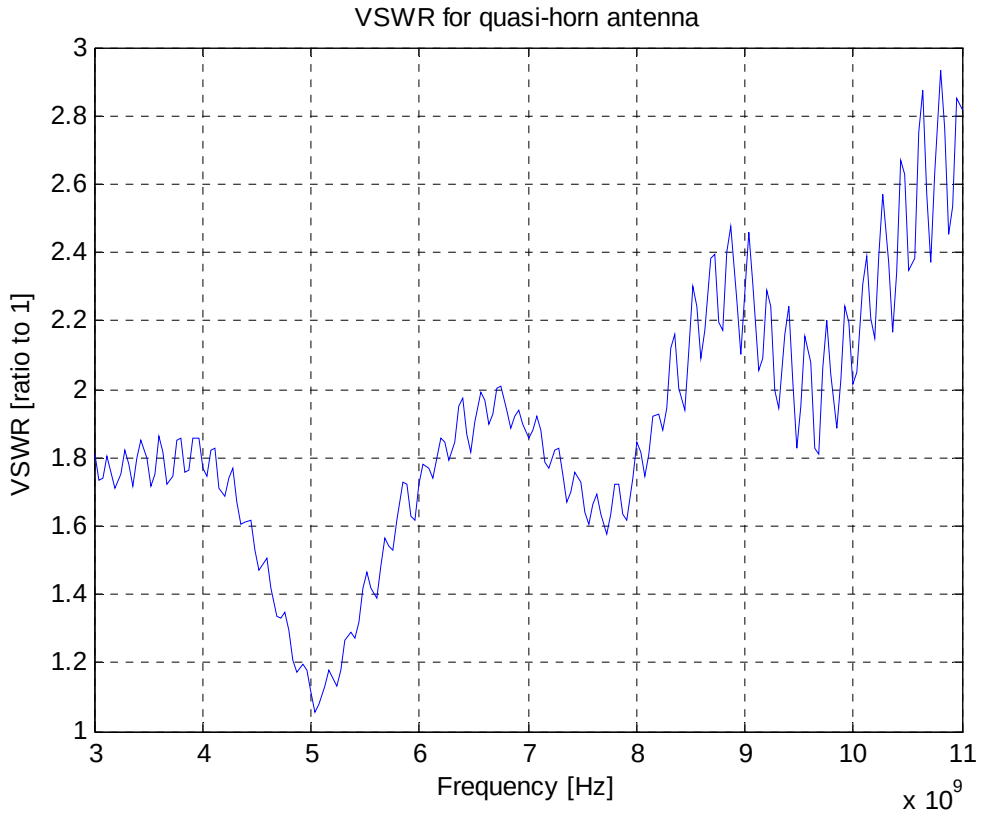

Figure 35. VSWR for the quasi-horn antenna.

Gain and HPBW

The quasi-horn antenna did not give a high boresight gain. The maximum boresight gain is about 5 dBi at 4 GHz and decreases to less than 0 dBi at 6 GHz as shown in figure 36. HPBW was also fluctuating decreasingly from 120 degrees at 3.5

GHz to 65 degrees at 6 GHz as shown in figure 37. Figure 38 shows the normalized power pattern- in linear scale- for the quasi-horn antenna at 4.5 GHz (that is the peak frequency for Pulse ON 220). A full set of graphs showing the normalized power pattern at different frequencies for the quasi-horn antenna is provided in appendix B. Further research on the quasi-horn antenna was terminated at this point and the focus was turned to planar microstrip antennas such as the Vivaldi antenna.

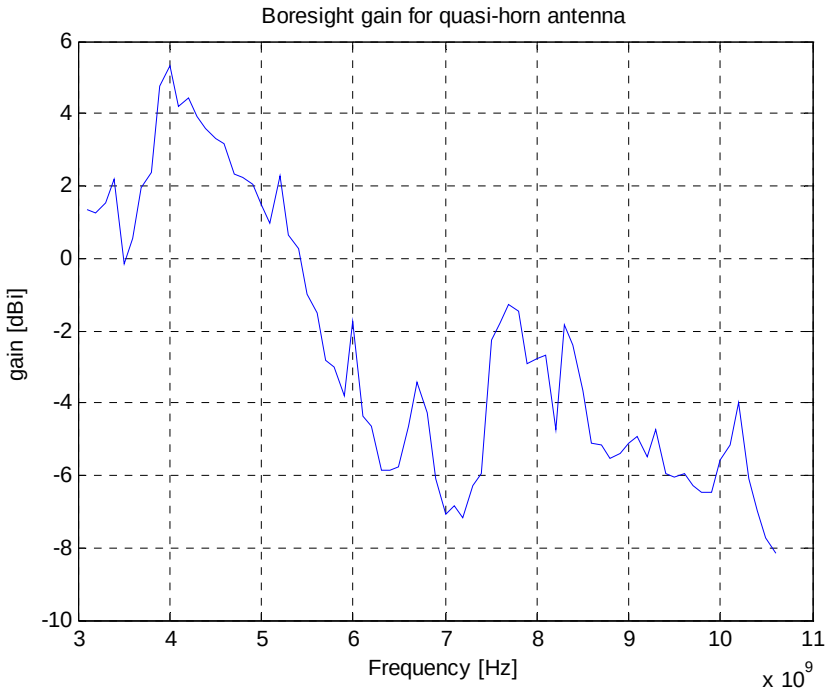

Figure 36. Boresight gain for the quasi-horn antenna.

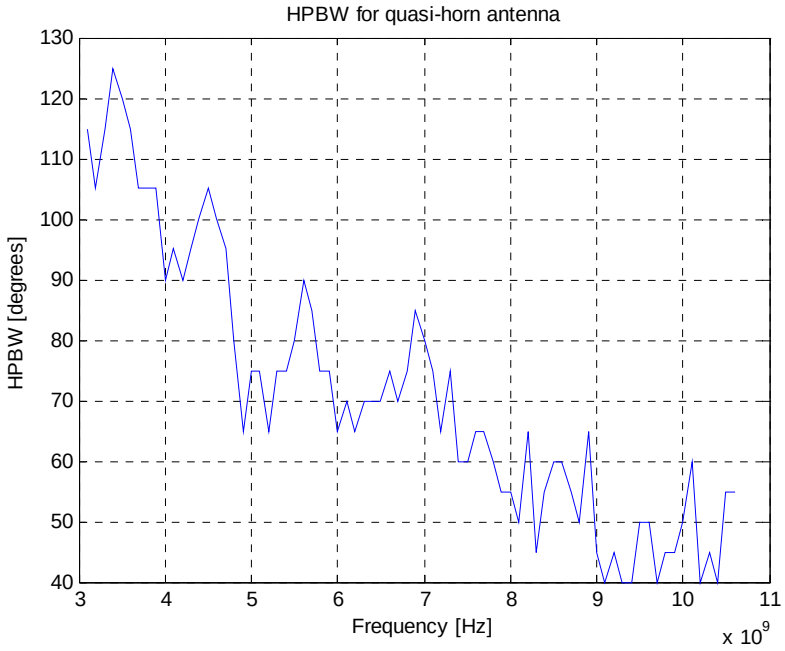

Figure 37. HPBW for the quasi-horn antenna.

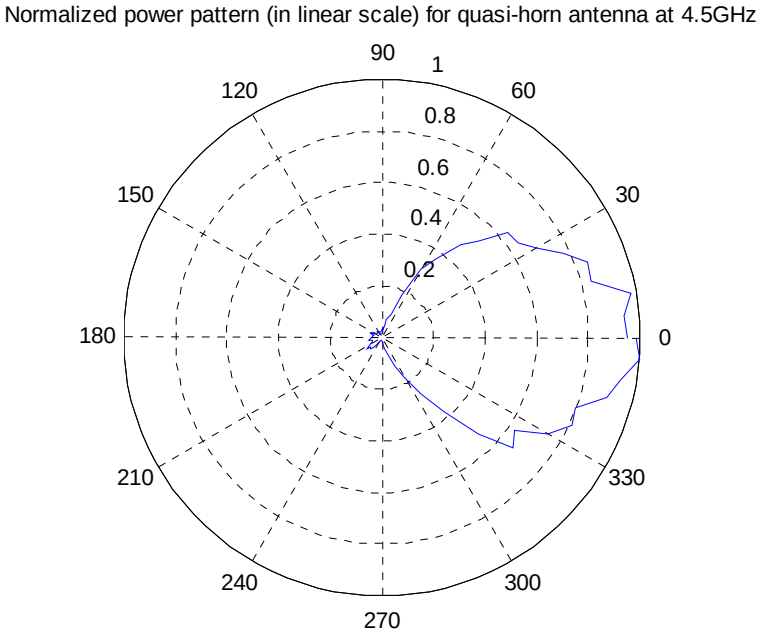

Figure 38. The normalized power pattern (in linear scale)
for the quasi-horn antenna at 4.5 GHz.

PCB Transmission Line Antenna and Corner Reflectors

Printed circuit board (PCB) transmission lines are popular due to their low cost and ease of manufacture. The transition between impedance of a particular transmission line and free space impedance is limited only by properties of the geometry in question and the dielectric constant of the materials used. For these reasons low-cost efficient antennas have been built in forms of striplines, microstrip, and slot lines on PCBs. Many of these antennas rely on tapered PCB transmission lines to achieve broadband matches [10]. The most famous form of planar transmission line antennas involves a transition from a microstrip transmission line to a slot transmission line. The Time Domain's Pulse ON 200 is an example of a bottom-fed elliptical dipole antenna that features a microstrip-to-dual-notch transition, shown in figure 39. Pulse ON 200 is matched to the UWB frequencies and has the VSWR measured in figure 40, on the other hand the boresight gain was as low as 1 dBi below 8 GHz due to the omni-directional nature of the antenna pattern. The boresight gain of the antenna was measured at MSU-Bozeman and is shown in figure 41.

Figure 39. Pulse ON 200 UWB antenna features a microstrip-to-dual-notch transition.

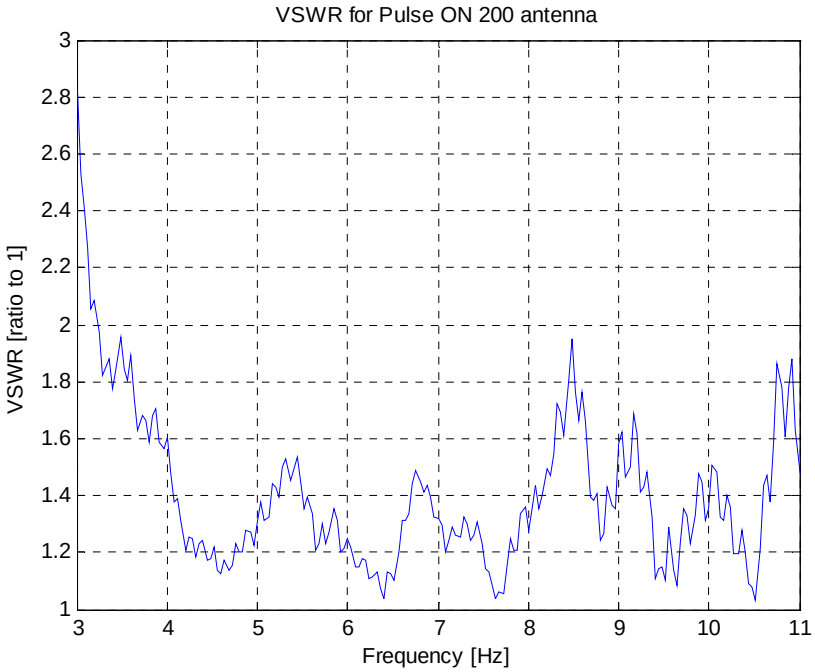

Figure 40. VSWR for Pulse ON 200 UWB antenna.

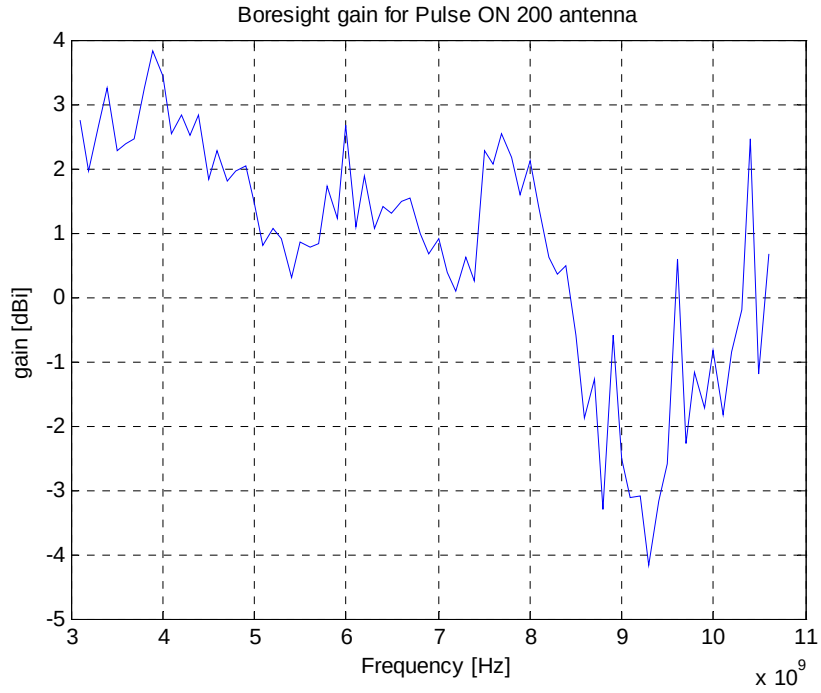

Figure 41. Boresight gain for Pulse ON 200 UWB antenna.

While the Pulse ON 200 antenna has a near-perfect impedance match in the UWB range, it does not provide the directivity required for radar applications. To increase the directivity of the antenna, corner reflectors are used to direct the antenna radiation. A corner reflector offers a more directional, higher gain system than using a typical planar reflector [10]. The antenna is placed at a distance d from the corner of a 90° corner reflector as shown in figure 42. Schantz finds the boresight gain to be maximized for $d = 0.38\lambda_c$ [10]. For $\lambda_c = 80\ mm$ in the UWB range, d= 30.4 millimeters. A 90° corner reflector of copper is added to the Pulse ON 200 antenna tested in the previous section and the configuration is shown in figure 43.

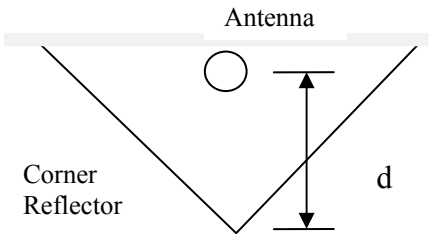

Figure 42. Antenna placed a distance d from a corner of a 90° corner reflector.

Figure 43. A 90° corner reflector of copper is added to the Pulse ON 200 antenna.

The addition of the corner reflector resulted in an average HPBW of 65 degrees below 9.5 GHz as opposed to omni-directional pattern without the reflectors. Figure 44 shows the normalized power pattern (in linear scale) for both the Pulse ON 220 antenna, and the Pulse ON 220 antenna with corner reflectors at 4.5 GHz. The measured HPBW is shown in figure 45. Appendix C provides the normalized power pattern at different frequencies for the Pulse ON 220 antenna with reflector. As a result of adding the corner reflector, the boresight gain of the new system is higher by up to 5 dBi in the 3-6 GHz area, which is the operational BW for the Pulse ON 220 radar system, as shown in figure 46. As expected when adding copper reflectors, the VSWR of the new system increased above its original value as shown in figure 47.

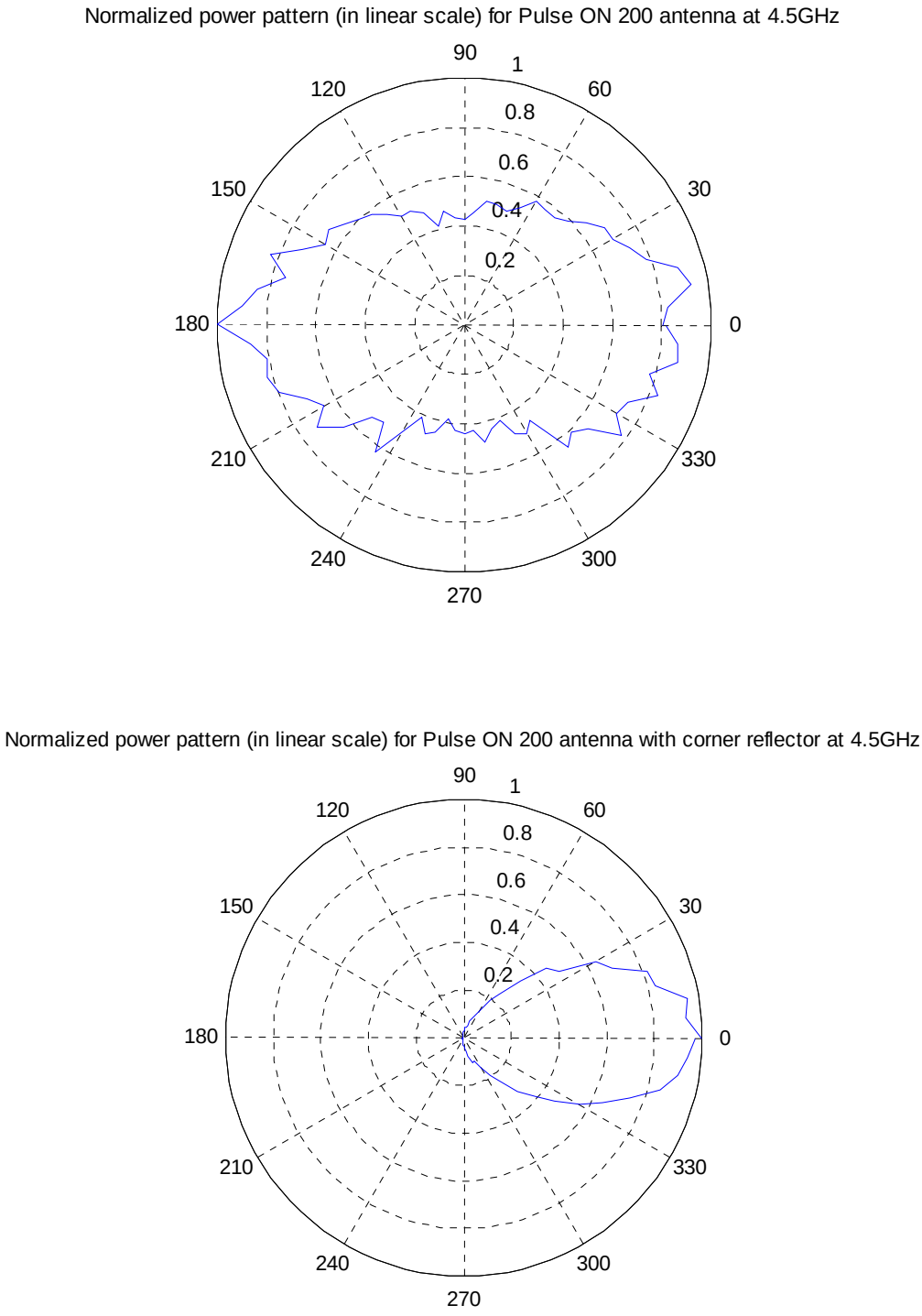

Figure 44. The normalized power pattern (in linear scale) for the Pulse ON 220 antenna (top), and the Pulse ON 220 antenna with corner reflectors at 4.5 GHz (bottom).

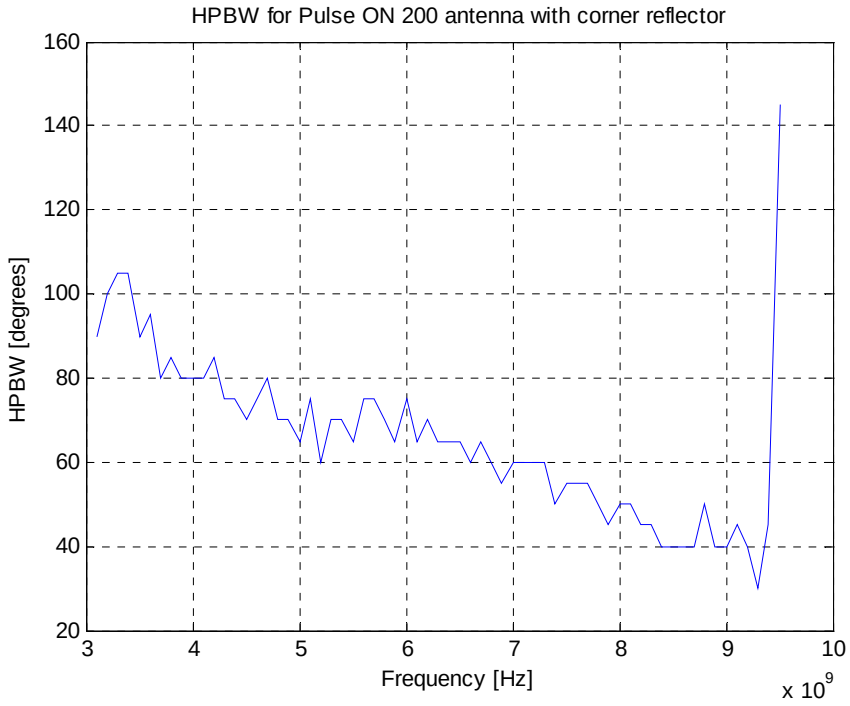

Figure 45. HPBW for Pulse ON 200 UWB antenna with corner reflector.

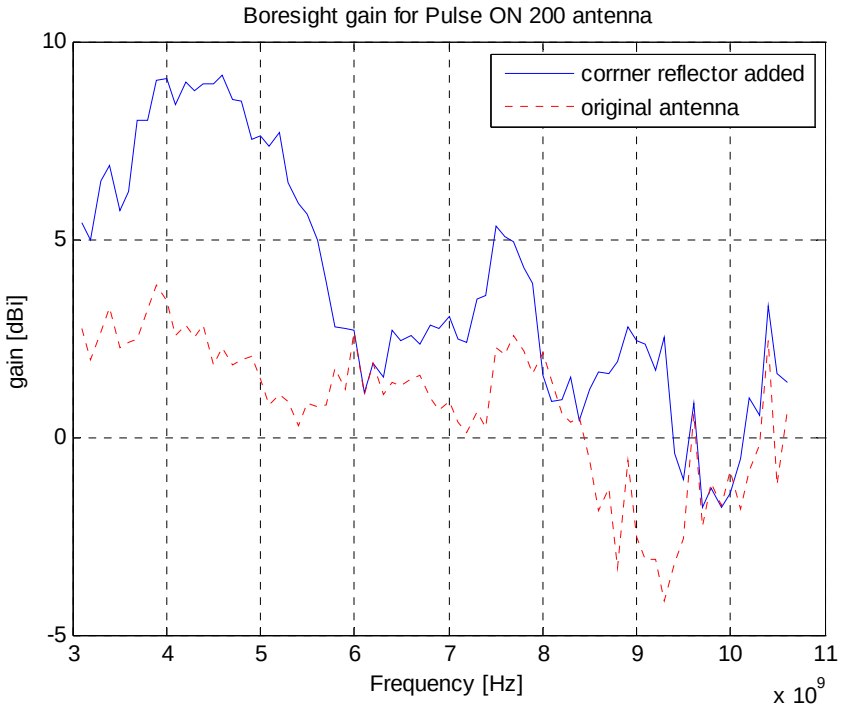

Figure 46. Boresight gain for Pulse ON 200 UWB antenna with corner reflector compared to the original antenna.

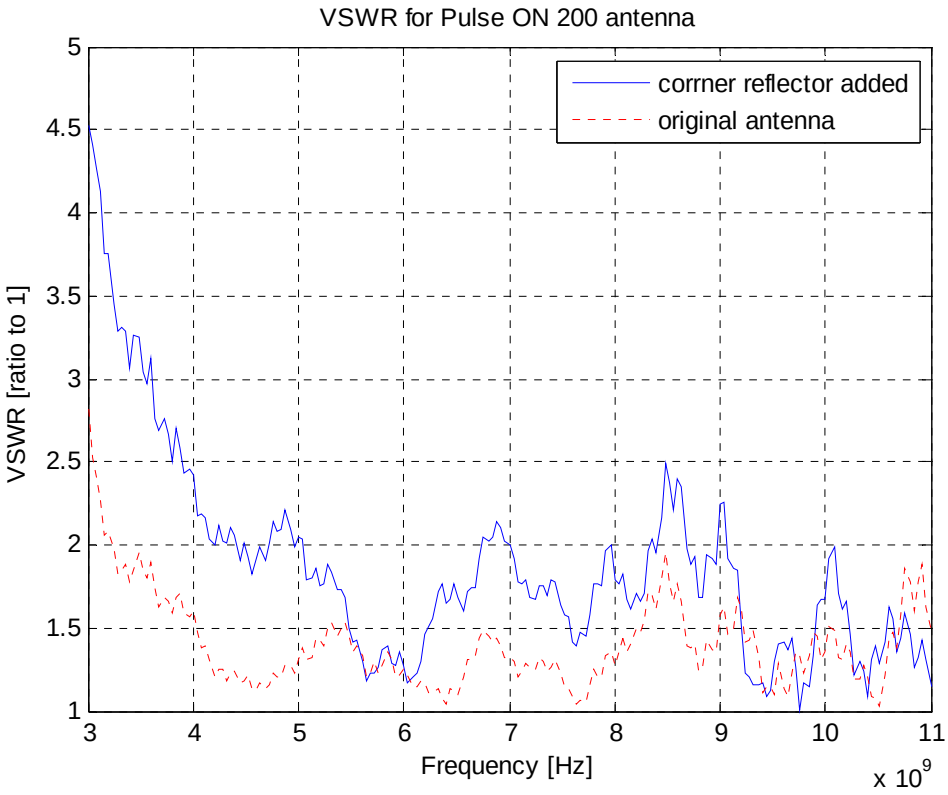

Figure 47. VSWR for Pulse ON 200 UWB antenna with corner reflector compared to the original antenna.

Vivaldi Antenna

Vivaldi antenna is a two-dimensional slot antenna. The design of a Vivaldi antenna involves a gradual transition from a microstrip transmission line to a slot transmission line that then flares out to form horn-type radiating elements. Planar horn antennas offer high gain in a simple, low-cost structure [10]. A Vivaldi antenna is:

> Formed by elliptically tapering the inner and outer edges of the slot line conductors of the antipodal Vivaldi radiator. ……..The antipodal Vivaldi antenna comprises tapered radiating slot and feeding transition. The symmetric tapered radiating slot is formed by two arms printed on opposite surfaces of a dielectric substrate. The feeding transition consists of a 50 Ω microstrip line linearly tapered to a parallel strip line to feed the tapered slot radiator, whereas the ground trace is elliptically tapered [3].

Figure 48 shows a three-dimensional view of the Vivaldi antenna.

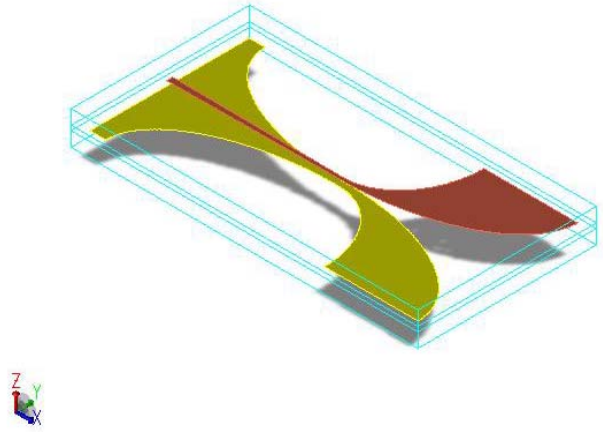

Figure 48. A three-dimensional view of a Vivaldi antenna simulated in ADS.

Planar Vivaldi antennas have been used in radar-like communications since 1979 [21]. UWB communications studies have shown that Vivaldi antennas can preserve the shape of transmitted UWB pulses [22]. The performance of the Vivaldi antennas, however, is limited by the need for a wideband balun. A type of Vivaldi antenna, known as the antipodal Vivaldi antenna, has been developed that overcame this problem by enabling a simple microstrip feed method. Several papers have been written on the design of antipodal Vivaldi antennas. The designs in some of these papers are inspected, simulated, tested, and optimized in this project for optimum performance in the desired frequency band of operation.

Design and Simulation

The physical characteristics of the Vivaldi antenna that affect its operation are defined by its dimensions in both the tapered slotline radiator and the feed line transition, shown in figure 49. The critical dimensions in the feed line transition section are the line

width W_s and the board height h. According to Brzezina [22], the ratio between the microstrip width and the board height (or thickness) is given by equation 17.

$$\frac{W_s}{h} = \frac{8e^A}{e^{2A}-2} \qquad \text{Equation 17}$$

where $$A = \frac{Z_0}{60}\sqrt{\frac{\varepsilon_r+1}{2}} + \frac{\varepsilon_r-1}{\varepsilon_r+1}\left(0.23+\frac{0.11}{\varepsilon_r}\right).$$

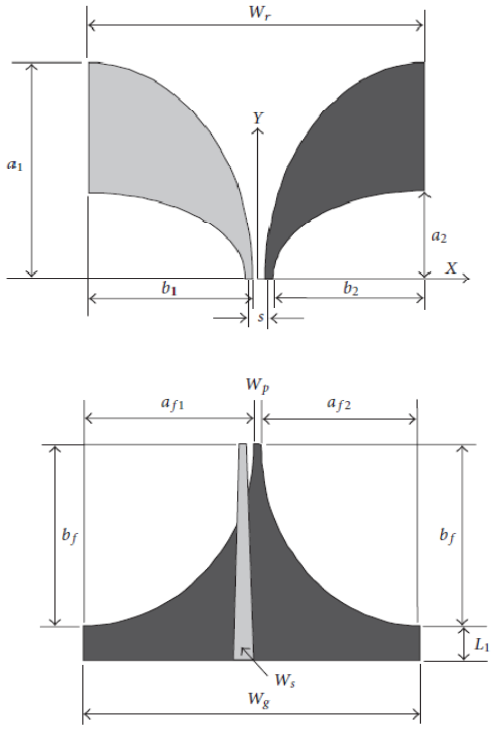

Figure 49. The tapered slotline radiator (top), and the feed line transition (bottom) of antipodal Vivaldi antenna [23].

In the tapered slotline radiator section of the Vivaldi antenna, the critical dimension is the width W_r which is defined by the highest frequency f_H as shown in equation 18 [24].

$$W_r < \frac{c}{f_H\sqrt{\varepsilon}}$$ Equation 18

The substrate materials used in this project were FR4 which has an ε_r= 4.5-j0.001 and thickness of 1.588 millimeters, and RO4003 with ε_r= 3.38-j0.002 and thickness of 0.813 millimeters. The antenna was simulated first using the dimensions in [23], shown in table 3, see figure 49, following the procedure in the "Design and simulation" section of chapter 6. The resulting VSWRs for the two substrate materials are shown in figure 50.

Table 3. Initial dimensions for the Vivaldi antenna
(all dimensions in mm).

a_1	b_1	a_2	b_2	W_g	W_s	W_p	a_{f1}	a_{f2}	*S*	*bf*
50	25	20	24	51	1.86	1.0	26	24	0.5	25

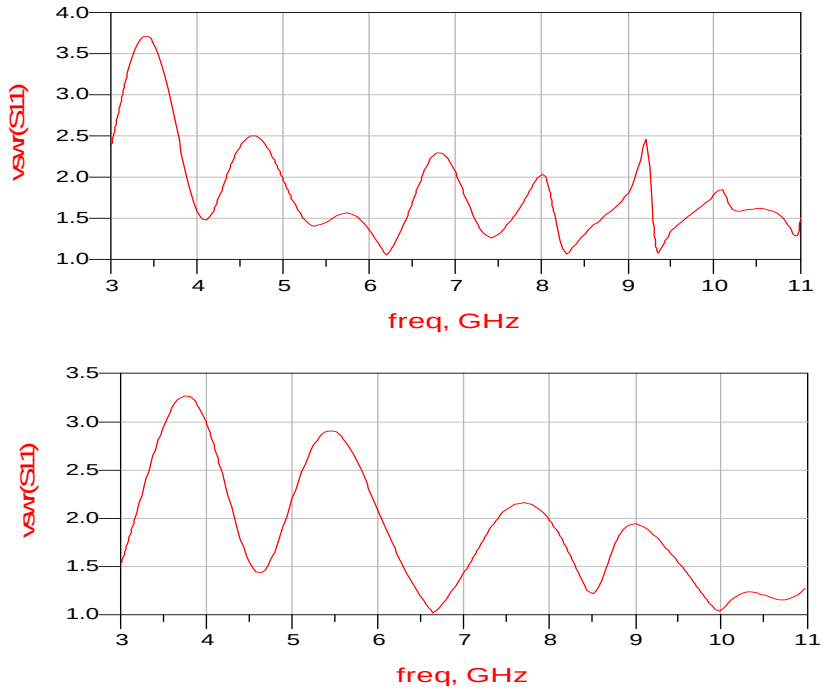

Figure 50. VSWR simulation results for the Vivaldi antenna built with dimensions in table2 on FR4 (top), and RO4003 (bottom).

By decreasing the gap *S* to 0 mm instead of 0.5 millimeters, a slight improvement was achieved in the simulation results of VSWR for the antenna built using RO4003 substrate, as shown in figure 51.

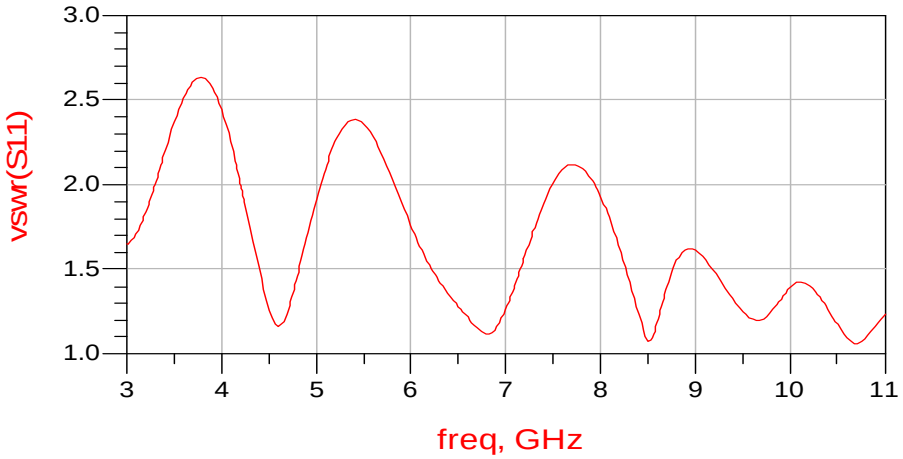

Figure 51. VSWR simulation results for the Vivaldi antenna built with S= 0 mm on FR4.

Finally, the length *bf* in the feed structure was increased to 50 millimeters and the resulting VSWRs had lower values and stayed under 2:1 for most of the desired frequency range. The VSWRs graphs for the designs with longer feeds are shown in figure 52. As explained in chapter 6, correct radiation patterns were not obtainable from the simulation programs used in this project, therefore the radiation patterns are discussed in the next section “Building and Testing”.

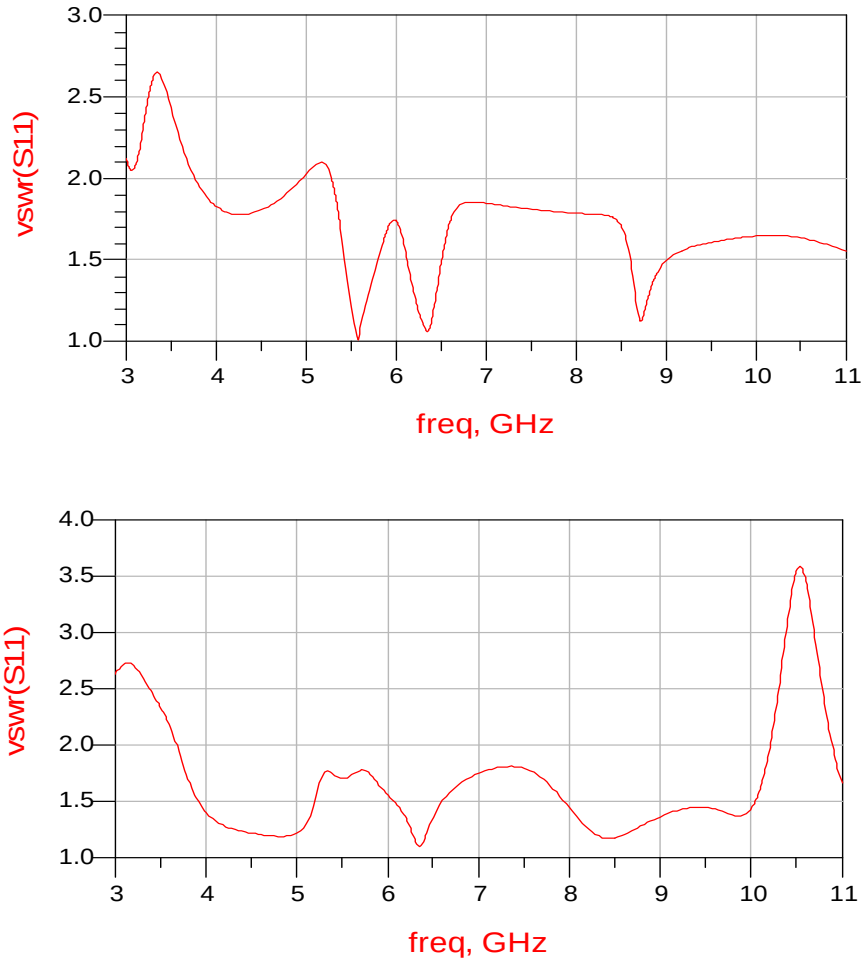

Figure 52. VSWR simulation results for the Vivaldi antenna built with Longer feed structure on FR4 (top), and RO4003 (bottom).

Building and Testing

The antipodal Vivaldi antenna with the long feed structure simulated above was built and tested at MSU-Bozeman as described in chapter 6. The measured VSWR for the antenna built on an FR4 substrate was similar to the simulated values except for a high peak at 3.3 GHz as shown in figure 53. The antenna built on RO4003 had more peaks than expected from the simulation in the measured VSWR as seen in figure 54.

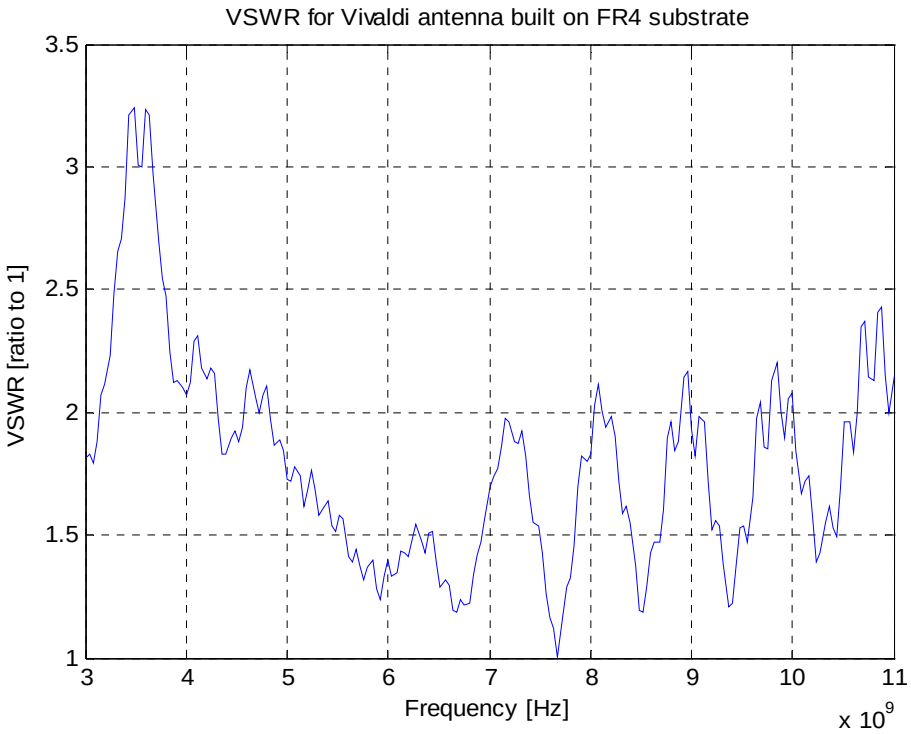

Figure 53. Measured VSWR for Vivaldi antenna built on FR4 substrate.

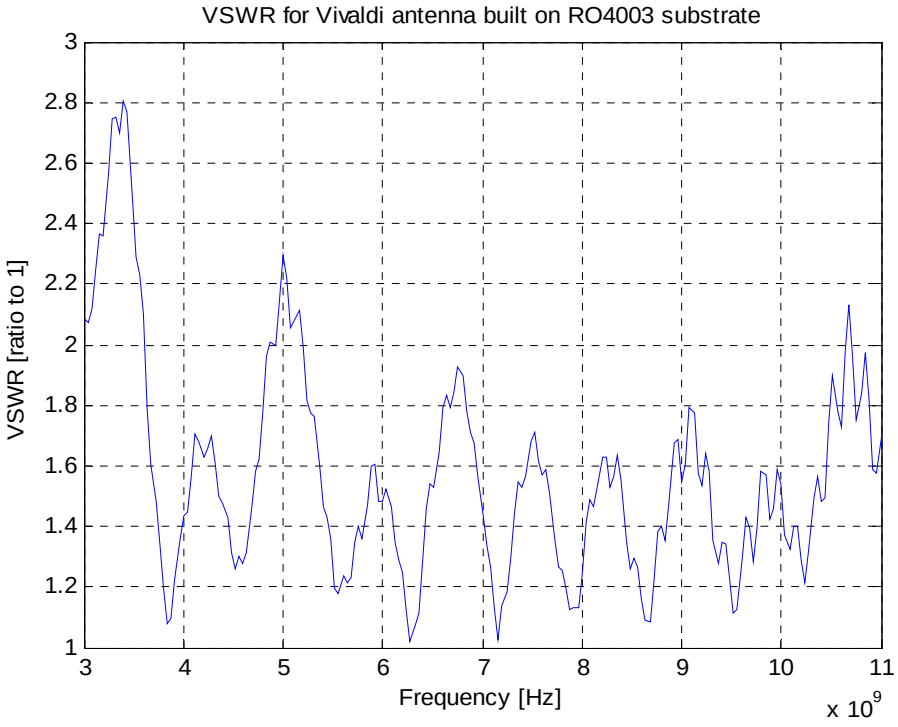

Figure 54. Measured VSWR for Vivaldi antenna built on RO4003 substrate.

Gain: Both designs had an acceptable boresight gain between 4 GHz- 6GHz as shown in figures 55, 56.

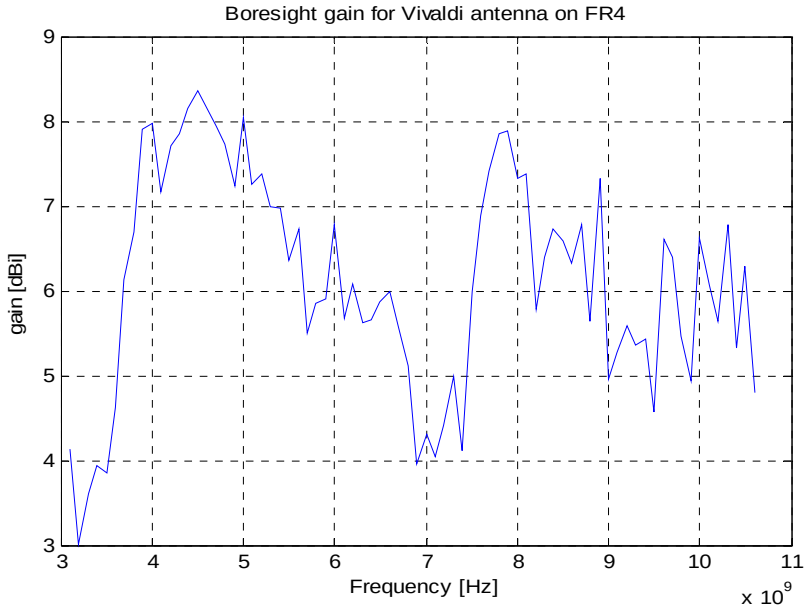

Figure 55. Boresight gain for Vivaldi antenna on FR4 substrate.

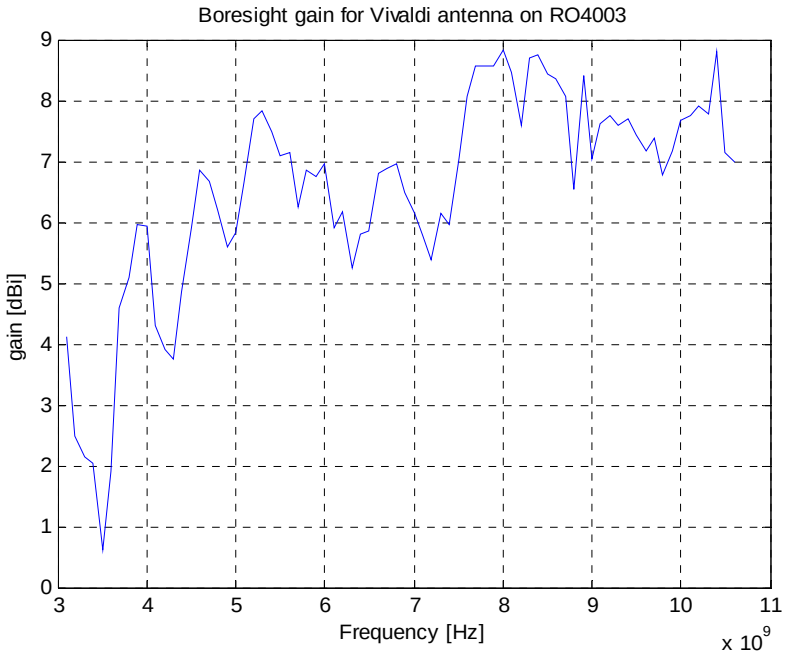

Figure 56. Boresight gain for Vivaldi antenna on RO4003 substrate.

HPBW: The Vivaldi antenna built using FR4, when measured had a decreasing HPBW from 110 ° at 3.1 GHz to 80° at 6 GHz as shown in figure 57. A sample of the normalized power patter at 4.5 GHz is shown in figure 58, while a full set of normalized power patter graphs is provided in Appendix D. The antenna built using RO4003 substrate has an average of 90° HPBW below 6 GHz as shown in figure 59. A sample of the normalized power patter at 4.5 GHz –the peak power for Pulse ON 220 radar system- is shown in figure 60, while a full set of normalized power pattern graphs is provided in Appendix E.

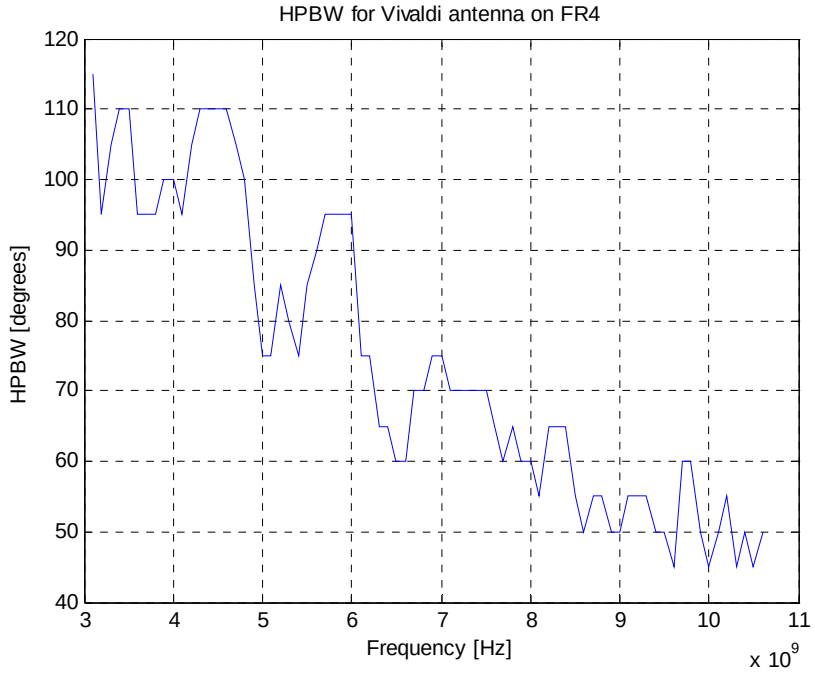

Figure 57. HPBW for Vivaldi antenna on FR4 substrate.

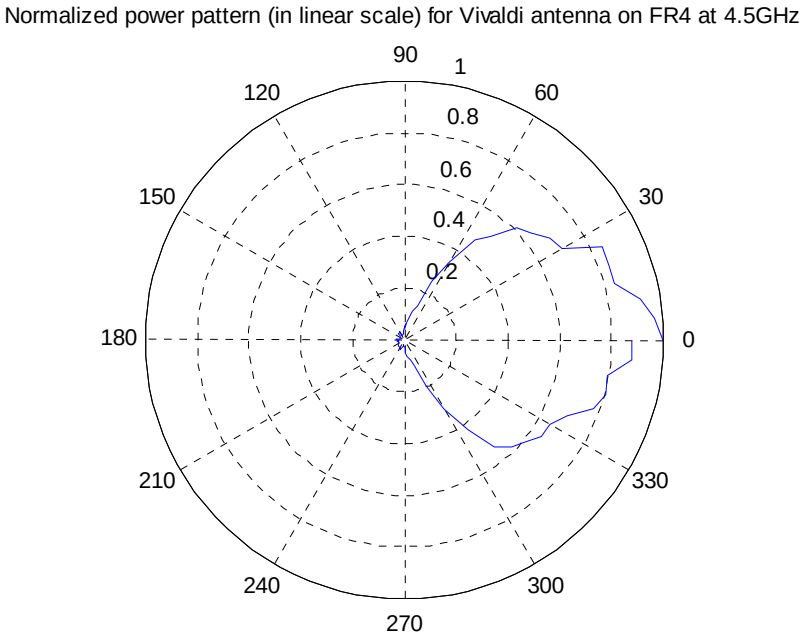

Figure 58. Normalized power pattern for Vivaldi antenna built on FR4 substrate at 4.5 GHz.

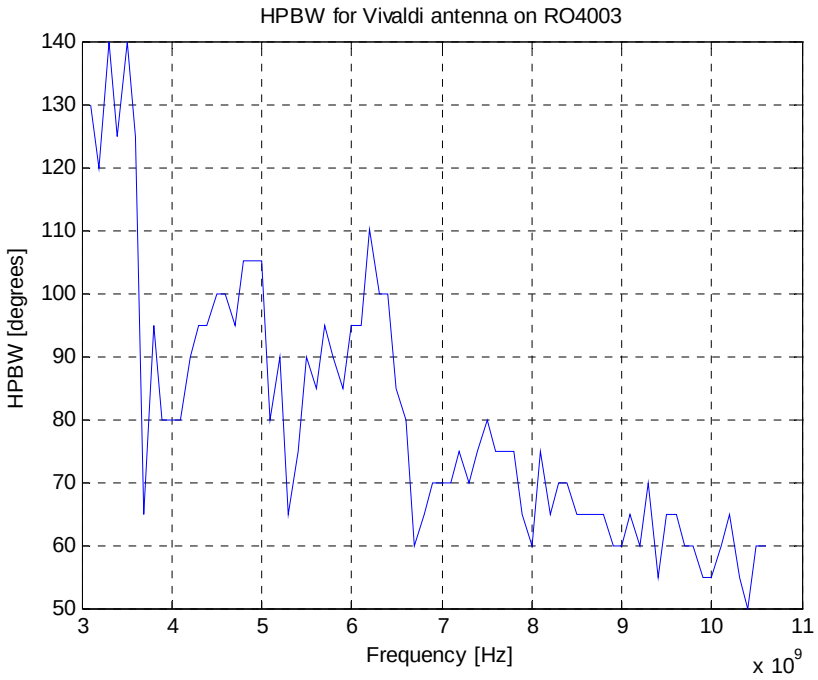

Figure 59. HPBW for Vivaldi antenna on RO4003 substrate.

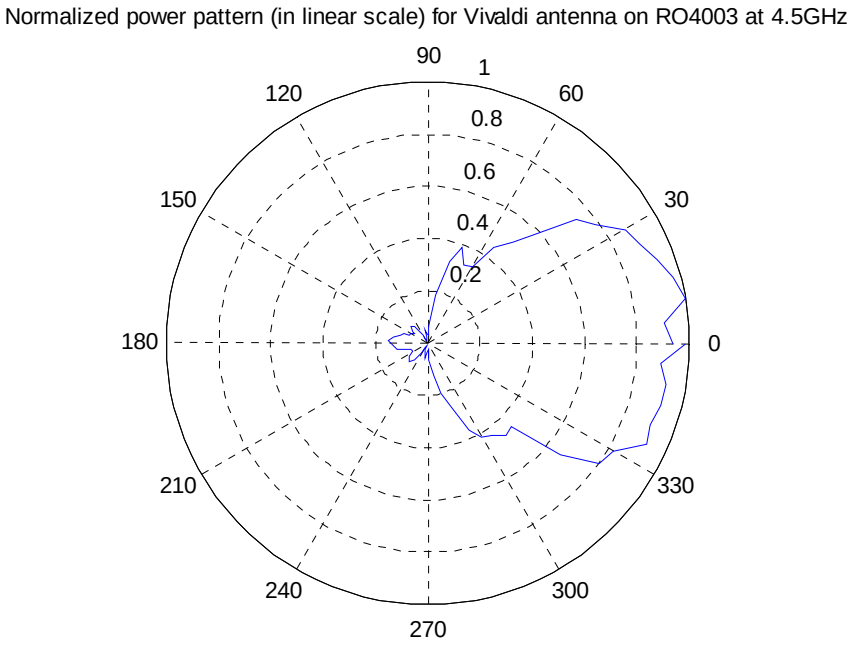

Figure 60. Normalized power pattern for Vivaldi antenna built on RO4003 substrate at 4.5 GHz.

Bowtie Antenna

In general, radiation characteristics depend on the ratio between the physical length of the antenna L and the wavelength λ. From this fact, Rumsey observed that an antenna that is only described by angles and is itself infinite in length is inherently self-scaling and thus frequency independent in gain, HPBW, and VSWR [3]. Figure 61 (a) is an example of an antenna that obeys Rumsey's principle. An infinite antenna is impossible to build, thus several techniques have been suggested to make antennas effectively infinite. A bowtie antenna introduces one of these techniques by truncating the infinite sheet as shown in figure 61 (b). A bowtie antenna violating Rumsey's design

properties will not be frequency-independent; however, it exhibits parameter stability over a very wide frequency band.

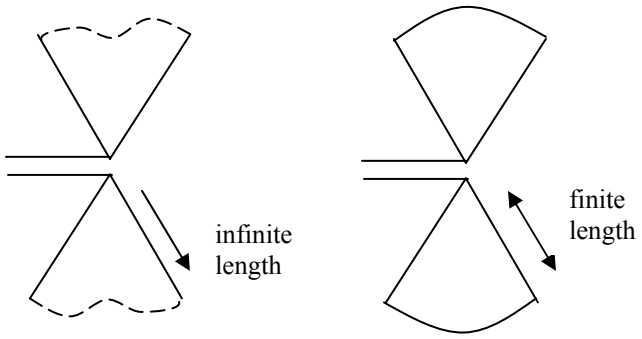

Figure 61. A frequency independent wideband antenna in a) theoretical realization and b) practical realization (bow-tie antenna). [3]

The bowtie antenna is a flat plate variation of the biconical antenna, which is known for its wide-band capability. Bowtie antennas are designed in different forms as shown in figure 62. The folded bowtie antenna is favored for its high directivity in both azimuth and elevation planes. Lai introduced a horn-like structure of a bowtie using copper flares to form a folded bowtie antenna [25].

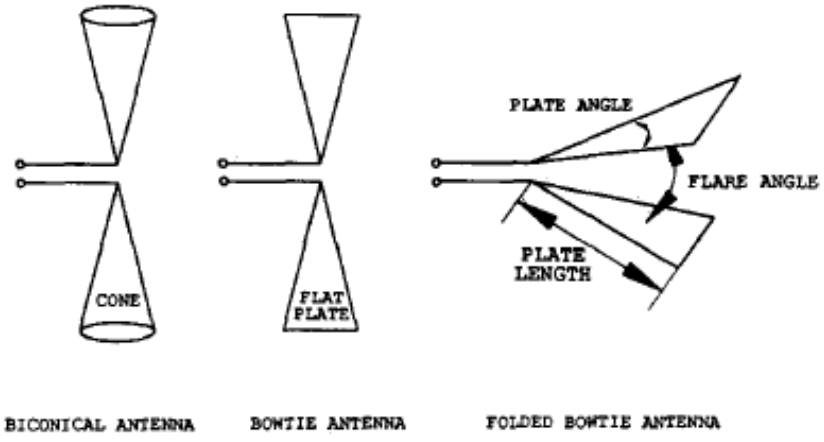

Figure 62. A few wideband bow-tie antenna types.

The bowtie antenna introduced here consists of a slotline tapered to form a Vivaldi exponential to provide a gradual transition for impedance matching purposes. The slotline then expands in a linear fashion at a specified flare and terminates in a rolled edge. The slotline and bowtie antenna join together starting at the beginning of the Vivaldi taper section, as shown in figure 63 [25]. The angles of the flares and the length of the plates define the lower frequency of the antenna [1].The directivity in the azimuth (horizontal) and elevation (vertical) planes are dependent upon the plate angle and the flare angle consecutively.

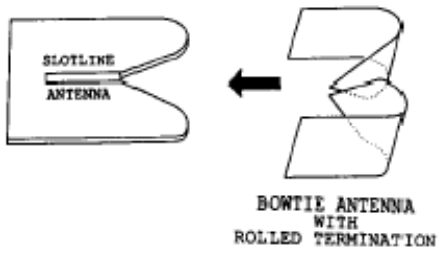

Figure 63. The bowtie antenna consists of a slot line Vivaldi and a rolled-flare termination [25].

The bowtie antenna is very broad band; however, in practice, it is difficult to find an equally broad-band and balanced feed structure. The impedance depends principally on the fine details of the structure of the feed region; the significant variation in the impedance of bowtie antennas shown proves that they are hard to match [10]. Lai proposed a Y-Y transition –first introduced by Gupta [26] - to match the microstrip and slotline transmission lines [25]. The slot line and microstrip widths depend on the dielectric constant of the substrate material and its thickness. For a 50 $\boldsymbol{\Omega}$ characteristic impedance the width of the microstrip (w) required can be calculated using equation 19 [27].

$$Z_0 = \frac{87.0}{(\varepsilon_r + 1.41)^{1/2}} \ln\left[\frac{5.98h}{0.8w + t}\right]$$ Equation 19

where h= substrate height, t= metal thickness, ε_r= the dielectric constant of the substrate.

RO4003 substrate has an ε_r= 3.38 and thickness of 0.813 mm, w= 1.6 mm. Calculation of the slotline width (w_s) is complicated, and bound formulas are used in the process, as described by Gupta [26]. An online calculator was used to calculate the required slotline width for a 50 $\boldsymbol{\Omega}$ match on the same substrate [28], and the optimal width of the slotline (w_s) was found to be 1 micrometers. This requires sophisticated production processes to implement. Using the Y-Y transition on cheap materials like RO4003 would be impractical. Use of more expensive substrates that have high dielectric constant -ε_r10.8- for a wider w_s would defeat the purpose of building cheap antenna design. A simpler balun design introduced by Kim utilizes a microstrip-to-coplanar stripline transition. This transition provided good performance with low insertion return losses for the whole UWB frequency range [29]. An illustration of this balun design is shown in figure 64, and the dimensions for the design used on RO4003 substrate are given in table 4. The balun is bent without sacrificing the balun performance resulting in a reduction in the length of the balun in the coplanar stripline direction by more than half of its original length.

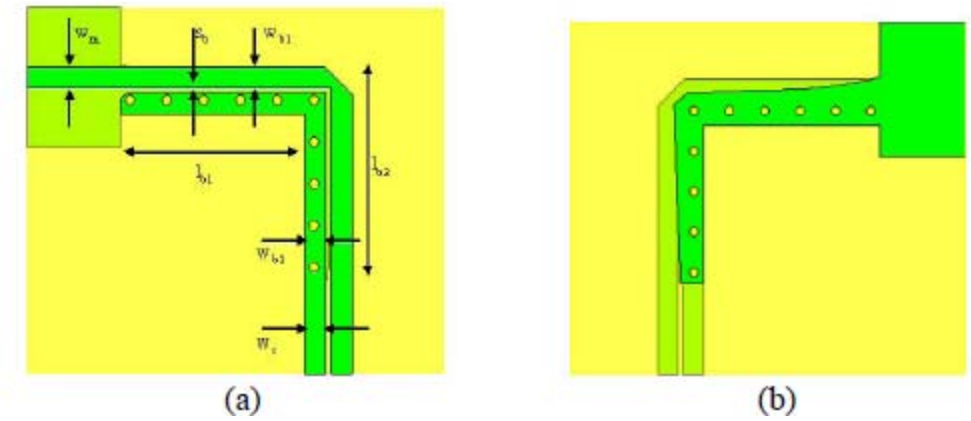

Figure 64. Illustration of (a) top view and (b) bottom view of the balun [29].

Table 4. Balun design dimensions for the bowtie antenna
(all dimensions in mm).

coplanar stripline gap, s_b	L_{b1}, L_{b2}	w_{b1}, w_m	w_{b2}, w_c
0.245	9.8	1.127	1.127

Design and Simulation

The bowtie antenna was realized on a RO4003 substrate (ε_r= 3.38 and thickness of 0.813 mm), and simulated for the VSWR of its planar structure in ADS following the simulation procedure in chapter six. A three dimensional view of the design is presented in figure 65, and the layer stackup is shown in figure 66.

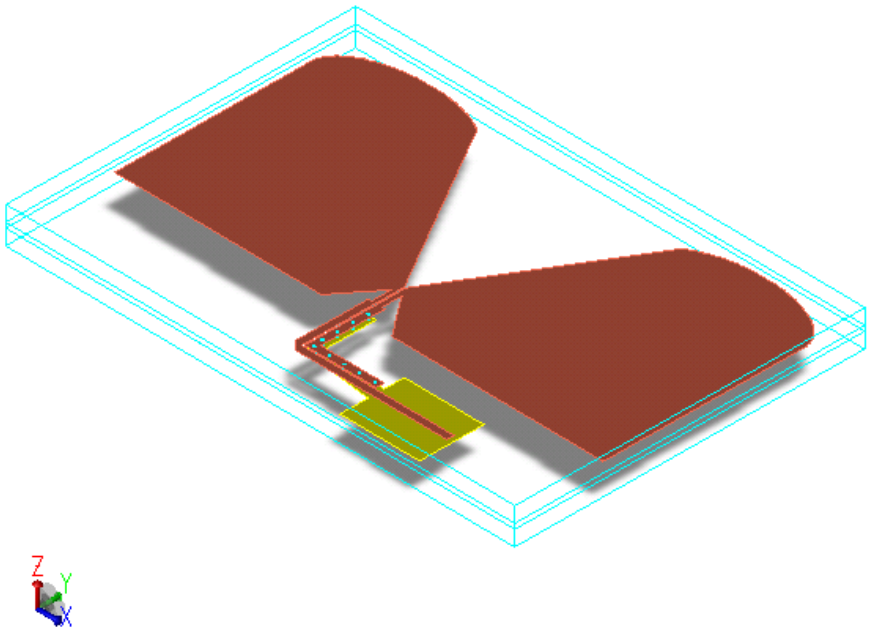

Figure 65. A three dimensional view of the bowtie antenna in ADS.

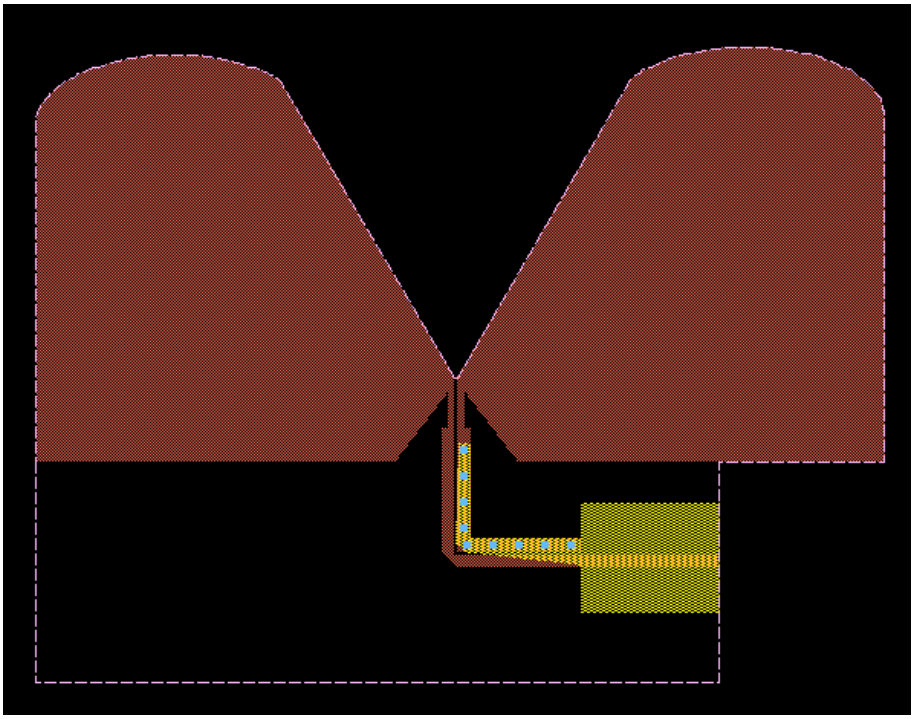

Figure 66. The layer stackup of the bowtie antenna in ADS: top copper layer in red, bottom ground layer in yellow, board outline as dashed line, and vias are shown as blue circles.

While the feed structure dimensions are critical, several other dimensions in the radiating element of the antenna have a great effect on its performance as well. The rolled edge terminations at the end of the bowtie are added to minimize edge diffractions. They can, however, greatly reduce the performance of the antenna if not designed carefully. Heedy used the moment method and the uniform geometrical theory of diffraction to provide a guide for designing such edge termination [30]. The ratio of the ellipse radii forming the edge termination need to remain at 2:1 for best performance in all designs. A good value for the minimum radius of the ellipse was found experimentally to be 6.35 mm. As mentioned before the flare angle defines the elevation directivity, but, along with the length of the plates, it also plays a role in defining the lower frequency of the antenna. Several flare angles and plate lengths were inspected and two designs showed acceptable VSWR values when simulated.

The first design (design A) had an opening flare angle of 60° and a plate length of 127 mm, slightly smaller than the half wavelength of the lower frequency that of 1 GHz ($\frac{\lambda_m}{2}$= 150 mm). At this point the project had turned to using the Novelda R2A radar system which has a -10 dB bandwidth between 1-6 GHz (refer to chapter three for more details). For this reason the lower frequency was set to 1 GHz. The VSWR for this design is shown in figure 67.

The second design (design B) had the same flare angle of 60° but the plate length was pushed down to a value slightly smaller than $\frac{\lambda_m}{4}$ (34.75 mm). The resulting VSWR is shown in figure 68. Both designs showed a VSWR < 2:1 for the desired frequency range 1-6 GHz. Addition of the copper flares was expected to increase VSWR values while

providing higher directivity in the azimuth plane. This will be discussed in the next section.

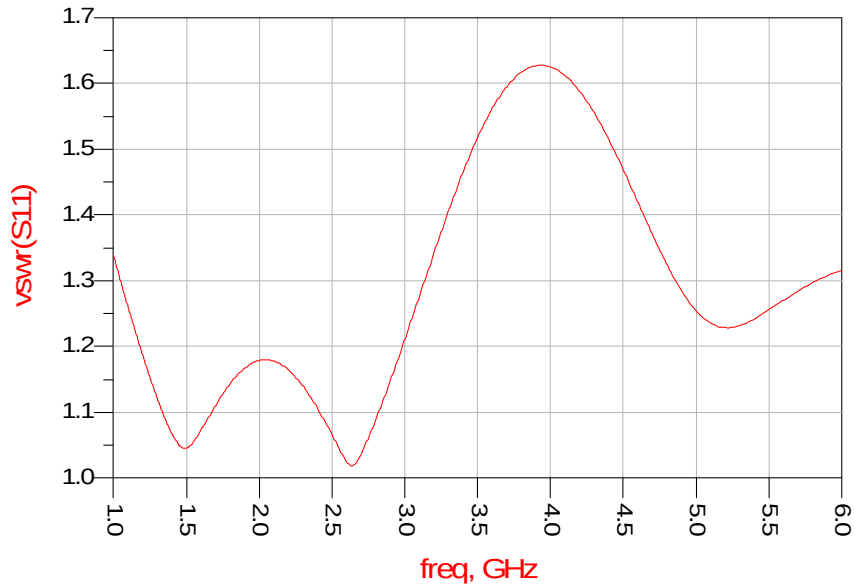

Figure 67. Simulated VSWR for the bowtie antenna (design A).

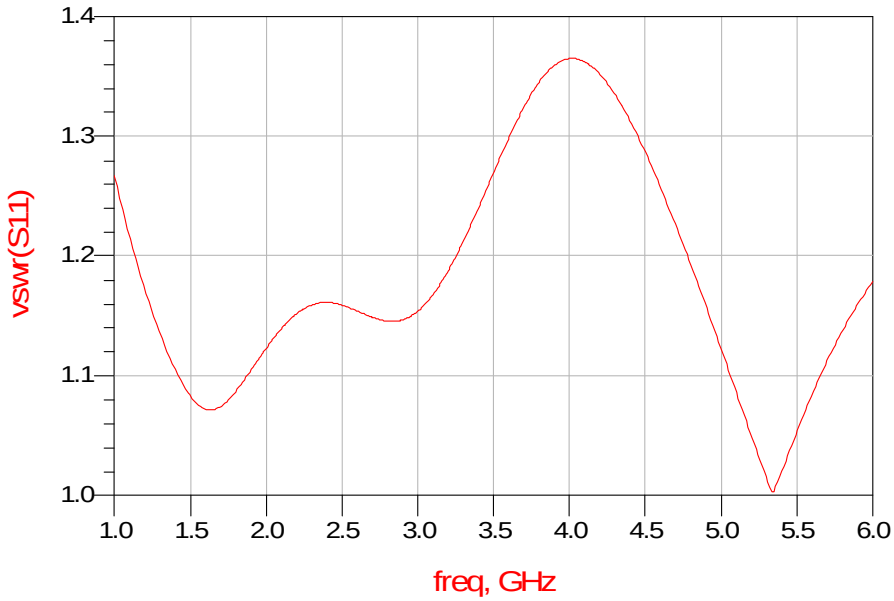

Figure 68. Simulated VSWR for the bowtie antenna (design B).

Building and Testing

The antennas were built on RO4003 with the same characteristics as in the simulation phase, and tested for performance before adding the copper flares to the PCBs. Experiments were carried out with the copper flares to find the optimum dimensions for each design.

Design A: (plate length= 127 mm) had a VSWR different from simulation with a high peak at 1.7 GHz. Addition of the copper flares reduced the peak at the low frequency but added another 2.5:1 VSWR peak at 2.6 GHz as shown in figure 69. The VSWR remained under 2:1 for most of the desired frequency range except between 2.3-3 GHz.

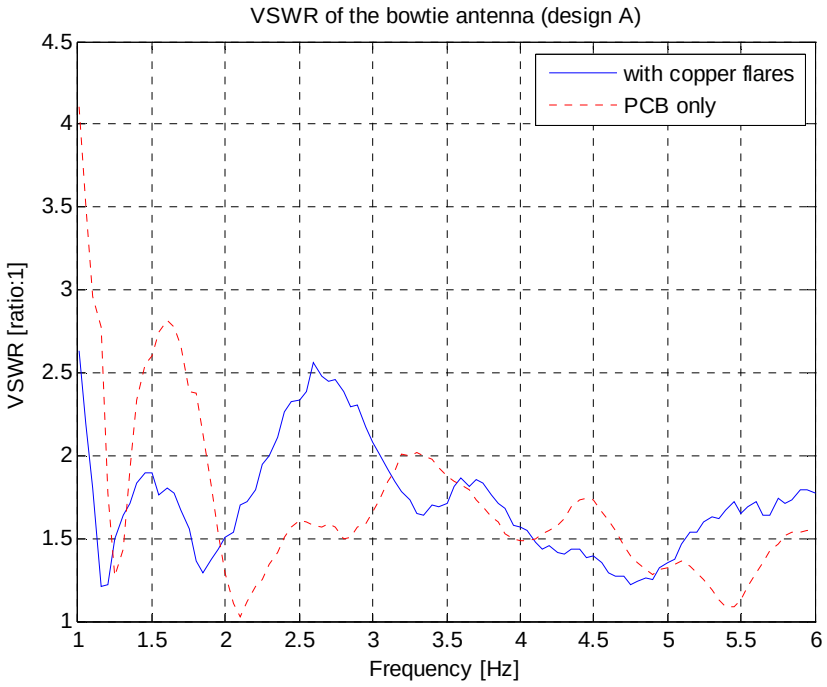

Figure 69. Measured VSWR for the bowtie antenna (design A) with (blue), and without copper flares (red).

Since a smaller plate (flare) angle increased the directivity of the antenna in the azimuth plane, the flare was shaped and tested to reach the smallest possible flare angle. For Design A, 23° was the lowest value that could be reached before getting unacceptable return loss values. Figure 70 shows a picture of an assembled prototype of the bowtie antenna (design A). The HPBW was measured in both the azimuth and elevation planes with and without the copper flares. In the azimuth plane, the HPBW decreased with the increasing of frequency with no improvement from adding the copper flares, as shown in figure 71. In the elevation plane, however, adding the copper flares improved the HPBW by up to 40° as shown in figure 72. HPBW values as low as 40° were achieved in this design. The normalized power patterns at the peak frequency in both planes are shown in figure 73, and the full set of pattern plots are provided in appendices F, G.

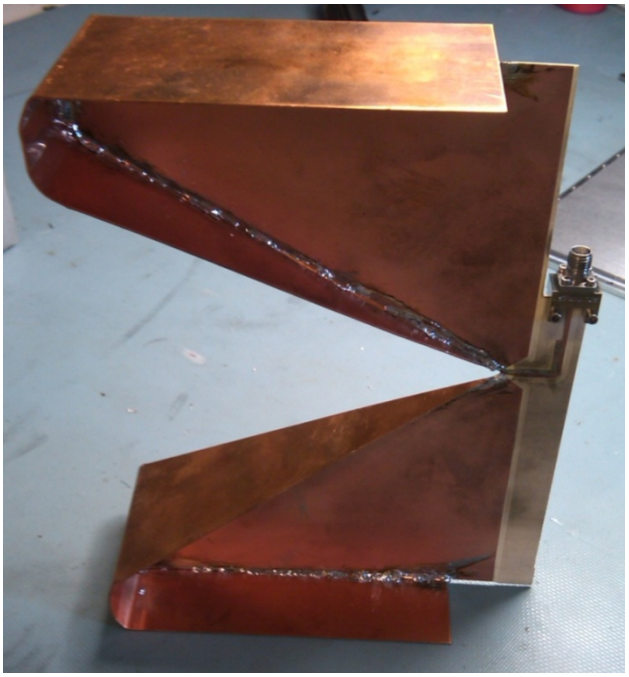

Figure 70. An assembled prototype of the bowtie antenna (design A).

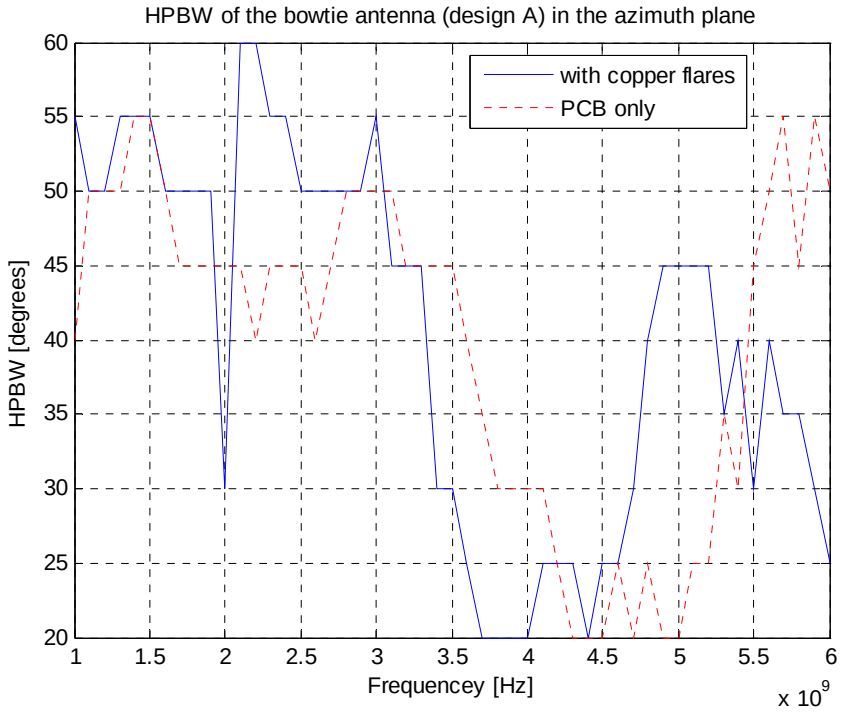

Figure 71. Measured HPBW in the azimuth plane for the bowtie antenna (design A).

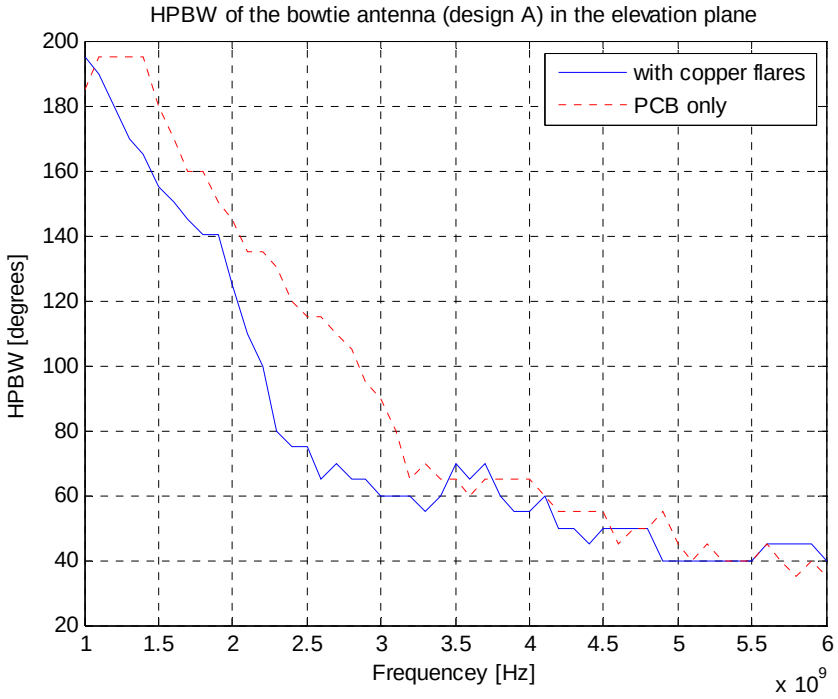

Figure 72. Measured HPBW in the elevation plane for the bowtie antenna (design A).

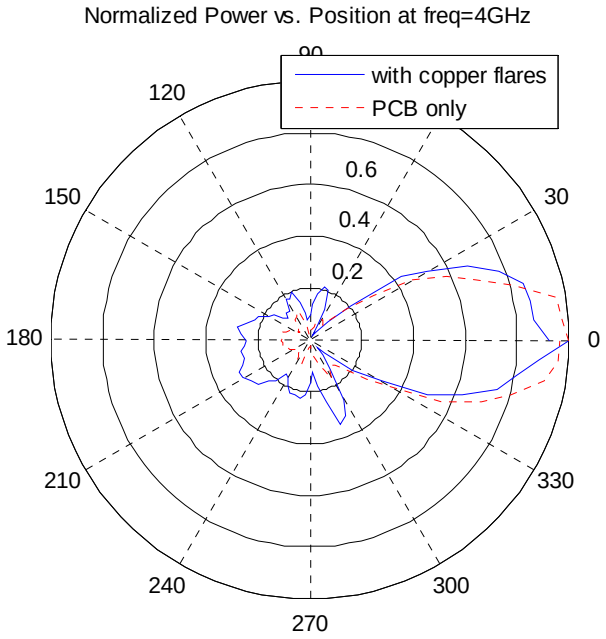

Bowtie antenna (design A) in the elevation plane

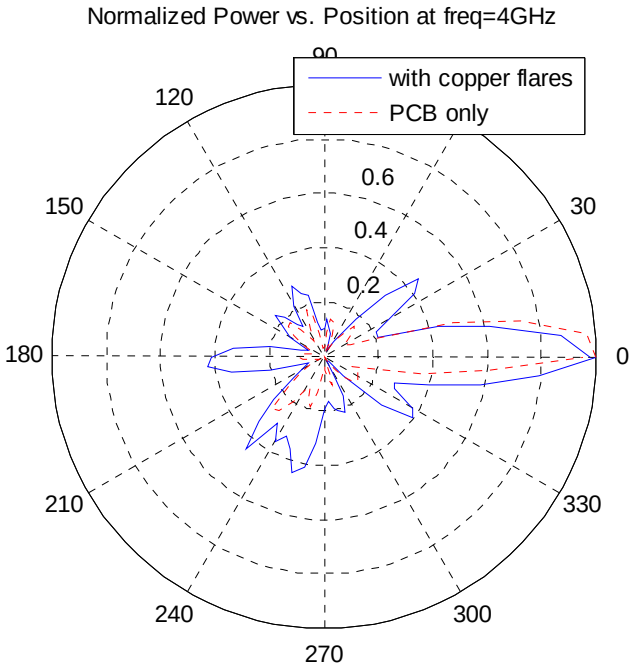

Bowtie antenna (design A) in the azimuth plane

Figure 73. Normalized power patterns in linear scale for the bowtie antenna (design A); in the elevation plane (top) and the azimuth plane (bottom).

Finally, the antenna boresight gain was measured with and without the copper flares. Not surprisingly, the gain was higher by 1 to 4 dBi for the antenna with the copper flares. This design showed a gain of 8 dBi +/- 1 dB only in the desired range of frequencies, as shown in figure 74.

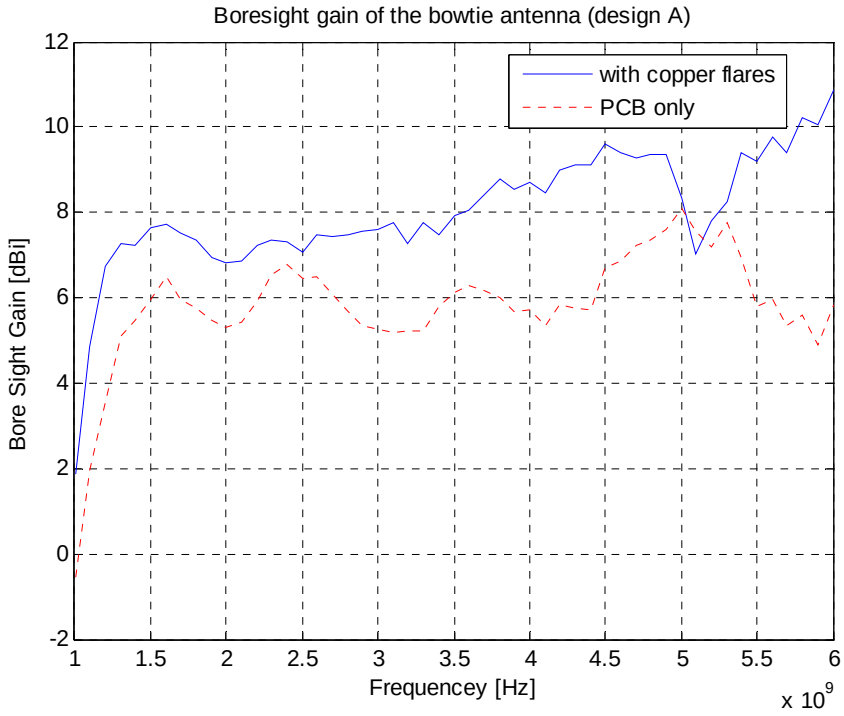

Figure 74. Measured boresight gain for the bowtie antenna (design A).

Design B: The bowtie antenna built following design B (plate length= 34.75 mm) also showed a different VSWR from the simulation results. Addition of the copper flares in this design improved the VSWR in the entire frequency band, as shown in figure 75. The VSWR remained under 2:1 for almost all the desired range of frequencies.

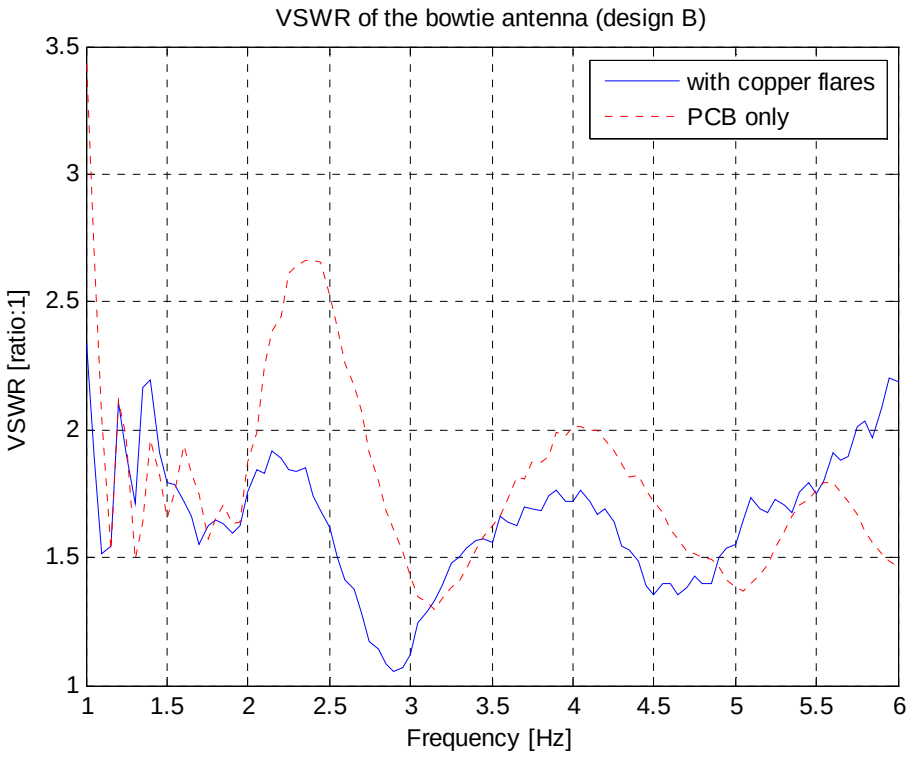

Figure 75. Measured VSWR for the bowtie antenna (design B) with (blue), and without copper flares (red).

For this design, the lowest value that could be reached for the flare angle, before getting unacceptable return loss, was 30°. Figure 76 shows a picture of design B of the bowtie antenna.

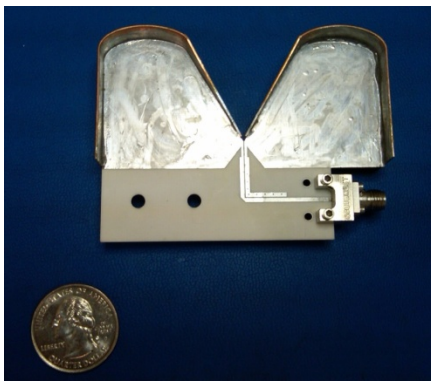

Figure 76. An assembled prototype of the bowtie antenna (design B).

The HPBW was measured in both the azimuth and elevation planes. In the azimuth plane, the antenna had better HPBW values without the copper flares. A minimum value of only 40° was reached for HPBW, as shown in figure 77. In the elevation plane, however, adding the copper flares improved the HPBW by as much as 50° at certain frequencies as shown in figure 78. This design had an HPBW value of only 150° at the peak frequency for the Novelda R2A in the elevation plane, but it has a 60° HPBW in the azimuth plane. The normalized power patterns at the peak frequency in both planes are shown in figure 79, and appendices H, I contain the full set of power pattern for this antenna.

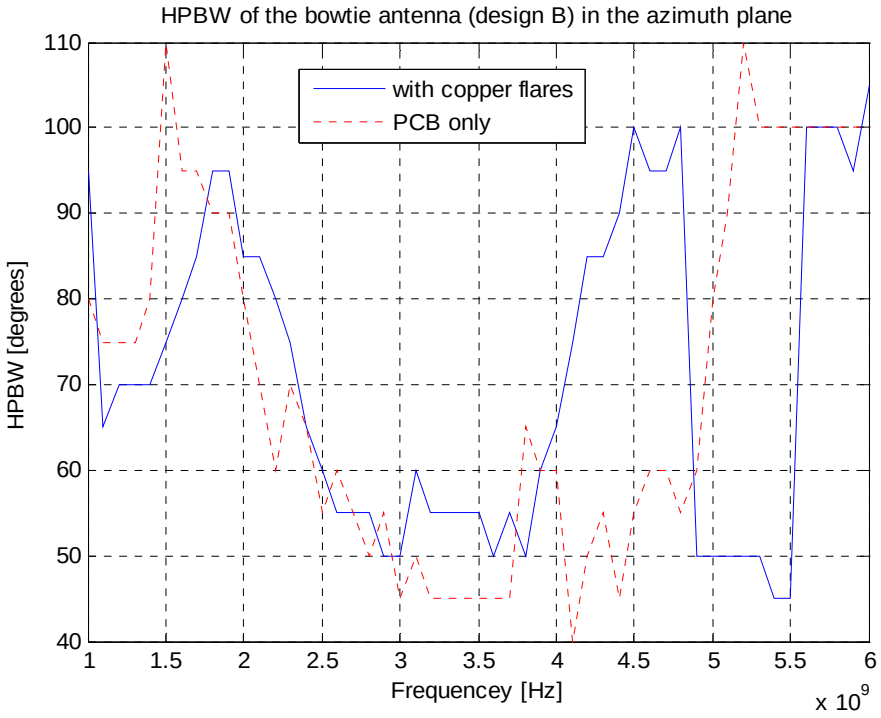

Figure 77. Measured HPBW in the azimuth plane for the bowtie antenna (design B).

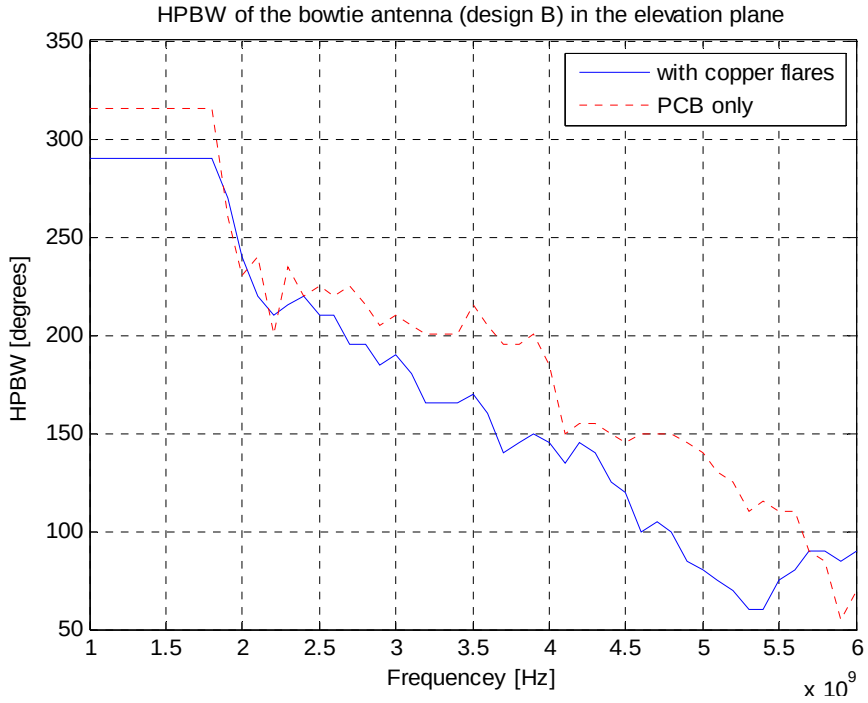

Figure 78. Measured HPBW in the elevation plane for the bowtie antenna (design B).

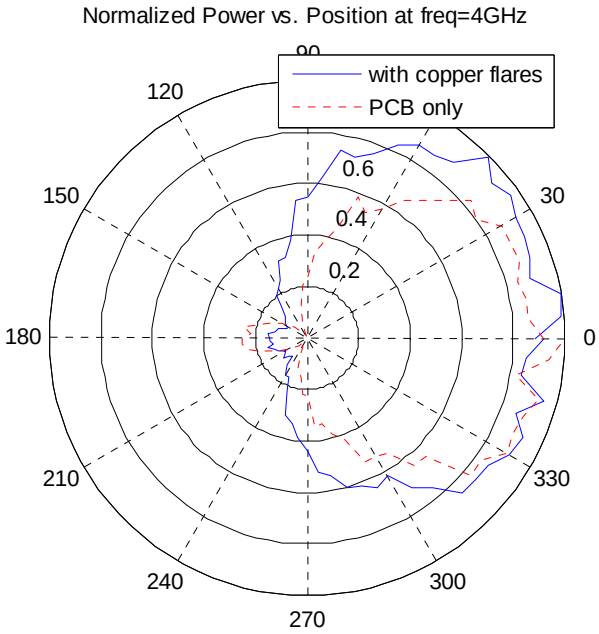

Bowtie antenna (design B) in the elevation plane

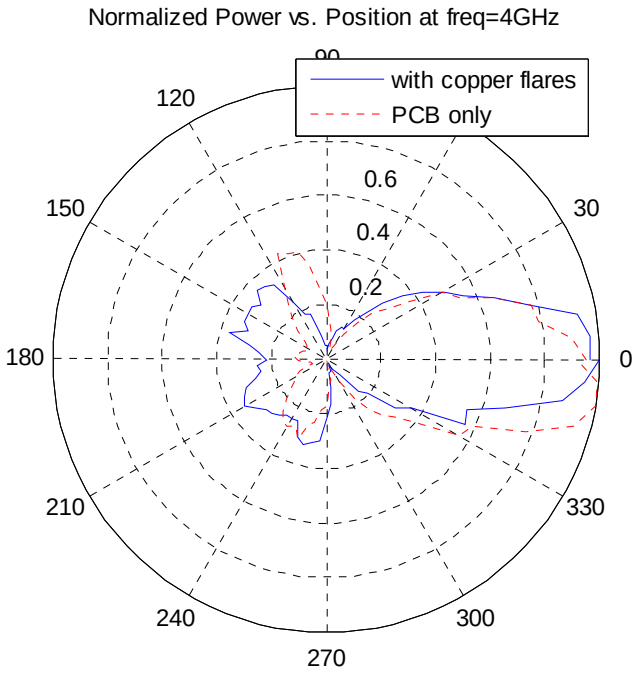

Bowtie antenna (design B) in the azimuth plane

Figure 79. Normalized power patterns in linear scale for the bowtie antenna (design B); in the elevation plane (top) and the azimuth plane (bottom).

The boresight gain was low for design B of the bowtie antenna compared to design A, but adding the copper flares increased the gain by 1 dB for most of the bandwidth as shown in Figure 80. The boresight gain for this antenna was not flat in the 1-6 GHz band, However, a gain of 5.5 dBi is measured at the 4 GHz, which is the peak frequency of the Novelda R2A transmit signal.

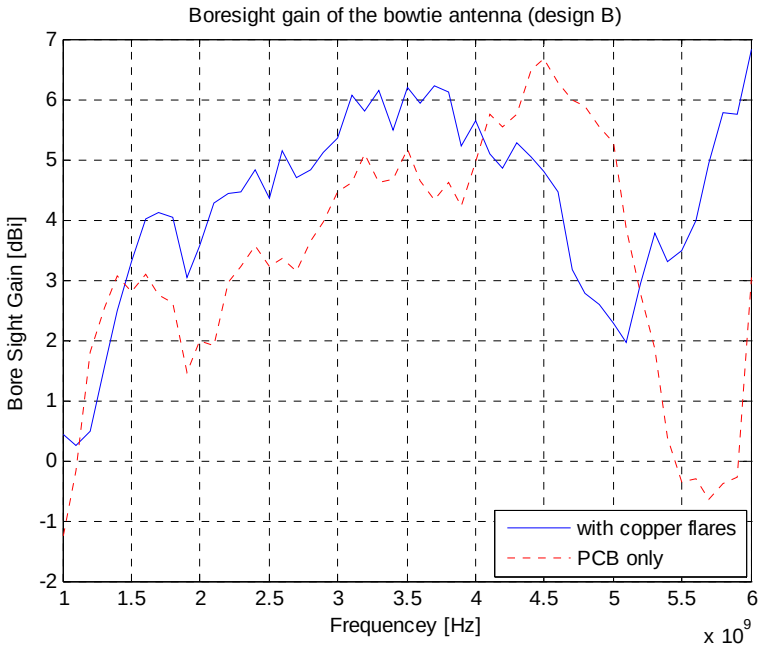

Figure 80. Measured boresight gain for the bowtie antenna (design B).

CHAPTER 8

DESIGN COMPARISONS

In this chapter, the antennas are compared for performance based on the factors considered in their design, driven by the overall system requirements. These factors include VSWR, HPBW, boresight gain, frequency of operation, and physical profile. The antennas are categorized according to the target UWB radar system. The two Radar systems considered here are:

- The Time Domain's Pulse ON 220 which has a 10 dB bandwidth between 3.5 and 5.2 GHz and a peak frequency of 4.4 GHz.

- The Novelda R2A which has a 10 dB bandwidth extending from 1 GHz to 6 GHz and a peak frequency of 4 GHz.

See chapter three for more details on the transmit signal for the two systems.

Time Domain Pulse ON 220

The candidate antenna designs for this system are the LPDA, quasi-horn, Pulse ON 200 with corner reflector, and the Vivaldi antennas. The LPDA antenna had the disadvantage of high VSWR. The quasi-horn antenna had relatively low boresight gain that makes it a bad choice for use in snow measurements. The Vivaldi antenna manufactured on RO4003 had a low boresight gain as well. The Pulse ON 200 antenna with corner reflector and the Vivaldi antenna on FR4 both had high gain and similar characteristics. The Vivaldi antenna, however, had the advantage of being a two-

dimensional antenna. Table 5 summarizes these designs and their measured characteristics.

Table 5. Antenna designs comparison for the Pulse ON 220 radar system.

Parameter / Antenna (Dimensions)	Bandwidth	VSWR	Boresight gain at peak frequency (4.4 GHz)	HPBW at peak frequency (4.4 GHz)	Boresight gain	HPBW
LPDA (145x68 mm)	3.5-5.2 GHz	> 2:1	8 dBi	75°	5.5-10.2 dBi	70-80°
Quasi-horn (105x63x35 mm)	3.5-5.2 GHz	< 2:1	3.5 dBi	95°	0-5.2 dBi	65-125°
Pulse ON 200 with corner reflector (50x60x110 mm)	3.5-5.2 GHz	< 2.5:1	8.7 dBi	70°	5.7-9 dBi	60-95°
Vivaldi on FR4 (50x110 mm)	3.5-5.2 GHz	< 3:1	8.4 dBi	110°	4-8.4 dBi	75-110°
Vivaldi on RO4003 (50x110 mm)	3.5-5.2 GHz	< 2.2:1	5 dBi	100°	0.7-7.7 dBi	65-140°

Novelda R2A

Two antennas were designed to be used with the Novelda R2A radar system, Design A and Design B of the bowtie antenna. While Design A had the disadvantage of being large in size, it showed high directivity in both, azimuth and elevation planes and a high boresight gain that is constant for most of the desired bandwidth. Design B was comparable to Design A in terms of VSWR but had less directivity and lower boresight gain as shown in table 6. One main advantage Design B had is its small size that makes it suitable for mobile applications using the Novelda R2A system.

Table 6. Antenna designs comparison for the Novelda R2A radar system.

Parameter / Antenna (Dimensions)	Bandwidth	VSWR	Boresight gain at peak frequency (4GHz)	HPBW at peak frequency (4GHz)	Boresight gain	HPBW
Bowtie, Design A (140x170x51 mm)	1-6 GHz	< 2.6:1	8.5 dBi	Azimuth= 20° Elevation= 55°	2-11 dBi	Azimuth= 20-60° Elevation= 40-195°
Bowtie, Design B (58x79x17 mm)	1-6 GHz	< 2.2:1	5.7 dBi	Azimuth= 65° Elevation= 145°	0.2-6.2 dBi	Azimuth= 45-105° Elevation= 60-290°

CHAPTER 9

DESIGN EVALUATION

The final phase in the design process was evaluation. After the antennas were tested they were evaluated in different environments for their performance in snow measurements. The evaluations included Matlab simulations, in-lab tests, and field tests. The antennas evaluated were the Vivaldi antenna built on FR4, the Design A and the Design B bowtie antennas. Each antenna was evaluated for performance with the corresponding radar system as explained in the next sections.

Via Matlab Simulation

A simulation environment in Matlab was built to simulate the behavior of a UWB pulse sent using the antennas introduced in this thesis as used for snow depth measurement. The simulation assumed a boresight radiation pattern on a flat surface of snow at a distance of 1 meter from the antenna. The snowpack was assumed to be 2 meters deep and containing an ice layer at 1 meter from the surface. The setup of the simulation experiment is shown in figure 81. A more complex simulation is being built to take radiation from side lobes and scattering effects into account. For this thesis, however, perpendicular-to-snow-surface beam radiation was assumed and scattering effects were not taken into account.

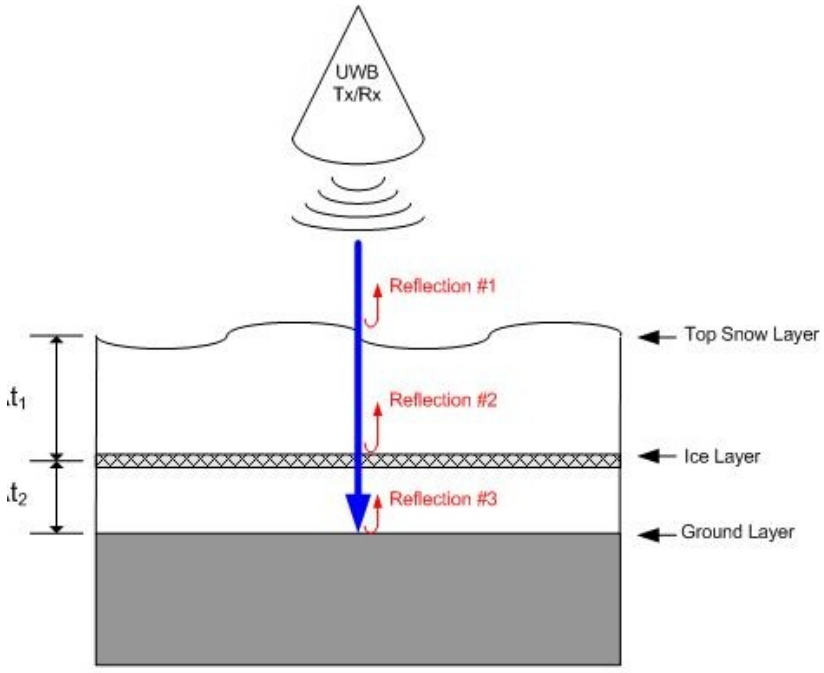

Figure 81. The simulated experiment setup for the Matlab simulation environment.

The simulation used a brief UWB Gaussian pulse as the transmit signal. The signal was repeatedly sent through the snowpack and reflected back off the surface, ice layer inside, and the ground. The reflected waves were then received and integrated to increase the signal to noise ratio (SNR) of the reflection. The integrated wave contains information about the location of each layer and the system performance is assessed by the ability to recognize the layer locations in the signal. A general pulse was created initially using a high order derivative of a Gaussian pulse but later replaced by a replica of the signal generated by the Time Domain Pulse ON 220 system. The signal had a 1.5 Vpp amplitude as shown in figure 82. The Vivaldi antenna was used in this model as the transmitter and the receiver antenna. The transmit signal after adding the antenna gain was tested versus the FCC UWB outdoor mask and its PSD is shown in figure 83.

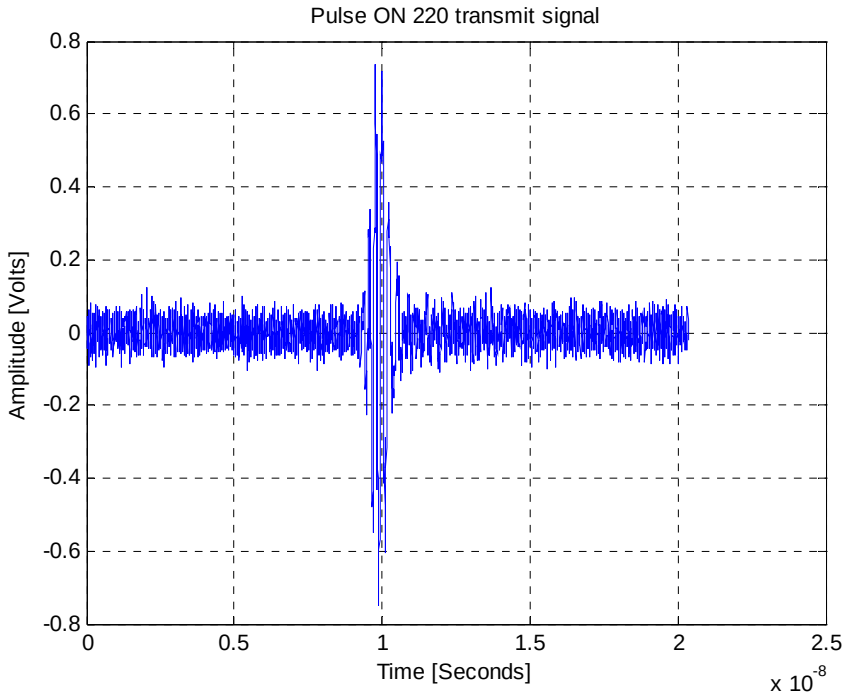

Figure 82. Time Domain Pulse ON 220 UWB pulse.

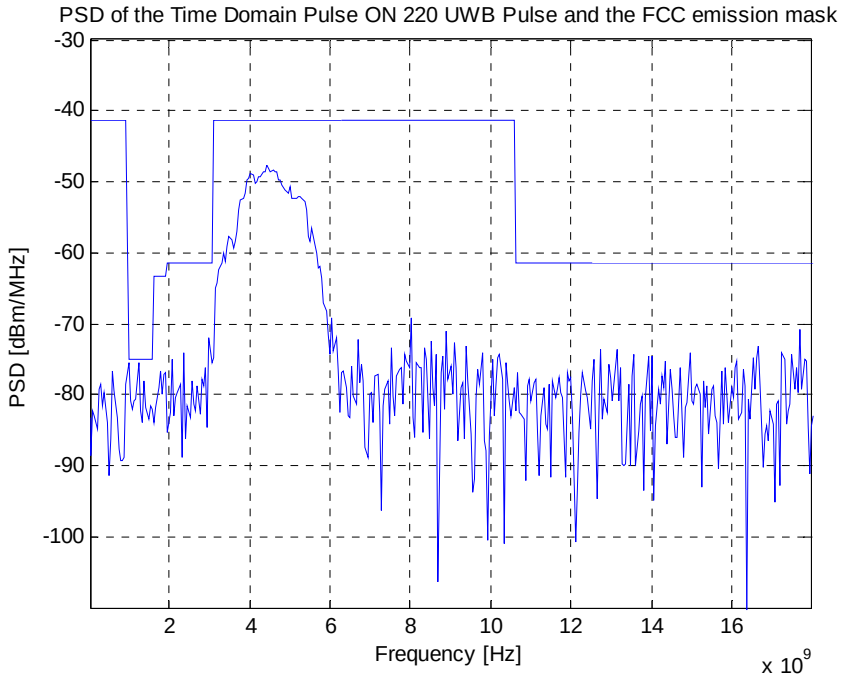

Figure 83. The PSD of the radiated Pulse ON 220 signal using the Vivaldi antenna and the FCC UWB outdoor mask.

When a signal hits a surface between two media of different dielectric constants, some of the energy in the signal is reflected and the rest is transmitted. Skolnik summarizes the laws that govern the reflection of signals from surfaces between different media in *Radar Handbook* [31]. If the incident signal has a power Pi and the reflected signal has a power Pr and the power absorbed by the second medium is Pt, the relation between the powers in these signals is given by equations 20, 21 [31].

$$P_{r=}P_iR \qquad \text{Equation 20}$$

where R is the reflection coefficient

$$P_{t=}P_iT \qquad \text{Equation 21}$$

where T = 1-R = the transmission coefficient

The reflection coefficient, R is a function of the dielectric constants of the two media between which the signal is reflected and is calculated using equation 22.

$$R = \frac{\sqrt{\varepsilon_1}-\sqrt{\varepsilon_2}}{\sqrt{\varepsilon_1}+\sqrt{\varepsilon_2}} \qquad \text{Equation 22}$$

where $\varepsilon_1, \varepsilon_2$ are the dielectric constants of medium 1 and medium 2 respectively.

In this model, four different layers exist through which the signal travels and the transmission and reflection coefficients were calculated whenever a transition between layers occurs. The layers are air, snow, ice, and ground. The dielectric constant (relative permittivity) for air is 1. Snow, however, does not have a constant value for relative permittivity. Relative permittivity of snow varies dramatically based on the snow density which in itself is a function of depth. Ulaby characterizes dielectric constants for a variety

of media including snow and provides a formula for calculating its relative permittivity that is given by equation 23 [32].

$$\varepsilon_{snow} = (1 + 0.51\rho_s)^{3} \quad \text{Equation 23}$$

where $\rho_s$is snow density in gm/cm^3

While snow density is a function of several variables, research showed that snow density can be calculated as a function of distance from the surface of dry snow. Lundberg used six year average measurements of peak snow depth and snowpack mean density at 11 locations in the Swedish mountains to provide a depth-dependent snowpack density [33]. Lundberg showed that for distance d> 2m, ρ_s has a constant value of 358. For snow at distance d< 2m, however, ρ_s is not constant but can be calculated using equation 24.

$$\rho_s = 148 + 105d \quad \text{Equation 24}$$

where d is the depth of the snow.

An average value of d= 1 m was used in this simulation resulting in ε_{snow}= 1.44. The relative permittivity of ice is affected slightly by temperature, but a common value for ε_{ice} is 3.15. Finally, the ground relative permittivity $\varepsilon_g$is given by equation 25.

$$\varepsilon_g = (1 + 0.44\rho_s)^2 \quad \text{Equation 25}$$

where $\rho_s$is the density of the ground surface.

The common value of ρ_s=2.6654 gm/cm^3 was used for ground surface density resulting in ε_g=4.7.

After parameters were set for the different layers in the model, the behavior of the signal was simulated taking reflection coefficients, transmission coefficients, and different losses into account. A path loss, given by equation 26, was applied to the transmitted signal.

$$P_L = (1/4\pi d\lambda)^2 \qquad \text{Equation 26}$$

In the snow another loss factor was introduced, that is signal attenuation. Attenuation in any medium is given as a value per distance. In snow, this value is not always constant since it depends on the moisture content of snow, temperature, snow density, and frequency. For the purpose of evaluation, a conservative value of 10 dB/m was used for attenuation in the simulation. The attenuation is usually much smaller for dry snow. Taking all these parameters into account, the simulation was run for a 1 milliseconds integration period assuming a 9.6 MHz duty cycle on the UWB pulse generator. Finally, White Gaussian noise was added to the reflected signal to emulate the environment effect on the signal. The resulting received signal is shown in figure 84 after converting the time scale into distance while considering the different speed for the signal in air and snow and correcting for bias. The surface of the snow introduced a massive reflection in the received signal; while the next two reflections, from the ice layer and from the ground, were much smaller due to signal attenuation in the snow. A clearer image of the portion of the received signal that contains the ice and ground reflections is

shown in figure 85. Even though the reflection from the ground was relatively small, its magnitude was about 6 dB higher than the noise in the received signal. The Matlab script for this simulation is provided in appendix J. At this point the focus was turned to physical measurements in controlled environment. The process of in-lab evaluation is presented in the next section for both the Pulse ON 220 and the Novelda R2A systems.

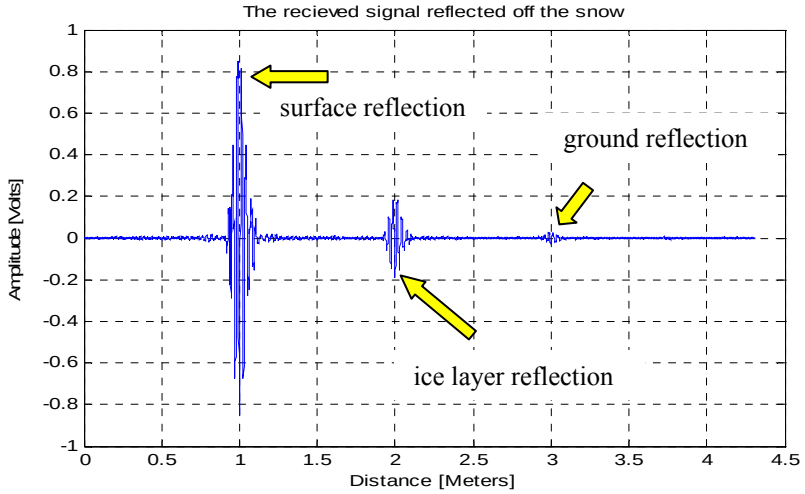

Figure 84. The simulation result for the received signal showing the locations of each reflection in meters.

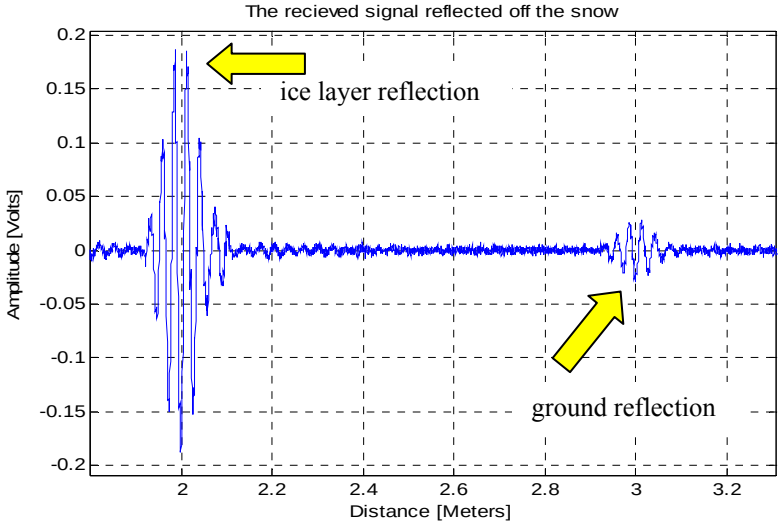

Figure 85. The simulation result for the received signal showing the ice and ground reflections.

Lab Tests

In-lab tests were conducted for two purposes, evaluating and having a better understanding of the UWB radar systems to be used, and to capture reference signals to be used for calibration when conducting field measurements. This provided the chance to test the different antenna designs and evaluate their performance using the actual UWB radar systems. The tests were conducted in the anechoic chamber to create a reflections-free environment. The Vivaldi antenna built on FR4 was tested with the Time Domain's Pulse ON 220 system. The Design A and Design B of the bowtie antenna were tested with the Novelda R2A system.

Time Domain's Pulse ON 220 System

Two Vivaldi antennas were connected to the transmitter and receiver ports of the Time Domain's Pulse ON 220 radar and placed inside the empty anechoic chamber for capturing a reference signal. The reference signal is shown in figure 86. A foil-wrapped ball was then placed in the anechoic chamber to serve as a point reflector. The radar then was used to send multiple pulses and capture their reflection from the surface of the ball. The Pulse ON 220 system integrates 1024 pulses at 9.6 MHz repetition frequency. The reference signal was subtracted from the reflection signal and the result is shown in figure 87. Hardware artifacts resulted in a noisy section in the reflected signal between 0 and 120 cm. The ball showed a strong reflection at the expected distance, while secondary peaks existed. More efficient algorithms needed to be developed to better interpret the measured reflected signal.

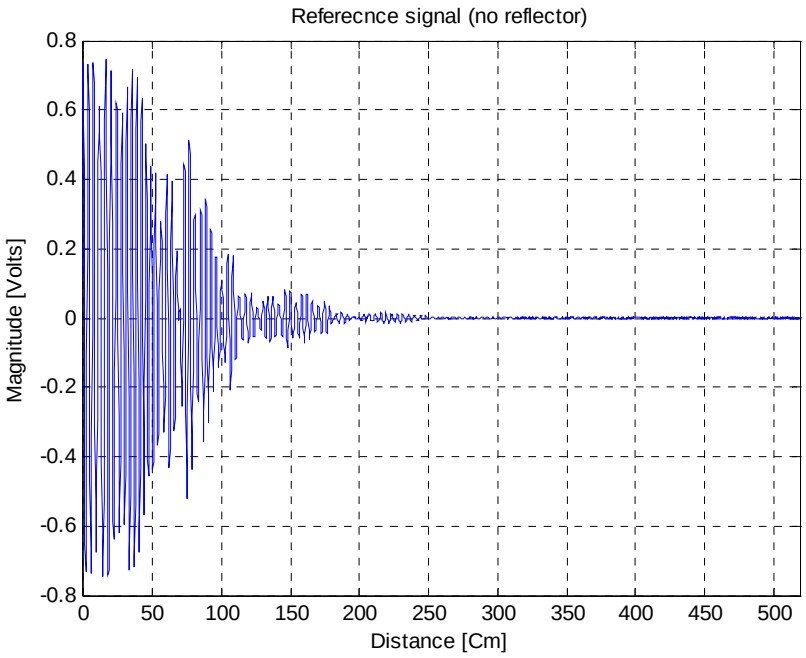

Figure 86. The reference signal for Pulse ON 220 using the Vivaldi antenna inside the anechoic chamber.

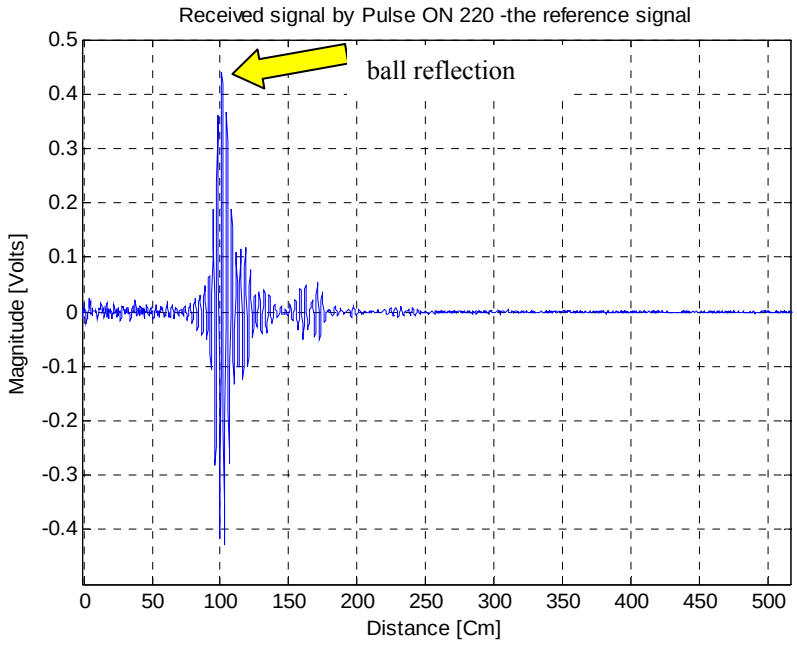

Figure 87. The resulting signal from subtracting a reference signal from the measured reflection off a foil-wrapped ball placed at about 1 meter from the radar.

Novelda R2A System

Following the same procedure described in the previous section, the Novelda R2A radar system was used to evaluate the performance of the Design A and Design B bowtie antennas. The Novelda R2A system allows for different repetition rates and the number of pulses that are integrated. The repetition frequency for this experiment was set to 48 MHz, and 3000 pulses were integrated to form the received signal. A scan of the empty chamber was captured for a reference and a metal plate was then used for a more realistic target as opposed to using a ball. The system using Design B antennas and the target inside the anechoic chamber are shown in figure 88.

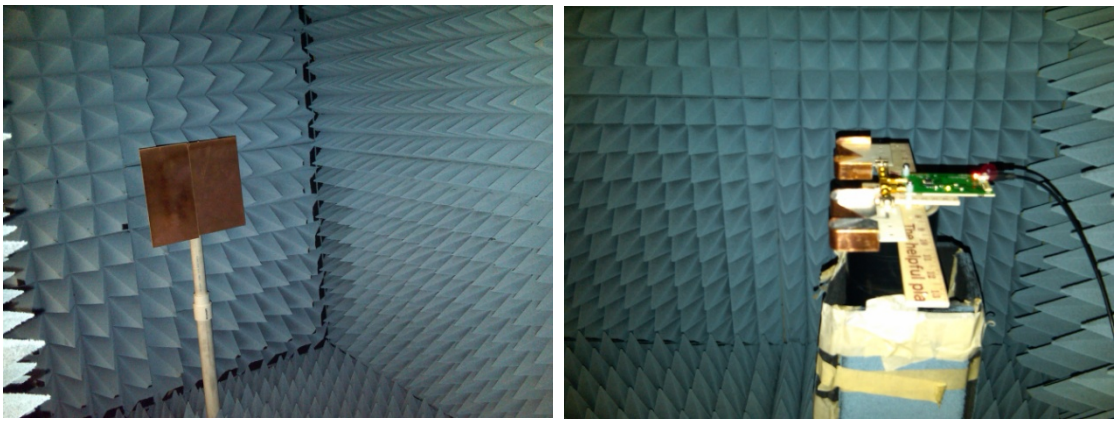

Figure 88. Novelda R2A radar with the Design B bowtie antennas (right) and a target metal plate (left) inside the anechoic chamber.

Subtraction of the reference signal from the reflected pulses was not enough to measure the target distance with the R2A system. Correlation-based DSP algorithms developed by Justin Hadella, a Flat Earth engineer and former MSU graduate student, were used to interpret the distance to the target. The processes these algorithms follow

are outside the scope of this thesis. The location of the target in the reflected signal was obvious using both antennas as shown in figures 89 and 90. As expected the reflection using the Design B antenna was smaller than its counterpart using the Design A bowtie antenna.

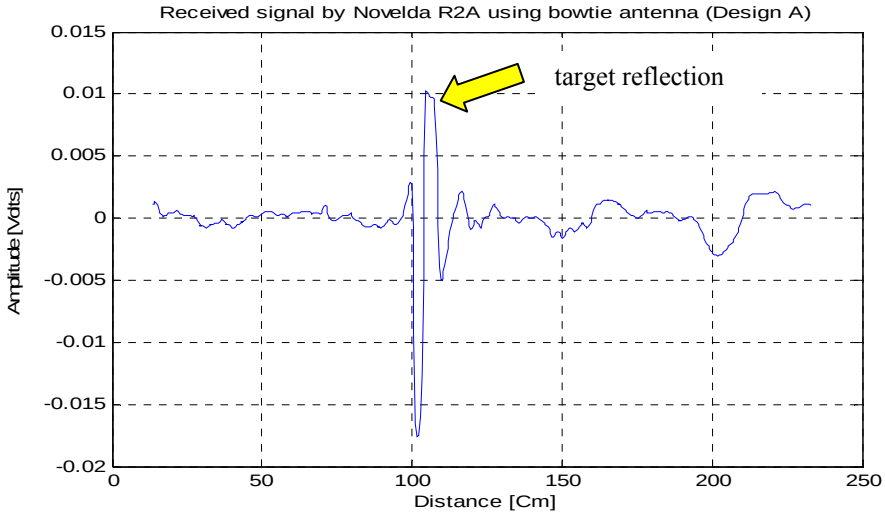

Figure 89. The processed received signal using the Design A bowtie antenna showing the location of the target plate.

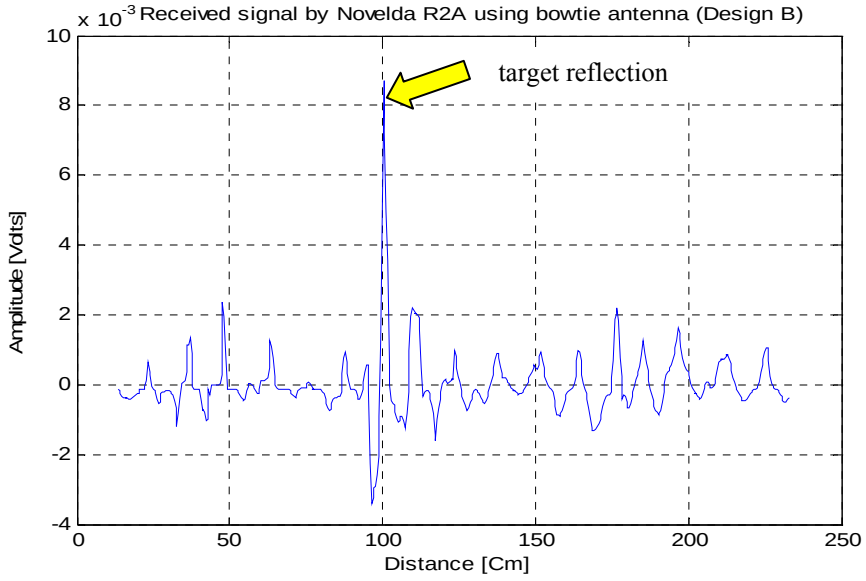

Figure 90. The processed received signal using the Design B bowtie antenna showing the location of the target plate.

Field Test

In this test the Pulse ON 220 system was used to measure the depth of a snowpack using the Vivaldi antennas as shown in figure 91.

Figure 91. Experiment setup for measuring snow depth using the Pulse ON 220 radar system and the Vivaldi antennas.

A reference signal was used to subtract the noise associated with hardware and environment artifacts from the received signal. To capture a reference signal, the antennas were directed at the sky and the received signal was recorded. The reference signal is shown in figure 92. The same settings as used in the in-lab experiment were used here. The repetition frequency was set by default to 9.6 MHz and 1024 scans were integrated to create the reflection signal.

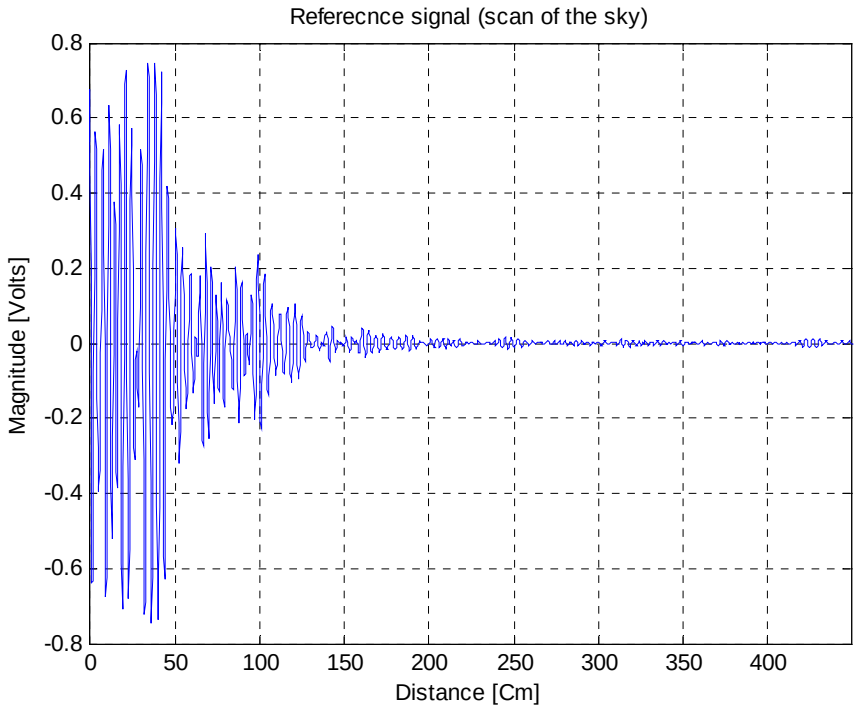

Figure 92. The reference signal for measuring snow depth using the Pulse ON 220 radar system and the Vivaldi antennas (antennas pointed at the sky).

The antennas were placed 90 cm above the surface of the snowpack that is 85 cm deep. The reflected signal was captured and the reference signal was subtracted for a cleaner signal. The unprocessed received signal is shown in figure 93, while figure 94 shows the received signal after subtracting the reference scan. The reflection from the surface is seen as a spike at 90 cm, while the reflection from the ground was very small due to signal attenuation in the snow. Several reflections appeared in the signal after the top surface reflection. More complex algorithms are being developed to distinguish between these reflections and find the ground reflection for depth measurement.

At this point, due to the weather and the unavailability of packed snow, no field tests were performed using the bowtie antennas with the Novelda R2A radar system.

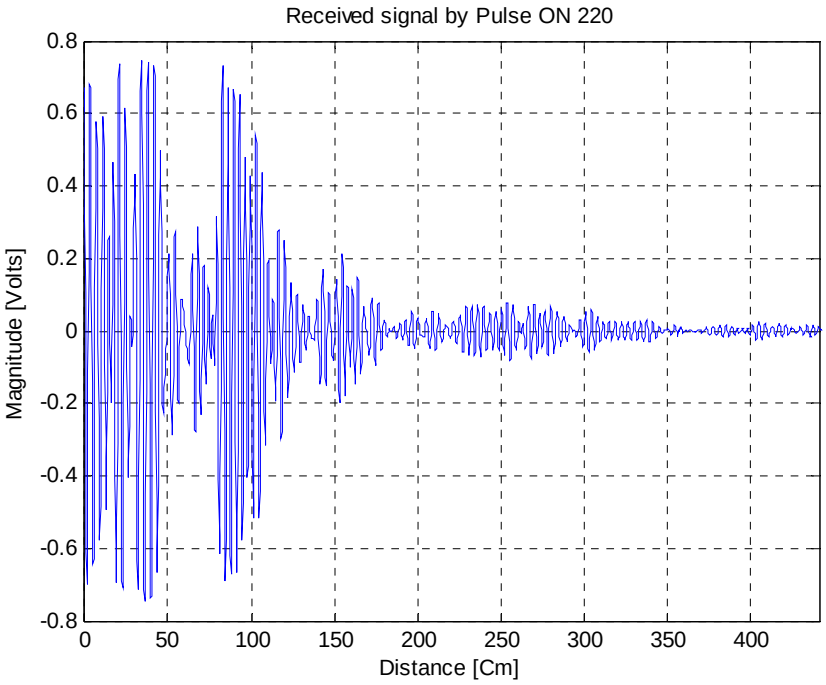

Figure 93. The received signal from snow using the Pulse ON 220 radar system and the Vivaldi antennas.

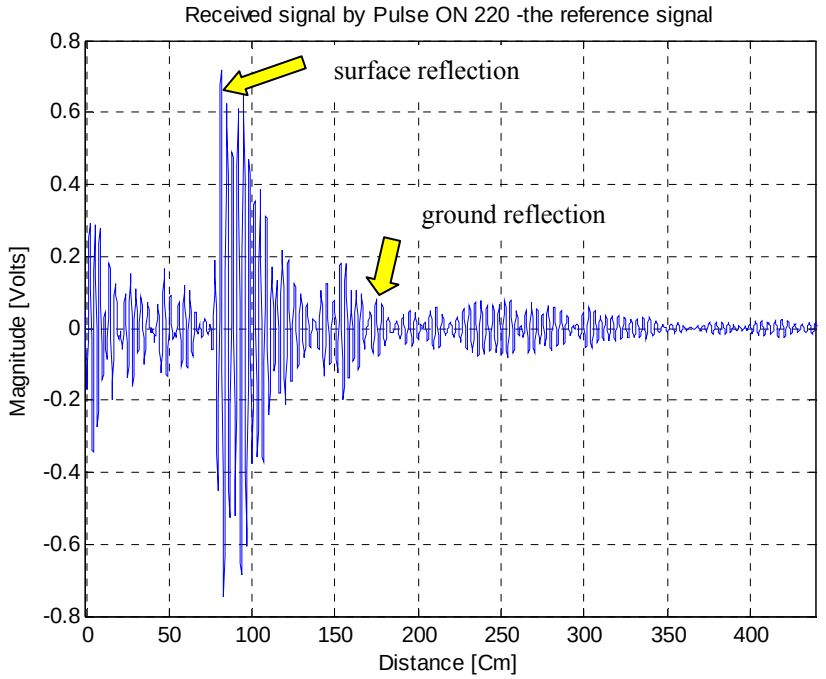

Figure 94. The received signal from snow after subtracting the reference signal using the Pulse ON 220 radar system and the Vivaldi antennas.

CHAPTER 10

CONCLUSIONS AND FUTURE WORK

Conclusions

In this thesis, a comprehensive study of UWB antennas for snow depth measurement was presented. The study included design, simulation, testing, and optimization of the antennas for use in practical UWB radar applications. Antennas were designed for two different systems with two frequency bandwidths in the UWB range. The target application for the antennas was snow measurements; therefore high gain and directivity were the focus of the design. One of the main reasons for using UWB in snow measurements is moving to a chip-scale technology. To maximize this advantage, the size of the antennas was considered as well in the design process.

Studying the tradeoffs of each antenna, the Vivaldi antenna built on FR4 substrate proved to be practical for use with the Time Domain's Pulse ON 220 system. For the Novelda R2A system, the two designs (A and B) of the bowtie antenna showed high performance when tested and evaluated for the target application. These designs have a good match in their bandwidth, high directivity, and high boresight gain at the frequency of operation. Even though the Design B antenna had a relatively low boresight gain when compared to the Design A antenna, it has the advantage of being small in size while keeping a high directivity, making it an optimal choice for mobile applications.

The results and discussion presented in this thesis should provide a guide to the basics in UWB antenna design, the fundamental requirements of UWB antennas, and design, testing and characterization of UWB antennas. The Vivaldi and the bowtie antennas presented here should provide a potential solution to current UWB radar systems to be used in snow measurements and other applications demanding high gain and directivity in UWB.

Future Work

Future work is needed to look into simulation programs that are able to provide gain and pattern plots for the designs besides return loss measurements. Better results could be achieved if more data can be collected in the simulation phase resulting in less modification needed after building the physical antenna. Other substrate materials could be used in future designs as well. In planar antenna designs, the antenna parameters are directly related to the dielectric characteristics and thickness of the substrate material used.

Finally, packaging was not considered in this research. The packing material for enclosure (known commercially as radome material) can help increase or decrease the performance of the antenna. Packing should be designed carefully taking into account the dielectric characteristics of the materials used and the physical profile affecting the antenna performance.

REFERENCES CITED

[1] Oppermann, Hamalainen, and Linatti, *UWB Theory and Applications,* Wiley, 2004.

[2] Federal Communications Commission, First Report and Order 02-48, 2002.

[3] B. Allen et al., *Ultra-wideband Antennas and Propagation for Communications, Radar and Imaging,* Wiley, 2007.

[4] Di Benedetto, and Giancola, *Understanding Ultra Wide Band Radio Fundamentals,* Prentice Hall PTR, 2004.

[5] C. A. Balanis, *Antenna Theory Analysis and Design*, 3rd edition, Wiley-Interscience, 2005.

[6] Merrill Skolnik, *Radar Handbook,* 2nd edition, McGraw-Hill, 1990.

[7] *IEEE Transaction on Antenna and Propagation,* Vol. AP-17, No. 3, May 1969.

[8] "System Analysis Module User's Manual, PulsON® 220TM UWB Radio," *Time Domain Corporation*, Cummings Research Park, May 2008, on the web: www.timedomain.com.

[9] *IEEE Transaction on Antenna and Propagation,* Vol. AP-31, No. 6, May 1983.

[10] Hans Schantz, *The Art And Science of ULTRAWIDEBAND ANTENNAS,* Artech House, 2005.

[11] R. J. Fontana, and Richley, *Observations on Low Data Rate, Short Pulse UWB Systems,* 2007 IEEE International Conference on Ultra-Wideband (ICUWB), Singapore, September 2007.

[12] Dwayne Folden, *Automated Antenna Test and Characterization Facility,* Montana State University, September 2007.

[13] Dwayne Folden, *UWB Radar Antenna: Simulation and Testing*, Montana State University, 2007.

[14] V. H. Rumsey, *Frequency Independent Antennas,*1975 National Convention Record, pt. 1, pp 114-118.

[15] American Radio Relay League and R. Dean Straw, *The ARRL Antenna Book: The Ultimate Reference for Amateur Radio Antennas, Transmission Lines And Propagation,* 21st edition, May 1, 2007.

[16] C. K. Campbell, et al., *Design of a Stripline Log Periodic Dipole Antenna, Antennas and Propagation*, IEEE Transactions on [legacy, pre - 1988], 1977.

[17] D. M. Pozar, *Microwave Engineering*, Addison-Wesley, New York, 1990.

[18] Y. Li and Zheng Zhou, *A Novel Ultra-wideband Microstrip Quasi-horn Antenna Using Stepped Dielectric Substrate,* ISCIT, Sapporo, Japan, October, 2004.

[19] C. Nguyen, J. Lee, and J. Parkl, *Ultra-wideband microstrip quasi-horn antenna,* Electronics Letters, June 2001, Vol. 37, No.12.

[20] Jeongwoo Han, *Development of an Electronically Tunable Ultrawideband Radar Imaging Sensor and its Components*, PhD dissertation, Texas A&M, May 2005

[21] P. Gibson, *The Vivaldi aerial*, in Proc. 9th Eur. Microwave Conf., 1979, pp. 101–105.

[22] Grzegorz Brzezina, *Planar Antennas in LTCC Technology with Transceiver Integration Capability for Ultra-Wideband Applications*, IEEE Transactions on Microwave Theroy and Techniques, vol. 54, no. 6, June 2006.

[23] Xianming Qing et al., *Parametric Study of Ultra-Wideband Dual Elliptically Tapered Antipodal Slot Antenna*, International Journal of Antennas and Propagation, Volume 2008, Article ID 267197.

[24] Y. Yang, Y. Wang, and A. E. Fathy, *DESIGN OF COMPACT VIVALDI ANTENNA ARRAYS FOR UWB SEE THROUGH WALL APPLICATIONS*, Progress In Electromagnetics Research, PIER 82, 401–418, 2008.

[25] Albert K. Y. Lai, Albert L. Sinopoli, and Walter D. Burnside, *A Novel Antenna for Ultra-Wide-Band Applications*, IEEE TRANSACTIONS ON ANTENNAS AND PROPAGATION, VOL. 40, NO. 7, JULY 1992.

[26] K.C. Gupta, *Microstrip Lines and Slotlines*, Artech House, Inc., 1979.

[27] Andrew J Burkhardt, Christopher S Gregg and J Alan Staniforth, *Calculation of PCB Track Impedance*, on the web: http://www.polarinstruments.com/support/cits/IPC1999.pdf

[28] Slot Line Calculator, On the web: http://www1.sphere.ne.jp/i-lab/ilab/tool/sl_line_e.htm.

[29] Young-Gon Kim, Dong-Sik Woo, Kang Wook Kim, Young-Ki Cho, *Design of Bow-Tie-Type UWB Antennas Using an Ultra-wideband Balun*, 1-4244-0878, IEEE, 2007.

[30] David J. Heedy, *An Aperture-Matched Compact Range Feed Horn Design*, IEEE TRANSACTIONS ON ANTENNAS AND PROPAGATION. VOL. AP-33, NO. 11, NOVEMBER 1985.

[31] Skolnik, *Radar Handbook*, 2nd Edition, McGraw-Hill, Inc., 1990.

[32] Ulaby, *Microwave Remote Sensing Active and Passive*, *Volume II Radar Remote Sensing and Surface Scattering and Emission Theory*, Addison-Wesley Publishing Company, 1982.

[33] A. Lundberg, *Snow density variations: consequences for ground-penetrating radar*, HYDROLOGICAL PROCESSES, 20, 1483–1495 (2006)

APPENDICES

APPENDIX A

NORMALIZED POWER PATTERN (IN LINEAR SCALE) FOR LPDA ANTENNA

Normalized power pattern (in linear scale) for LPDA antenna at 3.1GHz

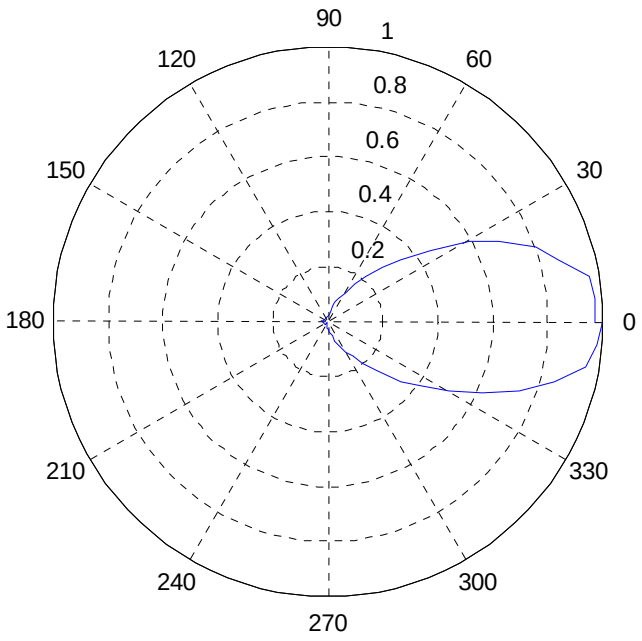

Normalized power pattern (in linear scale) for LPDA antenna at 3.5GHz

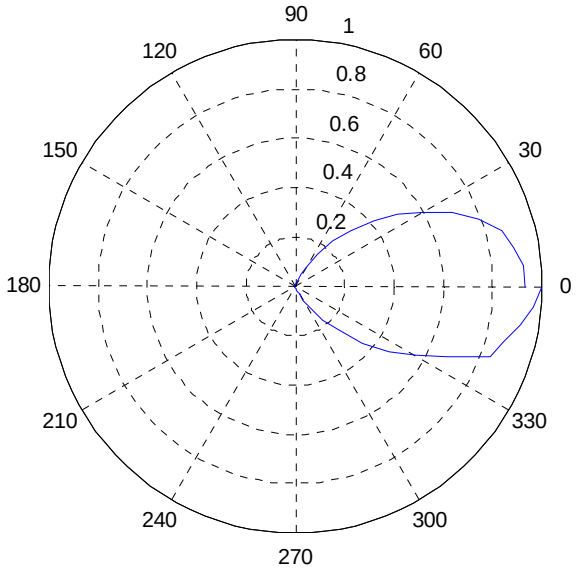

Normalized power pattern (in linear scale) for LPDA antenna at 4GHz

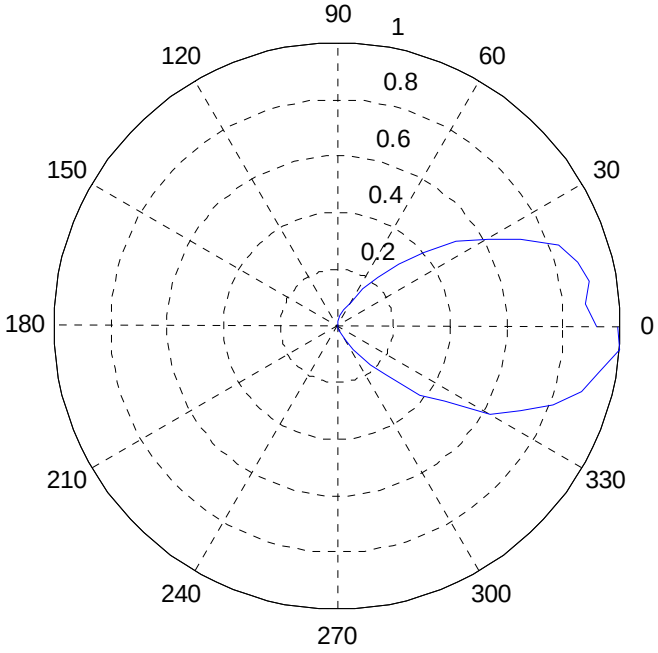

Normalized power pattern (in linear scale) for LPDA antenna at 4.5GHz

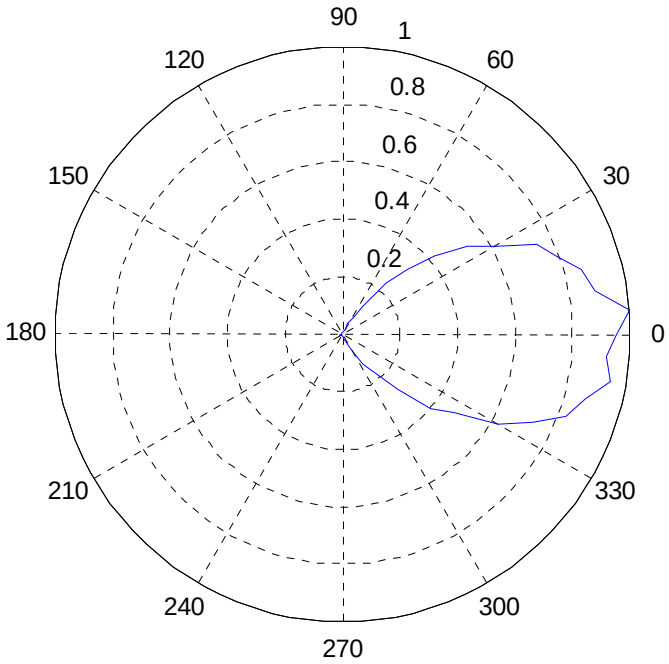

Normalized power pattern (in linear scale) for LPDA antenna at 5GHz

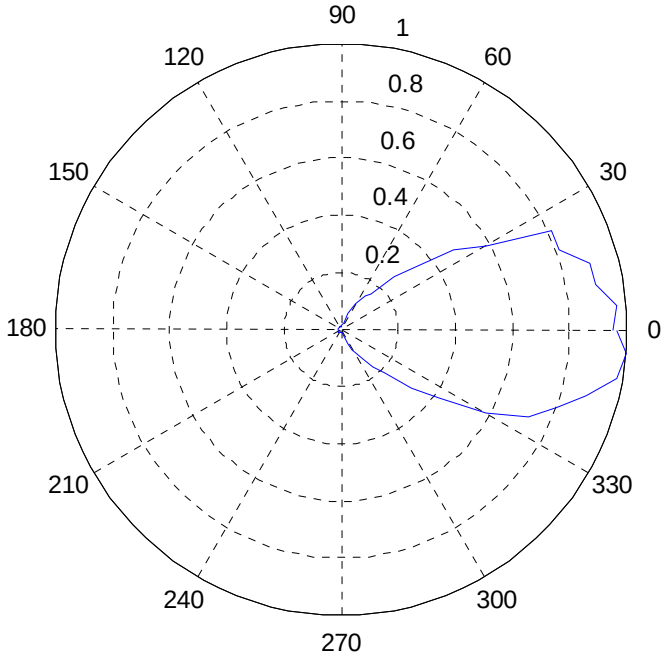

Normalized power pattern (in linear scale) for LPDA antenna at 5.5GHz

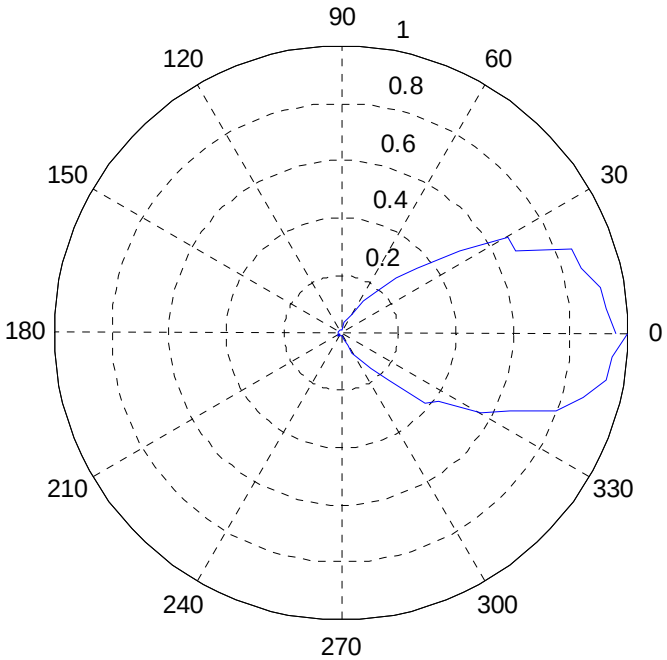

Normalized power pattern (in linear scale) for LPDA antenna at 6GHz

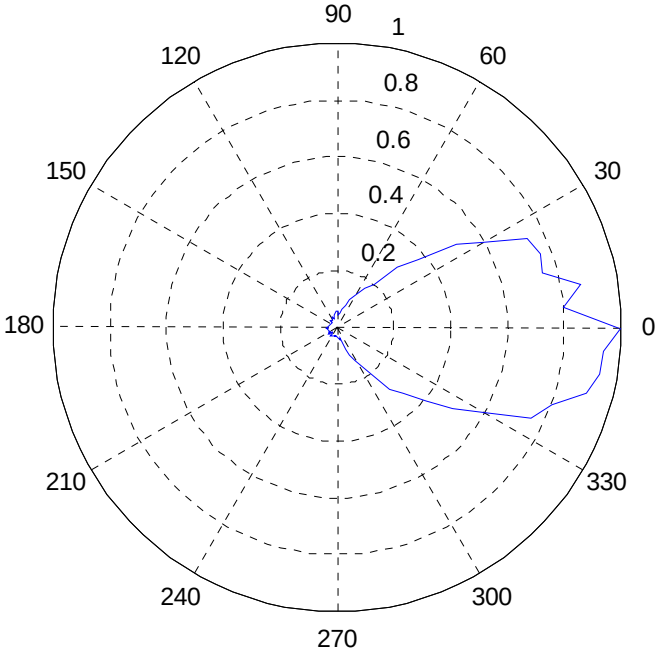

Normalized power pattern (in linear scale) for LPDA antenna at 6.5GHz

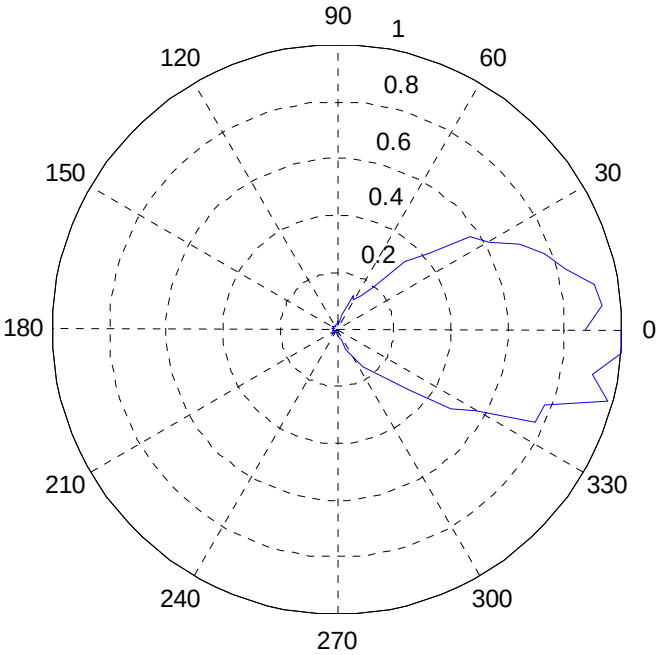

Normalized power pattern (in linear scale) for LPDA antenna at 7GHz

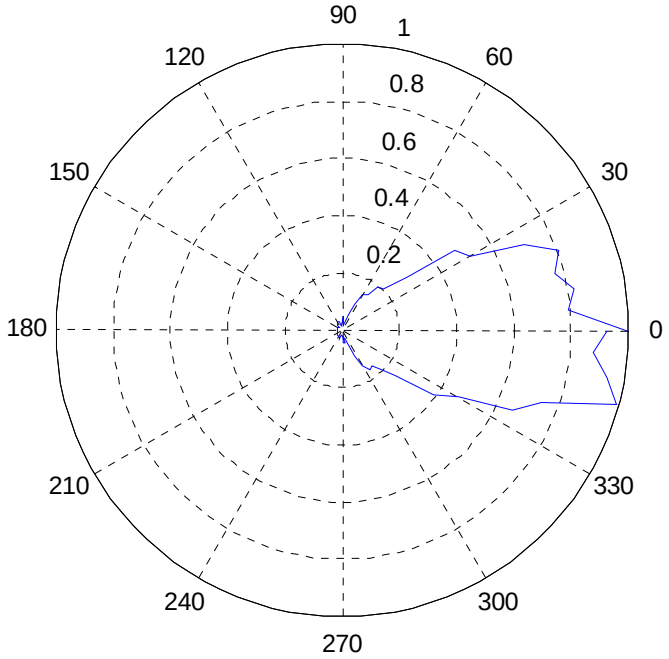

Normalized power pattern (in linear scale) for LPDA antenna at 7.5GHz

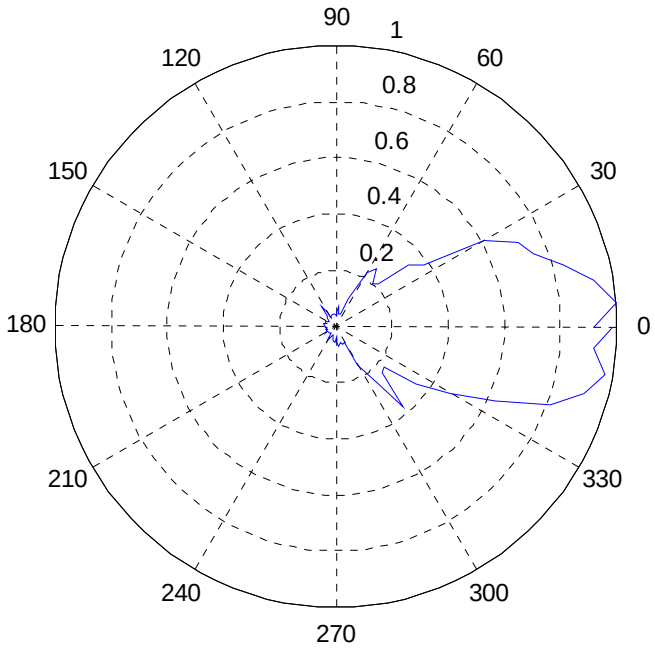

Normalized power pattern (in linear scale) for LPDA antenna at 8GHz

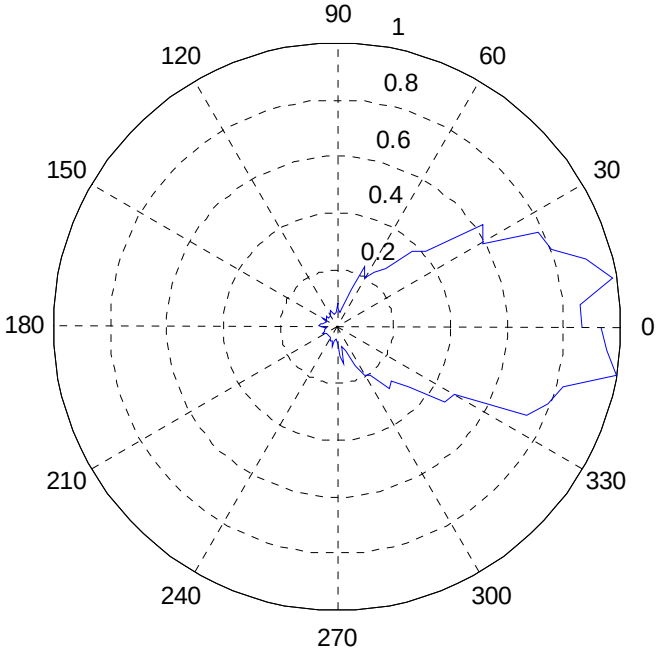

Normalized power pattern (in linear scale) for LPDA antenna at 8.5GHz

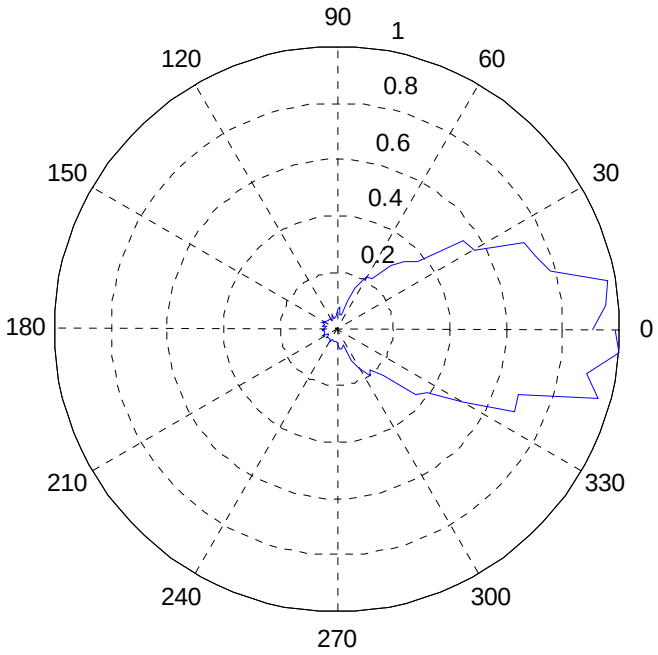

Normalized power pattern (in linear scale) for LPDA antenna at 9GHz

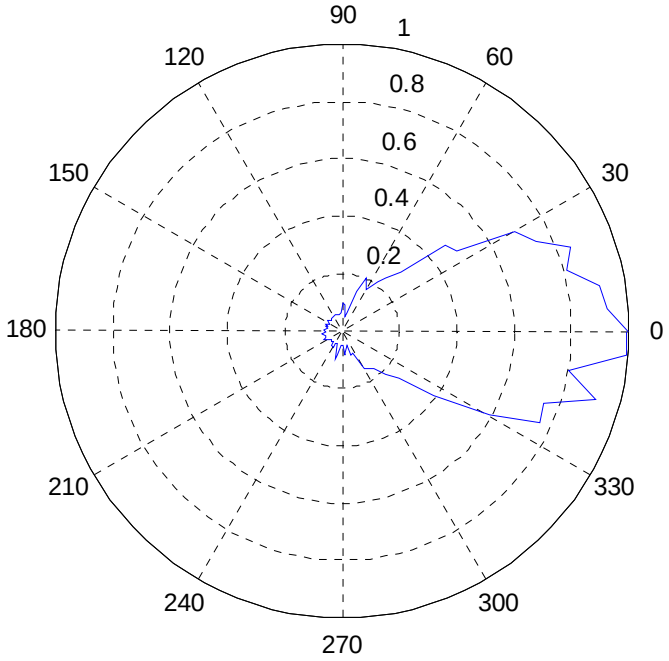

Normalized power pattern (in linear scale) for LPDA antenna at 9.5GHz

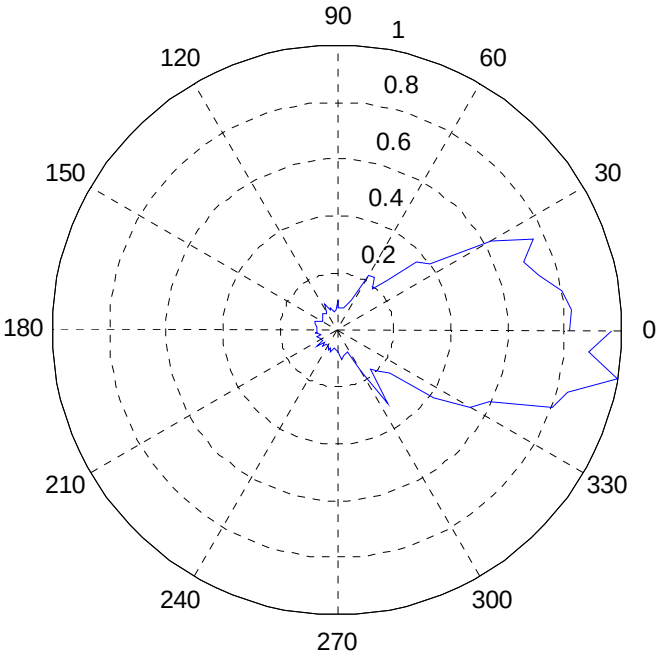

Normalized power pattern (in linear scale) for LPDA antenna at 10GHz

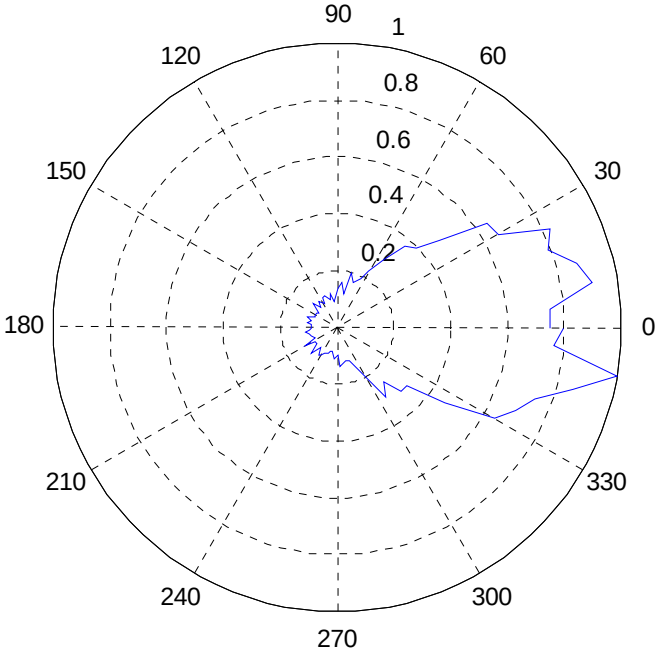

Normalized power pattern (in linear scale) for LPDA antenna at 10.5GHz

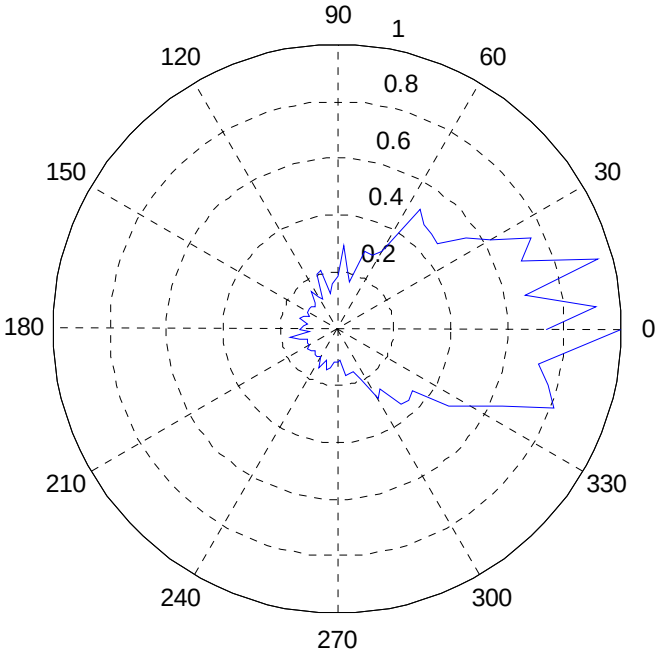

APPENDIX B

NORMALIZED POWER PATTERN (IN LINEAR SCALE) FOR QUASI-HORN ANTENNA

Normalized power pattern (in linear scale) for quasi-horn antenna at 3.1GHz

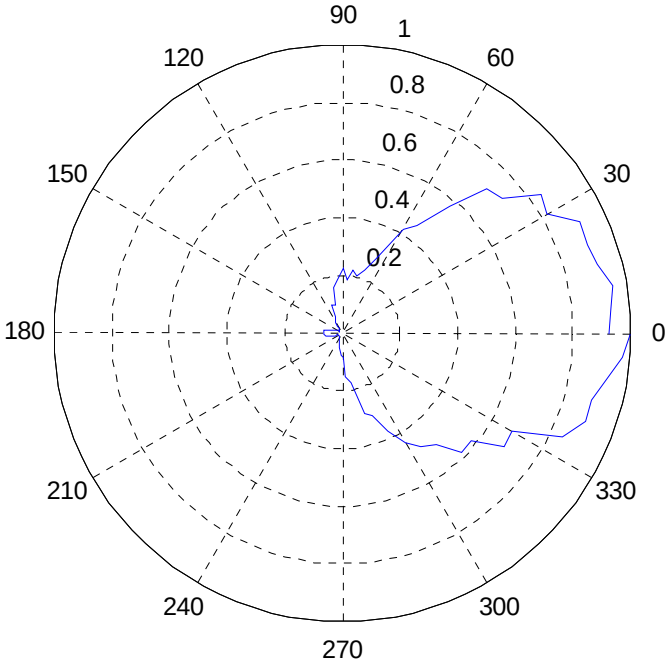

Normalized power pattern (in linear scale) for quasi-horn antenna at 3.5GHz

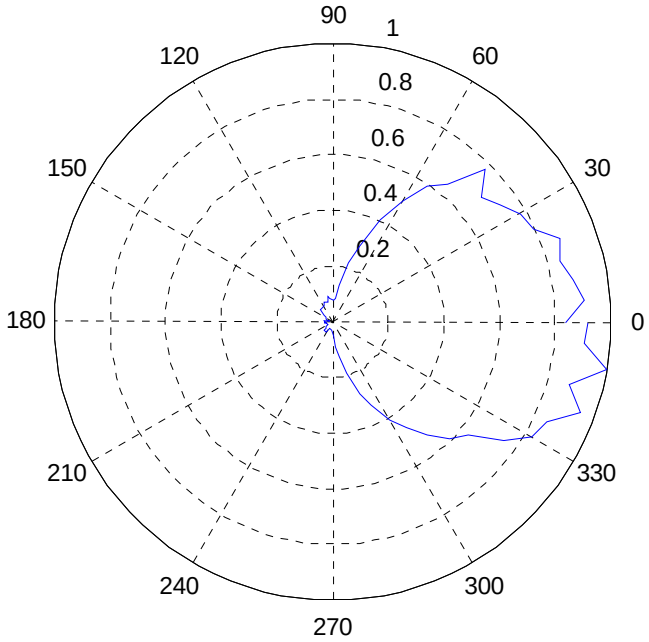

Normalized power pattern (in linear scale) for quasi-horn antenna at 4GHz

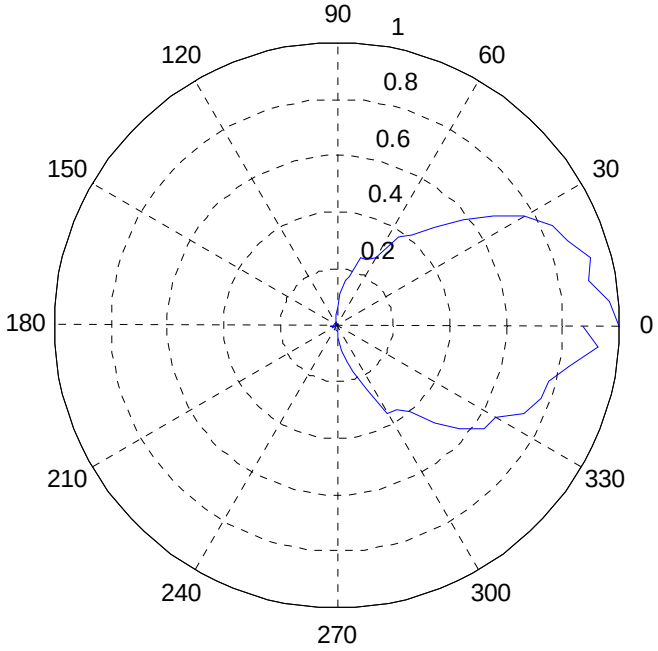

Normalized power pattern (in linear scale) for quasi-horn antenna at 4.5GHz

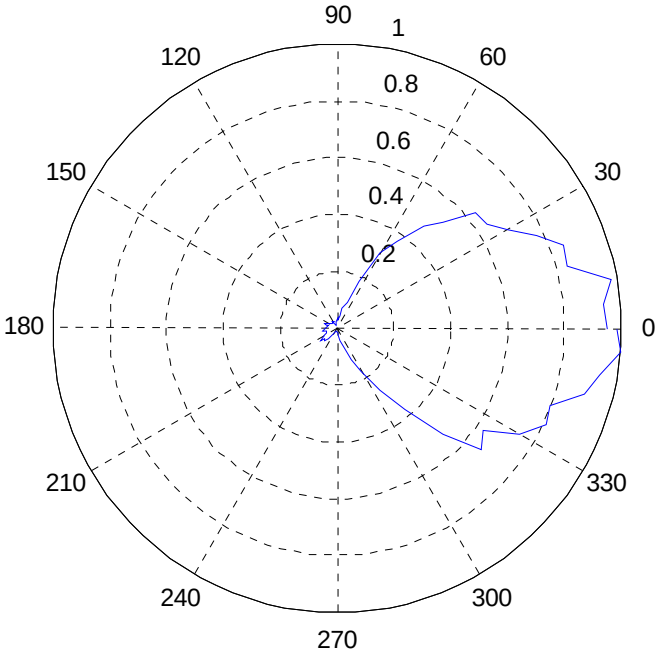

Normalized power pattern (in linear scale) for quasi-horn antenna at 5GHz

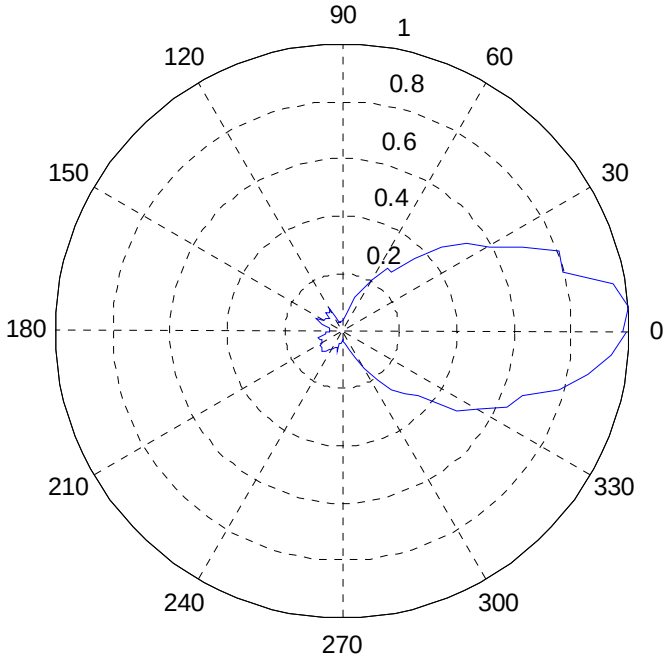

Normalized power pattern (in linear scale) for quasi-horn antenna at 5.5GHz

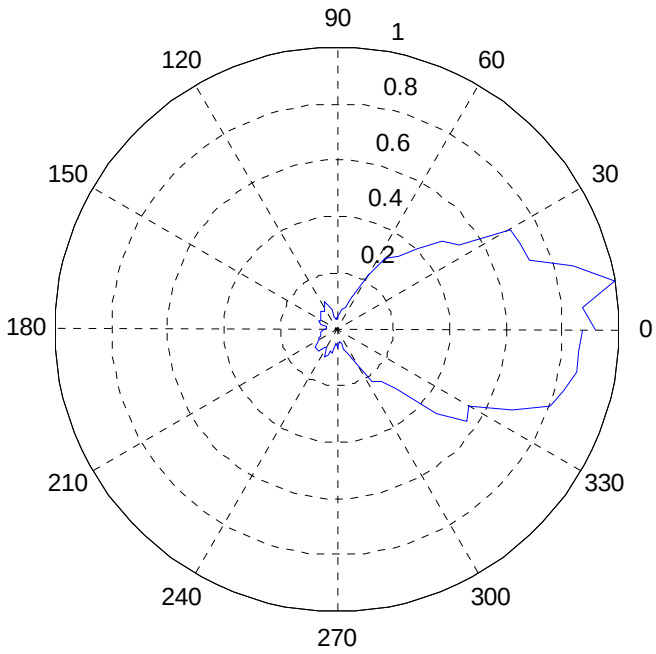

Normalized power pattern (in linear scale) for quasi-horn antenna at 6GHz

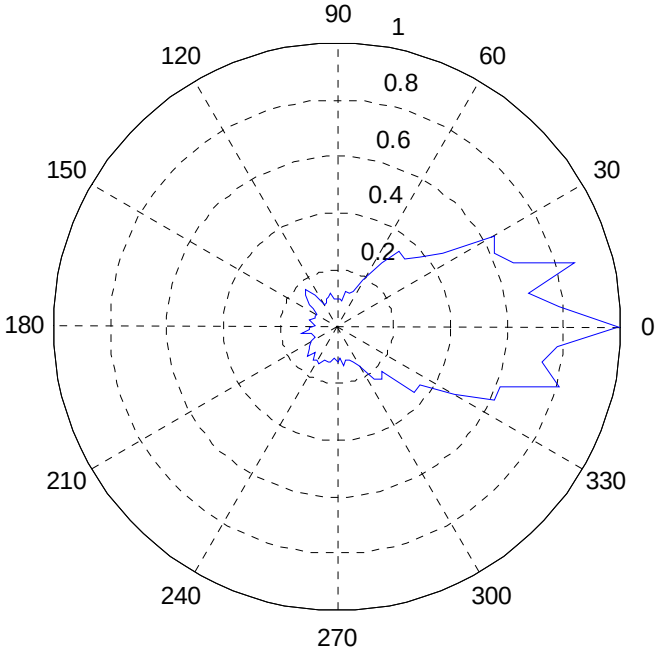

Normalized power pattern (in linear scale) for quasi-horn antenna at 6.5GHz

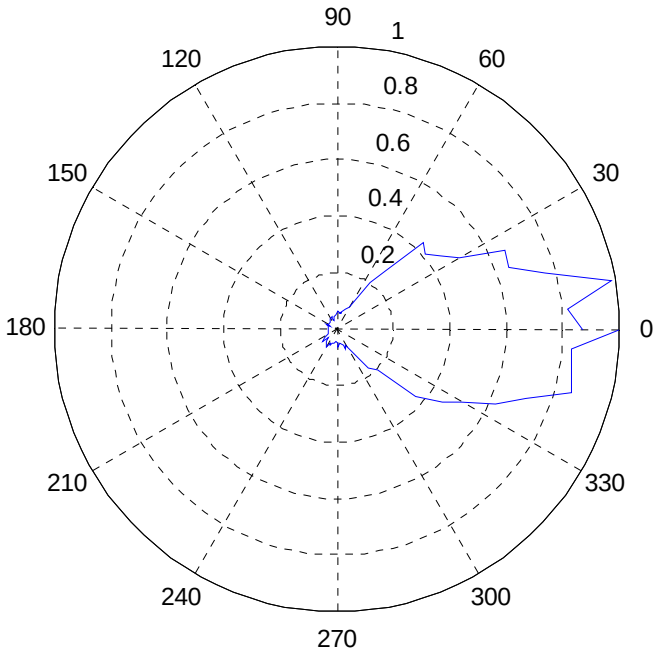

Normalized power pattern (in linear scale) for quasi-horn antenna at 7GHz

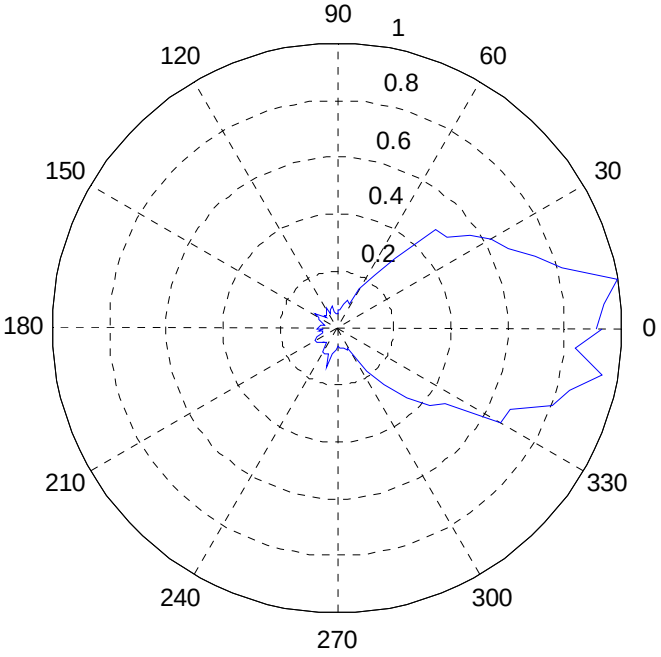

Normalized power pattern (in linear scale) for quasi-horn antenna at 7.5GHz

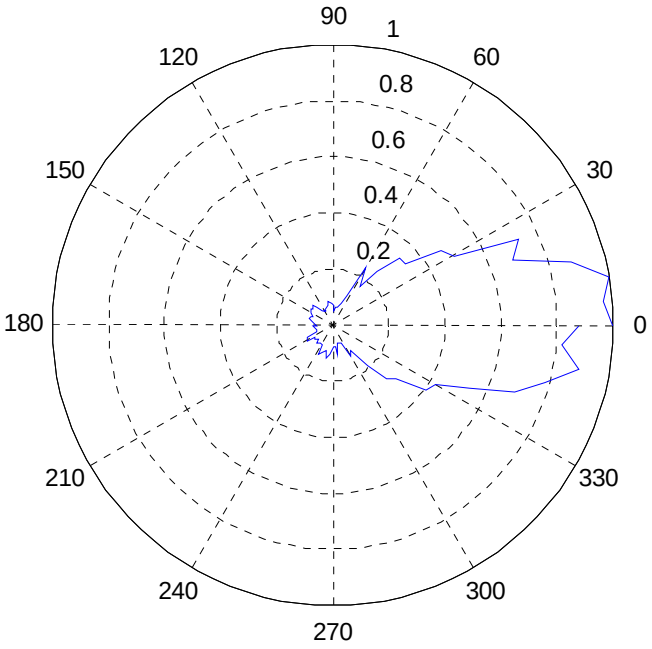

Normalized power pattern (in linear scale) for quasi-horn antenna at 8GHz

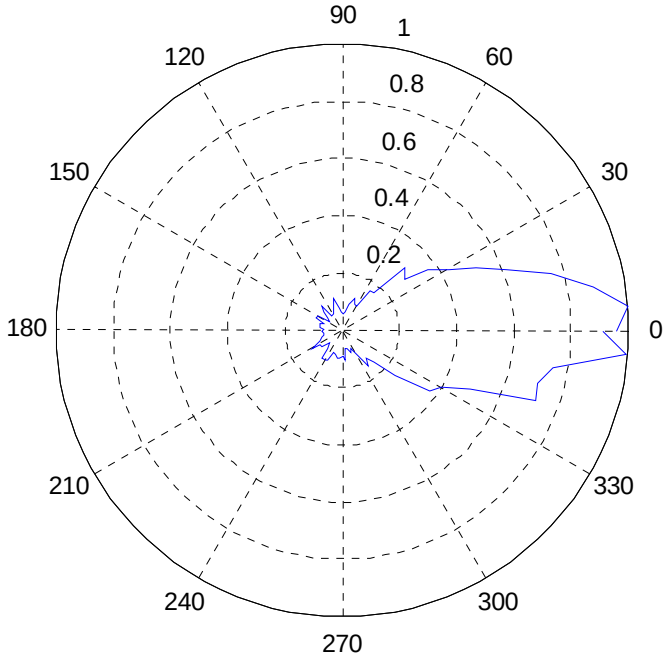

Normalized power pattern (in linear scale) for quasi-horn antenna at 8.5GHz

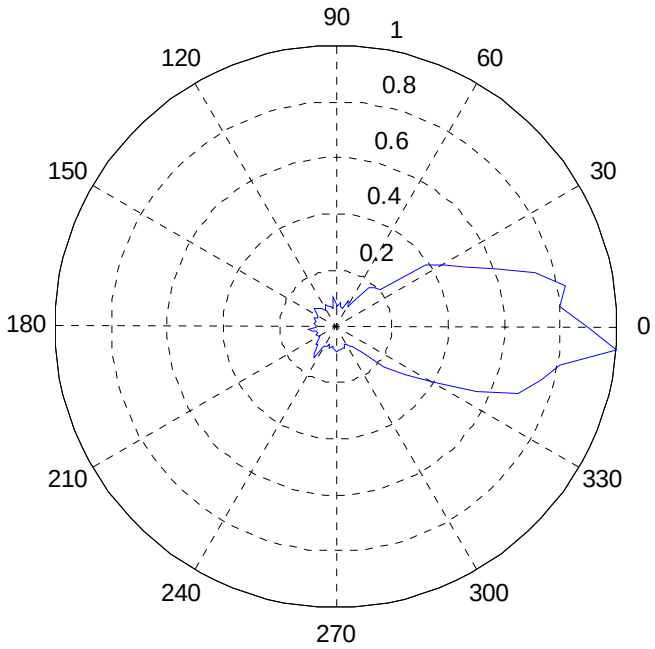

Normalized power pattern (in linear scale) for quasi-horn antenna at 9GHz

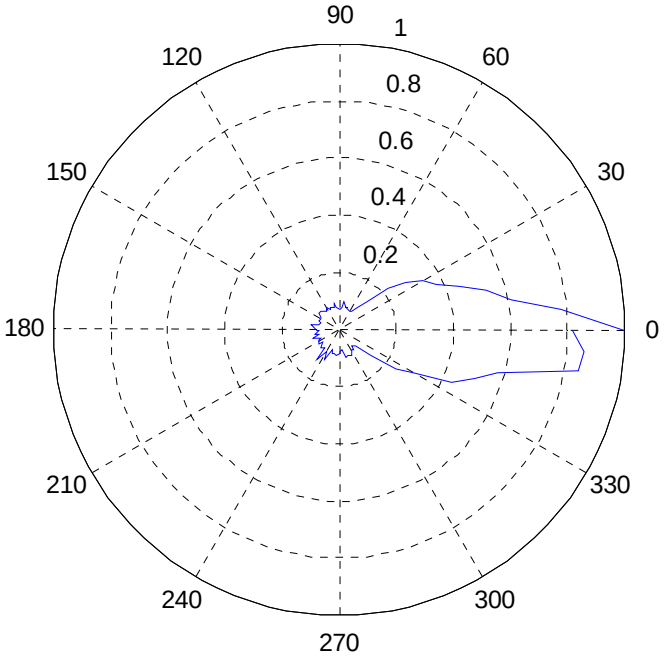

Normalized power pattern (in linear scale) for quasi-horn antenna at 9.5GHz

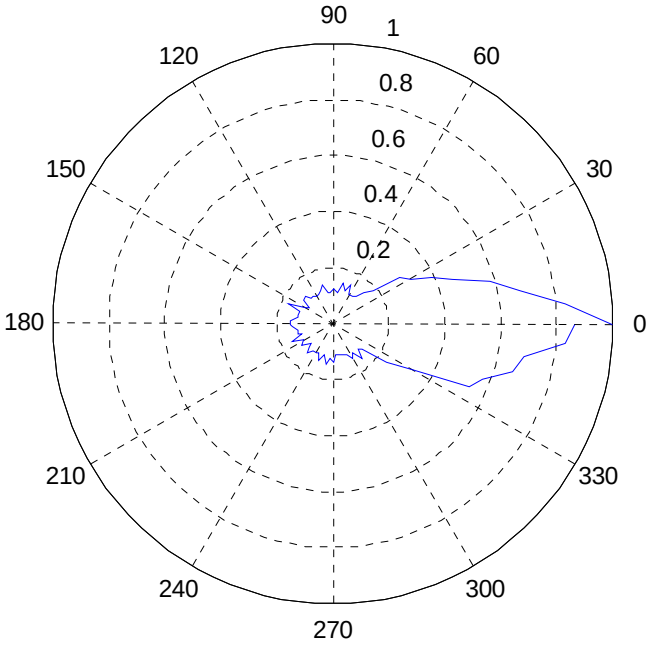

Normalized power pattern (in linear scale) for quasi-horn antenna at 10GHz

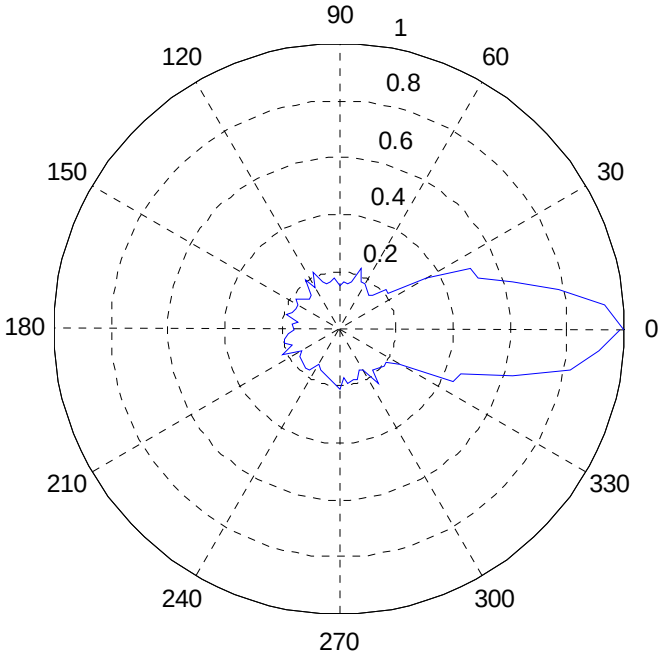

Normalized power pattern (in linear scale) for quasi-horn antenna at 10.5GHz

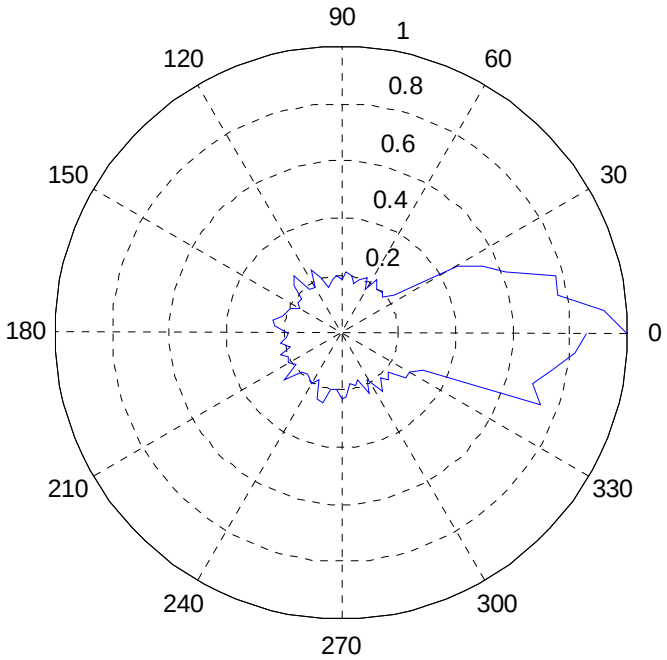

APPENDIX C

NORMALIZED POWER PATTERN (IN LINEAR SCALE) FOR PULSE ON 200 ANTENNA WITH CORNER REFLECTOR

Normalized power pattern (in linear scale) for Pulse ON 200 antenna with corner reflector at 3.1GHz

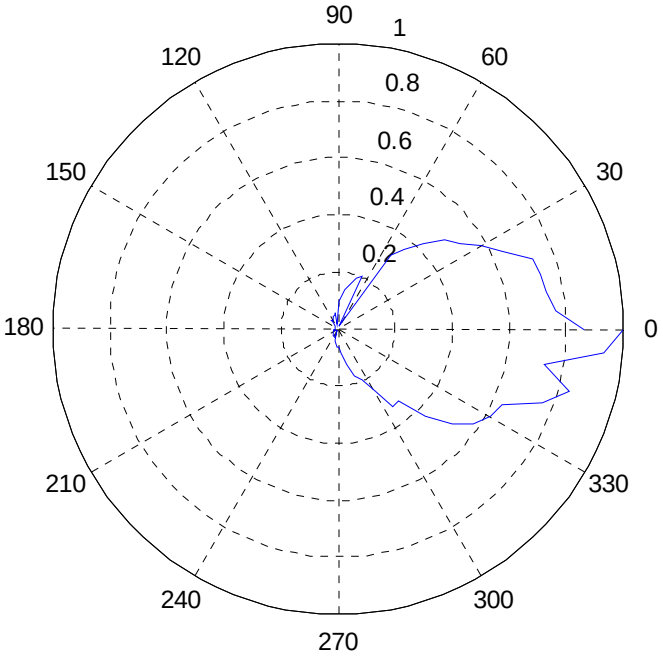

Normalized power pattern (in linear scale) for Pulse ON 200 antenna with corner reflector at 3.5GHz

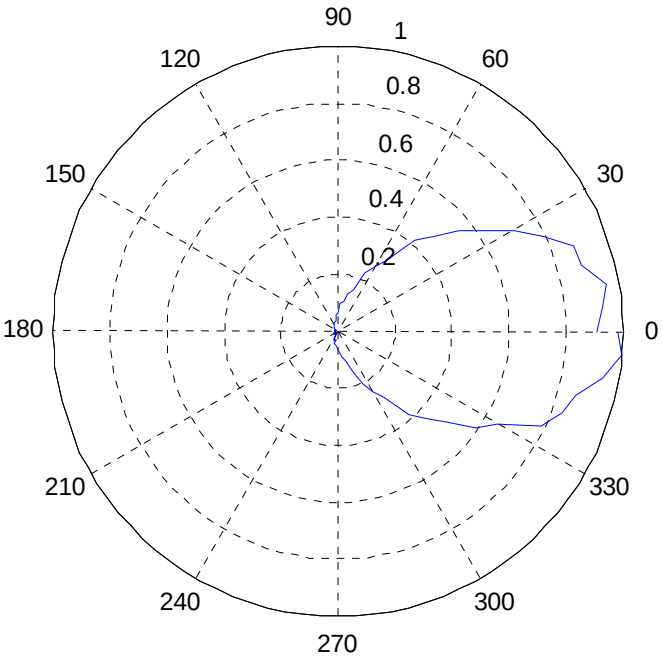

Normalized power pattern (in linear scale) for Pulse ON 200 antenna with corner reflector at 4GHz

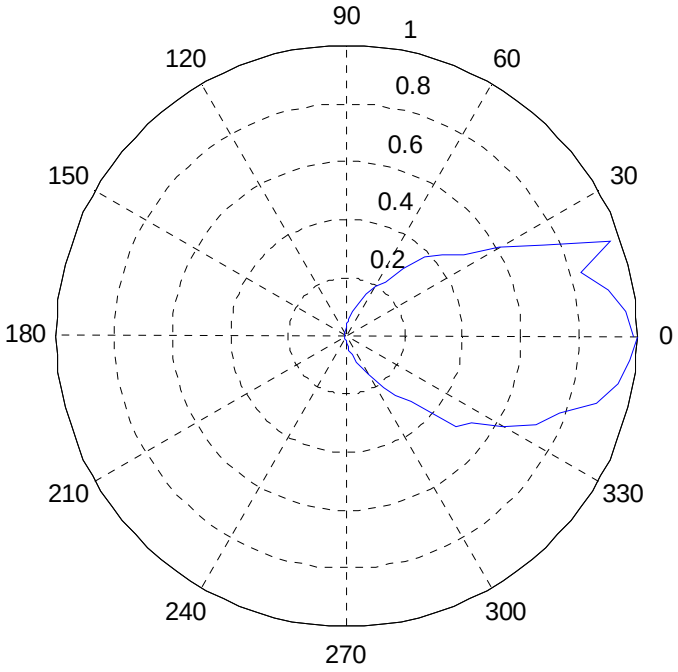

Normalized power pattern (in linear scale) for Pulse ON 200 antenna with corner reflector at 4.5GHz

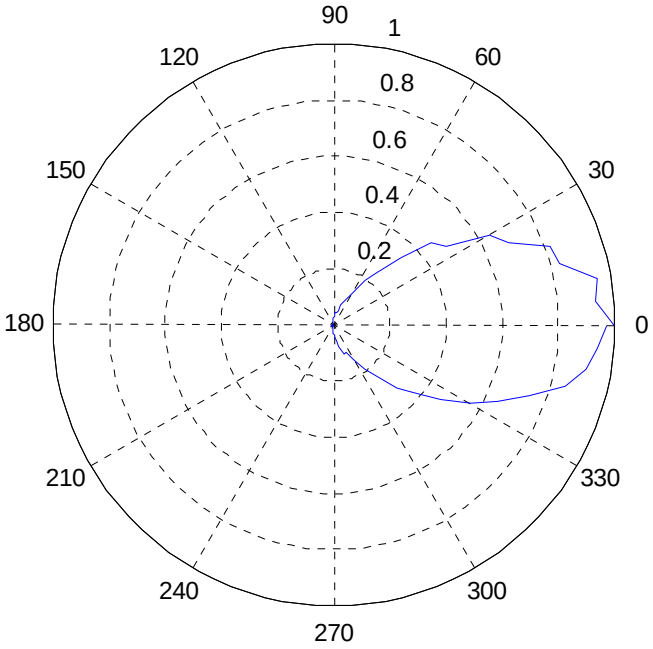

Normalized power pattern (in linear scale) for Pulse ON 200 antenna with corner reflector at 5GHz

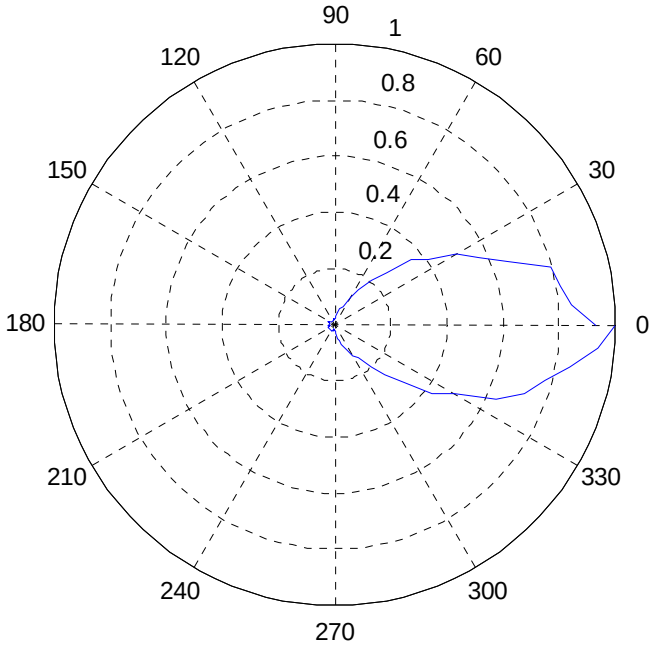

Normalized power pattern (in linear scale) for Pulse ON 200 antenna with corner reflector at 5.5GHz

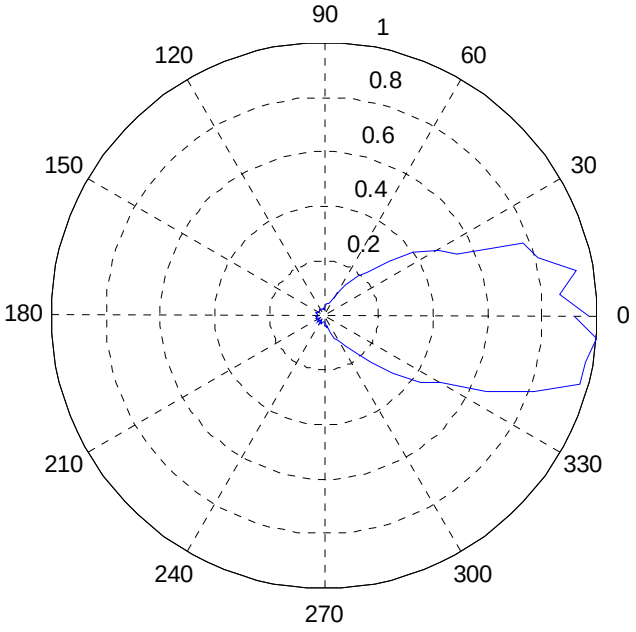

Normalized power pattern (in linear scale) for Pulse ON 200 antenna with corner reflector at 6GHz

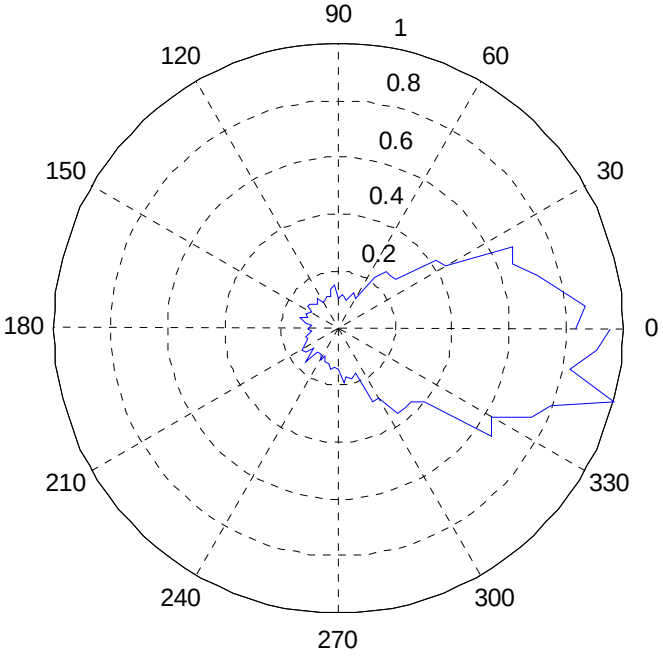

Normalized power pattern (in linear scale) for Pulse ON 200 antenna with corner reflector at 6.5GHz

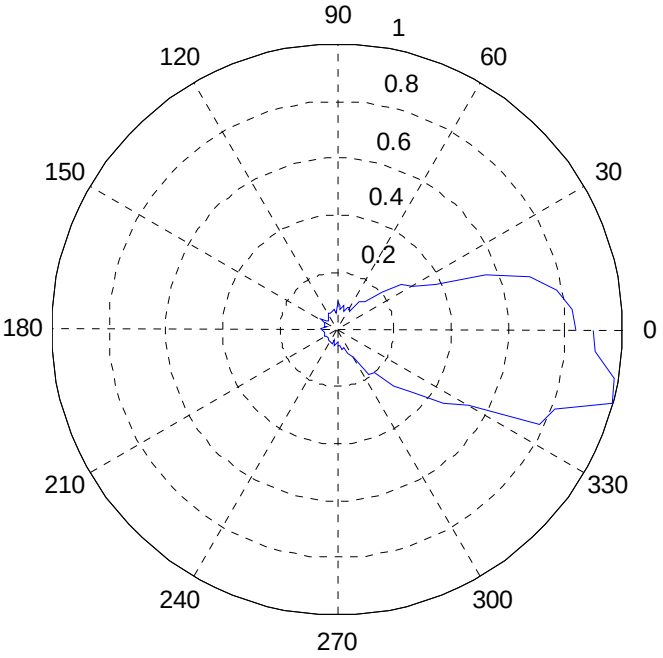

Normalized power pattern (in linear scale) for Pulse ON 200 antenna with corner reflector at 7GHz

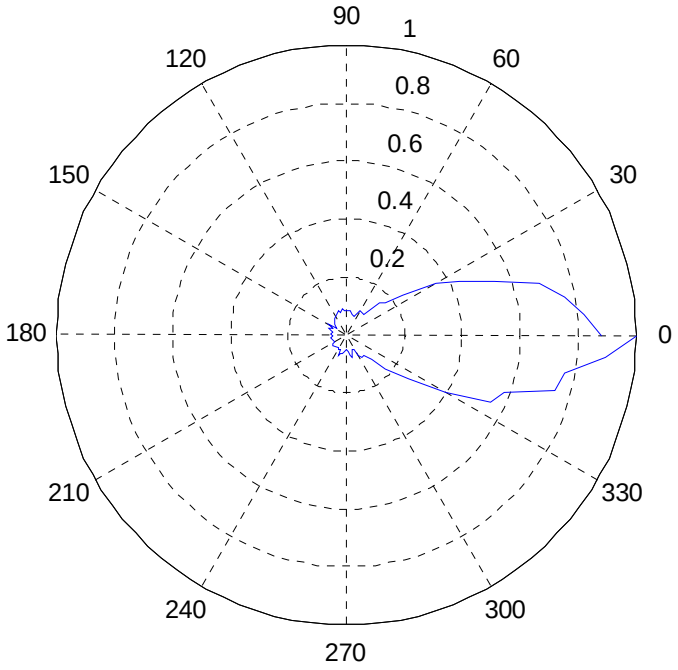

Normalized power pattern (in linear scale) for Pulse ON 200 antenna with corner reflector at 7.5GHz

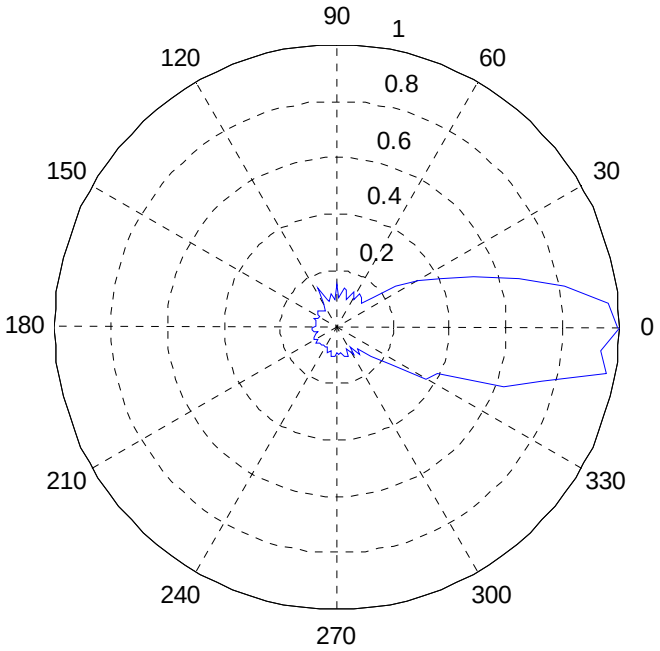

Normalized power pattern (in linear scale) for Pulse ON 200 antenna with corner reflector at 8GHz

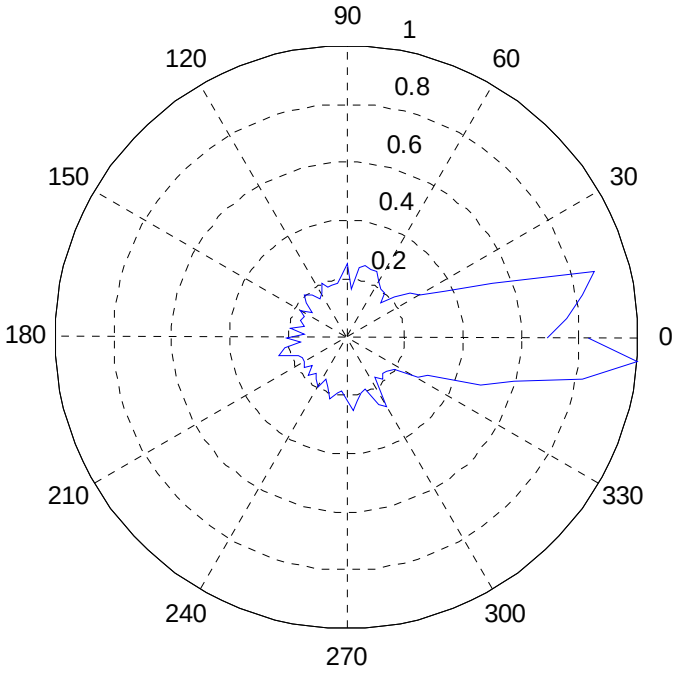

Normalized power pattern (in linear scale) for Pulse ON 200 antenna with corner reflector at 8.5GHz

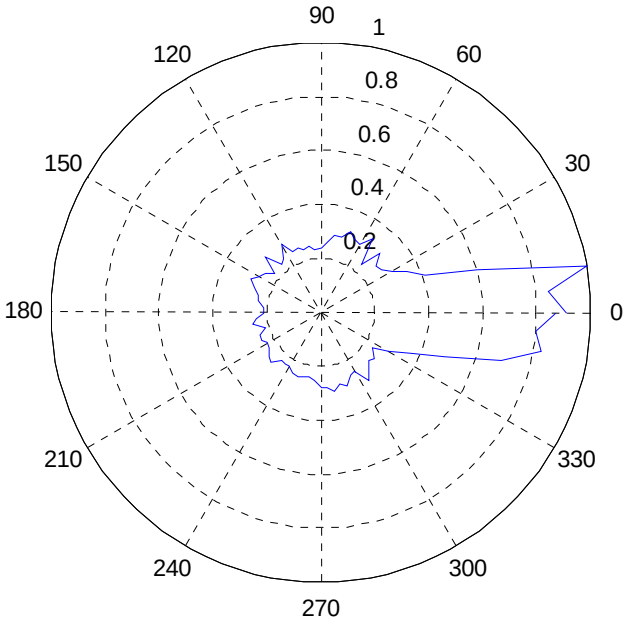

Normalized power pattern (in linear scale) for Pulse ON 200 antenna with corner reflector at 9GHz

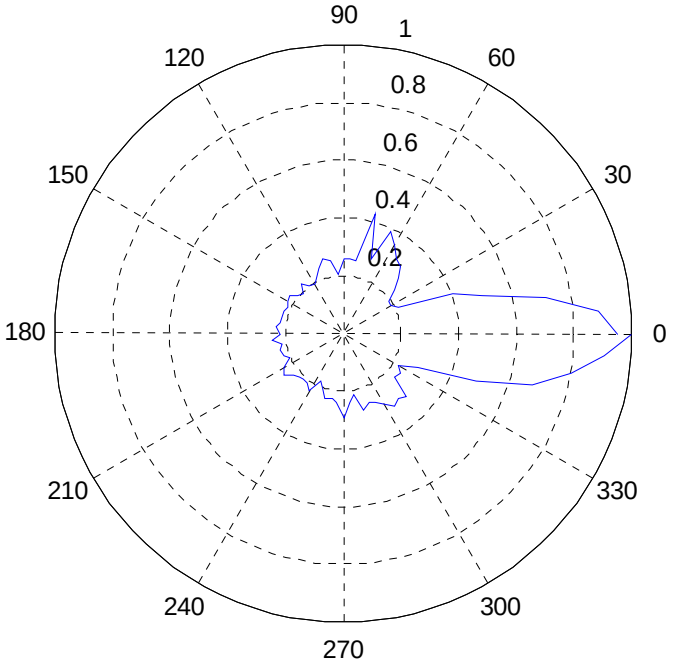

Normalized power pattern (in linear scale) for Pulse ON 200 antenna with corner reflector at 9.5GI

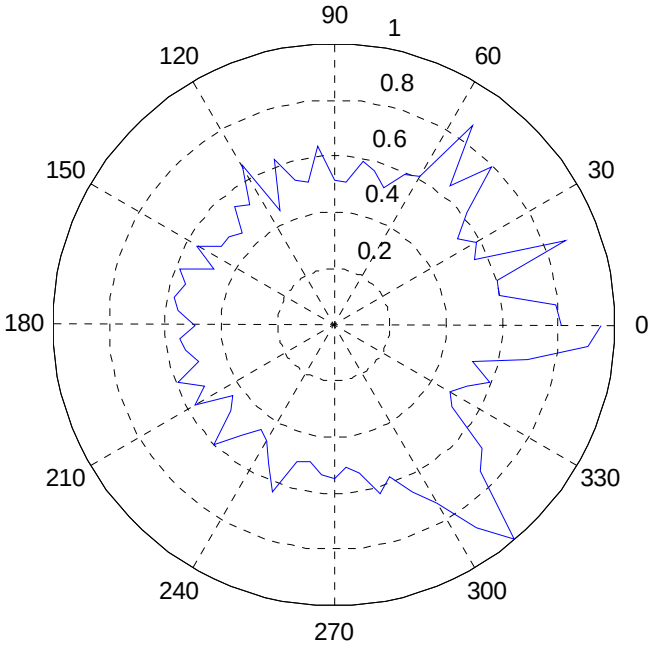

Normalized power pattern (in linear scale) for Pulse ON 200 antenna with corner reflector at 10GH

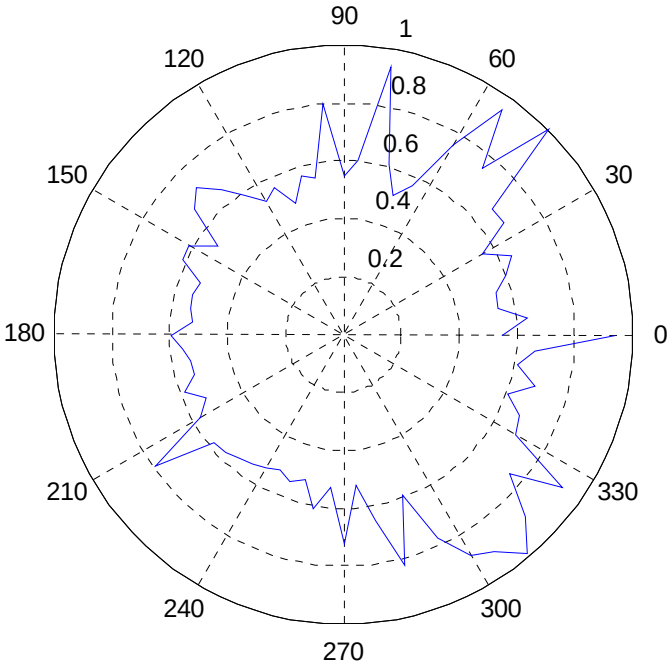

Normalized power pattern (in linear scale) for Pulse ON 200 antenna with corner reflector at 10.5GHz

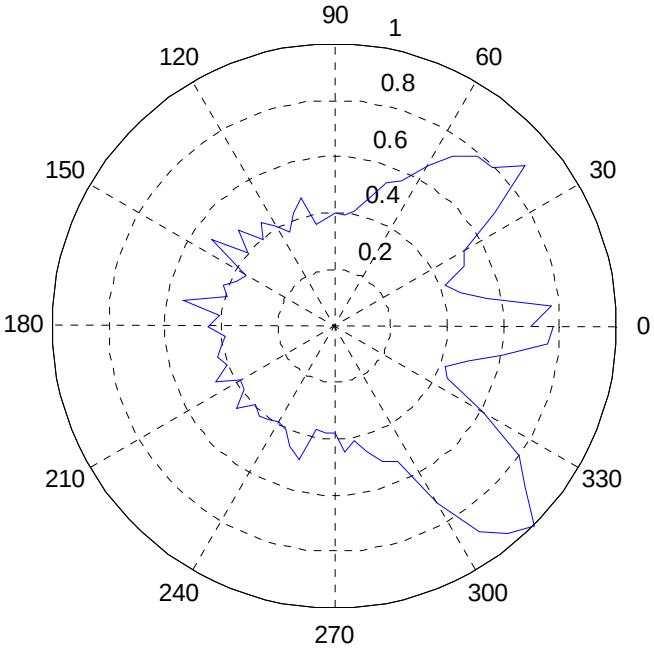

APPENDIX D

NORMALIZED POWER PATTERN (IN LINEAR SCALE) FOR VIVALDI ANTENNA ON FR4 SUBSTRATE

Normalized power pattern (in linear scale) for Vivaldi antenna on FR4 at3.1GHz

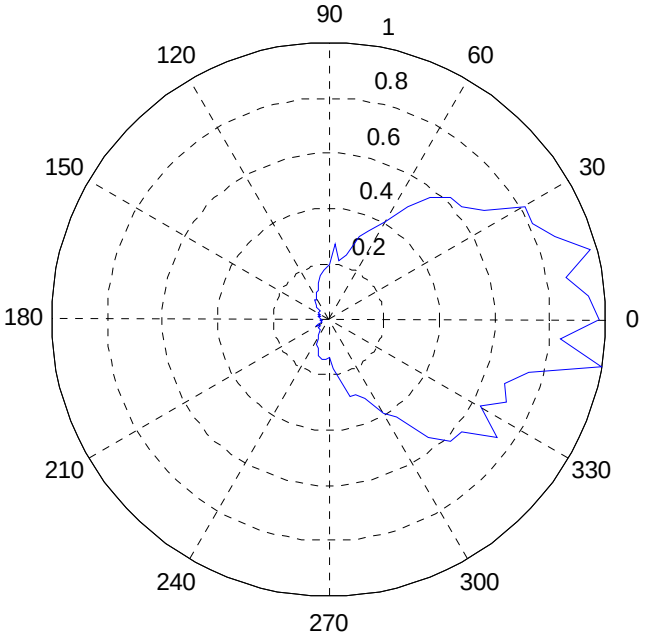

Normalized power pattern (in linear scale) for Vivaldi antenna on FR4 at 3.5GHz

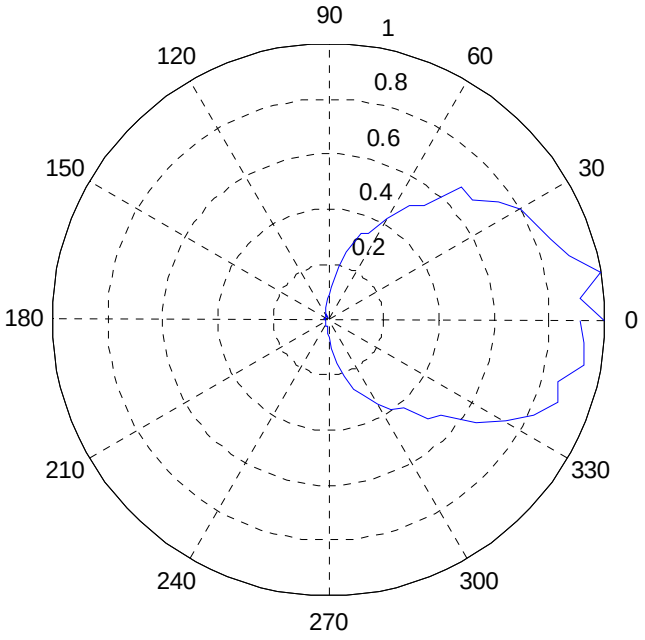

Normalized power pattern (in linear scale) for Vivaldi antenna on FR4 at 4GHz

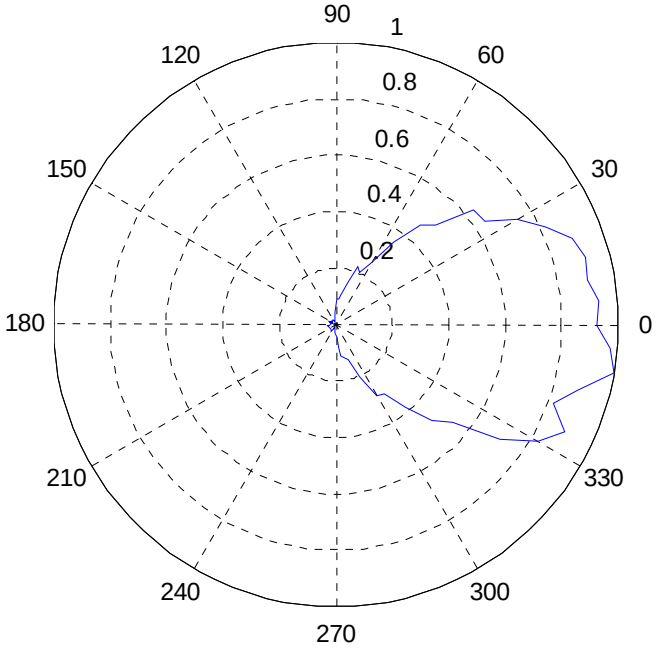

Normalized power pattern (in linear scale) for Vivaldi antenna on FR4 at 4.5GHz

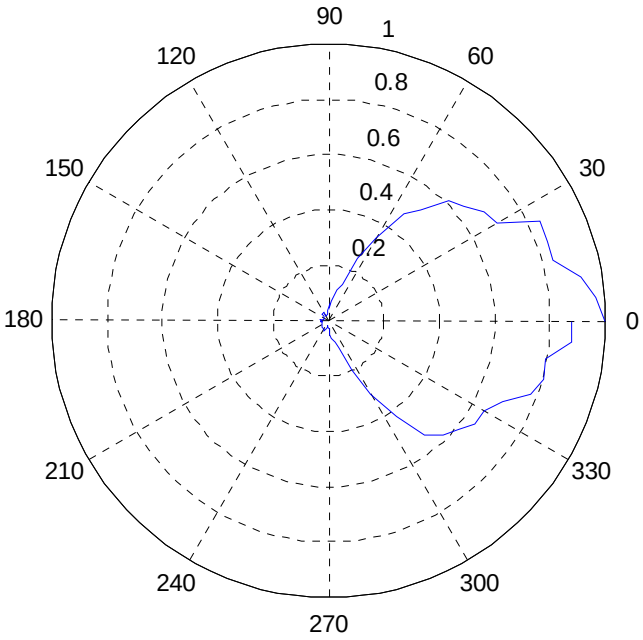

Normalized power pattern (in linear scale) for Vivaldi antenna on FR4 at 5GHz

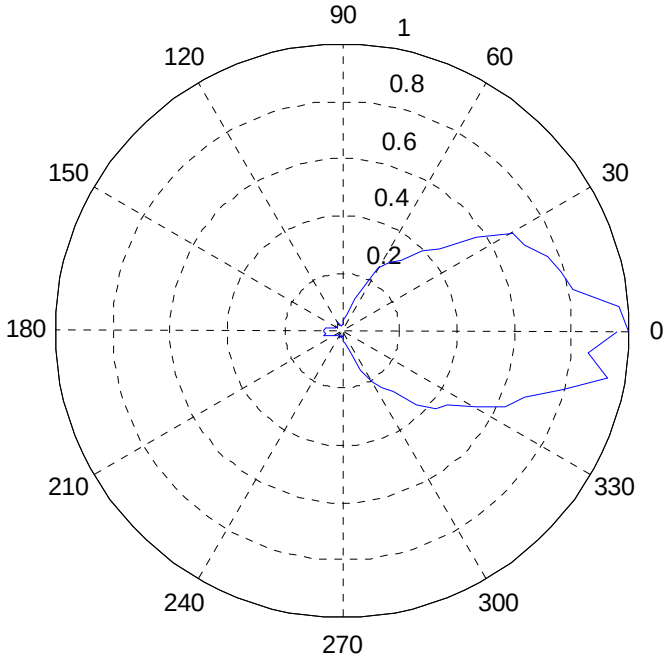

Normalized power pattern (in linear scale) for Vivaldi antenna on FR4 at 5.5GHz

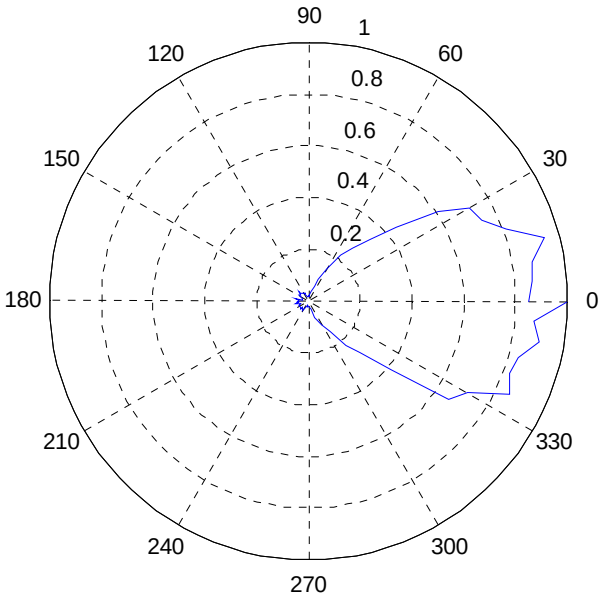

Normalized power pattern (in linear scale) for Vivaldi antenna on FR4 at 6GHz

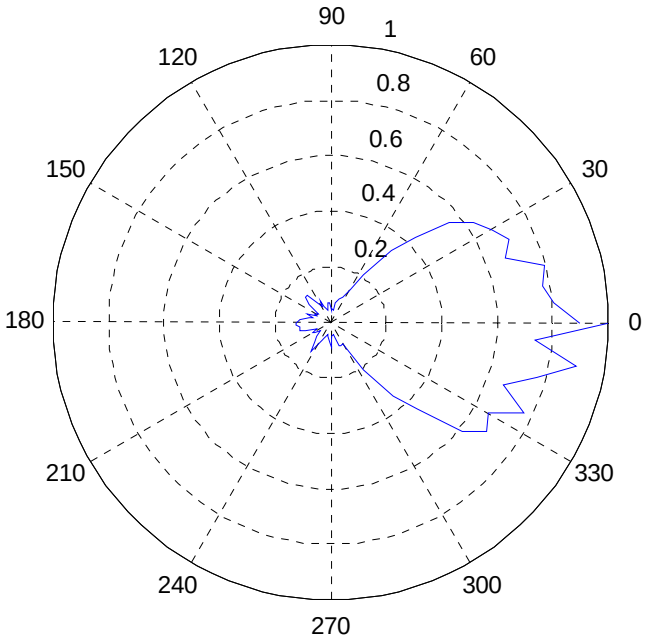

Normalized power pattern (in linear scale) for Vivaldi antenna on FR4 at 6.5GHz

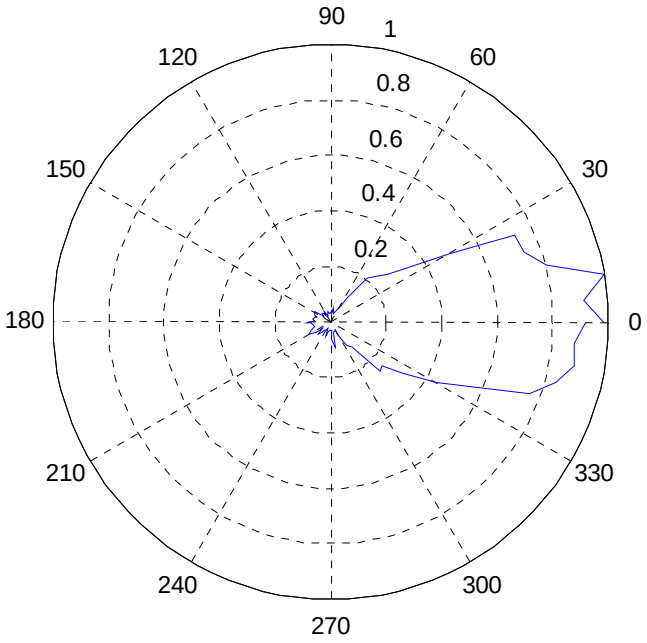

Normalized power pattern (in linear scale) for Vivaldi antenna on FR4 at 7GHz

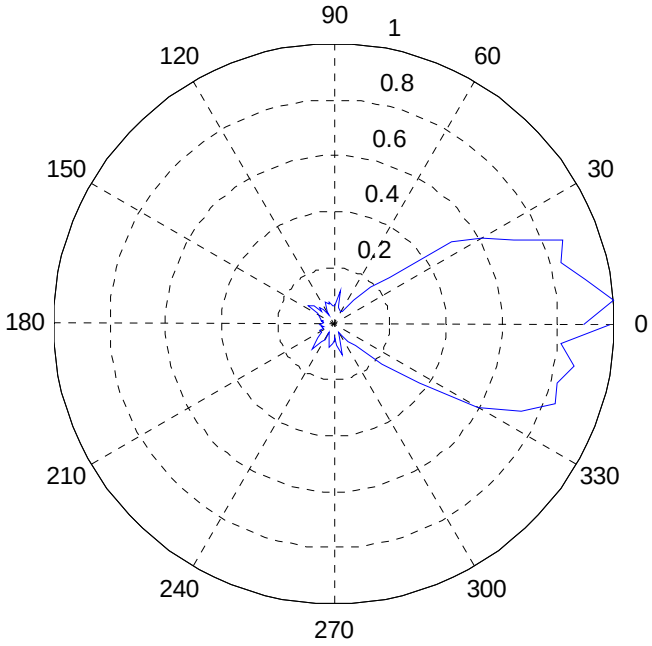

Normalized power pattern (in linear scale) for Vivaldi antenna on FR4 at 7.5GHz

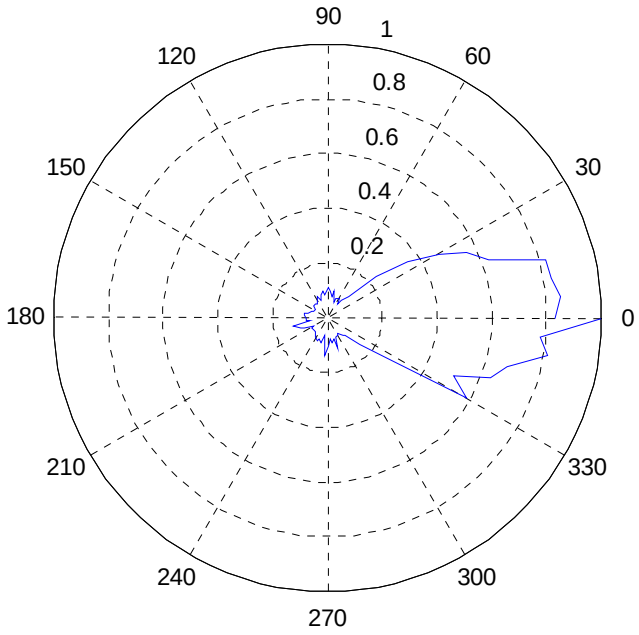

Normalized power pattern (in linear scale) for Vivaldi antenna on FR4 at 8GHz

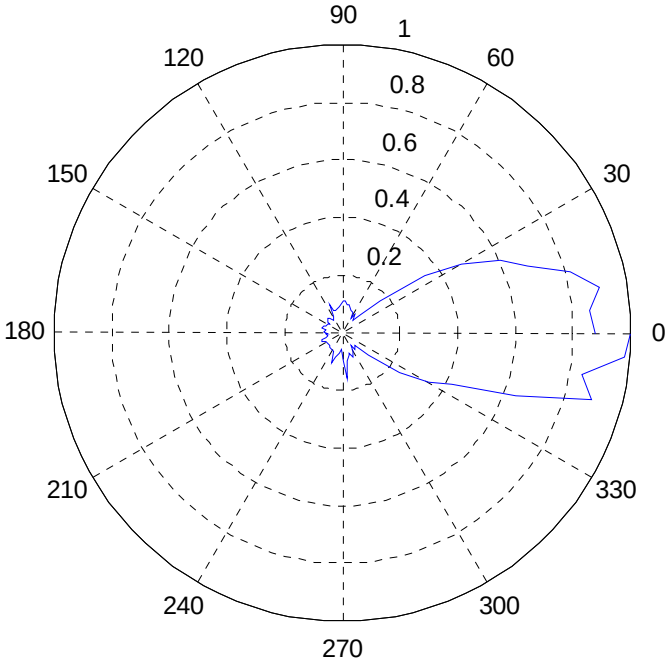

Normalized power pattern (in linear scale) for Vivaldi antenna on FR4 at 8.5GHz

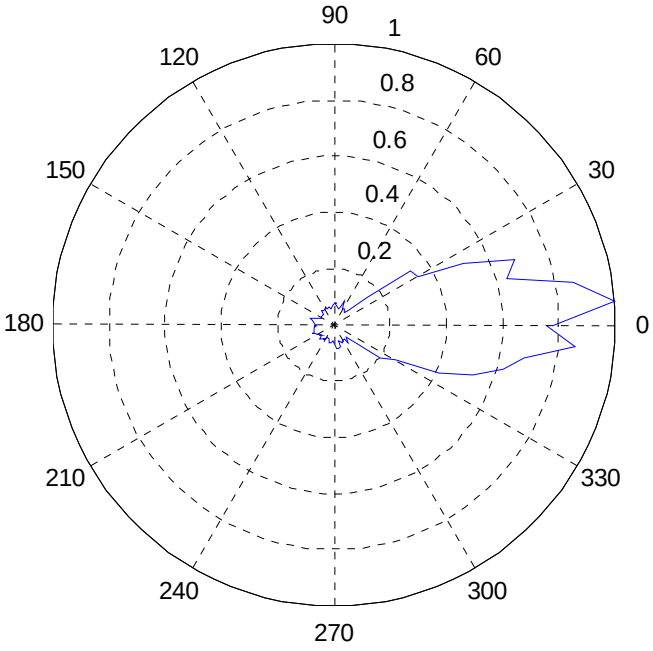

Normalized power pattern (in linear scale) for Vivaldi antenna on FR4 at 9GHz

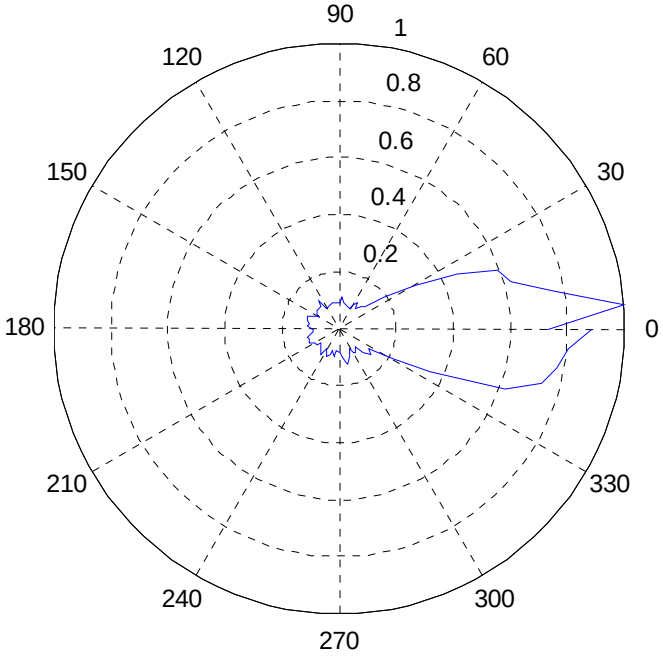

Normalized power pattern (in linear scale) for Vivaldi antenna on FR4 at 9.5GHz

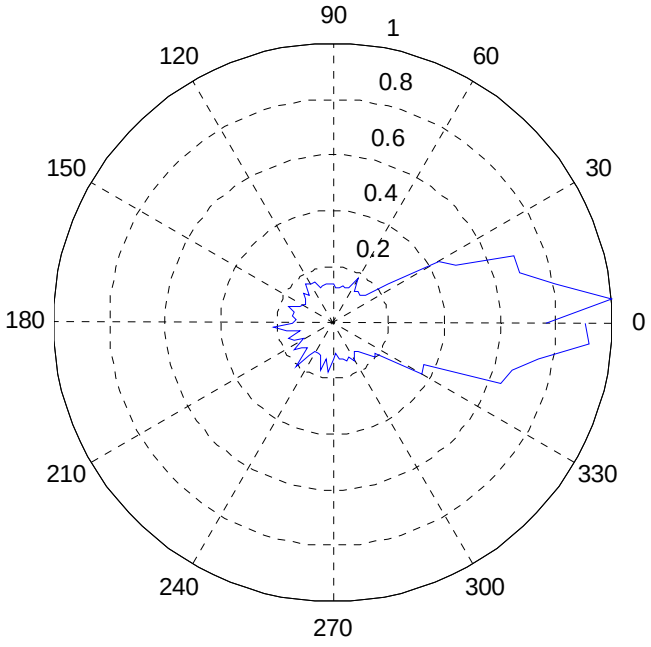

Normalized power pattern (in linear scale) for Vivaldi antenna on FR4 at 10.5GHz

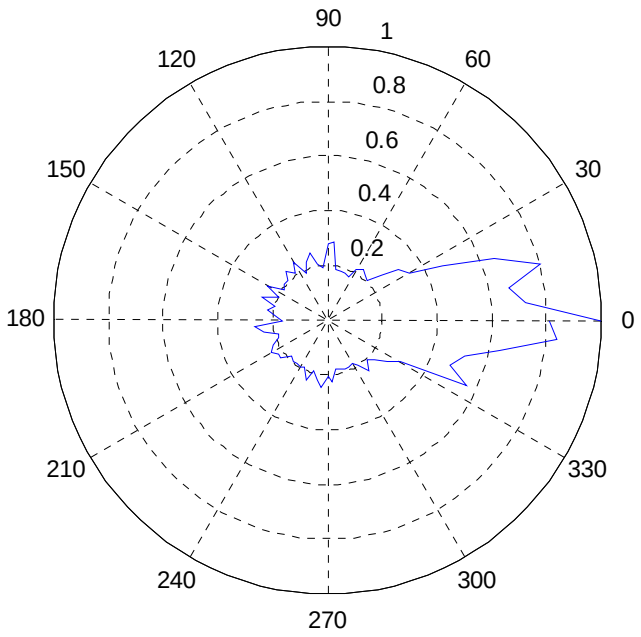

Normalized power pattern (in linear scale) for Vivaldi antenna on FR4 at 10GHz

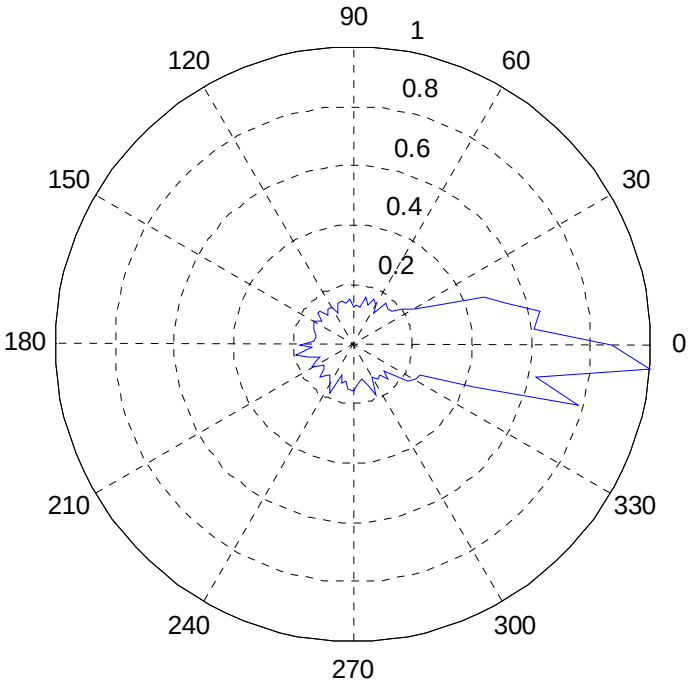

APPENDIX E

NORMALIZED POWER PATTERN (IN LINEAR SCALE) FOR VIVALDI ANTENNA ON RO4003 SUBSTRATE

Normalized power pattern (in linear scale) for Vivaldi antenna on RO4003 at3.1GHz

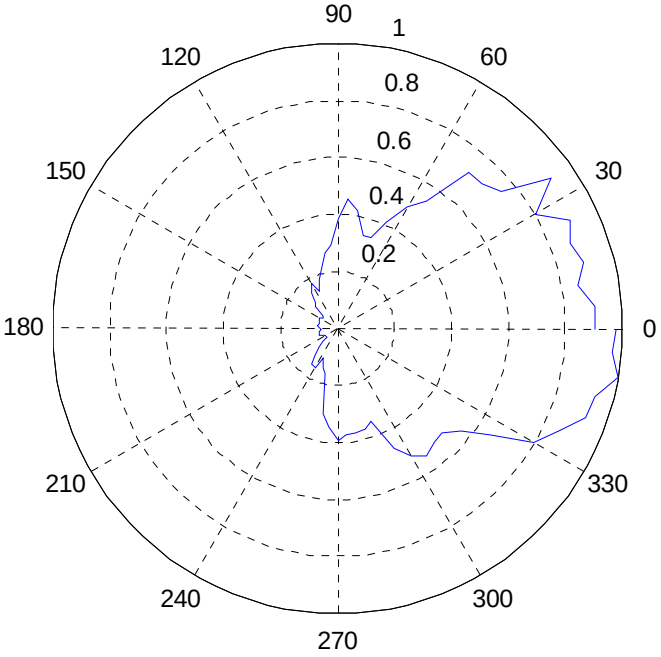

Normalized power pattern (in linear scale) for Vivaldi antenna on RO4003 at 3.5GHz

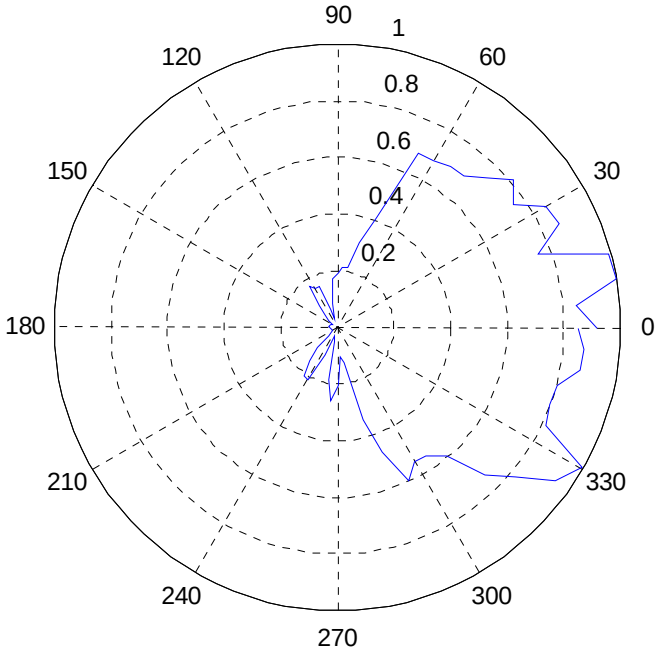

Normalized power pattern (in linear scale) for Vivaldi antenna on RO4003 at 4GHz

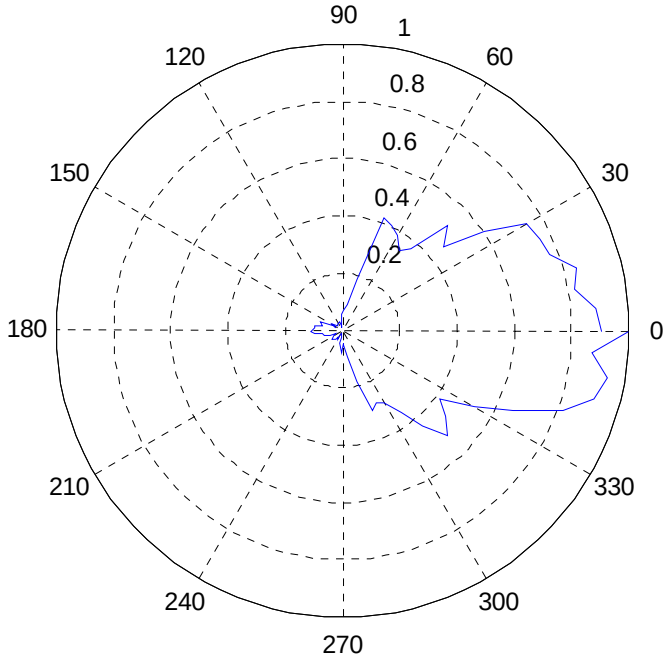

Normalized power pattern (in linear scale) for Vivaldi antenna on RO4003 at 4.5GHz

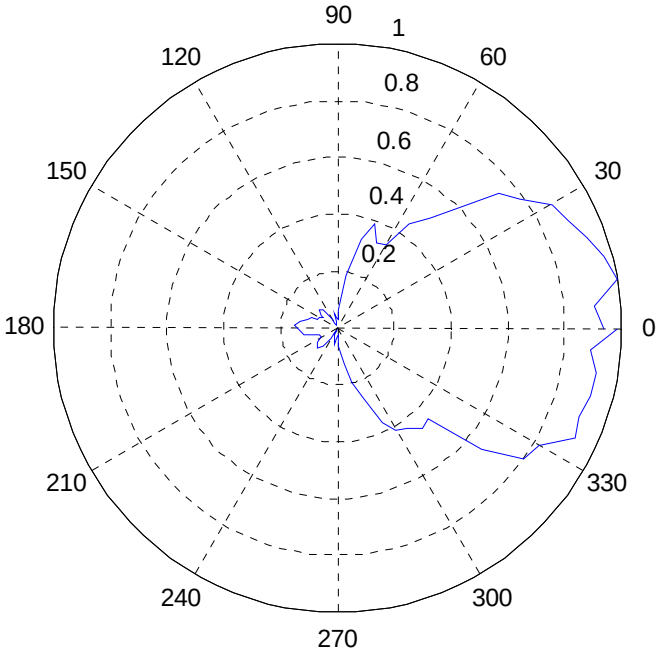

Normalized power pattern (in linear scale) for Vivaldi antenna on RO4003 at 5GHz

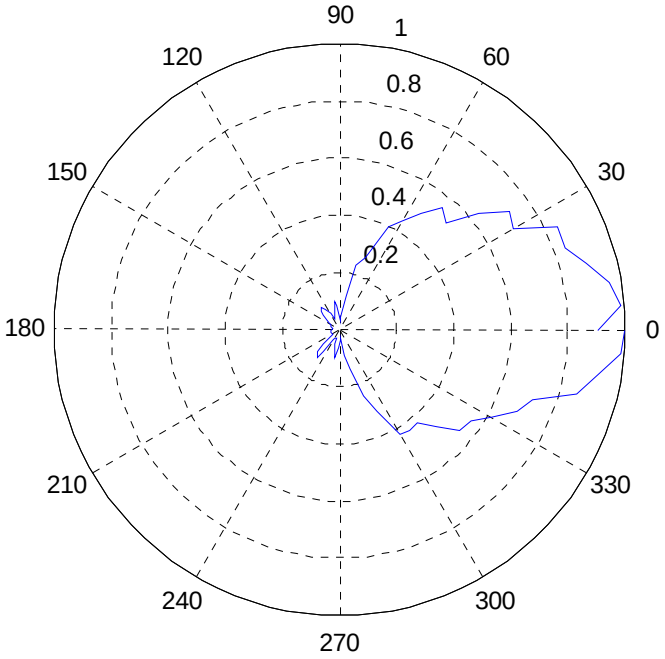

Normalized power pattern (in linear scale) for Vivaldi antenna on RO4003 at 5.5GHz

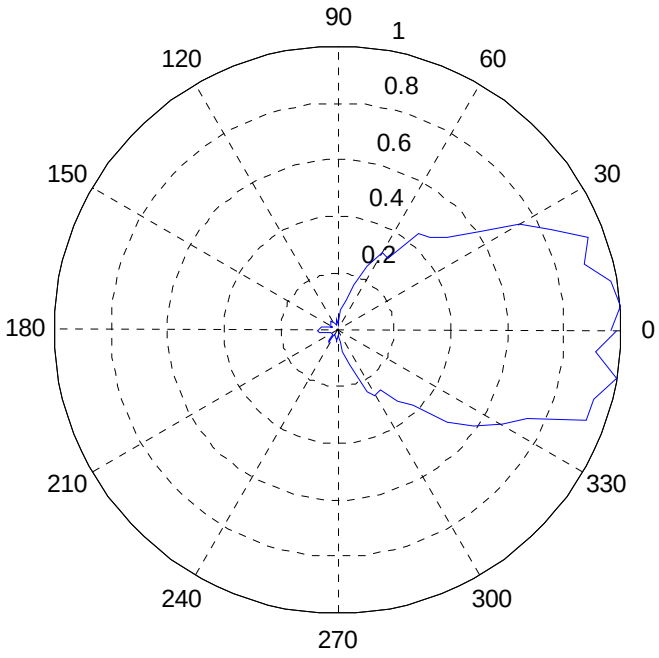

Normalized power pattern (in linear scale) for Vivaldi antenna on RO4003 at 6GHz

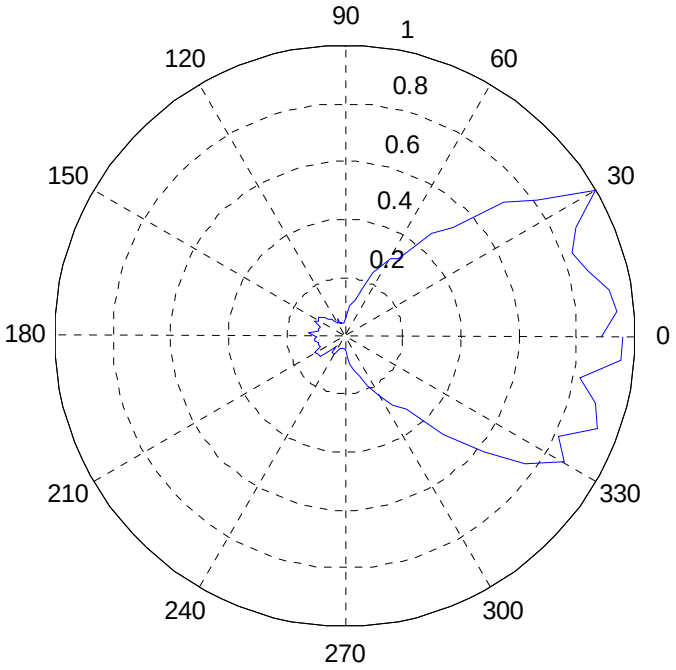

Normalized power pattern (in linear scale) for Vivaldi antenna on RO4003 at 6.5GHz

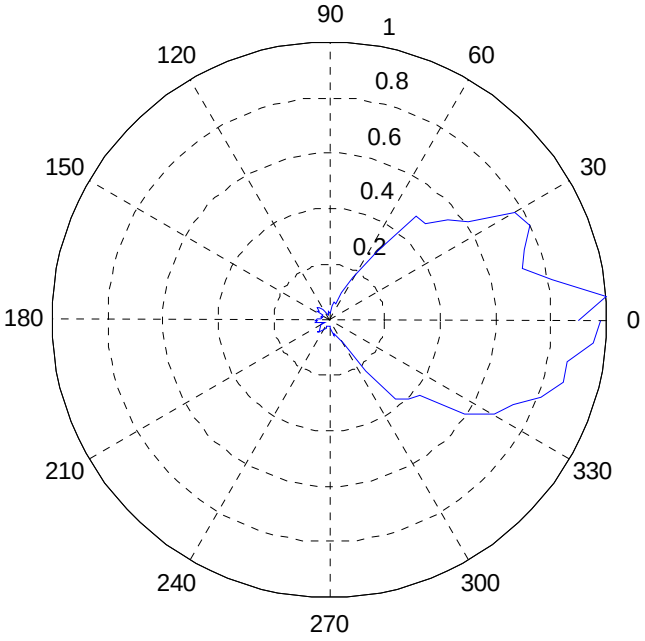

Normalized power pattern (in linear scale) for Vivaldi antenna on RO4003 at 7GHz

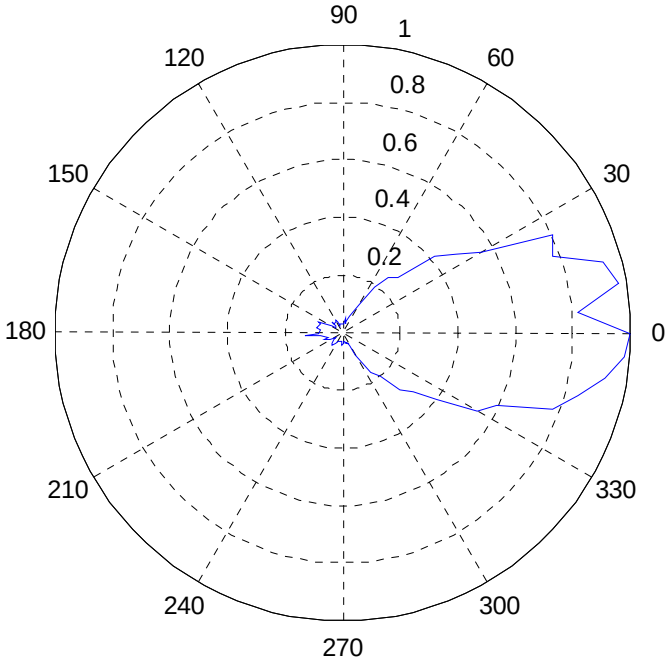

Normalized power pattern (in linear scale) for Vivaldi antenna on RO4003 at 7.5GHz

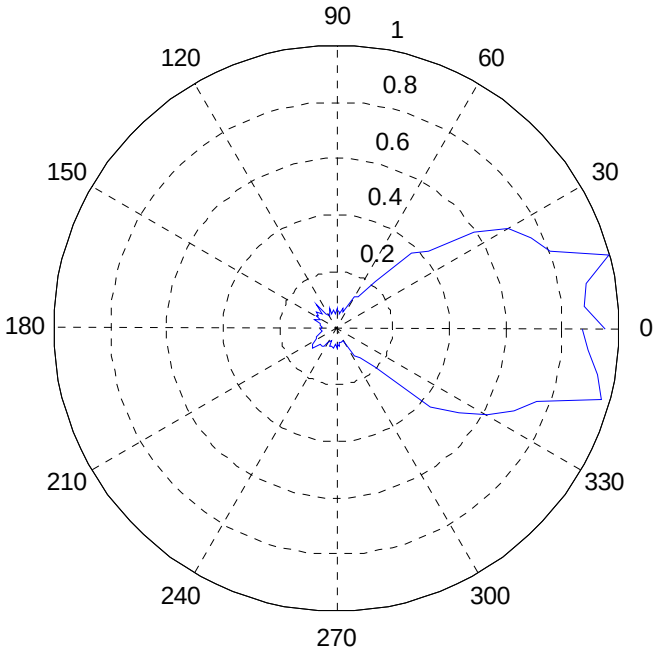

Normalized power pattern (in linear scale) for Vivaldi antenna on RO4003 at 8GHz

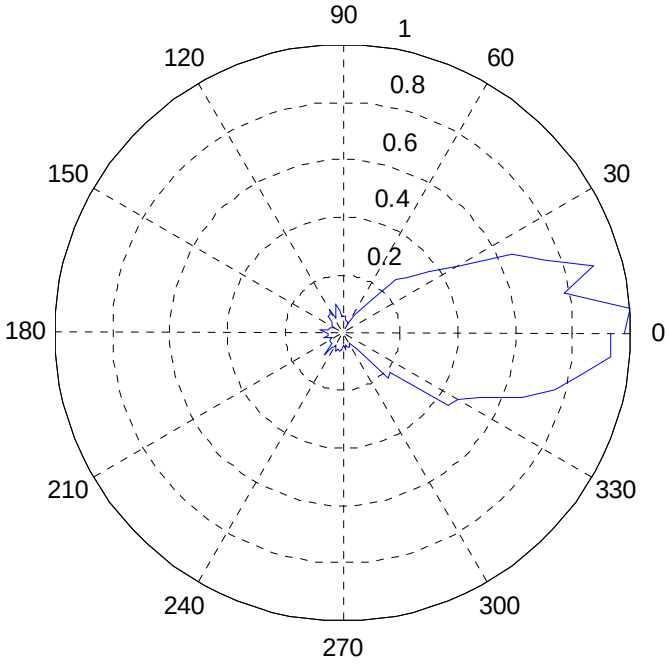

Normalized power pattern (in linear scale) for Vivaldi antenna on RO4003 at 8.5GHz

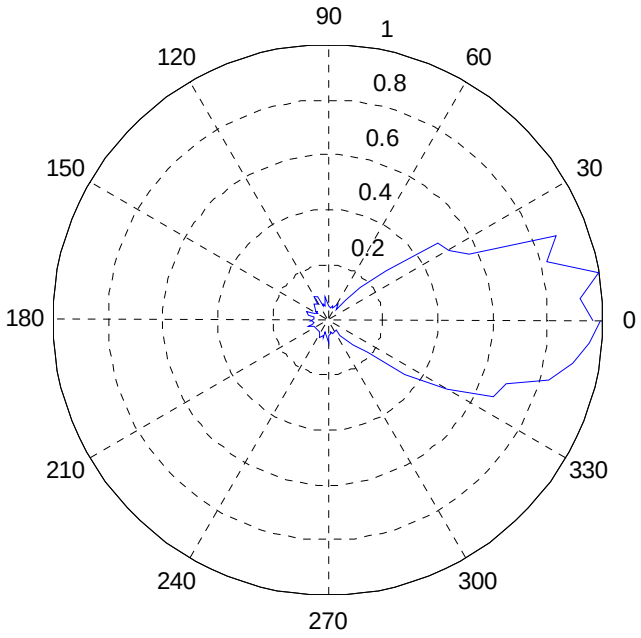

Normalized power pattern (in linear scale) for Vivaldi antenna on RO4003 at 9GHz

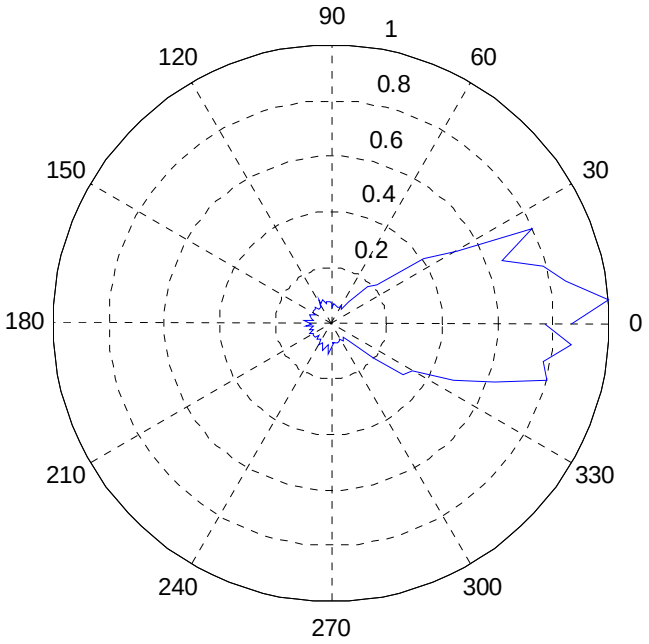

Normalized power pattern (in linear scale) for Vivaldi antenna on RO4003 at 9.5GHz

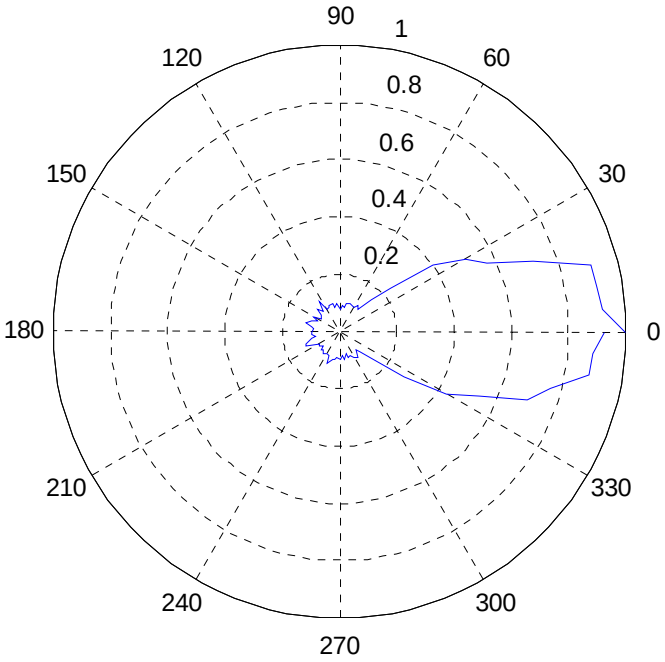

Normalized power pattern (in linear scale) for Vivaldi antenna on RO4003 at 10GHz

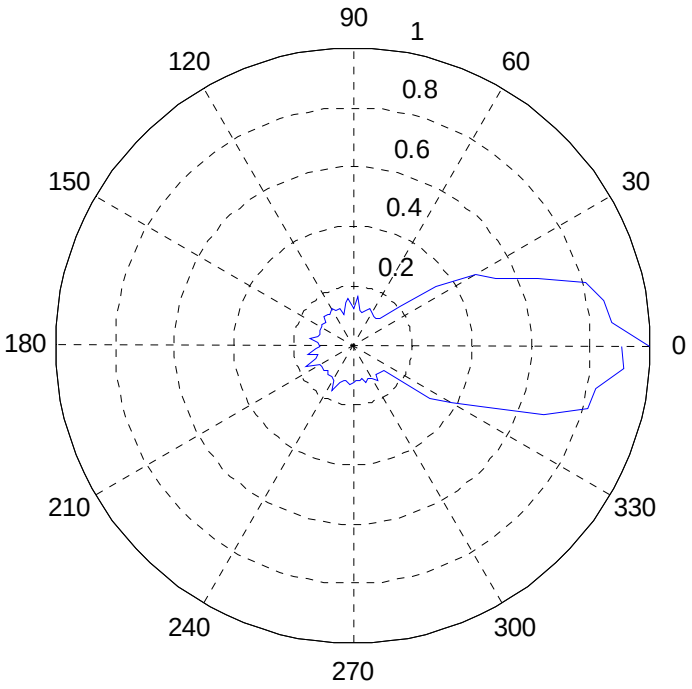

Normalized power pattern (in linear scale) for Vivaldi antenna on RO4003 at 10.5GHz

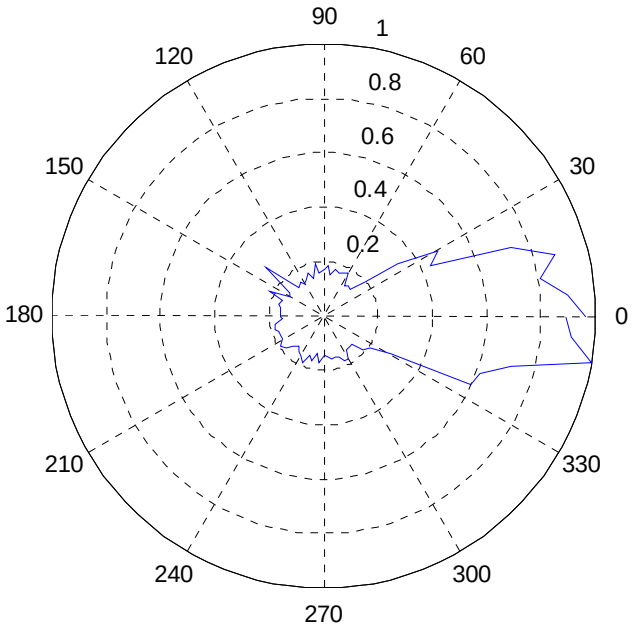

APPENDIX F

NORMALIZED POWER PATTERN (IN LINEAR SCALE) FOR BOWTIE ANTENNA (DESIGN A) IN THE ELEVATION PLANE

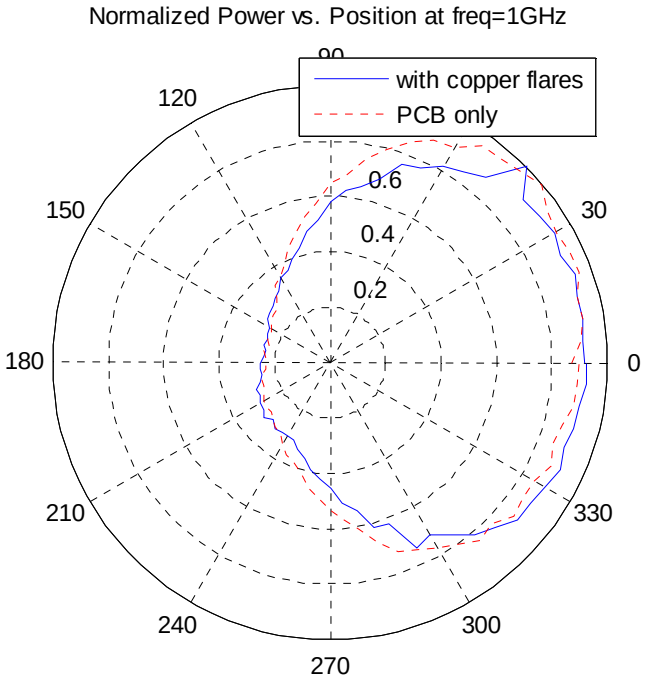

Bowtie antenna (design A) in the elevation plane

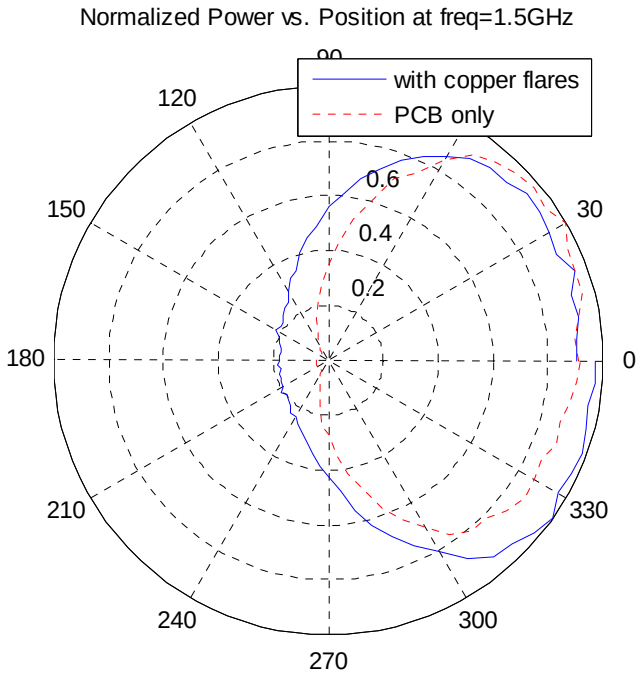

Bowtie antenna (design A) in the elevation plane

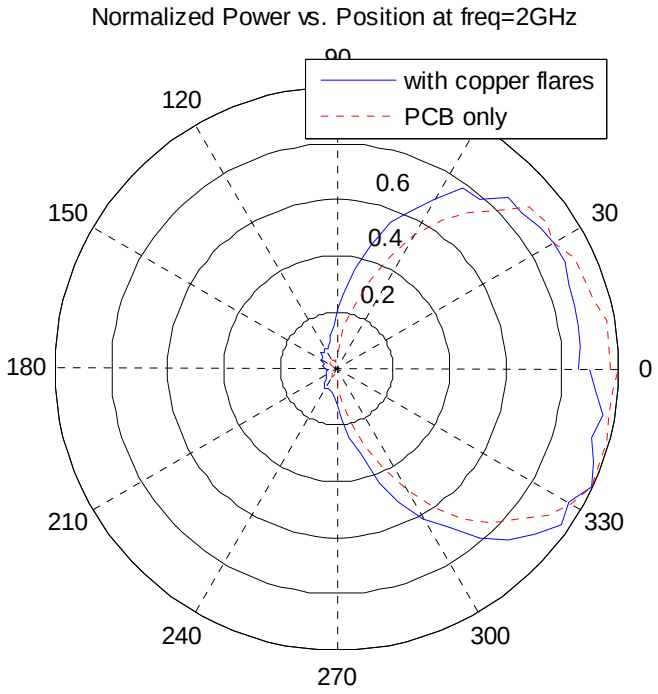

Bowtie antenna (design A) in the elevation plane

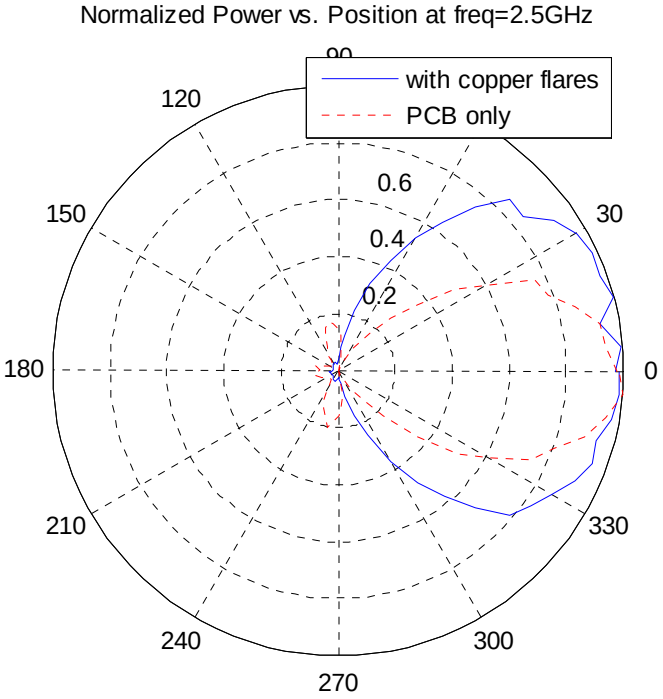

Bowtie antenna (design A) in the elevation plane

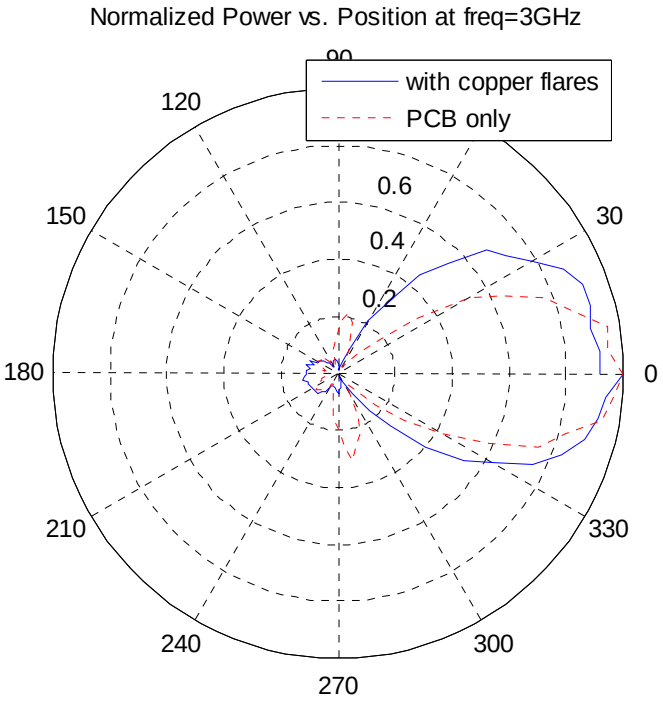

Bowtie antenna (design A) in the elevation plane

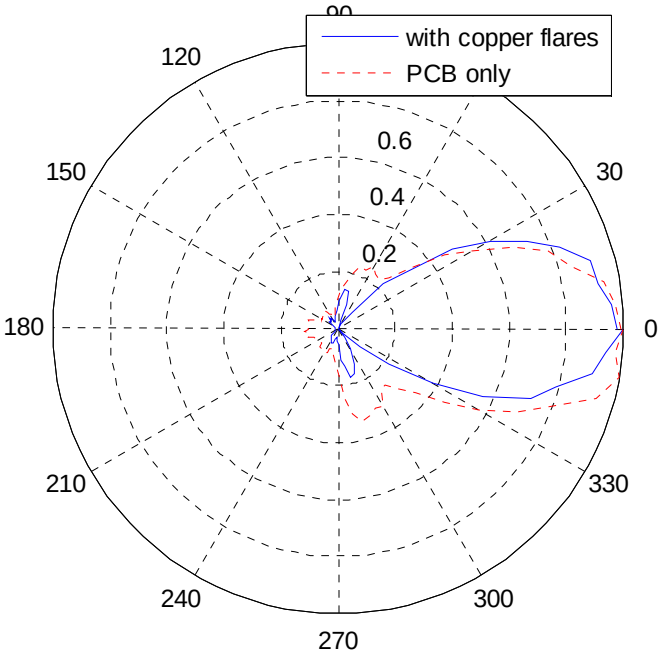

Bowtie antenna (design A) in the elevation plane

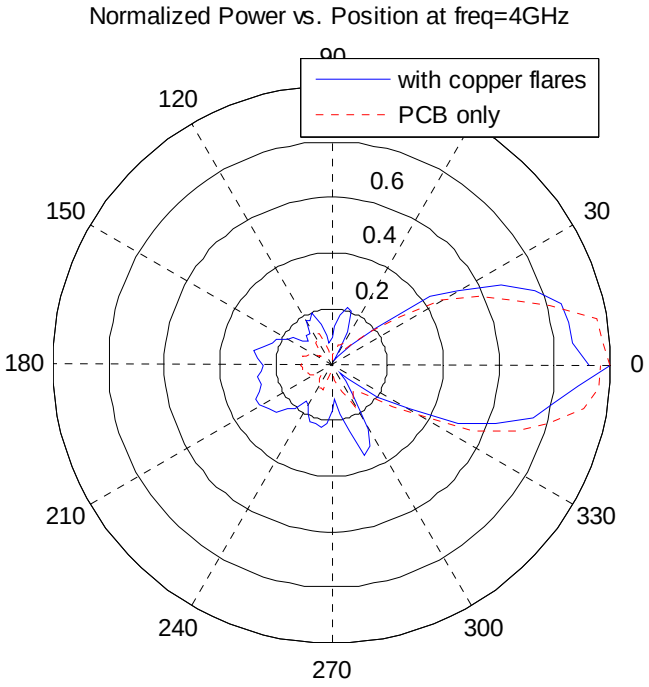

Bowtie antenna (design A) in the elevation plane

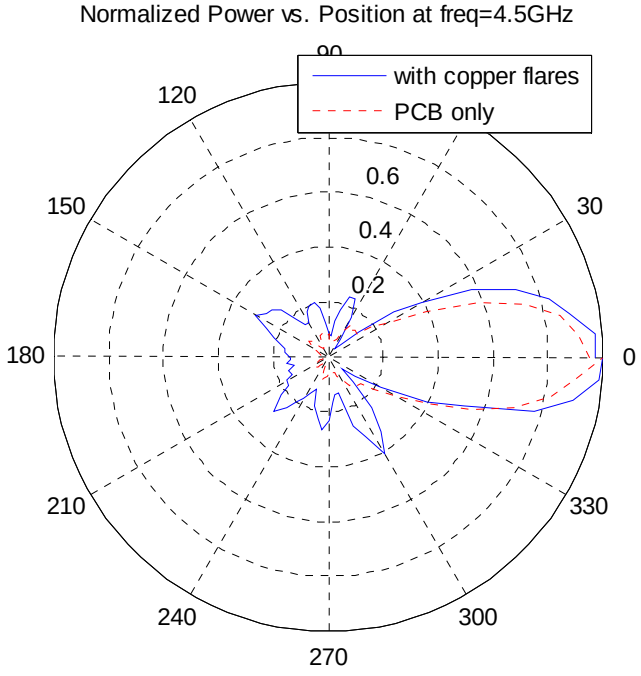

Bowtie antenna (design A) in the elevation plane

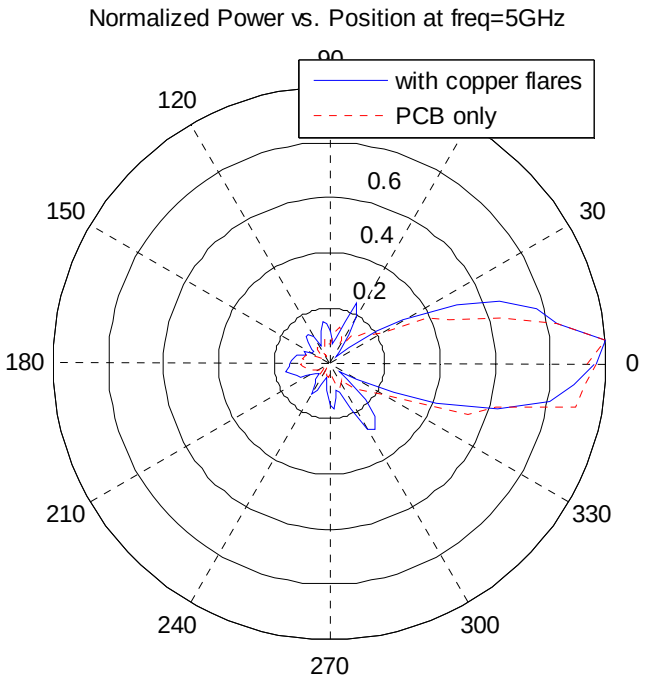

Bowtie antenna (design A) in the elevation plane

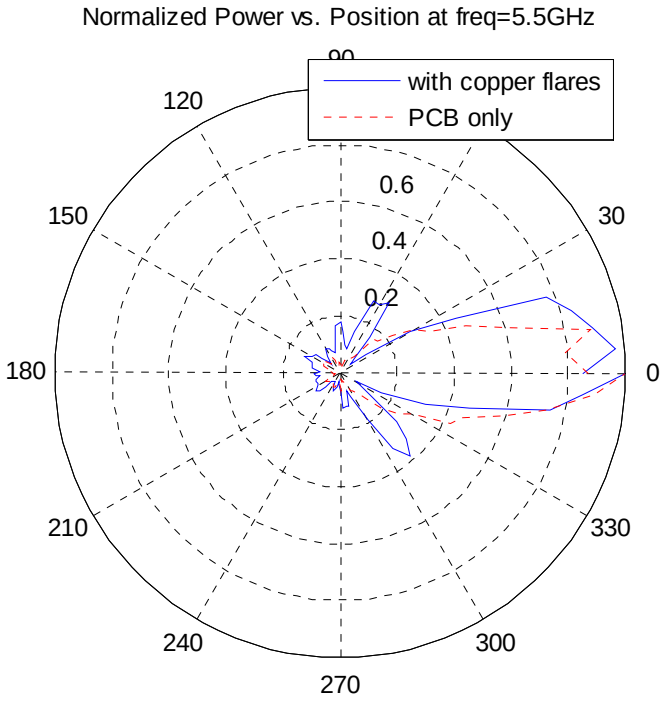

Bowtie antenna (design A) in the elevation plane

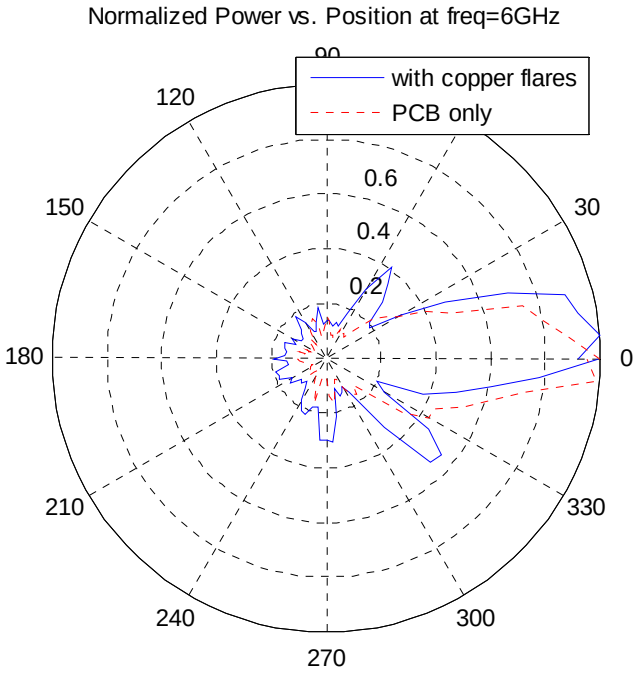

Bowtie antenna (design A) in the elevation plane

APPENDIX G

NORMALIZED POWER PATTERN (IN LINEAR SCALE) FOR BOWTIE ANTENNA (DESIGN A) IN THE AZIMUTH PLANE

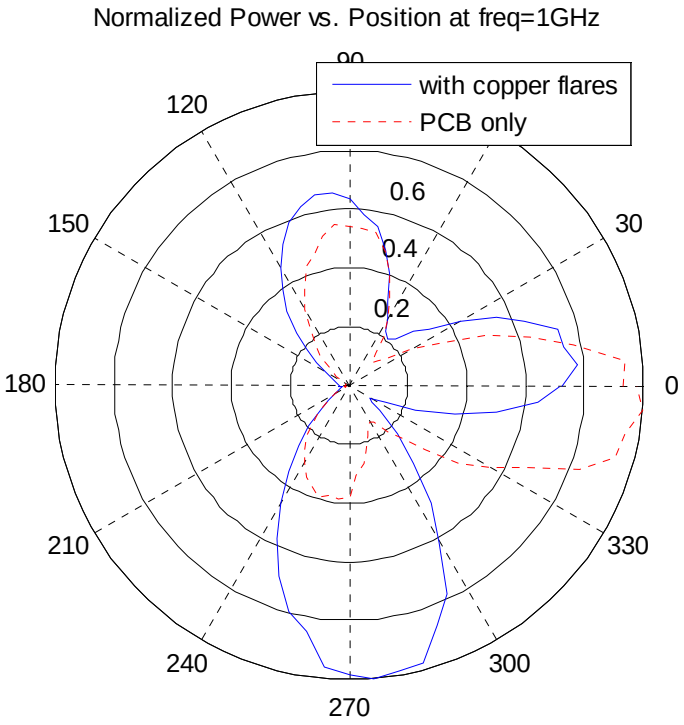

Bowtie antenna (design A) in the azimuth plane

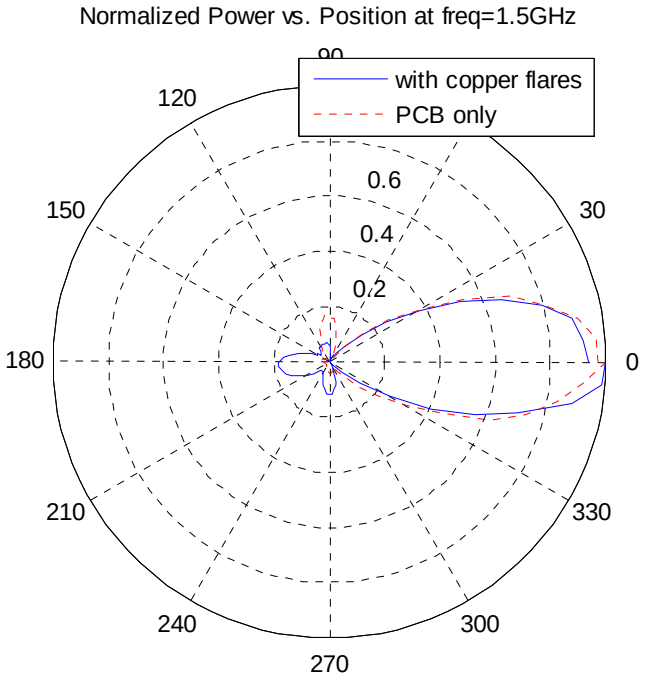

Bowtie antenna (design A) in the azimuth plane

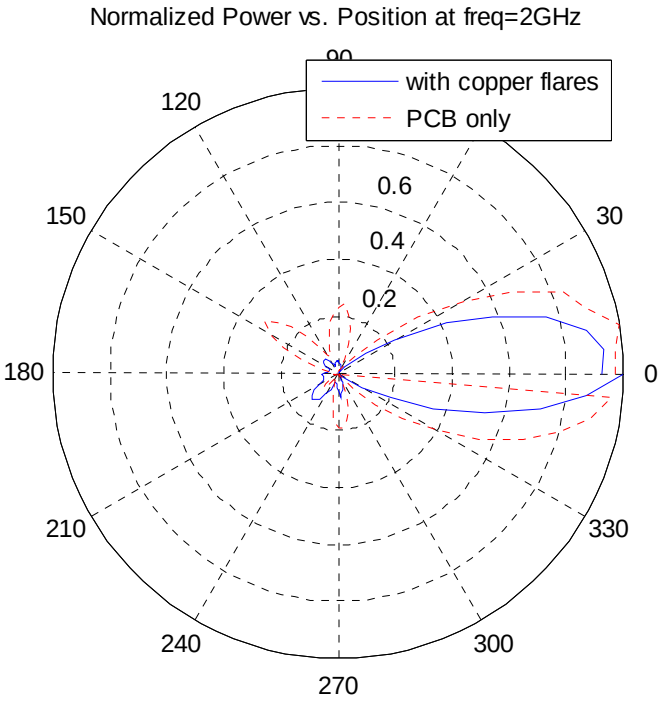

Bowtie antenna (design A) in the azimuth plane

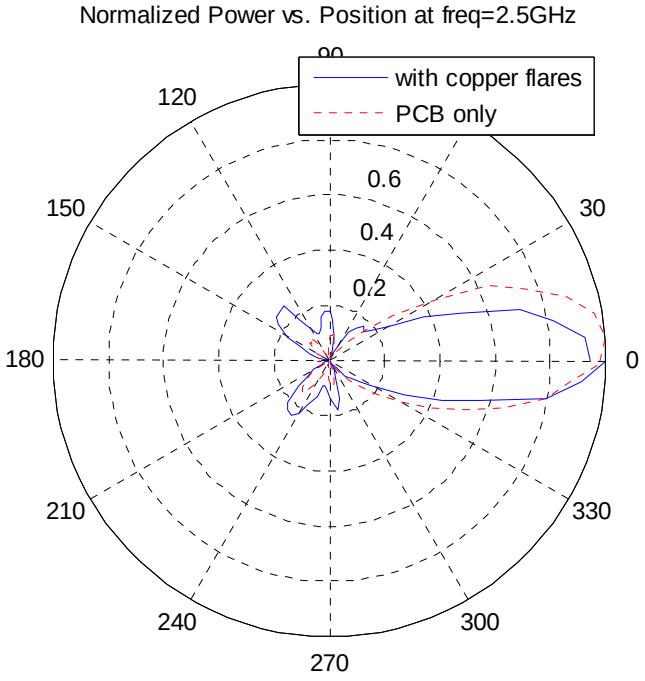

Bowtie antenna (design A) in the azimuth plane

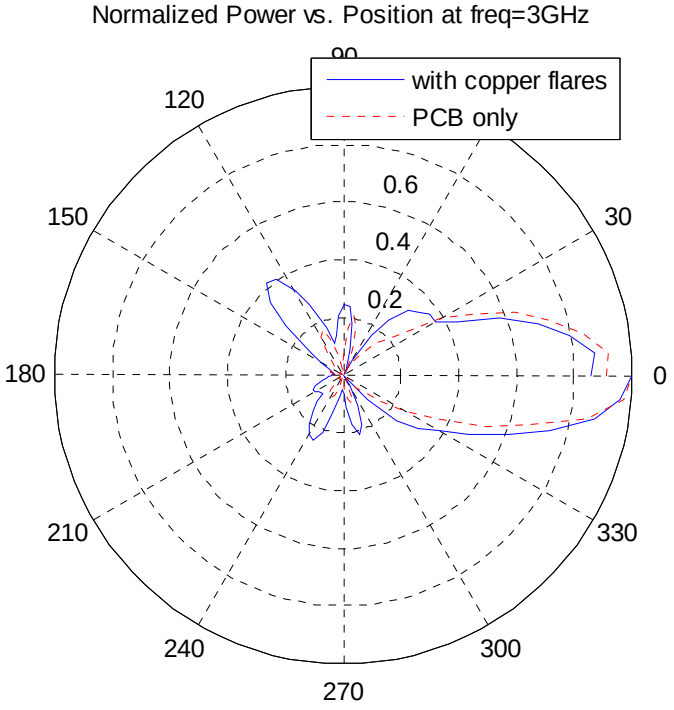

Bowtie antenna (design A) in the azimuth plane

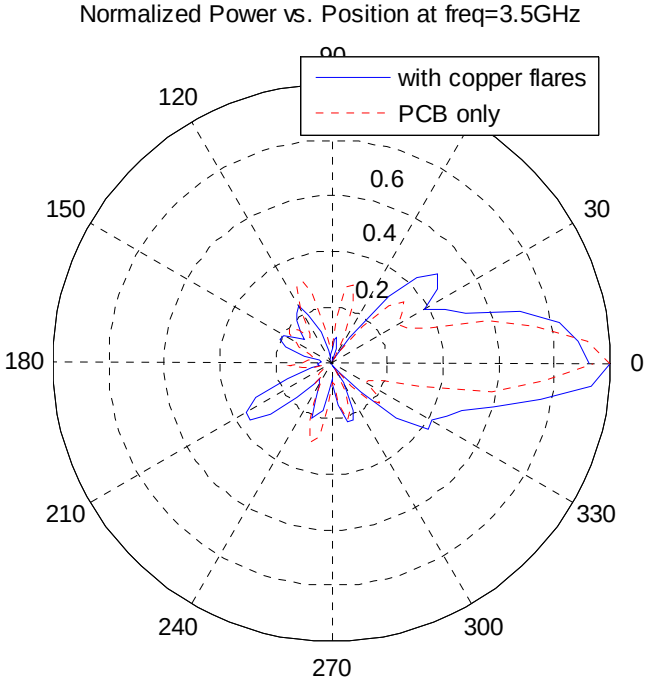

Bowtie antenna (design A) in the azimuth plane

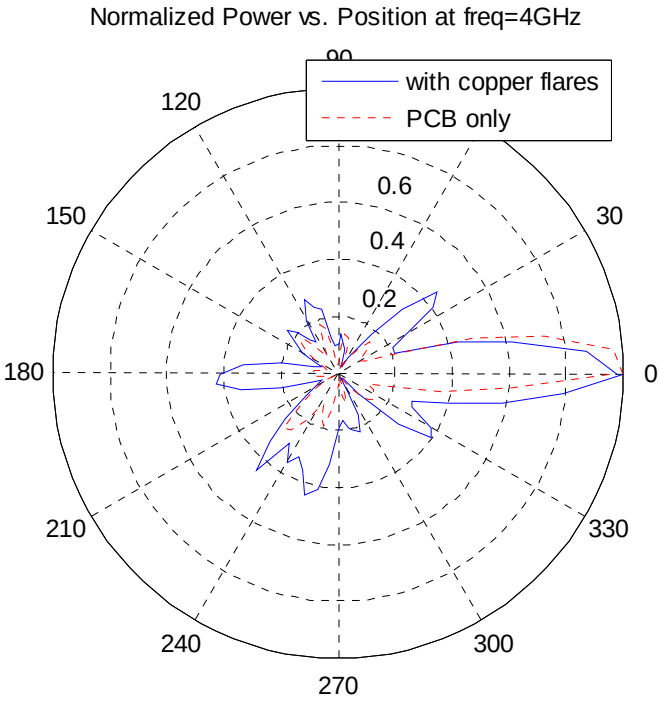

Bowtie antenna (design A) in the azimuth plane

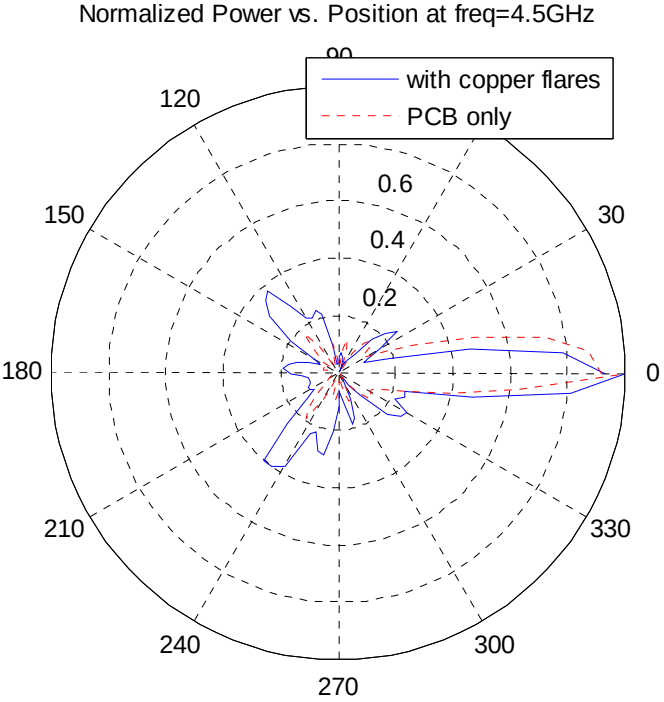

Bowtie antenna (design A) in the azimuth plane

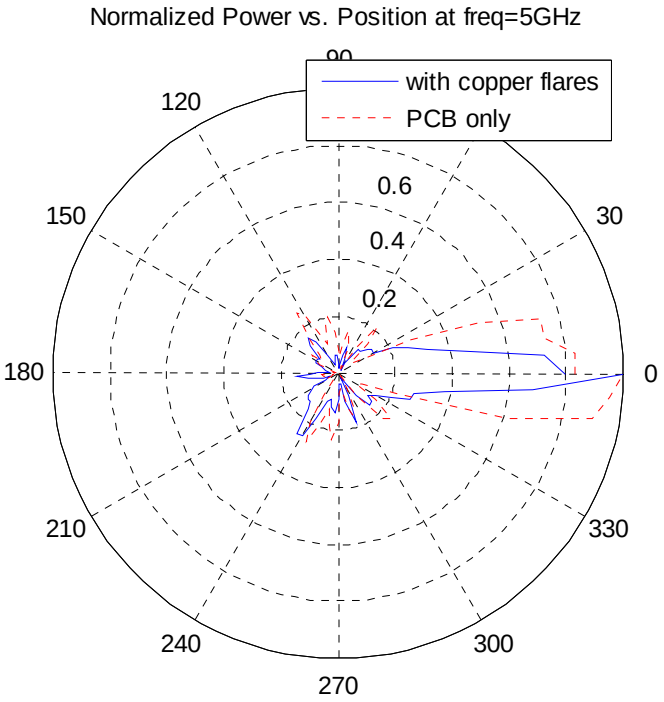

Bowtie antenna (design A) in the azimuth plane

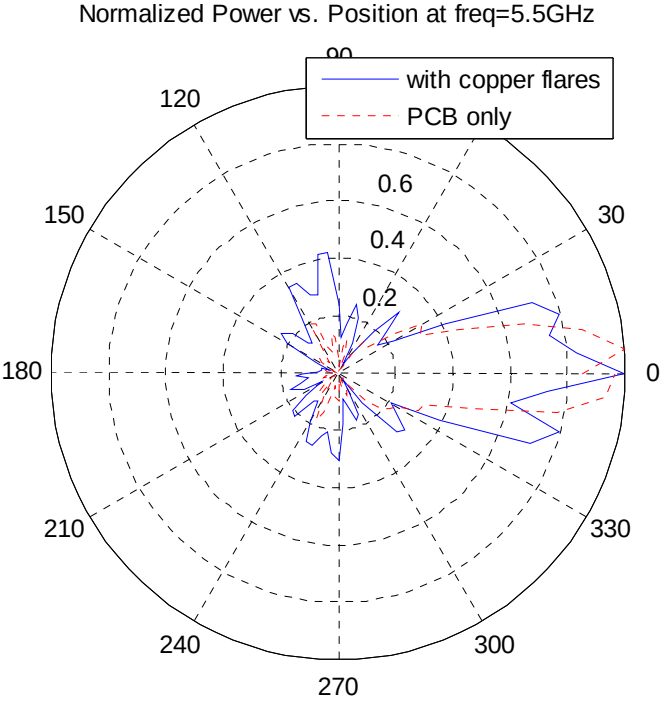

Bowtie antenna (design A) in the azimuth plane

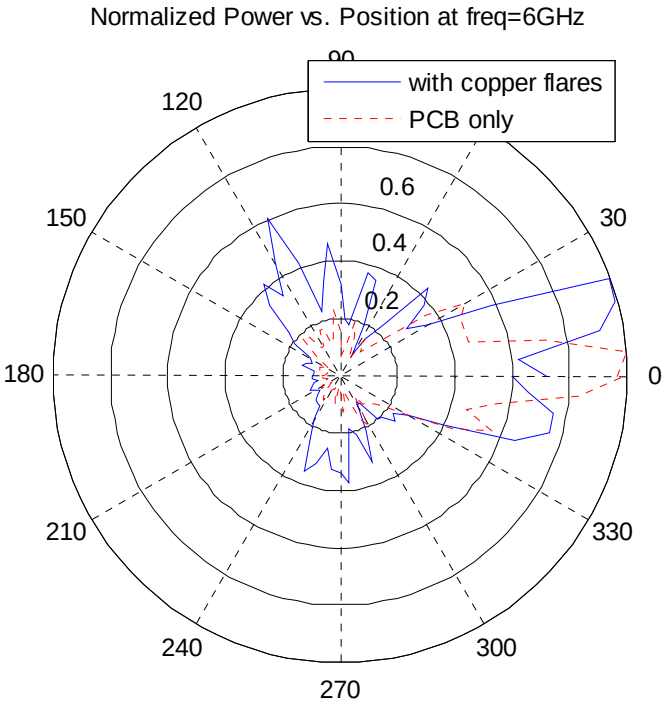

Bowtie antenna (design A) in the azimuth plane

APPENDIX H

NORMALIZED POWER PATTERN (IN LINEAR SCALE) FOR BOWTIE ANTENNA (DESIGN B) IN THE ELEVATION PLANE

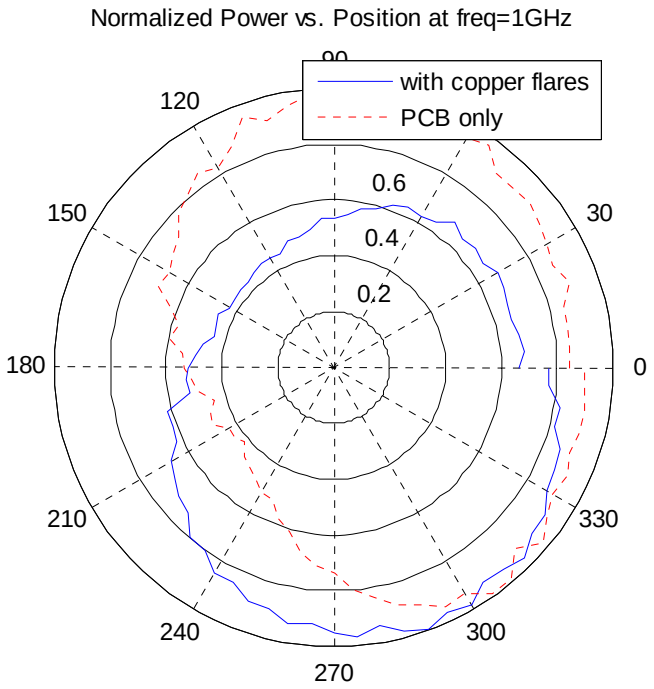

Bowtie antenna (design B) in the elevation plane

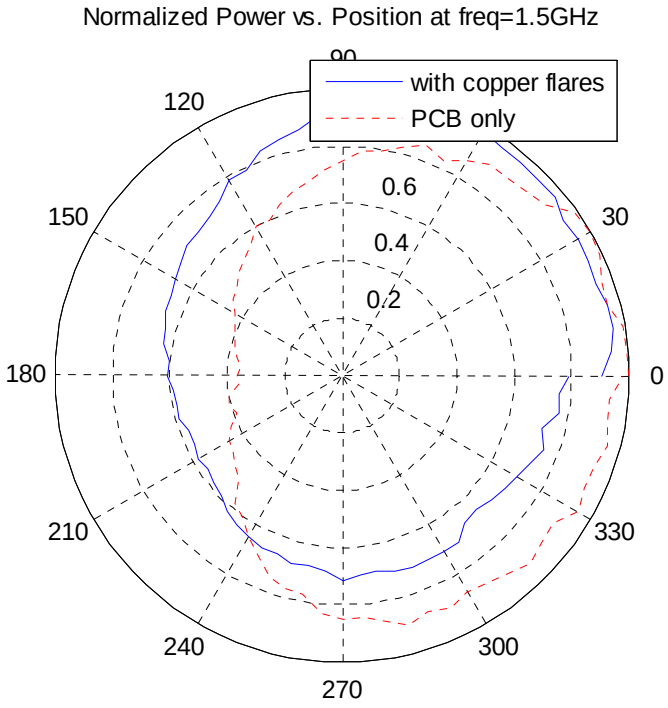

Bowtie antenna (design B) in the elevation plane

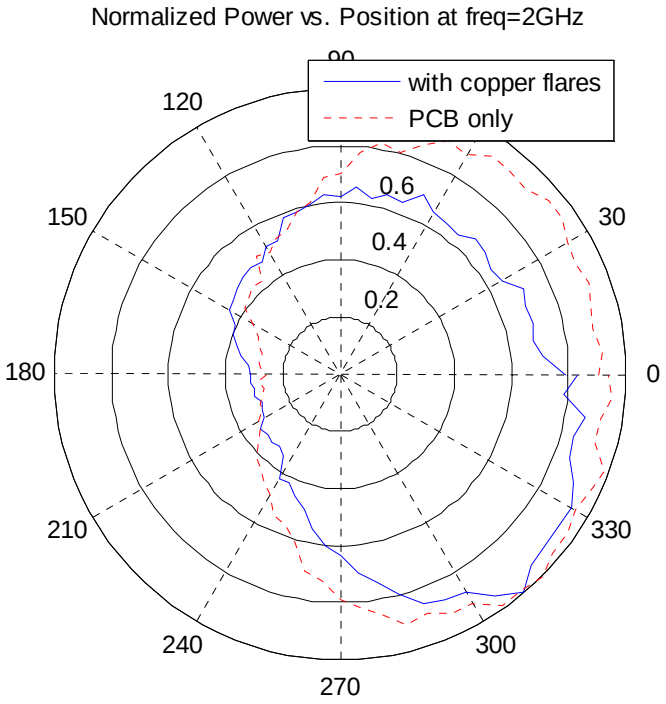

Bowtie antenna (design B) in the elevation plane

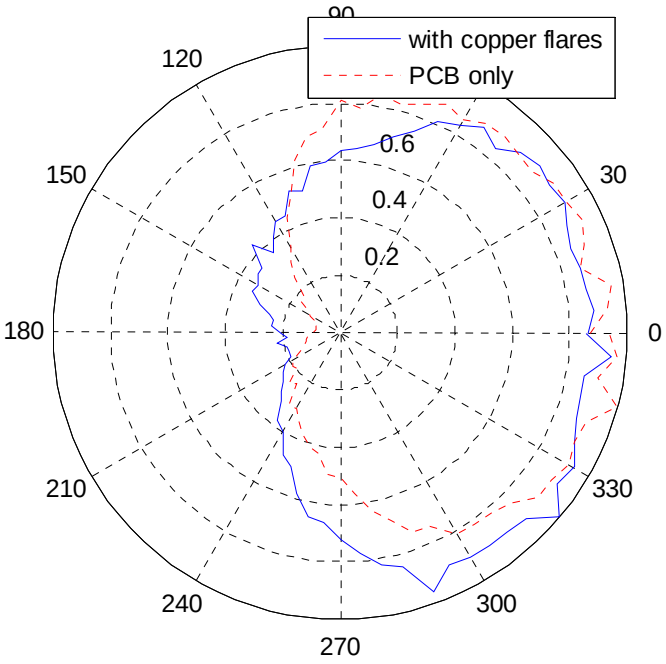

Bowtie antenna (design B) in the elevation plane

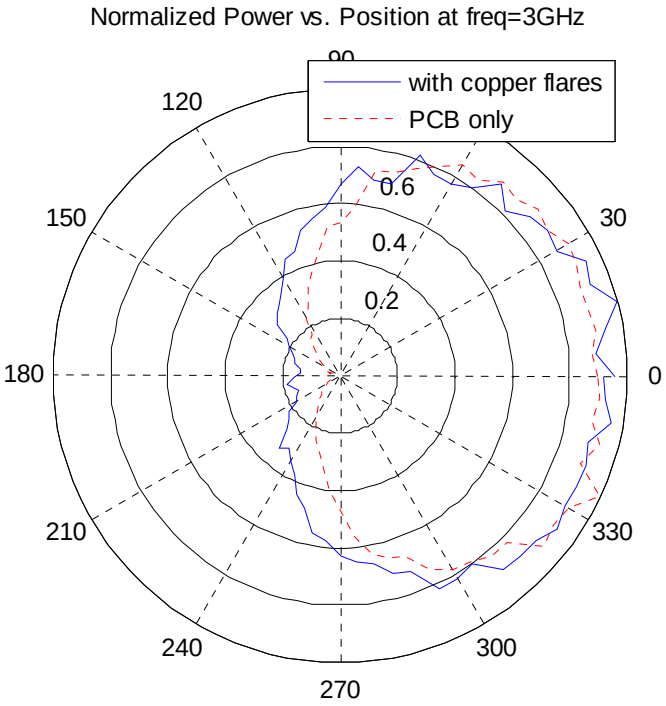

Bowtie antenna (design B) in the elevation plane

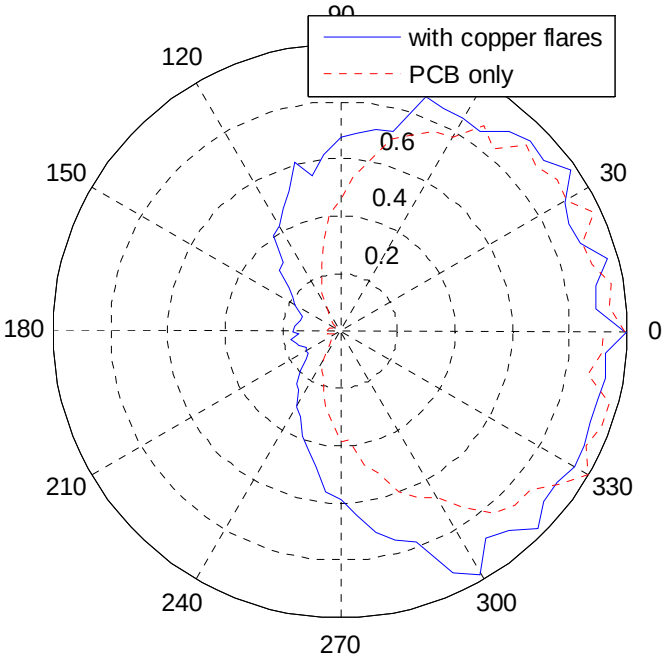

Bowtie antenna (design B) in the elevation plane

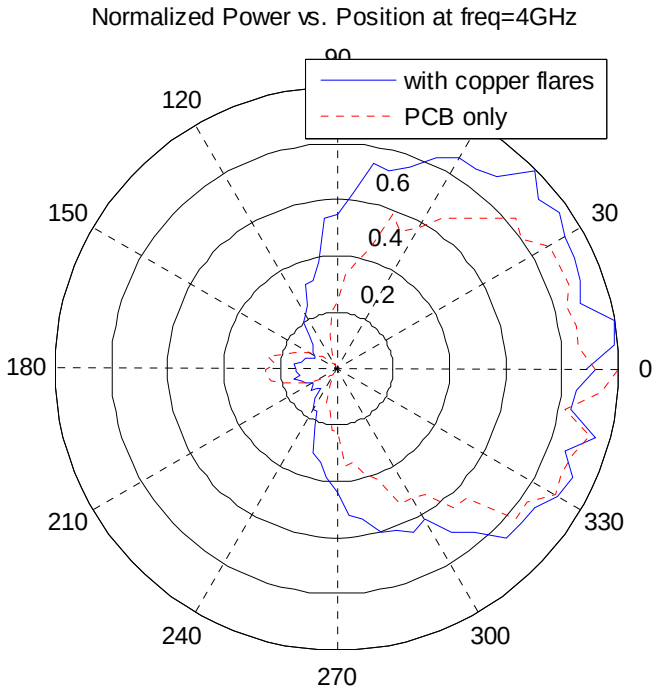

Bowtie antenna (design B) in the elevation plane

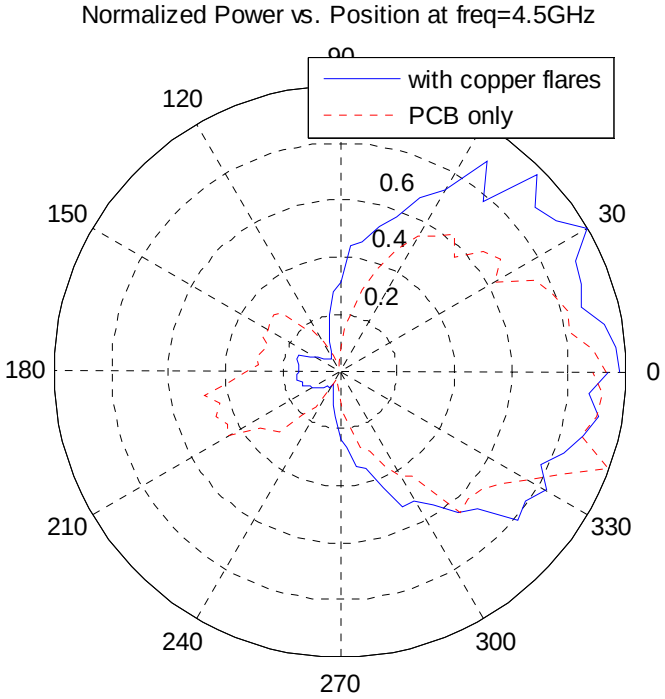

Bowtie antenna (design B) in the elevation plane

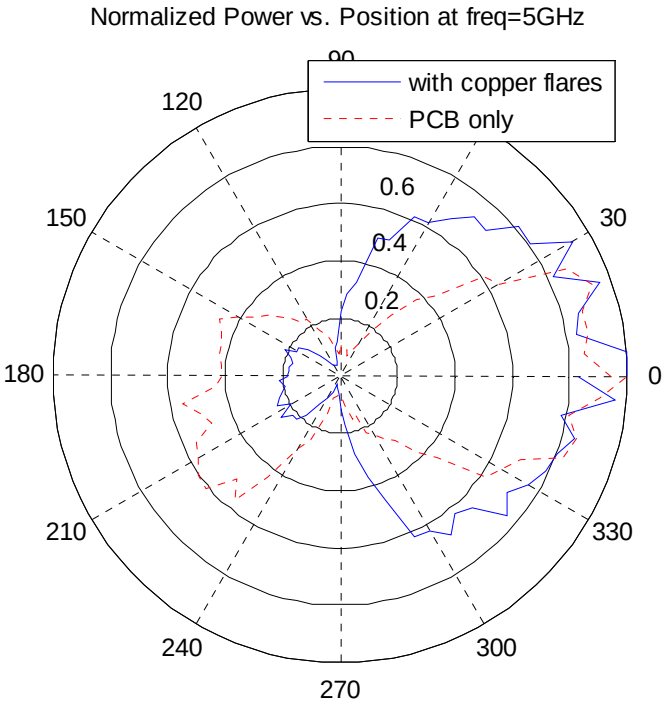

Bowtie antenna (design B) in the elevation plane

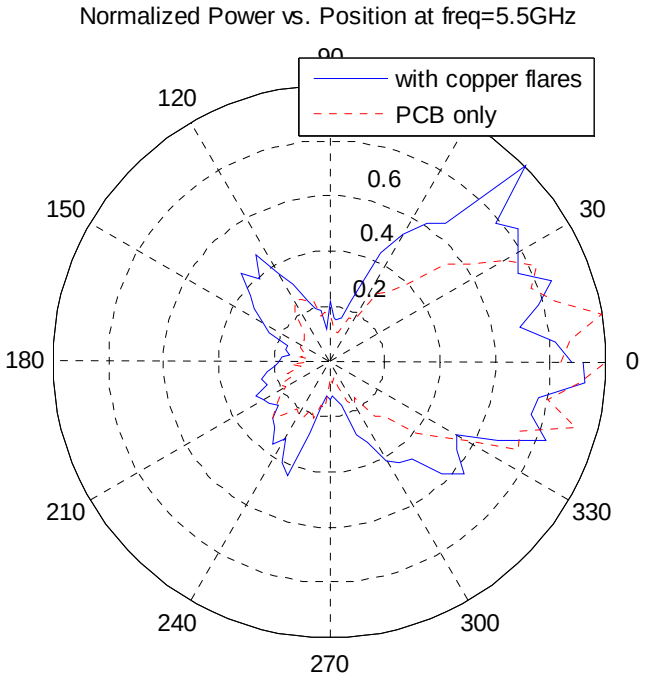

Bowtie antenna (design B) in the elevation plane

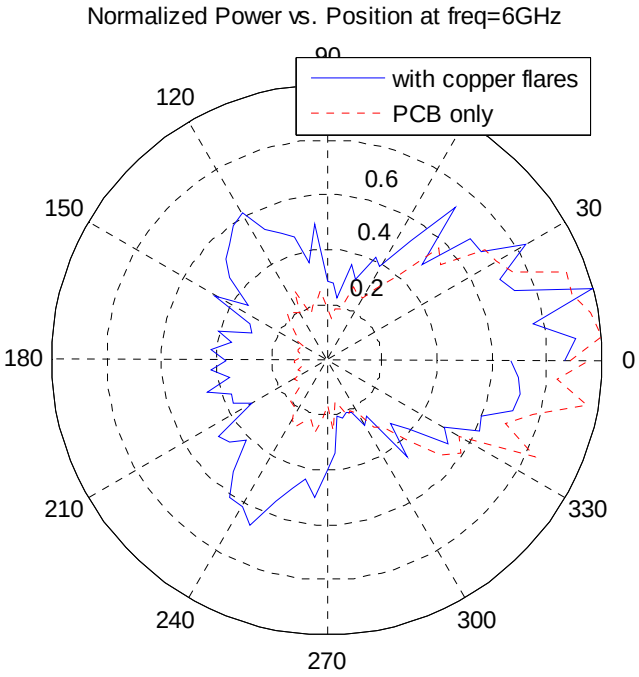

Bowtie antenna (design B) in the elevation plane

APPENDIX I

NORMALIZED POWER PATTERN (IN LINEAR SCALE) FOR BOWTIE ANTENNA (DESIGN B) IN THE AZIMUTH PLNE

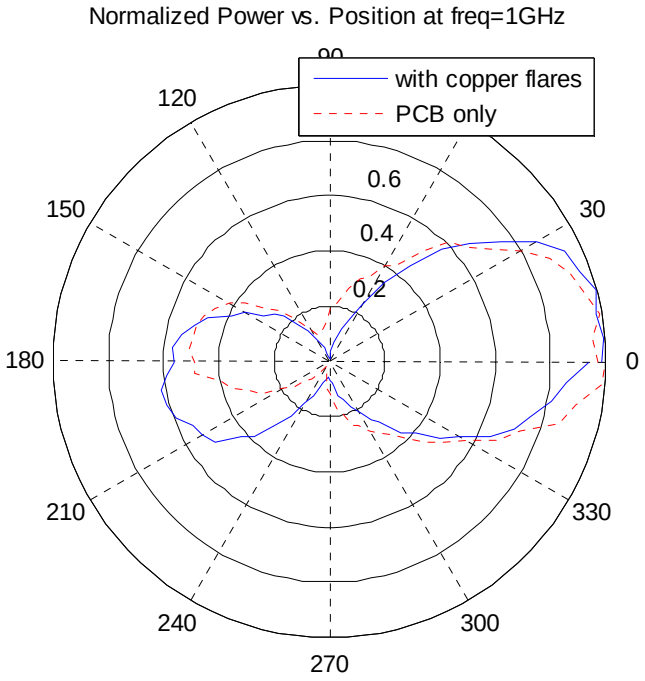

Bowtie antenna (design B) in the azimuth plane

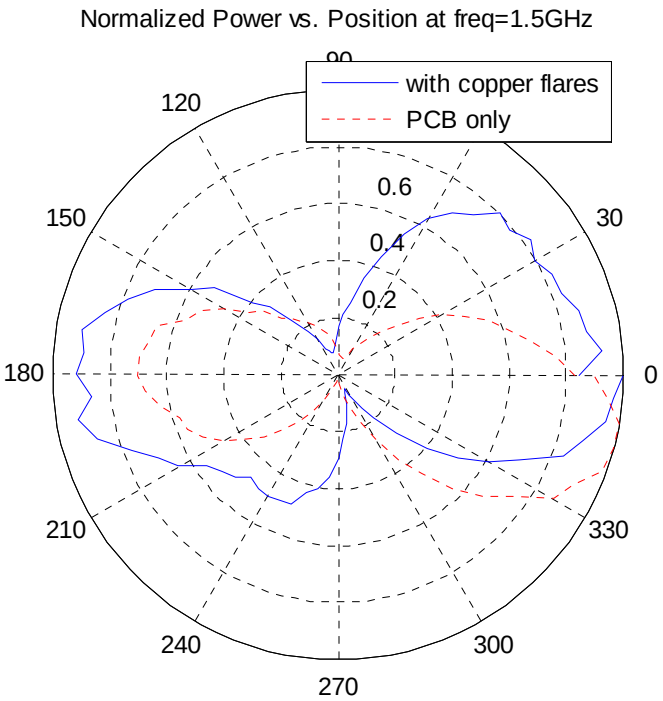

Bowtie antenna (design B) in the azimuth plane

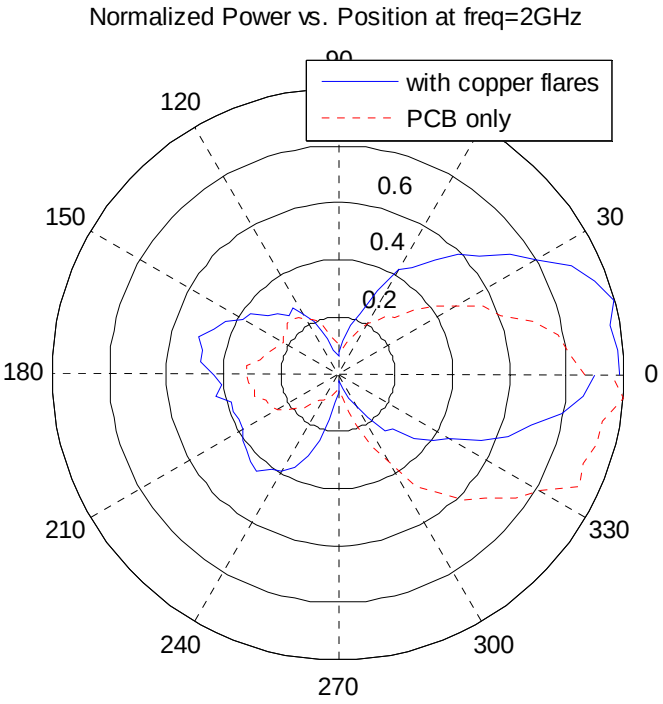

Bowtie antenna (design B) in the azimuth plane

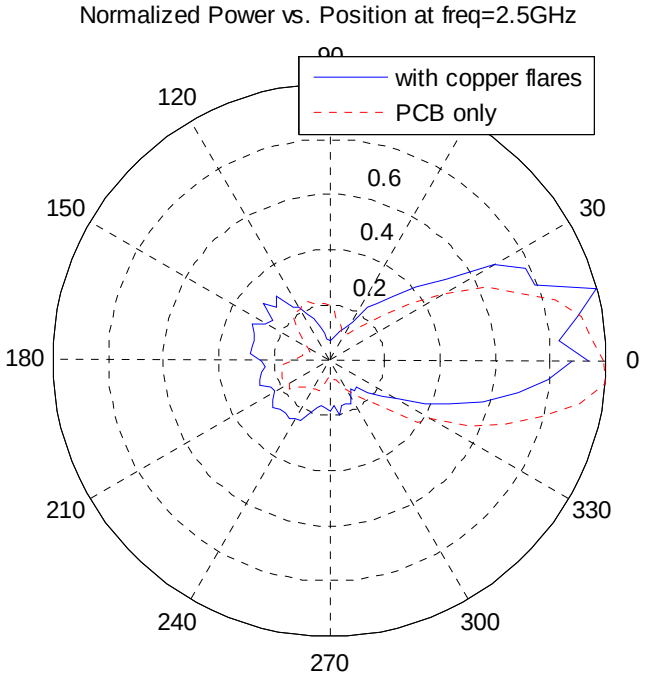

Bowtie antenna (design B) in the azimuth plane

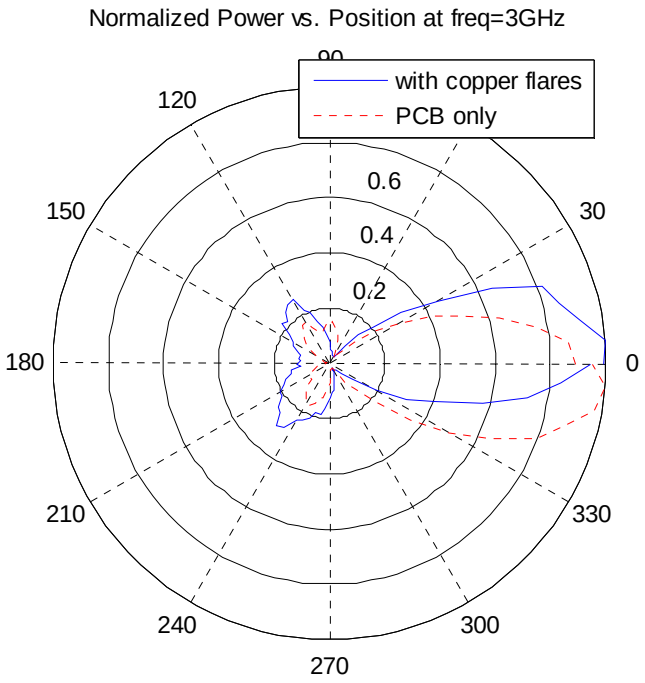

Bowtie antenna (design B) in the azimuth plane

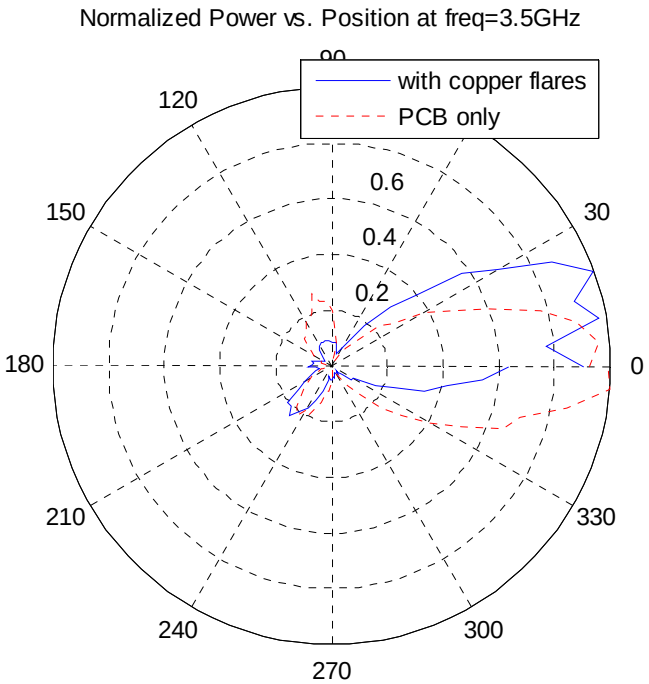

Bowtie antenna (design B) in the azimuth plane

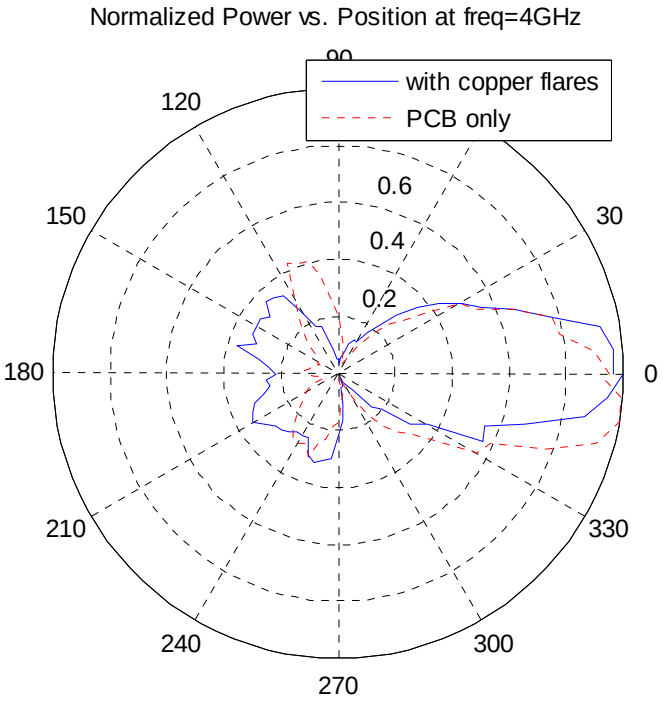

Bowtie antenna (design B) in the azimuth plane

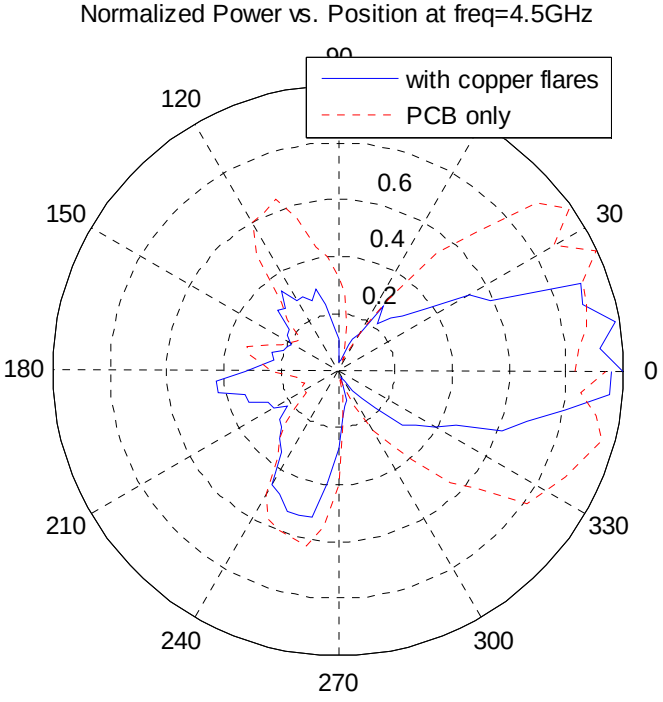

Bowtie antenna (design B) in the azimuth plane

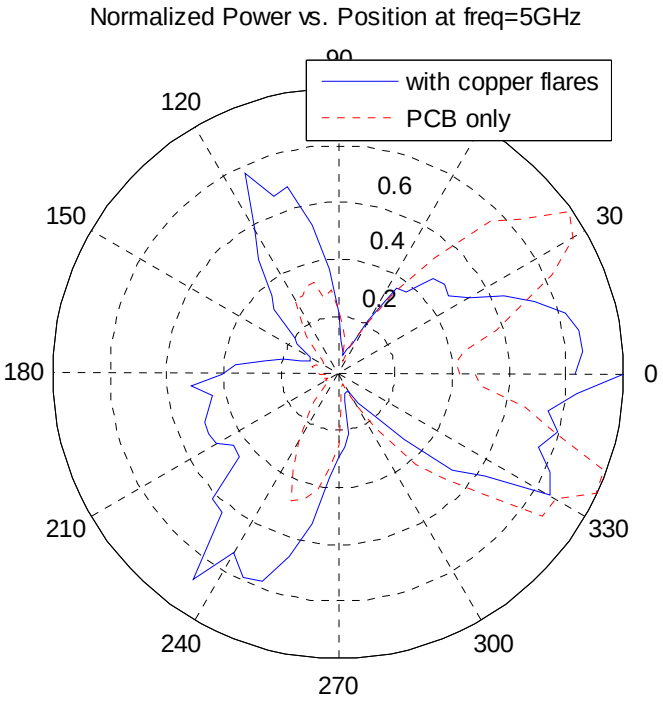

Bowtie antenna (design B) in the azimuth plane

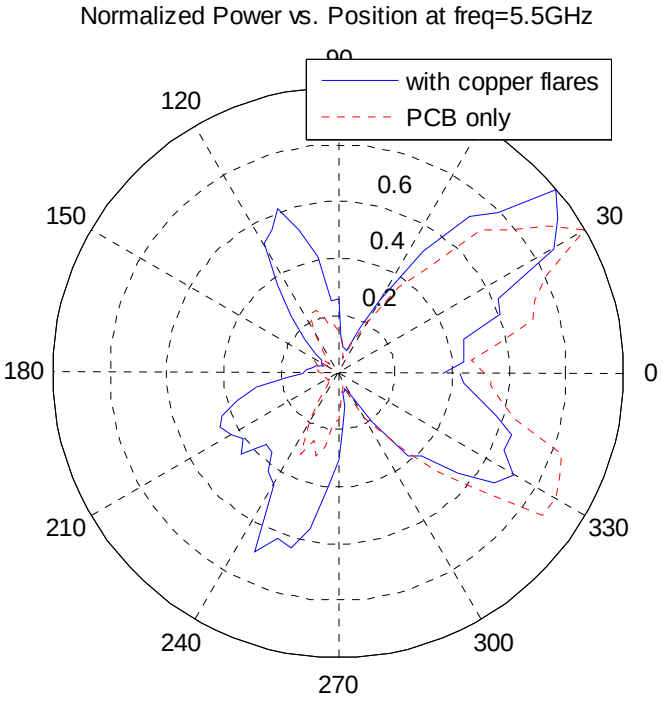

Bowtie antenna (design B) in the azimuth plane

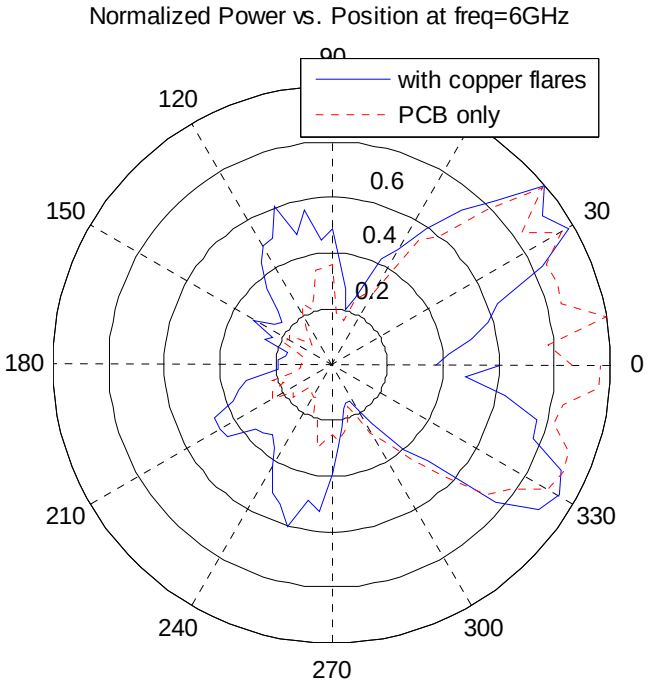

Bowtie antenna (design B) in the azimuth plane

APPENDIX J

MATLAB SCRIPT FOR SNOW DEPTH MEASUREMENT SIMULATION

```
%
% Snow measurements simulation using Pulse ON 220 and Vivaldi antenna,
%
%
% Programmed by: John Mosy
% October 2009
%
% Main function: calls TxRx for transmission and reflection simulation
%
%




clear; % clear all old variables



% Generating the UWB signal to be transmitted:

% using Pulse ON 220, the signal is loaded from the provided file
% suing the follwoing function:
[t, signal] = read_sent_signal();
signal= signal.*0.75; % the normalized value is scalled to the actual
values

% calculating df:
dt= t(2)-t(1);            % resolution in time
N= size(signal,2);        % number of points in the signal
df= 1/ (N*dt);            % frequency resolution



% snow parameters:
epsilon_snow= 1.44; % epsilon_snow= (1+.51Ps)^3,
                    % Ps(Snow density)= (148+105d)e-3, d is set to 1
(avg.)
                    % Ps = .2530 gm/cm3

%speed of the signal in air and snow:
c=299792458;            % speed of light =~3e8
% the signal speed in snow is reduced due to the epsilon r of snow
v= c/sqrt(epsilon_snow); % speed of the signal in the snow



% plotting the signal before adding the antenna gain:
figure();
plot(t,signal);
title('Pulse ON 220 transmit signal');
xlabel('Time [Seconds]');
```

```
ylabel('Amplitude [Volts]');
grid on;


% converting into frequency domain to apply antenna gain:
signal_fft1=fft(signal,N);  % fft for the signal

% Vivaldi antenna gain:
gain= absolute_gain_array(size(signal_fft1,2)/2,df);

% Applying the gain to the signal:
signal_fft(1:size(signal_fft1,2)/2)=
signal_fft1(1:size(signal_fft1,2)/...
    2).*gain;
signal_fft(size(signal_fft1,2)/2+1:size(signal_fft1,2))=
signal_fft1(...
    size(signal_fft1,2)/2+1:size(signal_fft1,2)).*fliplr(gain);


eirp= real(ifft(signal_fft));

% plotting the EIRP (signal+gain):
figure();
plot(t,eirp);
grid on;
title('EIRP= Pulse ON 220 transmit signal + Vivaldi antenna gain');
xlabel('Time [Seconds]');
ylabel('EIRP [Volts]');



% generation of and comparison with the FCC emission mask:
% using function 7.10 to generate the mask,
% using code from function 7.11 to compare with mask
% of Di Benedetto, Understanding Ultra Wide Band , Prrntice Hall PTR,
2004


Ts= 1/9.6e6; % Ts= 1/PRF of P220
fs= 1/dt; % sampling frequency
% the FCC emmision mask for UWB handhels ad outdoor devices(FCC,
2002),P186
emissionmask = cp0703_generate_mask(N,fs);
% the following code was modified from line 62 to 62+17, function 7.11
    X=fft(eirp,N);
            % conversion from MATLAB spectrum to Fourier spectrum
            X=X/N;
            % DOUBLE-SIDED ESD of the waveform
            E = fftshift(abs(X).^2/(df^2));
            % SINGLE-SIDED ESD of the waveform
            Ess = 2.*E((N/2+1):N);
            % PSD of the combination in dBm/MHz
```

```
            PSD = 10 * log10 ((1/Ts) * Ess / 377) + 90;
%+(30+60):
                                                    %30 for dBm, 60 for
/MHz
               [PSDPeak, ind_peak]=max(PSD);
               PSDPeak;
Tp= t(size(t,2))-t(1);
max_allowable_p= 7.5e-8*(Ts/Tp)^2;  % value set by the FCC mask
max_allowable_p_indBm= 10*log10(max_allowable_p)+30;
Power= 1/Ts .* Ess.*df / 377;
[max_Power, ind_max]= max(Power);
max_Power_indBm = 10*log10(max_Power)+30;

            P= sum(1/(10e-9).* Ess.*df / 377);
            Total_Power_dBm=10*log10(P)+30;

%%%%%%%%%%%%%%% plot the signal and the FCC emission mask on the same
graph
frequency=linspace(0,df*size(PSD,2),size(PSD,2));
figure();
plot(frequency,PSD);
hold on;
plot(frequency,emissionmask);
grid on;
title('PSD of the Time Domain Pulse ON 220 UWB Pulse and the FCC
emission mask');
xlabel('Frequency [Hz]');
ylabel('PSD [dBm/MHz]');



% surface of snow is considered the refernce d=0
% an ice layer is placed at d=1m
% the ground is at a distance d=2m from the snow surface
% the array d contains these values:
d= [0,1,2];


% the variable NR is the number the measurment is repated and the
reflected
% signals are summed together:
NR= 9.6e3;  % 1 ms measurment time


% calculating bandwidth and the peak frequency
threshold=-10;      % -10 dB threshold as defined for UWB
[Ess,f_high,f_low,BW,f_peak]=cp0702_bandwidth(signal,dt,threshold);
f= round(f_peak/100e6)*100e6;  % frequency of operation


% Generating the reflected signal off the snow
net_ref= TxRx(eirp,dt,f,N,d);
```

```
% creating an array that will sum all the reflected signals:
final_net_ref = zeros(size(net_ref));



% the time array for the final reflected signal:
final_time=
linspace(dt,dt*size(final_net_ref,2)+dt,size(final_net_ref,2));


% adding the reflected signals:
for count_NR=1:1:NR
    final_net_ref= final_net_ref+ net_ref;

end



% next lines are needed for the initialization the reflected signal
with
% noise (final_boresight)
K= 1.3806505e-23 ;% boltezman constant
T=290;             % tempreature
B=BW;              % bandwidth
noise_val=K*T*B;  % KTB, in watts
% generating the noise; the parameters are: n,m,p(v.)
final_noise=wgn(1,size(final_net_ref,2),noise_val,50,'linear');

% the signal + noise:
final_bore_sight_noise= final_net_ref +final_noise;


% adding the noise according to the number of repetitions
for i= 1: 1: NR-1
    % each time is generetaed randomly and independant from the
previous
K= 1.3806505e-23 ;% boltezman constant
T=290;             % tempreature
B=BW;              % bandwidth
noise_val=K*T*B;  % KTB, in watts
final_noise=wgn(1,size(final_net_ref,2),noise_val,50,'linear');
%n,m,p(v.),

final_bore_sight_noise= final_bore_sight_noise +final_noise;
end
```

```
% converting time to distance

set1= (fix(N*dt+2*1/c)/dt);
d1=final_time(1:set1).*c;
d2= final_time(set1+1:length(final_time)).*v;
distances= [d1 d2]./2-1.07; % bias

% plotting the reflected signal:
figure();
plot(final_time,final_bore_sight_noise);
grid on;
title('Received signal ');
xlabel('Time [Seconds]');
ylabel('Amplitude [Volts]');


figure();
plot(distances(2700:length(distances)),final_bore_sight_noise(2700:leng
th(final_bore_sight_noise)));
grid on;
title('The recieved signal reflected off the snow');
xlabel('Distance [Meters]');
ylabel('Amplitude [Volts]');



%%% end main
```

```
%
% Snow measurements simulation using Pulse ON 220 and Vivaldi antenna,
%
%
% Programmed by: John Mosy
% October 2009
%
% reading the signal sent by PulseOn 220
% returns signal array containing [time, value of signal]
%
% Programmed by: John Mosy
% Spervisor: Richard Wolff
%

function [time,signal]= read_sent_signal()


[numeric, txt, raw]= xlsread('P210MultipathFreeWaveform.xls');

i=1;
while (isnan(numeric(i+1,1))==1)
    i=i+1;
end

firstelem= i+1;
lastelem= size(numeric,1);
time= numeric(firstelem:lastelem,1)';
time= time.*1e-9;
signal= numeric(firstelem:lastelem,3)';


%%% end read_sent_signal
```

```
%
% Snow measurements simulation using Pulse ON 220 and Vivaldi antenna,
%
%
% Programmed by: John Mosy
% October 2009
%
% This function adds the antenna gain to the UWB signal
%

function [gain]= absolute_gain_array(size, df)




% loading the boresight gain array for the vivaldi antenna:
boresightgain= csvread('VivaldiBoresightGain.csv');


% frequancies in the fft
frequencies =linspace(0,df*size,size);


for i=1:1:length(frequencies)


    if frequencies(i)<3.1e9
        gain(i)= 10.^(boresightgain (1,2)./20);
    elseif frequencies(i)>10.6e9
        gain(i)=10.^(boresightgain (length(boresightgain),2)./20);
    else
        for j=1:length(boresightgain)
        if frequencies(i)>= boresightgain(j,1)-50e6 &&...
                frequencies(i)< boresightgain(j,1)+50e6
            gain(i)=10.^(boresightgain(j,2)./20);
        end
        end

    end

end




%%% end absolute_gain_array
```

```
%
% FUNCTION 7.10 : "cp0703_generate_mask"
%
% This function generates a discrete vector representing
% the FCC indoor % modified for outdoor mask
% emission mask for UWB devices
%
% The function receives in input:
% 1) the number of points in the frequency domain 'N'
% 2) the sampling frequency 'fs'
%
% The function returns a vector of N/2 points,
% 'emissionmask', representing the emission mask in the
% frequency range [0 , fs/2]
%
% Programmed by Luca De Nardis
% modified by: John Mosy for the outdoor values instead of indoor
%


function [emissionmask] = cp0703_generate_mask(N,fs)

df = fs / N;                % fundamental frequency
emissionmask = zeros(N/2);
n1 = round(0.96e9/df);
n2 = round(1.61e9/df);
n3 = round(1.99e9/df);
n4 = round(3.1e9/df);
n5 = round(10.6e9/df);

a(1:n1)=-41.3;
b(1:(n2-n1))=-75;
c(1:(n3-n2))=-63.3;
d(1:n4-n3)=-61.3;
e(1:n5-n4)=-41.3;
f(1:(N/2-n5))=-61.3;
emissionmask=[a b c d e f];
% positivefrequency=linspace(0, fs/2, N/2);
% semilogx(positivefrequency,emissionmask);
% axis([8e8 20e9 -78 -40]);



%%% end cp0703_generate_mask
```

```
%
% Snow measurements simulation using Pulse ON 220 and Vivaldi antenna,
%
%
% Programmed by: John Mosy
% October 2009
%
% This function generates the reflected signal off the snow
% The input parameters are: the EIRP signal, time resolution dt, peak
% frequency f, number of points in the signal N, array of distances d
% The output is: the reflected signal net_ref
%




function [net_ref]= TxRx(eirp, dt, f, N, d)




% snow parameters:
epsilon_snow= 1.44; % epsilon_snow= (1+.51Ps)^3,
                    % Ps(Snow density)= (148+105d)e-3, d is set to 1
(avg.)
                    % Ps = .2530 gm/cm3

epsilon_air= 1;
epsilon_ice= 3.15;   % affected by tempreature but normally =3.15
epsilon_ground= 4.7; % = (1+.44Ps)^2, Ps=2.6544
attunuation_factor= 10; %10dB/meter

% the reflection coeffitient and rabsorbtion losses of the laye:
% reflection and transmission coefficients:

 %R(air/snow),  Preflected= Ras*Pincident
 %R(snow/air),  Preflected= Rsa*Pincident
 %R(snow/ice),  Preflected= Rsi*Pincident
  Ras=((sqrt(epsilon_air)-sqrt(epsilon_snow))/...
  (sqrt(epsilon_air)+sqrt(epsilon_snow)))^2;
  %= R(air/snow),  Preflected= Ras*Pincident
  Tas=1-Ras; %transmission coeffecient
  Rsi=((sqrt(epsilon_snow)-sqrt(epsilon_ice))/...
  (sqrt(epsilon_snow)+sqrt(epsilon_ice)))^2;
  %= R(snow/ice),  Preflected= Rsi*Pincident
  Tsi=1-Rsi; %transmission coeffecient

  Rse=((sqrt(epsilon_snow)-sqrt(epsilon_ground))/...
  (sqrt(epsilon_snow)+sqrt(epsilon_ground)))^2;
  %= R(snow/earth), Preflected= Rse*Pincident
```

```
c=299792458;            % speed of light =~3e8
% the signal speed in snow is reduced due to the epsilon r of snow
v= c/sqrt(epsilon_snow); % speed of the signal in the snow
% calculating the maximum possible delay to construct the return signal
% array:
max_delay= 2*1/c+ 2*2/v;

% a fixed number of samples for the reflected signal array
num_smp= round(max_delay/dt);

tot_num_smp = num_smp+N; % maximum number of points in a reflected
signal
% for a maximum traveled distance
reflected_sgnl(1:tot_num_smp)=0;

% going through snow:

 for t=1:1:size(d,2)


ref_sgnl= eirp;

 dist=d(t);% distance for delay, d(t) is the
 t_delay= 2*1/c+ 2*dist/v; % time delay value
 num_smp= round(t_delay/dt);

% adding path loss:
if d(t)==0 % 2 cases: -in air only, -in air and snow
    ref_sgnl=ref_sgnl*1/(4*pi*2*1*f/c); % attenuation in air only
else                                    % loss in air and snow
    ref_sgnl=ref_sgnl*1/(4*pi*2*(1+dist)*f/c);
end

if t==1  % reflection off the surface
    ref_sgnl=Ras.*ref_sgnl;
elseif t==2 % reflection off the ice layer
    ref_sgnl=(Tas^2)*Rsi.*ref_sgnl.*sqrt(10^(-attunuation_factor/...
        10*2*d(t)));
elseif t==3 % reflection off the ground
    ref_sgnl=(Tas^2)*(Tsi^2)*Rse.*ref_sgnl.*sqrt(10^(...
        -attunuation_factor/10*2*d(t)));
end

%  ref_sgnl(1:num_smp)=0; % adding the delay as zeros at
% the begining of the signal

 reflected_sgnl(num_smp+2911:num_smp+3377)=ref_sgnl(2911:3377);
                           % filling the rest w/ zeros to meet the
fixed
                           % length for a reflected signal
```

```
%
ref_sgnl(num_smp+1+size(reflected_sgnl,2):...
%                                   tot_num_smp)=0; % change here
%                                   %%%%%%%%%%%%%%%%%%%%%%%%%

 end % end snow layers counter

N= size(reflected_sgnl,2);
% applying the gain at the reciever:
% converting into frequency domain to apply antenna gain:
signal_fft1=fft(reflected_sgnl,N);  % fft for the signal

df= 1/ (N*dt);            % frequency resolution

% Vivaldi antenna gain:
gain= absolute_gain_array(size(signal_fft1,2)/2,df);

% Applying the gain to the signal:
signal_fft(1:size(signal_fft1,2)/2)=
signal_fft1(1:size(signal_fft1,2)/...
    2).*gain;
signal_fft(size(signal_fft1,2)/2+1:size(signal_fft1,2))=
signal_fft1(...
    size(signal_fft1,2)/2+1:size(signal_fft1,2)).*fliplr(gain);


net_ref= real(ifft(signal_fft));




 %%% end TxRx
```

```
%
% FUNCTION 7.7 : "cp0702_bandwidth"
%
% Evaluates the bandwidth of the input 'signal' with
% sampling rate 'dt'
% Bandwidth is evaluated according to the given 'threshold'
% (in dB)
% 'BW' is the bandwidth
% 'f_high' is the higher limit
% 'f_low' is the lower limit
%
% Programmed by Guerino Giancola / Luca De Nardis
%
% modified by: John Mosy; return values added: f_peak
% supervisor: Richard Wolff
%

function [Ess,f_high,f_low,BW,f_peak] = ...
   cp0702_bandwidth(signal,dt,threshold)

% ---------------------------------------------------------
% Step One - Evaluation of the single-sided Energy Spectral
%            Density
% ---------------------------------------------------------

% sampling frequency
fs = 1 / dt;
% frequency smoothing factor
frequencysmoothingfactor = 8; %8;
% number of samples (i.e. size of the FFT)
N = frequencysmoothingfactor * length(signal);
% fundamental frequency
df= 1/(N * dt);

% double-sided MATLAB amplitude spectrum
X = fft(signal,N);
% conversion from MATLAB spectrum to Fourier spectrum
X = X/N;
% DOUBLE-SIDED ENERGY SPECTRAL DENSITY
E = abs(X).^2/(df^2);
% SINGLE-SIDED ENERGY SPECTRAL DENSITY
Ess = 2.*E(1:floor(N/2));

% -----------------------------------------------
% Step Two - Evaluation of the frequency bandwidth
% -----------------------------------------------

% Epeak is the peak value of the ESD
[Epeak,index] = max(Ess);
% peak frequency
f_peak = index * df;

% Eth is the value of the ESD corresponding to the given
```

```
% threshold
Eth = Epeak*10^(threshold/10);

% iterative algorithm for evaluating high and low
% frequencies

imax = index;
E0h = Ess(index);

while (E0h>Eth)&(imax<=(N/2))
    imax = imax + 1;
    E0h = Ess(imax);
end

f_high = (imax-1) * df;             % High Frequency

imin = index;
E0l = Ess(index);

while (E0l>Eth)&(imin>1)&(index>1)
    imin = imin - 1;
    E0l = Ess(imin);
end

f_low = (min(index,imin)-1) * df;   % Low Frequency

% end of iterative algorithm

% Signal Frequency Bandwidth
BW = f_high - f_low;




%%% end cp0702_bandwidth
```

```
function y = wgn(varargin)
%WGN Generate white Gaussian noise.
%   Y = WGN(M,N,P) generates an M-by-N matrix of white Gaussian noise.
%   P specifies the power of the output noise in dBW.
%
%   Y = WGN(M,N,P,IMP) specifies the load impedance in Ohms.
%
%   Y = WGN(M,N,P,IMP,STATE) resets the state of RANDN to STATE.
%
%   Additional flags that can follow the numeric arguments are:
%
%   Y = WGN(..., POWERTYPE) specifies the units of P.  POWERTYPE can
%   be 'dBW', 'dBm' or 'linear'.  Linear power is in Watts.
%
%   Y = WGN(..., OUTPUTTYPE); Specifies the output type.  OUTPUTTYPE
can
%   be 'real' or 'complex'.  If the output type is complex, then P
%   is divided equally between the real and imaginary components.
%
%   Example: To generate a 1024-by-1 vector of complex noise with power
%            of 5 dBm across a 50 Ohm load, use:
%            Y = WGN(1024, 1, 5, 50, 'dBm', 'complex');
%
%   Example: To generate a 256-by-5 matrix of real noise with power
%            of 10 dBW across a 1 Ohm load, use:
%            Y = WGN(256, 5, 10, 'real');
%
%   Example: To generate a 1-by-10 vector of complex noise with power
%            of 3 Watts across a 75 Ohm load, use:
%            Y = WGN(1, 10, 3, 75, 'linear', 'complex');
%
%   See also RANDN, AWGN.

%   Copyright 1996-2003 The MathWorks, Inc.
%   $Revision: 1.11.4.3 $  $Date: 2004/04/12 23:01:28 $

% --- Initial checks
error(nargchk(3,7,nargin));

% --- Value set indicators (used for the strings)
pModeSet    = 0;
cplxModeSet = 0;

% --- Set default values
p        = [];
row      = [];
col      = [];
pMode    = 'dbw';
imp      = 1;
cplxMode = 'real';
seed     = [];

% --- Placeholders for the numeric and string index values
```

```
numArg = [];
strArg = [];

% --- Identify string and numeric arguments
%     An empty in position 4 (Impedance) or 5 (Seed) are considered
numeric
for n=1:nargin
   if(isempty(varargin{n}))
      switch n
      case 4
         if(ischar(varargin{n}))
            error('The default impedance should be marked by [].');
         end;
         varargin{n} = imp; % Impedance has a default value
      case 5
         if(ischar(varargin{n}))
            error('The default seed should be marked by [].');
         end;
         varargin{n} = [];  % Seed has no default
      otherwise
         varargin{n} = '';
      end;
   end;

   % --- Assign the string and numeric vectors
   if(ischar(varargin{n}))
      strArg(size(strArg,2)+1) = n;
   elseif(isnumeric(varargin{n}))
      numArg(size(numArg,2)+1) = n;
   else
      error('Only string and numeric arguments are allowed.');
   end;
end;

% --- Build the numeric argument set
switch(length(numArg))

   case 3
      % --- row is first (element 1), col (element 2), p (element 3)

      if(all(numArg == [1 2 3]))
         row    = varargin{numArg(1)};
         col    = varargin{numArg(2)};
         p      = varargin{numArg(3)};
      else
         error('Illegal syntax.')
      end;

   case 4
      % --- row is first (element 1), col (element 2), p (element 3),
imp (element 4)
      %
```

```
      if(all(numArg(1:3) == [1 2 3]))
         row    = varargin{numArg(1)};
         col    = varargin{numArg(2)};
         p      = varargin{numArg(3)};
         imp    = varargin{numArg(4)};
      else
         error('Illegal syntax.')
      end;

   case 5
      % --- row is first (element 1), col (element 2), p (element 3),
imp (element 4), seed (element 5)

      if(all(numArg(1:3) == [1 2 3]))
         row    = varargin{numArg(1)};
         col    = varargin{numArg(2)};
         p      = varargin{numArg(3)};
         imp    = varargin{numArg(4)};
         seed   = varargin{numArg(5)};
      else
         error('Illegal syntax.');
      end;
   otherwise
      error('Illegal syntax.');
end;

% --- Build the string argument set
for n=1:length(strArg)
   switch lower(varargin{strArg(n)})
   case {'dbw' 'dbm' 'linear'}
      if(~pModeSet)
         pModeSet = 1;
         pMode = lower(varargin{strArg(n)});
      else
         error('The Power mode must only be set once.');
      end;
   case {'db'}
      error('Incorrect power mode passed in.  Please use ''dBW'',
''dBm'', or ''linear.''');
   case {'real' 'complex'}
      if(~cplxModeSet)
         cplxModeSet = 1;
         cplxMode = lower(varargin{strArg(n)});
      else
         error('The complexity mode must only be set once.');
      end;
   otherwise
      error('Unknown option passed in.');
   end;
end;

% --- Arguments and defaults have all been set, either to their
defaults or by the values passed in
```

```
%     so, perform range and type checks

% --- p
if(isempty(p))
   error('The power value must be a real scalar.');
end;

if(any([~isreal(p) (length(p)>1) (length(p)==0)]))
   error('The power value must be a real scalar.');
end;

if(strcmp(pMode,'linear'))
   if(p<0)
      error('In linear mode, the required noise power must be >= 0.');
   end;
end;

% --- Dimensions
if(any([isempty(row) isempty(col) ~isscalar(row) ~isscalar(col)]))
   error('The required dimensions must be real, integer scalars > 1.');
end;

if(any([(row<=0) (col<=0) ~isreal(row) ~isreal(col) ((row-
floor(row))~=0) ((col-floor(col))~=0)]))
   error('The required dimensions must be real, integer scalars > 1.');
end;

% --- Impedance
if(any([~isreal(imp) (length(imp)>1) (length(imp)==0) any(imp<=0)]))
   error('The Impedance value must be a real scalar > 0.');
end;

% --- Seed
if(~isempty(seed))
   if(any([~isreal(seed) (length(seed)>1) (length(seed)==0) any((seed-
floor(seed))~=0)]))
      error('The State must be a real, integer scalar.');
   end;
end;

% --- All parameters are valid, so no extra checking is required
switch lower(pMode)
   case 'linear'
      noisePower = p;
   case 'dbw'
      noisePower = 10^(p/10);
   case 'dbm'
      noisePower = 10^((p-30)/10);
end;

% --- Generate the noise
if(~isempty(seed))
```

```
   randn('state',seed);
end;

if(strcmp(cplxMode,'complex'))
   z = randn(2*row,col);
   y = (sqrt(imp*noisePower/2))*(z(1:row,:)+j*z(row+1:end,:));
else
   y = (sqrt(imp*noisePower))*randn(row,col);
end;









%%% end wgn
```